Xiaoxiang Zheng   *Editor*

Neural Interface: Frontiers and Applications

Advances in Experimental Medicine and Biology

Volume 1101

More information about this series at

Xiaoxiang Zheng
Editor

Neural Interface: Frontiers and Applications

Springer

Editor
Xiaoxiang Zheng
Qiushi Academy for Advanced Studies
Zhejiang University
Hangzhou, Zhejiang, China

Preface

Neural interfaces interact directly with the central nervous system (CNS) or peripheral nervous system (PNS) to restore brain function impaired by neural diseases or trauma or to enhance motor or cognitive functions for the abled individuals. The technology interfacing the brain is also known as brain-computer interface (BCI) or brain-machine interface (BMI). While the cochlear prosthesis and deep brain stimulation for Parkinson's disease have become reality, other neural interface applications are yet fully matured for decades. However, in recent years we have witnessed the great advances in this field, and the advances in neuroscience and engineering are speeding up neural interface technology, opening the door to assist, augment, repair, or restore sensorimotor or other cognitive functions and thus improving the quality of life for the individuals with disabilities. Medical applications such as NeuroPace for seizure detection/suppression and spinal cord stimulation for pain management are now becoming increasingly common. Neural interfaces are now being explored in applications as diverse as rehabilitation, accessibility, gaming, education, recreation, robotics, and human enhancement.

Neural interfaces also represent a powerful tool to address fundamental questions in neuroscience. We also have witnessed tremendous advancements in the field of neural interface with high impact not only in the development of neuroprosthetics but also in our basic understanding of brain function. Neural interface technology can be seen as a bridge linking engineering and neuroscience.

This book focuses on frontiers of neural interface technology, including hardware, software, neural decoding and encoding, control system, and system integration. It also covers the respects of applications in neuroprosthetics, neural diseases treatment, neurorobotics, and also the research paradigms for basic neuroscience. This book aims at providing the researchers, graduate students, and upper undergraduate students in a wide range of disciplines with a cutting-edge and comprehensive summary of researches on neural interfaces.

Editing such a book is tough, yet delightful, challenging, and fundamentally a team effort. Thus, I am in gratitude to a bevy of individuals without whom we could not have hoped to succeed. First and foremost, I sincerely thank Dr. Peng Zhang, a senior editor from Springer Nature, who invited me to edit this book, for his

understanding, support, and patience. I would like to thank all the authors who shared their works and wrote the manuscripts of their chapters. Their great contribution makes up this exciting work. I also would like to thank everyone who has helped me along the way but whom I did not mention explicitly.

Hangzhou, China   Xiaoxiang Zheng

Contents

About the Editor

Xiaoxiang Zheng is a professor at the Qiushi Academy for Advanced Studies, Zhejiang University. She is currently a member of the academic board of Key Laboratory for Biomedical Engineering of Ministry of Education at Zhejiang University and was the director of the College of Biomedical Engineering and Instrument Science, Zhejiang University, and executive member of the council of the Chinese Society of Biomedical Engineering. Dr. Zheng's research interests include neural engineering, microcirculation, and physiology of the cell. She has published more than 200 articles in these fields, over 100 of which are indexed by SCI or EI.

Contributors

Mojisola Grace Asogbon CAS Key Laboratory of Human-Machine Intelligence-Synergy Systems, Shenzhen Institutes of Advanced Technology (SIAT), Chinese Academy of Science (CAS), Shenzhen, China
Institute of Advanced Integration Technology, SIAT, Shenzhen, China
Shenzhen College of Advanced Technology, University of Chinese Academy of Sciences, Shenzhen, China

Rajmohan Bhandari University of Utah, Salt Lake City, UT, USA
Blackrock Microsystems, Salt Lake City, UT, USA

Junjun Chen Qiushi Academy for Advanced Studies, Zhejiang University, Hangzhou, China
Department of Biomedical Engineering, Zhejiang University, Hangzhou, China

Weidong Chen Qiushi Academy for Advanced Studies (QAAS), Zhejiang University, Hangzhou, People's Republic of China
Department of Biomedical Engineering, Key Laboratory of Ministry of Education Ministry, Zhejiang University, Hangzhou, People's Republic of China
College of Computer Science and Technology, Zhejiang University, Hangzhou, People's Republic of China

Zhe Chen Department of Psychiatry, Department of Neuroscience and Physiology, New York University School of Medicine, New York, NY, USA

Peng Fang CAS Key Laboratory of Human-Machine Intelligence-Synergy Systems, Shenzhen Institutes of Advanced Technology (SIAT), Chinese Academy of Science (CAS), Shenzhen, China
Institute of Advanced Integration Technology, SIAT, Shenzhen, China

Robert Franklin Blackrock Microsystems, Salt Lake City, UT, USA

Jiping He Neural Interface and Rehabilitation Technology Research Center, School of Automation, Huazhong University of Science and Technology, Wuhan, China
Beijing Advanced Innovation Center for Intelligent Robot and System, School of Mechatronical Engineering, Beijing Institute of Technology, Beijing, China
Center for Neural Interface Design, School of Biological and Health Systems Engineering, Arizona State University, Tempe, AZ, USA

Dingyin Hu Neural Interface and Rehabilitation Technology Research Center, School of Automation, Huazhong University of Science and Technology, Wuhan, China

Jian Huang Neural Interface and Rehabilitation Technology Research Center, School of Automation, Huazhong University of Science and Technology, Wuhan, China

Sui Huang Nurotron Biotechnology Inc., Irvine, CA, USA

Paul Oluwagbengba Idowu CAS Key Laboratory of Human-Machine Intelligence-Synergy Systems, Shenzhen Institutes of Advanced Technology (SIAT), Chinese Academy of Science (CAS), Shenzhen, China
Institute of Advanced Integration Technology, SIAT, Shenzhen, China
Shenzhen College of Advanced Technology, University of Chinese Academy of Sciences, Shenzhen, China

Yile Jin Qiushi Academy for Advanced Studies, Zhejiang University, Hangzhou, China
Department of Biomedical Engineering, Zhejiang University, Hangzhou, China

Julia Körner University of Utah, Salt Lake City, UT, USA

Qiuxia Lai Neural Interface and Rehabilitation Technology Research Center, School of Automation, Huazhong University of Science and Technology, Wuhan, China

Farah Laiwalla School of Engineering, Brown University, Providence, RI, USA

Moritz Leber University of Utah, Salt Lake City, UT, USA
Blackrock Microsystems, Salt Lake City, UT, USA

Guanglin Li CAS Key Laboratory of Human-Machine Intelligence-Synergy Systems, Shenzhen Institutes of Advanced Technology (SIAT), Chinese Academy of Science (CAS), Shenzhen, China
Institute of Advanced Integration Technology, SIAT, Shenzhen, China

Wei Li Neural Interface and Rehabilitation Technology Research Center, School of Automation, Huazhong University of Science and Technology, Wuhan, China

Xiao Li Neural Interface and Rehabilitation Technology Research Center, School of Automation, Huazhong University of Science and Technology, Wuhan, China

Chuang Lin CAS Key Laboratory of Human-Machine Intelligence-Synergy Systems, Shenzhen Institutes of Advanced Technology (SIAT), Chinese Academy of Science (CAS), Shenzhen, China
Institute of Advanced Integration Technology, SIAT, Shenzhen, China

Xuan Ma Neural Interface and Rehabilitation Technology Research Center, School of Automation, Huazhong University of Science and Technology, Wuhan, China

Masaki Nakanishi Institute for Neural Computation, University of California San Diego, San Diego, CA, USA

Sandeep Negi University of Utah, Salt Lake City, UT, USA
Blackrock Microsystems, Salt Lake City, UT, USA

Arto Nurmikko School of Engineering, Brown University, Providence, RI, USA

Gang Pan College of Computer Science and Technology, Zhejiang University, Hangzhou, People's Republic of China

Christopher F. Reiche University of Utah, Salt Lake City, UT, USA

Oluwarotimi Williams Samuel CAS Key Laboratory of Human-Machine Intelligence-Synergy Systems, Shenzhen Institutes of Advanced Technology (SIAT), Chinese Academy of Science (CAS), Shenzhen, China
Institute of Advanced Integration Technology, SIAT, Shenzhen, China

Florian Solzbacher University of Utah, Salt Lake City, UT, USA
Blackrock Microsystems, Salt Lake City, UT, USA

Xiaoan Sun Nurotron Biotechnology Inc., Irvine, CA, USA

Jing Wang Department of Anesthesiology, Perioperative Care and Pain Medicine, Department of Neuroscience and Physiology, New York University School of Medicine, New York, NY, USA

Ningyuan Wang Nurotron Biotechnology Inc., Irvine, CA, USA

Yijun Wang Institute of Semiconductors, Chinese Academy of Sciences, Beijing, China

Yuanyuan Wang Neural Interface and Rehabilitation Technology Research Center, School of Automation, Huazhong University of Science and Technology, Wuhan, China

Yueming Wang Qiushi Academy for Advanced Studies (QAAS), Zhejiang University, Hangzhou, People's Republic of China
College of Computer Science and Technology, Zhejiang University, Hangzhou, People's Republic of China

Zhaohui Wu College of Computer Science and Technology, Zhejiang University, Hangzhou, People's Republic of China

Kedi Xu Qiushi Academy for Advanced Studies (QAAS), Zhejiang University, Hangzhou, People's Republic of China
Department of Biomedical Engineering, Key Laboratory of Ministry of Education Ministry, Zhejiang University, Hangzhou, People's Republic of China
Zhejiang Provincial Key Laboratory of Cardio-Cerebral Vascular Detection Technology and Medicinal Effectiveness Appraisal, Zhejiang University, Hangzhou, People's Republic of China

Qi Xu Neural Interface and Rehabilitation Technology Research Center, School of Automation, Huazhong University of Science and Technology, Wuhan, China

Ming Yin University of Utah, Salt Lake City, UT, USA
Blackrock Microsystems, Salt Lake City, UT, USA

Dan Zhang Department of Psychology, Tsinghua University, Beijing, China

Jiacheng Zhang Qiushi Academy for Advanced Studies (QAAS), Zhejiang University, Hangzhou, People's Republic of China
Department of Biomedical Engineering, Key Laboratory of Ministry of Education Ministry, Zhejiang University, Hangzhou, People's Republic of China
Zhejiang Provincial Key Laboratory of Cardio-Cerebral Vascular Detection Technology and Medicinal Effectiveness Appraisal, Zhejiang University, Hangzhou, People's Republic of China

Peng Zhang Neural Interface and Rehabilitation Technology Research Center, School of Automation, Huazhong University of Science and Technology, Wuhan, China

Shaomin Zhang Qiushi Academy for Advanced Studies (QAAS), Zhejiang University, Hangzhou, People's Republic of China
Department of Biomedical Engineering, Key Laboratory of Ministry of Education Ministry, Zhejiang University, Hangzhou, People's Republic of China
Zhejiang Provincial Key Laboratory of Cardio-Cerebral Vascular Detection Technology and Medicinal Effectiveness Appraisal, Zhejiang University, Hangzhou, People's Republic of China

Nenggan Zheng Qiushi Academy for Advanced Studies (QAAS), Zhejiang University, Hangzhou, People's Republic of China
College of Computer Science and Technology, Zhejiang University, Hangzhou, People's Republic of China

Xiaoxiang Zheng Qiushi Academy for Advanced Studies (QAAS), Zhejiang University, Hangzhou, People's Republic of China
Department of Biomedical Engineering, Key Laboratory of Ministry of Education Ministry, Zhejiang University, Hangzhou, People's Republic of China
Zhejiang Provincial Key Laboratory of Cardio-Cerebral Vascular Detection Technology and Medicinal Effectiveness Appraisal, Zhejiang University, Hangzhou, People's Republic of China

Chapter 1
Advances in Penetrating Multichannel Microelectrodes Based on the Utah Array Platform

Moritz Leber, Julia Körner, Christopher F. Reiche, Ming Yin, Rajmohan Bhandari, Robert Franklin, Sandeep Negi, and Florian Solzbacher

Abstract The Utah electrode array (UEA) and its many derivatives have become a gold standard for high-channel count bi-directional neural interfaces, in particular in human subject applications. The chapter provides a brief overview of leading electrode concepts and the context in which the UEA has to be understood. It goes on to discuss the key advances and developments of the UEA platform in the past 15 years, as well as novel wireless and system integration technologies that will merge into future generations of fully integrated devices. Aspects covered include novel device architectures that allow scaling of channel count and density of electrode contacts, material improvements to substrate, electrode contacts, and encapsulation. Further subjects are adaptations of the UEA platform to support IR and optogenetic simulation as well as an improved understanding of failure modes and methods to test and accelerate degradation in vitro such as to better predict device failure and lifetime in vivo.

Authors Moritz Leber, Julia Körner and Christopher F. Reiche have contributed equally to this chapter.

M. Leber (✉) · M. Yin · R. Bhandari · S. Negi · F. Solzbacher (✉)
University of Utah, Salt Lake City, UT, USA

Blackrock Microsystems, Salt Lake City, UT, USA
e-mail: mleber@blackrockmicro.com; florian.solzbacher@utah.edu

J. Körner · C. F. Reiche
University of Utah, Salt Lake City, UT, USA

R. Franklin
Blackrock Microsystems, Salt Lake City, UT, USA

Keywords Utah electrode array (UEA) · Neural interface materials · Wireless technology · Accelerated aging · Advanced system integration

1.1 Application Areas and Challenges

Many neural interface electrode developments have been driven by government-sponsored research programs that focused on the restoration of motor or sensory function (neuroprosthetics). In recent years, increasing numbers of clinical research studies under FDA investigative device exemption (IDE) approvals have been carried out for a variety of interfaces. The Utah electrode array (UEA) is the only penetrating high-channel count device of its kind to have received FDA 510 (k) clearance and to have been used in such studies to date. Up until recently, the commercial sector however deemed this market to be too small and the technical hurdles and risks as too large to warrant investment. Subchronic monitoring and treatment of neurological disorders, such as epilepsy, and some peripheral and autonomic nervous system applications appear to have gained momentum in the commercial sector.

Key technological trends that can be observed are increasing channel count, enhanced biocompatibility through materials advances (porosity, coatings, etc.), the advent of devices for use in optogenetics and IR stimulation, advanced wireless (implantable and external) and novel system integration, and packaging concepts for these devices that, e.g., push the boundaries on electrode channel count into the 1000s of channels and beyond (the current Darpa NESD program targets 1 Mio channels for an implantable wireless device covering about 2×2 cm^2).

The clinical trends are driven by key opinion leaders with clinical research studies in human patients at Brown University/Massachusetts General Hospital, Stanford, University of Pittsburgh Medical Center, University of Pennsylvania, Chicago Northwestern, Case Western Reserve University, Caltech, UCLA, Columbia, University of Washington, and a growing number of centers in Europe. To an increasing extent, epilepsy patients are being used as a recruiting group for a variety of clinical studies.

With increasing channel count on the hardware side, new challenges arise on the software and data analysis side if one takes into account that the current state of the art in analysis of the data is to search for specific features or carry out spike sorting of action potential events. Data amounts can easily exceed terabytes from a single subject within a 24-h period for devices in the 100-channel range. Assuming 50,000 channels, this would pose a serious challenge. Data collection, storage, management, and also visualization, search, and analysis become intractable with current methods. In addition, while the transition from nonhuman primates to human subjects has great advantages, it also comes with a more stringent regulatory framework and Health Insurance Portability and Accountability Act (HIPPA)

regulations for protection of patient data. Future concepts for ultrahigh-channel count neural interfaces will thus likely have to mimic some of the architecture used in the human nervous system as well as in advanced sensor networks, where local "processors" can receive and process neural data at high resolution and depending on filters and parameters set by a central control unit can then either autonomously decide to pass on, compact, or discard data. Smart contextual visualization and search approaches could assume the role of a smart virtual assistant and become support tools for exploration of data.

1.2   Overview of Electrodes in the Field

There is a plethora of penetrating neural micro electrodes that has been published and demonstrated to varying degrees in vivo, mostly by academic institutions. Microwire electrodes were among the first implantable penetrating microelectrodes and were developed in the 1950s [25]. They are fabricated by cutting off the end of an insulated metal wire or by laser ablation of the insulation material around the sharpened tip of a wire [114]. With sufficient mechanical stiffness to withstand the insertion process into neural tissue, common materials for the 25–50 μm diameter wires are stainless steel, tungsten, iridium, and platinum-iridium alloys [25, 87, 114]. Several microwires can be assembled to an array, which is held together by a cast material such as biocompatible epoxy [114]. Further development led to the introduction of floating microelectrode arrays (FMAs), which are designed to move with the brain by "floating" on the surface of the brain and being mechanically decoupled from the skull. FMAs offer the advantage of being highly customizable regarding individual electrode length, position, and spacing [77]. The different electrodes are held together by lightweight substrates and are micro-welded to highly flexible insulated wires leading to the connector (Fig. 1.1a).

Besides microwire and FMA probes, silicon micromachined electrodes and arrays are prevalent in the field. The two main technologies include devices based on the Michigan style shank electrodes and the Utah electrode array (UEA). Both device types allow for high electrode density and electrode counts that are required for neural prosthetic applications [114], and they exhibit the advantage of micromachining batch process compatibility.

Michigan type microelectrodes consist of multiple electrode sites on a silicon shank and are fabricated using standard microfabrication techniques such as dopant diffusion, physical and chemical vapor deposition, photolithography, and etching processes [34, 125]. Furthermore, it is possible to assemble individual silicon shanks to three-dimensional array geometries [124].

In contrast, UEAs are immediately fabricated as a three-dimensional device. The UEA technology was developed at the University of Utah in the early 1990s [22] and is currently (as of 2019) the only FDA cleared microelectrode array for human
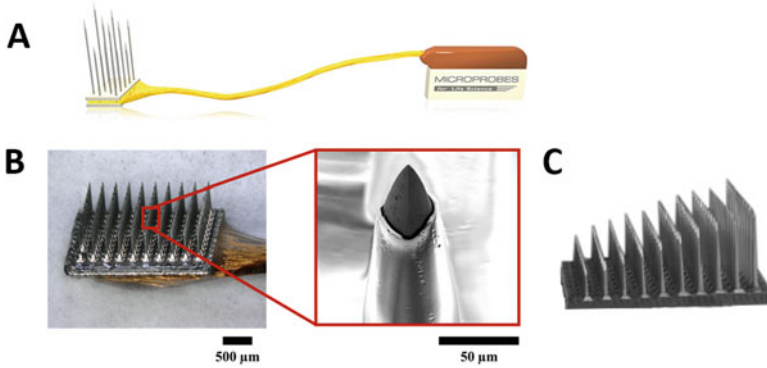
Fig. 1.1 (**a**) A floating microelectrode array architecture. The 18–36 microelectrodes of arbitrary lengths are held together by a lightweight ceramic platform and tethered to a connector by a thin and lightweight cable. (**b**) The Utah electrode array: a 10 × 10 grid of insulated boron doped silicon micro needles. Insulated gold wires are wire bonded before being encapsulated in medical grade silicone to form the assembled Utah electrode array. The magnification shows an active platinum coated electrode site at the tip of a parylene-C coated silicon shaft. (**c**) The Utah slant electrode array: a modification of the UEA with variable shaft lengths to access different depths in the tissue. (**a**. Image copyright and courtesy of Microprobes for Life Science. **c**. Image copyright and courtesy of Blackrock Microsystems LLC)

research use. The arrays consist of typically 10 × 10 electrodes, which are formed by cutting pillar geometries out of a highly p-doped silicon substrate with pre-structured insulation sites. The contact pads for each electrode are deposited and patterned on the back side of the wafer. A subsequent customized wet etching process sharpens the silicon pillars and forms a dense array of silicon needles with lengths varying from 500 to 1500 μm. The tips of the silicon needles are then metallized (typically with platinum or iridium oxide) in a sputtering process to improve the electrochemical charge transfer between the device and the surrounding biological media. To ensure biocompatibility and to protect the array from the foreign body response when implanted, the entire device is coated with parylene-C. Finally, the electrode sites are formed by removing the parylene-C encapsulation coating from the upper 30–50 μm of the metallized silicon tips. Insulated gold wires are wire bonded to the contact pads on the back of the UEA for each individual electrode and attach them to a connector. The bond sites are subsequently encapsulated with medical grade silicone.

Over two decades, the UEA was subject to multiple improvements and material changes [9]. The early UEA electrodes were insulated from each other by p-n junctions and the shafts were encapsulated with polyimide. The current UEA technology, however, uses glass lines between the shaft sites for insulation instead of p-n junctions and parylene-C instead of polyimide. As a modification of the standard UEA geometry with equal shaft lengths, the Utah slant electrode array (USEA) exhibits shaft lengths varying from 750 to 1500 μm. With the advantage of acting at different

depths in the tissue, the USEA is commonly implanted into the peripheral nervous system [18]. Figure 1.1b displays an assembled standard UEA with constant shaft lengths of 1000 μm and Fig. 1.1c a USEA with varying shaft lengths.

In addition to the Michigan probes and the UEA technology, recent research efforts led to the introduction of high-density and high-channel silicon-based micro-electrodes. Prominent technologies include the CMOS-based high-density micro-probe arrays [100] developed at IMTEK/Germany and the neuropixels probes [56] developed at Janelia Research Campus/USA.

1.3   Key Developments of the UEA Platform

1.3.1   Array Shape Variations

Over time, adjustments have been made to the standard UEA geometry to allow for a variety of applications and to improve stimulation and recoding [98].

All shafts of the standard UEA have the same length (Fig. 1.2a). The arrays can be fabricated with a widely varying number of electrodes, ranging from small 4×4 (16 electrodes) arrays to larger ones with 10×10 (100 electrodes). High-density UEAs can comprise over 200 electrodes within the same dimensions as the standard UEAs [106].

A commonly used variation of the UEA is the Utah slant electrode array (USEA), which features electrodes with different lengths in one and constant length in the other direction (Fig. 1.2b). These arrays are favorably used in stimulation and recording in peripheral nerves as they allow to reach different axons in varying depths within the nerve [11, 18]. Furthermore, USEA with particularly long elec-trodes (1–9 mm compared to the usual 0.5–1.5 mm) have been reported (long USEA), allowing specifically deep penetration into neural tissue [106].

Another development, especially for applications in retinal implants and periph-eral nerves, are convoluted shape UEAs. In that case, although all electrodes have the same lengths, they feature a varying penetration depth into the neural tissue due
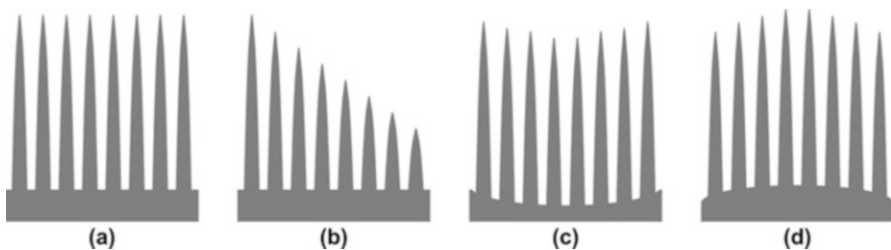
Fig. 1.2 Different geometries of the Utah electrode array: (**a**) standard UEA, (**b**) Utah slant electrode array, (**c**) and (**d**) convoluted shape UEA with concave and convex curvature, respectively

to the electrode base being curved, either in a convex or a concave fashion (Fig. 1.2c, d). According to Bhandari et al., this leads to a better integration of the array with the nerve geometry, consequently less extra-neural volume where fibrotic tissue can grow, and higher selectivity in stimulation as varying nerve sites can be reached [10].

1.3.2 Novel Architectures to Improve Tissue Response: The Natural Buoyancy Utah Electrode Array

Recording and stimulation performance of microelectrodes as well as foreign body response are critical factors limiting the longevity of neural interfaces and must be addressed in the design process [3, 19, 23, 62]. Shape, size, electrode material, tethering forces, and the implantation technique significantly influence the foreign body response to implanted neural electrodes [35, 77].

As an example, blood pulsation and head movements cause permanent relative motions of the brain with respect to the surrounding skull. Since the array must be implanted in the small space between skull and brain, it is subjected to these relative movements. Ideally, it would be advantageous for the electrodes to be mechanically decoupled from one another and to be able to float on the cerebral cortex. Minimizing the micromotions and resulting friction between the brain tissue and the implanted electrodes would reduce the risk of inflammation and the formation of an insulating sheath around the electrodes, leading to device insulation and failure. Numerical studies have shown that causes for severe foreign body response can be limited by flexible and/or soft implants [67, 109]. Hence, by eliminating the rigid backplane of the UEA, the mechanical mismatch between implant and tissue would be significantly reduced. Nevertheless, the backplane holding all 100 electrodes of the UEA in place is indispensable for the device handling and the high velocity insertion process during surgery. A dissolving and biodegradable backplane offering the required mechanical strength prior to and during the implantation process would therefore represent the ideal tradeoff solution. Once implanted, the dissolving backplane would decouple all electrodes from one another. Although the use of dissolvable implantation shuttles showed promising results by mitigating the foreign body response [60, 127], the fabrication of a high-channel count implant, such as the natural buoyancy Utah electrode array (NBUA) [65], with a dissolving backplane is unique.

The NBUA represents a modification of the conventional UEA, where the matrix of up to 10×10 microelectrodes is held together by the biocompatible dissolvable polyethylene glycol (PEG) material. The PEG provides a temporary rigid mechanical back-plane required for insertion of the array into the tissue. Once the 10×10 matrices of electrodes are inside the tissue, the PEG dissolves after it gets in contact with the biological fluid. At that point each electrode is floating independently from the others (Fig. 1.3).
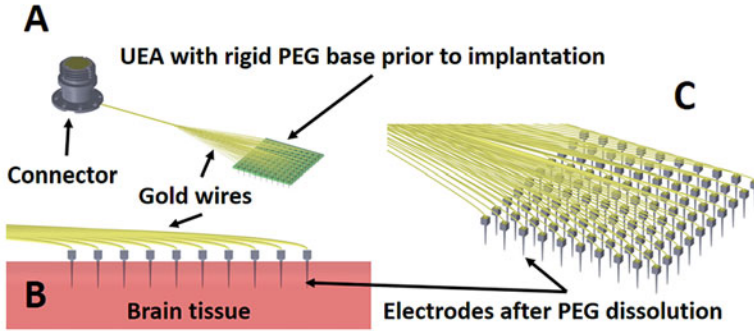
Fig. 1.3 Cartoon image of the dissolvable UEA prior to insertion (**a**). At this point all the 100 shafts are connected by PEG which represents the rigid backplane of the device required for the simultaneous insertion of all 100 electrodes. After insertion, PEG dissolves resulting in mechanically decoupled floating shafts (**b**, **c**). (Reprinted, with permission, from Leber et al. [65])

The fabrication of the NBUA comprises additional steps starting with a standard unwired UEA. Although the main modification is the substitution of the glass traces with PEG, the fabrication of single electrodes results in further challenges. The side walls of single electrodes, previously covered and protected by the glass traces, need to be encapsulated with parylene-C to avoid the exposure of silicon to the biological environment. Furthermore, the packaging process, which includes wire bonding and silicone encapsulation, needs to be adapted to decoupled single electrodes.

The first step in the fabrication process is the removal of the glass lines in between the different shafts of the standard Utah array while keeping the array in place. Glass lines are etched in hydrofluoric acid (HF). To keep the array in place and to protect the shaft and tip metal from HF, the UEA is entirely molded in photoresist with only the back side glass traces exposed. A polyethylene (PE) ring surrounds the array and serves as mold for the photoresist. After the HF etch, the photoresist is removed in acetone, releasing the singularized electrodes solely held together by a 3 μm thick parylene-C layer, which will subsequently be removed. Parylene-C is deposited again onto the array covering this time also the side walls of the electrodes, which were previously protected by the glass traces. Laser ablation disrupts the film connecting the single electrodes and forms the active electrode sites at the tip of each shaft.

Finally, all electrodes embedded in PEG and insulated gold wires are used to wire bond the bond sites on the back of each electrode to a connector. Silicone is applied using a thin platinum wire onto each bond site in order to provide additional mechanical strength to the bonds and to encapsulate the remaining exposed surface. The PEG is then removed from the tip side of the assembly by dipping the assembly into deionized water. The final device is shown in Fig. 1.4.

The PEG backplane has typically a mass of 300 mg, which dissolves in phosphate-buffered saline at room temperature in less than 45 minutes (Fig. 1.5). Electrical impedance spectroscopy experiments after dissolution yielded typical UEA impedance values for the single electrodes.
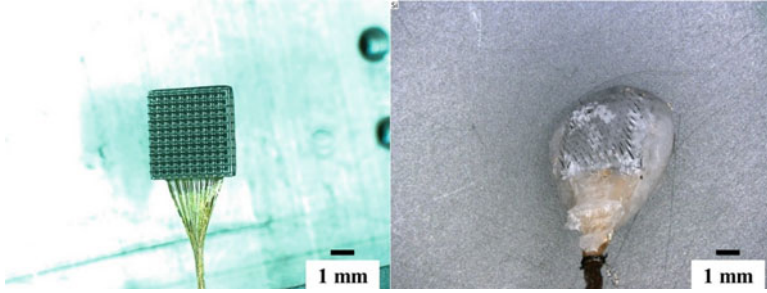
Fig. 1.4 Left: A standard UEA without dissolvable base for comparison. Right: The finalized NBUA device consists of 100 separated electrodes held in place by PEG and connected by gold wires to a connector. (© 2017 IEEE. Reprinted, with permission, from Leber et al. [65])
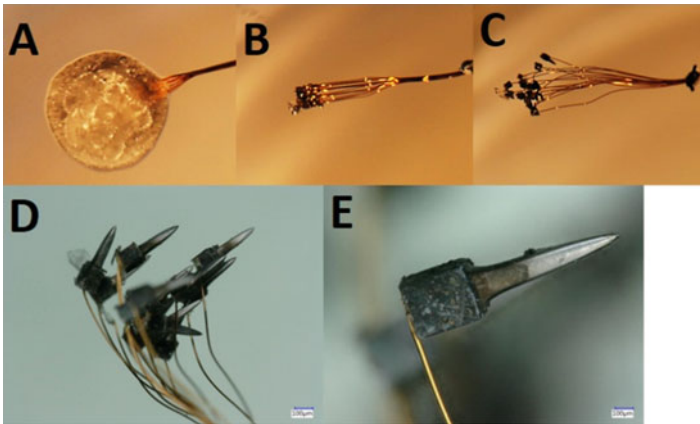
Fig. 1.5 A 4 × 4 device dissolving in PBS at room temperature. (**a**) Rear view of PEG-encapsulated device right after immersion in PBS (t = 0 min). (**b**) Rear view of device with dissolved PEG base (t = 45 min). (**c**) Same as (**b**) with deformed wire to demonstrate freely floating electrodes. (**d** and **e**) Close-up pictures of dissolved UEA and single electrode. (Reprinted, with permission, from Leber et al. [65])

It has not only been shown that the technology of a dissolving back plane is a promising evolution of the UEA, but it also offers the potential for many additional improvements. For once, PEG can be used as a carrier material for drug delivery to reduce inflammation or enhance neuronal growth. Furthermore, contacting the dissolving NBUA with highly flexible polymer-based ribbon cables will reduce the tethering forces induced by the currently used gold wires and provide even less mechanical mismatch between the implant and the tissue.

1.3.3   Ultrahigh-Channel Count Electrode Architectures

In order to reduce damage to and impact on the tissue in which stimulation and recording take place, it is beneficial for neural probes to have a small footprint. In case of the UEA, this requirement in combination with the 3D microelectrode geometry limits the number of active sites as only a certain number of electrodes fit within the device footprint due to the challenges of the dicing-based fabrication process. However, there is substantial interest to increase the number of active sites and their density to address larger fractions of the brain and nerve tissue as well as submillimeter neuroanatomical structures without increasing discomfort and risk of infection for the patient (Wark et al. 2013). Furthermore, the ability to simultaneously stimulate and record in a coordinated fashion at different locations is desired.

In order to enhance both coverage and resolution of the UEA architecture, different paths have been pursued:

1. Multiport devices that connect multiple UEAs to one percutaneous connector. This has allowed up to 1024 channels (sixteen 64-channel UEAs) to be attached to one connector (Fig. 1.6).
2. High-density (HD) UEAs that have a smaller pitch (200 μm, instead of 400 μm) between electrodes. These have been originally developed for the use in the peripheral nervous system as slant electrode arrays [118], but the technology is easily transferable to regular UEAs with constant shaft lengths.
3. Utah multisite electrode arrays (UMEAs) which are UEAs with multiple electrode sites per shank. This allows to increase the number of stimulation/recording sites while maintaining the same array footprint and form factor as the standard UEA [104]. Although initial demonstrators have shown up to 9 contacts per UEA

Fig. 1.6 Multiport UEA with 1024 channels (16 times 64 channel arrays attached to one connector). (Image copyright and courtesy of Blackrock Microsystems LLC)
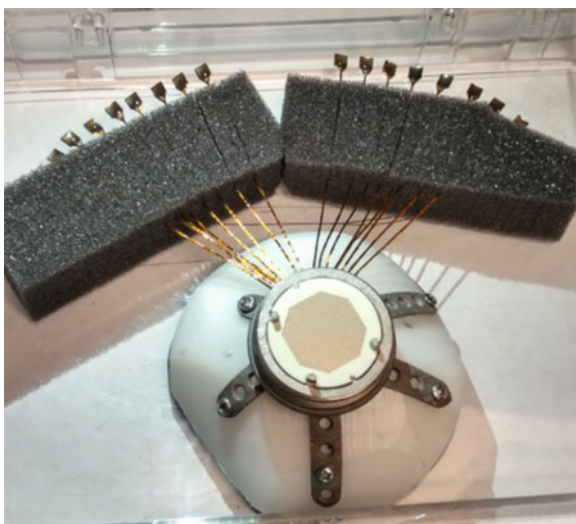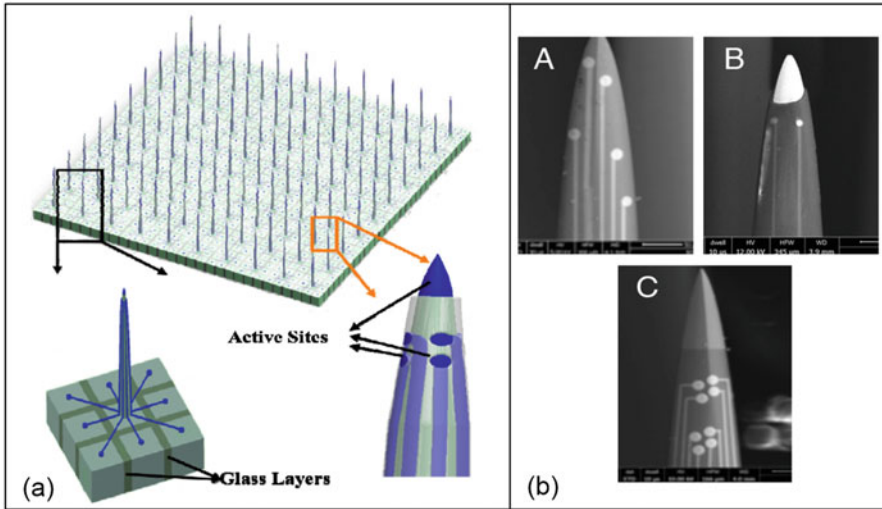
Fig. 1.7 (**a**) Concept of UMEA with up to nine active sites per electrode. (**b**) SEM micrographs of FIB fabricated UMEA with varying configurations: (A) 2 μm metal traces with multiple sites along shaft without tip electrode, (B) 5 μm diameter sites with 2 μm traces, (C) 2 pairs of 5 μm tetrodes. (A. Reprinted, with permission, from Shandhi et al. [103])

shank, practical implementations allow typically 3–4 contacts per shank (Fig. 1.7).

While the multiport and high-density devices are fabricated in the same way as the standard UEA with only small changes to the process, the creation of the Utah multisite electrode array requires significant modification and additional fabrication steps.

Each electrode of the UMEA has one active site at the electrode tip and up to eight active sites along the shaft. This requires the bottom of the electrode to be divided into nine isolated conductive squares which hold the contact pad for each site on the back (the shaft occupies one square). All active sites are connected to the contact pads via metal traces on the shaft's side, as seen in Fig. 1.7a [103]. In order to insulate all active sites from one another, a silicon nitride layer is deposited prior to metal sputtering [104].

Two approaches have been pursued to fabricate UMEAs: the serial direct writing by focused ion beam (FIB) patterning in combination with high-resolution scanning electron microscopy (SEM) [103] and a shadow mask process compatible with batch fabrication [104].

The FIB technique allows to deposit metal (platinum) patterns along the shafts of the UEA with precise control and reproducible resolution of <1 μm. It enables the creation of metal patterns of any shape (circles, square, ring, etc.), size, count, and location for neural recording and stimulation, on the tip of the electrode or along the shank of the Utah electrodes in various configurations [103].
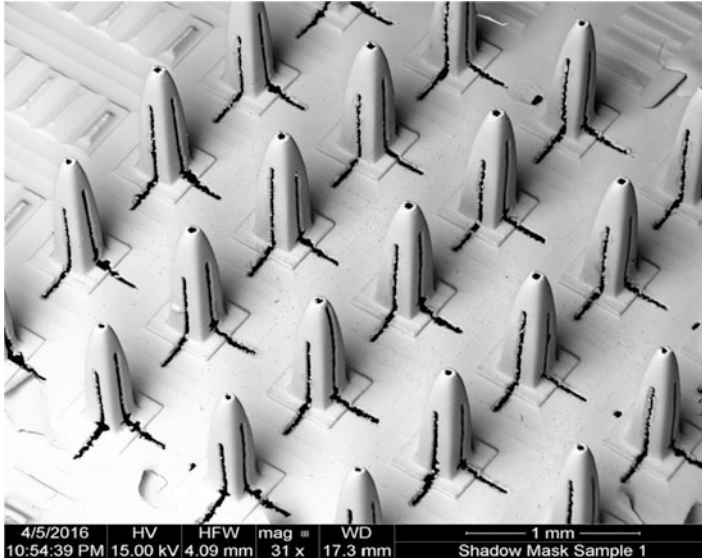
Fig. 1.8 SEM micrograph of the nickel shadow mask fabricated by electroplating and laser ablation on a sacrificial UEA. (Reprinted, with permission, from Shandhi et al. [104])

However, this approach is comparatively slow and expensive, as each active site needs to be written individually. Shandhi et al. have developed a process which addresses this challenge: first, a nickel shadow mask is created on a sacrificial UEA by electroplating and laser ablation (Fig. 1.8). After dissolution of the sacrificial UEA structure, this shadow mask can be used to deposit the metal traces and electrode sites by sputtering of platinum or another desired metal on another UEA during fabrication [104]. Although this approach requires additional fabrication steps compared to the standard UEA, it enables batch fabrication of arrays with an increased number of stimulation/recording sites while maintaining the footprint of a standard UEA.

This novel technology to pattern 3D UEA architectures opens new possibilities for commercial devices. For example, it enables the fabrication of different patterns (such as active sites in tetrode and laminar configuration) and/or in situ sensors for device and tissue health monitoring at the site of implantation. Figure 1.7b shows SEM micrographs of some of the fabricated UMEA configurations.

1.3.4 Improving the Stimulation and Recording Properties: Iridium Oxide and Roughened Electrodes

Neural stimulation and recording electrodes are generally characterized by their impedance, charge injection capacity (CIC), and surface area. It is common practice in the field to express the electrodes' impedance at the frequency of 1 kHz.

The CIC is defined as the highest amount of charge that can be delivered by an electrode within the leading phase of a stimulation pulse without inducing electrolysis of water, which is considered to have harmful effects on the surrounding tissue. Although the CIC is often assumed as a "safe" stimulation parameter, material degradation was observed at lower charge values [90, 91], and tissue damage can be induced by overexcitation of neural tissue regardless of the CIC [30].

The surface area can be differentiated into geometric surface area (GSA) and real surface area (RSA) that additionally considers surface roughness on a nanometer scale. Both impedance and CIC depend on the RSA: the impedance decreases while the CIC increases with increasing RSA [28]. Generally low impedance and high CIC values are desirable for neural stimulation and recording electrodes [119]. Microelectrodes like the UEA ensure high selectivity and spatial resolution to discriminate between single neurons. Consequently, they exhibit a rather small surface area (ca. 2000 μm^2 for UEA electrodes). Hence, a tradeoff must be made between small electrode sizes on the one hand and low impedance along with high CIC values on the other hand. As impedance and CIC depend not only on the GSA and RSA, but also on the material specific electrochemical charge transfer, two approaches to optimize impedance and CIC were pursued in research:

1. Exploration of various electrode coating materials regarding their charge transfer properties.
2. Creation of rough electrode surfaces to increase the RSA/GSA ratio.

Both approaches were investigated for the UEA technology by introducing sputtered iridium oxide as an alternative coating material to the well-established platinum and by roughening the silicon substrate material.

The Introduction of Iridium Oxide as UEA Coating Material
Over the years, iridium oxide has been shown to be one of the most promising electrode coating materials, especially due to its comparatively high CIC values [28]. Iridium oxide films can be created by using several techniques such as electrochemical activation by repeated oxidation and reduction in PBS to form activated iridium oxide films (AIROF) [90, 91], thermal decomposition of iridium salt on metal substrates [92], electrodeposition [72], or by sputtering processes [59]. Sputtered iridium oxide films (SIROF) have the advantage of the possibility to fine-tune process parameters to obtain the desired physical and electrical properties for neural stimulation and recording [80, 122]. Therefore, they were investigated as an alternative coating material to platinum for the UEA electrodes.

Negi et al. [80] studied the effect of pulsed DC reactive sputtering parameters on the resulting SIROF film quality [80]. The sputtering pressure was identified as the critical deposition parameter, which has a major impact on the film morphology, as well as the electrochemical properties of the coatings. At lower pressure values, the SIROF surface exhibits a granular morphology, transitioning to dendritic structures with increasing pressure. Furthermore, impedance and CIC values of the films were measured to be lowest and highest, respectively, at lower pressure values. Further studies confirmed the superior electrochemical properties of SIROF compared to AIROF and platinum. SIROF coated UEA electrodes yielded CIC values of 2 mC/cm^2 compared to 1 mC/cm^2 [83] and 0.3 mC/cm^2 [81] for AIROF and platinum coated electrodes, respectively. At the same time, the impedance values at 1 kHz for SIROF electrodes were measured to be lowest with 6–10 kΩ compared to 120 kΩ [83] and 125 kΩ [81] for AIROF and platinum, respectively. In addition to its superior CIC and impedance values, SIROF was shown to be more resilient against material degradation by analyzing the iridium content in PBS after continuous pulsing, using mass spectrometry [82].

Due to its superior material properties described above, iridium oxide has been validated as an alternative coating material for UEA electrodes and has demonstrated its usefulness in sophisticated human experiments [32].

Silicon Substrate Material Roughening for Improved Electrode Properties
Although SIROF coatings have been shown to substantially increase the charge injection properties and to decrease the impedance values of UEA electrodes, platinum is the best studied material for neural electrodes to date, with numerous reported acute and chronic in vivo studies. As a result, much research was conducted on roughening platinum electrode surfaces for improved charge transfer properties. The efforts to create high RSA/GSA ratio platinum surfaces include laser processing [40, 41], electrochemical roughening [15, 115, 121], and electroplating of platinum gray [123, 142] as well as platinum black [38, 71, 85] films. Whereas laser processing is a time-consuming serial processing technique and presents difficulties regarding the three-dimensional UEA geometry, electrochemical roughening and deposition methods add to the process complexity and, in the case of platinum black, raise concerns regarding their mechanical integrity. This led to a substantially new approach to create high RSA/GSA ratio electrode surfaces by roughening the silicon substrate instead of the coating material, allowing the conformal deposition of platinum in a simple sputtering process.

Various physical and chemical roughening processes to alter the silicon surface of UEA tips were investigated. Despite well-described silicon roughening techniques in literature, the unusual high aspect ratio of the UEA architecture required a tailored roughening process. A customized reactive ion etching (RIE) and Bosch-type deep reactive ion etching (DRIE) recipe were developed to roughen the silicon tips of the UEA before coating them with a 500-nm-thick platinum layer [64]. The initial RIE step creates a shallow, well-defined microstructure on the silicon surface, whereas the second DRIE step deepens the pores from the first RIE etch until a minimum electrode impedance is reached, indicating maximum RSA increase. The process
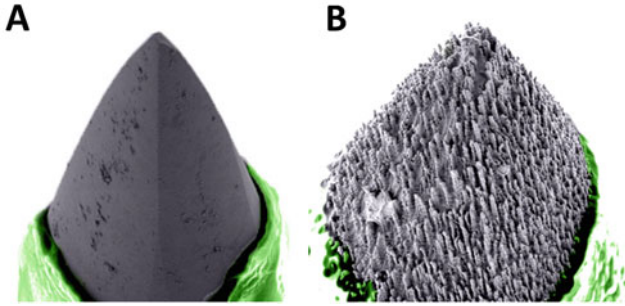
Fig. 1.9 Colored SEM images: (**a**) Standard platinum coated UEA electrode. (**b**) Roughened platinum coated UEA electrode

exhibits high controllability and has the advantage of batch fabrication compatibility, allowing to process the UEAs on wafer level. Fig. 1.9 displays a standard platinum coated UEA electrode and a roughened platinum coated UEA electrode.

Extensive soak testing in PBS over 500 days with regular impedance spectroscopy and CIC measurements demonstrated a decrease of impedance at 1 kHz by a factor of 0.32, and an increase of CIC by a factor of 1.8 of the roughened compared to standard UEA electrodes [63]. Furthermore, the roughened electrodes demonstrated an increased robustness toward stimulation-induced material failure. In a stress test, during which 1 million biphasic charge balanced pulses were applied to both roughened and standard electrodes, the roughened electrodes were found to be less susceptible to the degradation and delamination of the platinum coating.

Furthermore, first in vivo tests with the roughened UEAs were carried out in rodents. Although slightly higher platinum residuals in the neural tissue were detected for the roughened electrodes, a negative effect on the foreign body response and cytotoxicity could not be observed during a histological analysis of the neural tissue after 8 weeks of implantation into the cerebral cortices of rodents [63].

The substantially novel method of substrate material alteration toward increased RSA/GSA ratios of neural electrodes was only studied for platinum coatings to date. SIROF coated roughened UEA electrodes remain to be studied but are expected to even further increase the electrochemical properties such as the electrodes' impedance and CIC values.

1.3.5 Optrodes for Infrared and Optogenetic Stimulation

In the past, most devices that aim to interface with the nervous system and evoke action potentials in neurons relied on electrical stimulation. This is still the case, but there is an increasing interest in using electromagnetic radiation, both in infrared (IR) and visible wavelengths for neural stimulation as these optical methods carry the promise to address some of the challenges of electrical stimulation, such as

neuronal specificity, spatial resolution, stimulation-induced tissue damage, and stimulation artifacts [86, 120].

IR stimulation-based approaches have the advantage that they can be employed without preceding alterations to the neurons or their surroundings as the tissue absorbs the radiative energy and the resulting rapid temperature change induces stimulation due to many different processes and effects in the neural tissue [112].

In contrast, for the stimulation with visible wavelengths, the neurons have to be modified via optogenetics. In this technique, chosen as Nature's method of the year 2010 [79], virus vectors are used to genetically target specific neuron subtypes to express light-activated proteins in their cell membrane. Depending on the protein chosen, the thus genetically modified neurons can either be stimulated or inhibited by light irradiation in a specific wavelength range of the visible and near-infrared spectrum with very high specificity [86].

In order to take full advantage of the potential of optical stimulation, the efficient delivery of radiation deep into the neuronal tissue with high spatiotemporal resolution is required in many use cases. Furthermore, a corresponding device should also be able to record the resulting electrochemical response of the neurons to monitor the effect of the stimulation. The simplest penetrating light delivery approach is given by implanting an optical fiber into the neural tissue, often together with a penetrating or surface electrode for electrophysiological measurements of the response of the neural cells [5, 6, 39]. In more advanced approaches of integrated devices, either Michigan-style penetrating electrodes are upgraded with optical waveguides [26] or even whole micro light emitting diodes (μLED) [95, 126]. Alternatively, the UEA platform is adapted to benefit the optical stimulation techniques as discussed in the following.

A way to integrate a UEA-type device with a simple optical fiber approach is given by removing one of the electrodes and creating a hole in the back plane of a UEA via laser ablation. The missing electrode can then be replaced by aligning and fixing a so-called optrode, a metal coated tapered optical fiber, in its place (Fig. 1.10). This combines the relatively simple single site optical fiber stimulation with the spatiotemporal multichannel recording capability of UEA-type devices. Successful optogenetic stimulation with such a device was demonstrated both in vitro and in vivo [117, 141].

Alternatively, the UEA geometry and batch compatible fabrication method can be modified to create novel devices for multichannel light delivery. To create a device for IR radiation transmission, undoped silicon is used as a base material in the fabrication process and the contact pads of the UEA are replaced with an aluminum mask with windows to facilitate the alignment of butt-coupled optical fibers to the silicon needles that are acting as waveguides. Additionally, other fabrication steps necessary for the electrostimulation such as the metal electrode material deposition and the electrical insulation of the individual silicon needles are omitted. The resulting IR optrode array (Fig. 1.10a) was able to efficiently and selectively deliver IR radiation into tissue for stimulation [2, 27]. In order to further enhance the efficiency of the IR transmission and to add the possibility of delivering visible light into tissue for optogenetic stimulation, the base material for the
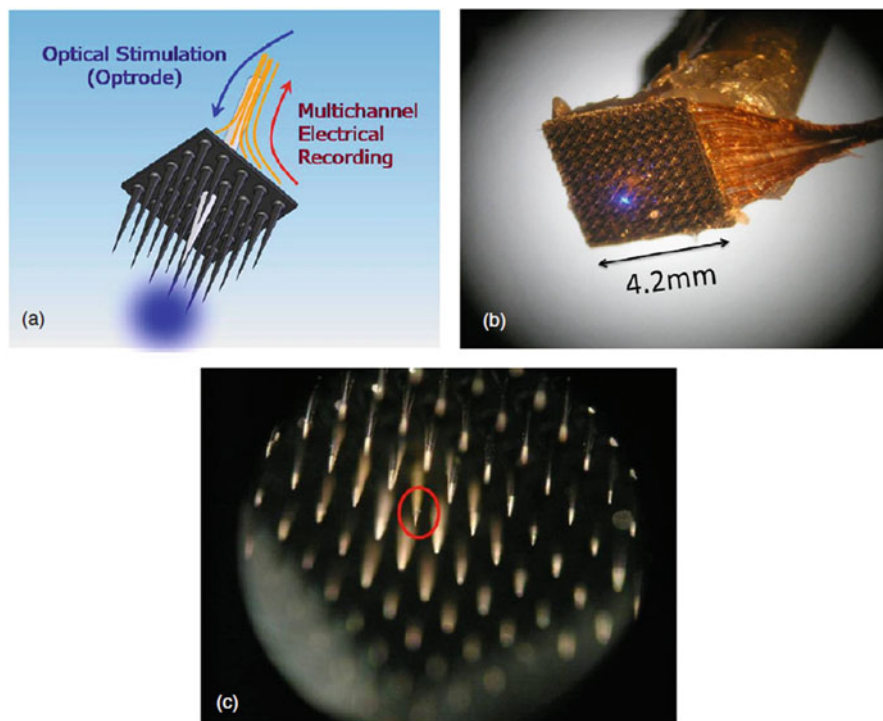
Fig. 1.10 Combination of a multi electrode array based on the Utah electrode array with a sharpened and metal coated optical fiber-based optrode. (**a**) Schematic of the device and (**b**) optical image with blue laser light being transmitted through the optrode. (**c**) Close-up optical image of the device. The position of the optrode between the electrodes is indicated. (Reprinted, with permission, from Zhang et al. [141])

device fabrication was changed from silicon to transparent silicate glass [1, 2]. However, glass behaves differently than silicon especially during the etching step of the UEA fabrication process and no sharp needles could be created this way. Therefore, several additional steps had to be added to the standard UEA fabrication process along with other smaller modifications to create a suitable device geometry. These additional steps include the use of a tapered dicing blade to pre-shape sharp optrode tips as well as a heat treatment step to smoothen the rough glass surface after etching [2, 17, 96].

The resulting passive glass Utah optrode array devices (Fig. 1.11b, c) can be used for light delivery using external stimulation sources. However, for neurological research and future clinical and neuroprosthetic applications, a fully integrated device, featuring both multichannel optical stimulation and electrical recording capacity, would be beneficial. Such a device is currently under development by a combination of the passive glass optrode array with a μLED array and an interposer layer to reduce cross-talk between optrodes (Fig. 1.12). By adding electrical
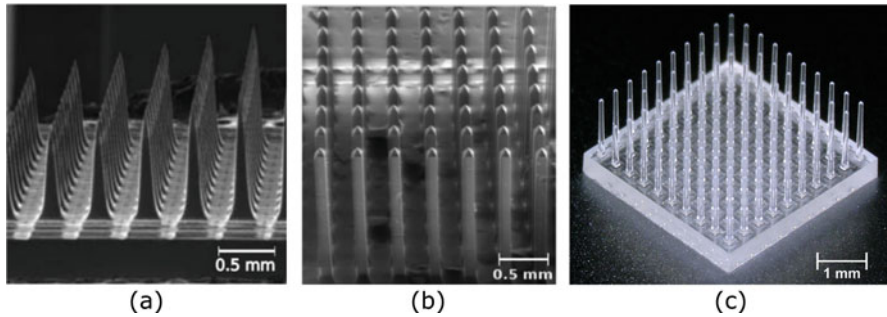
Fig. 1.11 SEM images of optrode arrays fabricated from (**a**) undoped silicon, (**b**) fused silica glass, and (c) optical image of an optrode array made from borosilicate glass. (**a**, **b** Reprinted, with permission, from Abaya et al. [2])
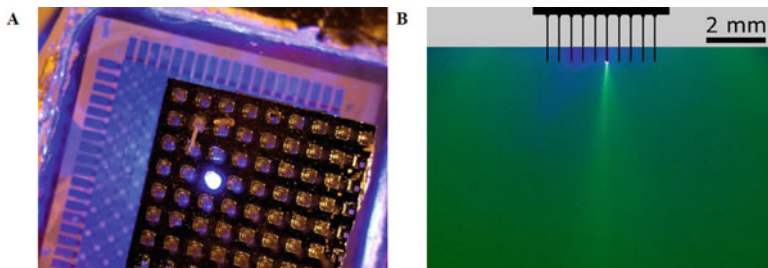
Fig. 1.12 Images of a glass optrode array with a special interposer to prevent cross talk, coupled to a μLED array. In (**a**), one of the μLEDs is turned on. (**b**) shows the emission profile of an optrode when immersed in fluorescein solution. (Reprinted, with permission, from Scharf et al. [96])

recording functionality to the array, a highly flexible device for optogenetic research applications will be created [96].

1.3.6   Advances in Encapsulation

An important requirement for implanted neural devices is the ability to perform their function in vivo for an extended amount of time to justify the risk and cost associated with implantation surgery. However, the physiological environment is hazardous to devices. Water and different ionic species dissolved in body fluids lead to corrosion and other electrochemical degradation processes of the various materials the device consists of, resulting in leakage currents or short circuits of electrical components. This will eventually lead to complete device failure. Therefore, the functional parts of the device, except the active electrode sites that are supposed to interact directly with the neural tissue, must be protected from the physiological environment by encapsulation.

Table 1.1 Methods and materials that can be used for the encapsulation of implantable neural devices along with their advantages and disadvantages

Method and material	Advantages	Disadvantages
Hermetic can [55]	Hermetic (airtight + waterproof), long lifetime	Large, assembly process complexity, need for feedthroughs
Silicon oxide ([43, 78])	Conformal, good insulation	Dissolves in body fluids (except for thermal SiO_2), needs to be defect free – > capacitively coupled electrodes
Silicon nitride ([97, 129])	Low WVTR, good dielectric properties, easy to deposit	Pin holes, dissolves in body fluids
Diamon-like carbon (DLC) [93]	Low friction, low wear, chemically inert, biocompatible, deposition at room temperature possible, doping can control electrical properties	Poor adhesion, tends to delaminate
Ultrananocrystalline diamond (UNCD) ([8, 128])	Chemically inert, biocompatible, high wear resistance, low friction surface	Requires high deposition temperatures
Silicon carbide ([29, 49, 66])	Very hard to dissolve/destroy, biocompatible, doping can control electrical properties, low water intake	Pin-holes, high temperature process, nonuniformity, cracks on polymer substrates
PTFE ([54, 69])	Low friction, biostable, biocompatible	Nonuniformity, byproduct incorporation
Silicone [116]	Biocompatible, cheap, widely used	Nonuniformity, high WVTR
Parylene ([51, 70])	Conformal, low deposition temperature, biocompatible, widely used	Relatively high WVTR, poor adhesion
Polyimide [88]	Biocompatible	Nonuniformity, high water absorption and WVTR

Any material that is used for encapsulation of implantable neural devices has to provide chemical resistance against biological media and their diffusion into the encapsulation material, biocompatibility, and long-term stability. It has to protect the inner parts of the device over extended periods of time in vivo by creating a near-hermetic isolation with a very low water vapor transmission rate (WVTR) [107]. Additionally, it has to ensure the proper electrical functionality of the devices, i.e. preferably should have high impedance and a low dielectric constant to reduce signal noise and ensure high selectivity for interaction with neural tissue [51].

Furthermore, the encapsulation steps need to be compatible with the fabrication or assembly processes, offer the potential for further miniaturization, and be compatible with wire-based or wireless data and power transmission. Identifying an encapsulation method and corresponding materials that fully satisfy all these requirements at the same time is very difficult [134].

Consequently, many different materials have been investigated for encapsulation purposes of implantable neural devices (Table 1.1). Methods can be divided into hermetic and near-hermetic encapsulation. The former can be realized as capsules or small implantable cans made of metal, glass, or ceramic and provide an airtight and

waterproof environment [129]. They are rather large which is a drawback for miniaturized implantable devices and, furthermore, require feedthroughs for electrical data and power transfer. Therefore, near-hermetic encapsulation using thin films, which at least significantly slow down the ingress of body fluids, has significant potential [129, 134].

Thin-film encapsulation materials can be grouped into polymeric (e.g. polytetrafluoroethylene (PTFE), silicone elastomers, polyimide, and parylene) and non-polymeric materials (e.g. silicon dioxide, silicon nitride, silicon carbide, and diamond-like carbon (DLC)). Non-polymeric materials require chemical vapor deposition (CVD) processes with rather high temperatures, which is not suitable for neural devices with active electronics that would not sustain these high temperatures. Furthermore, some of them dissolve in saline solution over time, are prone to structural defects (pin-holes), form non-conformal layers, and tend to delaminate.

Polymeric materials are very flexible, inexpensive, and require low process temperatures. Disadvantages include a high WVTR, problems in creating conformal and pin-hole free films, and material degradation as well as poor adhesion [129].

For implantable neural interfaces, many different encapsulation materials have been studied and continuously developed for creating conformal and long-term stable encapsulation. In the following, the ones relevant and used for the UEA will be discussed, which include parylene-C, silicon carbide, and more advanced parylene-C/Al$_2$O$_3$ bilayer structures.

1.3.6.1   Parylene-C

Parylene, a semicrystalline polymer for the family of thermoplasts, is a widely used material for encapsulation and insulation of biomedical devices. It exists in several variants, among which parylene-C and parylene-N are certified as class VI polymers for use in biomedical devices by the Food and Drug Administration (FDA) [73, 108].

In the following, we will focus on parylene-C which is used for the UEA. Information on other variants may be found elsewhere [36, 61].

Parylene-C has many advantageous properties: it is highly biocompatible, non-toxic, chemically inert, an excellent ion barrier, has a low dielectric constant (~3.15 at 60 Hz), relatively low water absorption rate (~0.1% in 24 h), high resistivity, and dielectric stability in saline. Furthermore, due to the possibility of employing a CVD process, a very conformal deposition down to the nanoscale and also for complex geometries which include sharp edges and crevices is possible [70, 73, 102, 105, 107, 130, 133].

Due to parylene-C being a polymer, it exhibits some of the corresponding drawbacks as well, which include a relatively poor adhesion to inorganic and metallic substrates and a certain permeability to water [73].

Parylene-C is deposited according to the *Gorham* method, which is a three-step CVD process [140]. First, the precursor (di-para-xylene dimer) is sublimated at ~130 °C. Next, by elevating the temperature to ~680 °C, the dimer is cracked into monomers. It is important to achieve a complete dissociation of dimers into monomers

to reduce the number of dimers in the deposited film. Reduction of the temperature (to at least <80 °C) allows the polymerization of the monomers on all available surfaces. The film grows due to a free radical chemical reaction process where first new carbon chains are formed (initiation) and then extended to higher molecular weight by attachment of monomers to the end of the chain [51, 101, 129]. Typical film thicknesses deposited on the UEA are 3–6 μm. Resulting film properties depend on the pressure, temperature, and deposition rate during the CVD process which provides a means to tailor the film's properties within a certain range [50].

The described CVD process has the additional advantage of not requiring any solvents or additives, which reduces the contamination of the film to a minimum and ensures almost defect free and conformal coverage, even of complex electrode geometries [51].

A problem which needs to be addressed during film deposition is the poor adhesion of parylene-C to metal and other inorganic surfaces. In case of the UEA, it has to stick well to silicon and platinum or iridium oxide, depending on the type of tip metallization used. Therefore, measures must be taken to increase the adhesion which include silanization, PECVD deposition of an interlayer, plasma surface treatment, heat treatment, and chemical modifications.

The use of silane (usually Silquest A-174) as adhesion promoter, which is vaporized onto the substrate before deposition, is a common method for the UEA [73, 105, 107]. The organo-silane creates a covalent bonding by functional groups between substrate and parylene-C [45, 135]. It is inexpensive and integrates very well in the process flow of UEA device fabrication.

Seymour et al. [102] developed a reactive parylene-C by adding a functional group and demonstrated that it improves adhesion and short-term insulation performance. Plasma surface treatment or chemical surface modifications of the substrate before parylene-C deposition increases the number of radical sites for covalent bonds, resulting in better adhesion [73]. This can even be enhanced by deposition of a plasma polymer as a thin interlayer between substrate and parylene-C [140]. Although that has been reported to be a very effective method, it requires another complex step and is therefore not used for the UEA [129]. Finally, the parylene-C coated UEA can be annealed to increase the physical interlock between substrate and thin film [73].

All of these methods address the adhesion problem but do not prevent moisture ingress over time.

The function of the UEA is based on the electrode tips being in contact with the neural tissue; hence, the encapsulation has to be removed from this area. Several methods have been proposed and studied, the most common one being the reactive ion etching (RIE) with oxygen plasma by using aluminum foil or photoresist as a mask [10, 107].

Yoo et al. employed laser ablation which is advantageous for mass production and allows to selectively treat individual electrodes. However, this process creates carbon debris and the amount thereof as well as the conformity of removal depend on the laser fluence. The debris can be removed by a subsequent short (1 min) oxygen

plasma etch. However, the laser ablation requires a tip metal which can withstand the laser power [138, 139].

Many experiments have been carried out (both in vivo and in vitro) to investigate the long-term stability of parylene-C encapsulation to ensure the safe and reliable performance of chronically implanted neural devices. Test devices include flat interdigitated electrode structures and functional UEAs, which are submerged in phosphate-buffered saline (PBS) solution for prolonged amounts of time (several hundred days to more than a year). Typical temperatures range from 37 °C (human body temperature) up to 80 °C to achieve accelerated aging processes.

Although parylene-C coating can withstand very harsh conditions, such as the use of different sterilization methods and heat treatment [101], all experiments indicated an increasing amount of failed test devices after being subject to physiological saline solution for prolonged times. The failure mechanisms are not yet fully understood, but investigations of failed devices found blistering, microcrack formation, microscopic delamination, and thinning of the parylene-C film. One reason is believed to be the steady water uptake of the material. Furthermore, imperfections at the interface between the electrode and parylene-C coating may induce electrical stresses leading to microcracks and delamination of the film. Once moisture and possibly ions permeate though the encapsulation, chemical reactions degrade the metal film underneath and eventually induce failure of the electrode [73, 130, 133]. These effects are observed for all variants of parylene, although with slightly different characteristics. For example, parylene-N is prone to microcrack formation but does not show delamination [73].

Failing electrodes exhibit an increased leakage current, decreased impedance modulus for low frequencies, and an increased area under the cyclic voltammetry curve used for testing the devices which indicate exposure of underlying metal [73, 105, 130].

To overcome these problems, the single material encapsulation has been advanced to a bilayer of parylene-C and Al_3O_3 which will be discussed in the next section.

1.3.6.2 Parylene-C/Al_2O_3 Bilayer Encapsulation

The use of a bilayer encapsulation evolved due to the observed long-term degradation of parylene-C films in physiological environment. The bilayer encapsulation allows combining the favorable properties of both materials to form a better and more durable encapsulation for neural implants. With parylene-C still being the outer layer in direct contact with tissue, the ease of regulatory approval is ensured with its proven performance in patients for up to 6 years.

Al_2O_3 thin films deposited by atomic layer deposition (ALD) feature the formation of conformal and pin-hole free layers, high hardness and abrasion resistance, good biocompatibility, and perfect electrical performance and are a very good moisture barrier with very low WVTR. However, the major drawback of ALD Al_2O_3 is that it corrodes easily in water and more so in PBS solution [130].

Table 1.2 Relevant properties for the UEA for both individual materials (ALD Al_2O_3 and parylene-C) and the bilayer of these two materials (information taken from [[129], Xie et al. 2014, [20]])

Properties	ALD Al_2O_3	Parylene-C	Effects of bilayer
Water vapor transmission rate (WVTR)	~10^{-6} g/m^2·day [57]	~1 g/m^2·day (from SCS coating)	Isolates water vapor from the device
Deposition temperature	Room temperature to 200 °C	Room temperature	Low temperature coating process
Barrier to ions	Yes	Yes	Good ion barrier
Biocompatible	Yes	Yes	Biocompatible coating
Insulation	10^{14} ohm-cm	10^{15} ohm-cm [133]	High insulation impedance
Coating process	Plasma-assisted ALD	CVD	Pin-hole free, uniform coating
Dissolution in water	Yes [4]	No	Prevents alumina dissolution

By combining ALD Al_2O_3 and parylene-C, this disadvantage is mitigated as parylene-C provides a good ion barrier. It therefore prevents ions from reaching and dissolving the Al_2O_3 layer. Table 1.2 summarizes the properties relevant for use in the UEA for both individual materials and the bilayer. Typical thicknesses used for the UEA are ~50 nm Al_2O_3 and ~3–6 μm parylene-C [21, 131, 133].

Several studies have been carried out since the development of the bilayer encapsulation to investigate its long-term performance for test samples (flat glass IDEs) and actual UEAs soaked in PBS at body temperature as well as for elevated temperatures (for accelerated aging) for prolonged amounts of time (months to more than a year) [21, 73, 130, 131, 134].

These investigations indicated that the bilayer on flat IDE test samples shows a better long-term stability in physiological environment than a single parylene-C film. A comprehensive study from Minnikanti et al. found a mean time to failure (MTTF) of 8 months for single parylene-C encapsulation in saline solution at 37 °C, while the MTTF for the bilayer was 36 months – an increase by a factor of 4.6 and very close to that of other materials like liquid crystal polymers (LCP; up to 2 years) [73]. The MTTF for single parylene-C is consistent with values reported from other groups which are 6–12 months. However, most of these tests were only performed on flat IDE samples which does not reflect the complex geometry of the UEA.

Xie et al. and Caldwell et al. performed lifetime tests on actual UEAs encapsulated with the bilayer. While Xie et al. reported an improved long-term stability even under an increased bias voltage [134], the more comprehensive study (increased number of samples/improved statistics) from Caldwell et al. did not find conclusive evidence for an improved lifetime of the bilayer, neither on more complex flat test samples with additional features nor for the full UEAs [21]. Furthermore, they observed that, if the encapsulation fails, the bilayer is destroyed faster than the single parylene-C film [21]. The rationale in that case is that solution ingress does not have a strong effect for a single parylene-C film. For the bilayer, however, solution

Fig. 1.13 Comparison of defect size for (**a**) single parylene-C encapsulation and (**b**) parylene-C/Al$_2$O$_3$ bilayer. (Reprinted, with permission, from Caldwell et al. [21])
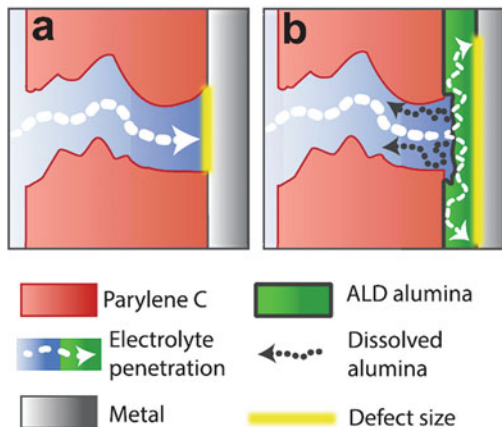
permeating through the outer parylene-C layer reaches the underlying Al$_2$O$_3$ film which dissolves, leading to the creation of an undercut and effectively to a growth of the defect site (Fig. 1.13).

These results clearly show that imperfections of the parylene-C layer have a much more severe effect in case of the bilayer. Hence, although the bilayer could be an important improvement in the encapsulation of neural devices for long-term implantation, the current materials combination still gives rise to problems and needs to be developed further to allow for chronic implantation over several years.

Steps along that way have to include the development of failure models in order to understand the causes for formation of imperfections and defects of the films. Based on that, materials and deposition processes can be improved. A suggestion made by Caldwell et al. is the use of higher deposition temperatures for the ALD Al$_2$O$_3$ which would create less impurities, thereby reducing the probability of dissolving the film [21]. Furthermore, it may become necessary to investigate the feasibility of other materials such as silicon carbide or oxide-nitride-oxide layers in the future [21].

As in the case of a single parylene-C film, the bilayer has to be removed from the electrode tips to ensure contact between tip metallization and tissue. Xie et al. proposed a three-step process similar to that of single parylene removal: (1) laser ablation of the parylene-C layer, (2) reactive ion etching with oxygen plasma to remove carbon debris and parylene-C residue, and (3) buffered oxide etch (BOE) to remove the Al$_2$O$_3$ layer and expose the tip metal [132, 133].

1.3.6.3 Silicon Carbide as an Alternative Encapsulation Material

Another material which fulfills the criteria for an encapsulation material for implantable devices (i.e. high hardness, chemical inertness, biocompatibility, low dielectric constant. and low moisture intake) is silicon carbide [29]. Hsu et al. developed a low

Fig. 1.14 Scanning
electron micrographs from
a-SiC$_x$:H films deposited on
UEA. The thickness of the
film was measured at
different sites along the
electrode shaft, and a wide
variation is observable.
(Reprinted, with permission,
from Hsu et al. [49])
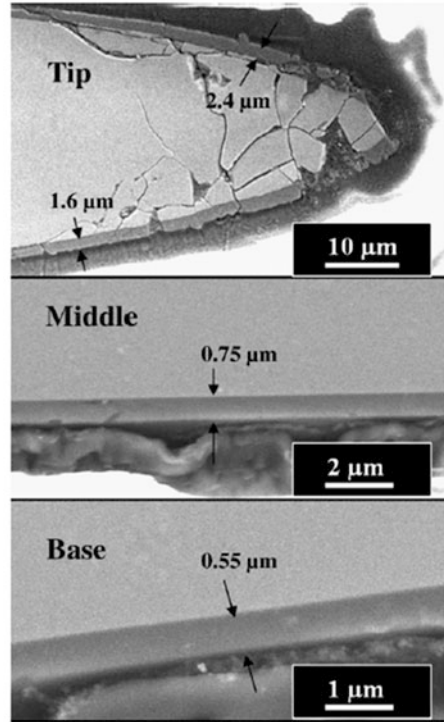
temperature process for the deposition of hydrogenated amorphous silicon carbide
(a-SiC$_x$:H) on test samples (IDEs) and UEAs and investigated the properties of the
resulting film with regard to stress, defect density, and dielectric constant. While for
the actual UEAs only the conformity and coating uniformity were studied with
electrode cross sections in scanning electron microscope (SEM), electrical tests
with coated IDEs soaked in saline solution were performed [49].

The a-SiC$_x$:H films were deposited by plasma-enhanced CVD at temperatures
below 200 °C and with hydrogen as dilution gas source and silane (SiH$_4$) and
methane (CH$_4$) as Si and C precursors. Through variation of process parameters
and subsequent characterization, it became evident that the quality of the deposited
film (strength of Si-C bond, film stress) can be optimized and tailored within a
certain range. However, while the results were promising for the flat IDE samples,
the encapsulation of the UEAs showed a rather large thickness variation along the
electrode shafts and a large pin-hole density (Fig. 1.14) [49]. Hence, the encapsula-
tion of UEA with silicon carbide was not viable.

Another issue that has been observed is that silicon carbide is hard to remove
which is crucial for the UEA as the metallized tips have to be exposed to get in
contact with tissue. Laser ablation and mechanical grinding have been reported but
led to alterations of the underlying metal film [29].

Despite these difficulties, silicon carbide stays in the focus as a possible material due to its good biocompatibility and promising results in IDE soak tests. Currently, it is being discussed if it is feasible to create an entire electrode from a-SiC allowing for greater flexibility of electrode structures.

1.3.6.4   Accelerated Aging

In order to evaluate the performance of any encapsulation, its short- and long-term performance in an in vivo environment and its possible failure modes have to be investigated. However, in the development of new processes and exploration of new materials, it is neither feasible nor reasonable to achieve this by chronic implantation studies due to the time and resources necessary for such studies. Therefore, one needs to test new encapsulation materials or processes in vitro in an experimental setup that mimics the physiological environment. This also avoids the ethical dilemma, high cost, and regulatory challenges associated with animal studies. However, these experiments are still time-consuming if the long-term performance has to be evaluated and therefore still pose a problem, especially since usually a large number of iterations are involved in device development. Therefore, accelerated aging methods have to be employed to estimate the lifetime performance of the encapsulation and the whole device in a reasonable amount of time.

A basic in vitro method to test the lifetime of biomedical devices is to immerse them in saline solution of physiological concentration at a temperature of 37 °C to mimic the human body temperature.

In order to induce accelerated aging of the device, a simple method is to increase the temperature of the solution above 37 °C as this will increase the rate at which chemical reactions proceed [46]. For polymeric encapsulation materials and assuming first-order reactions only, it can be shown by using chemical kinetics that increasing the temperature speeds up the reaction rate and therefore the aging process by a factor f:

$$f = \exp\left(\frac{R\left(T - 37^{\circ}C\right)}{E_{act}}\right)$$

where R being the universal gas constant (8.314 J mol^{-1}), T the elevated temperature, and E_{act} the activation energy of the aging reaction [52]. The application of this relation, however, has the challenge of determining the activation energy. This is avoided by employing the empirically determined "10-degree rule" which provides a conservative estimate about the accelerated aging process. It states that a temperature increase by 10 °C roughly doubles the rate of many polymeric reactions and therefore the aging process [46, 52]. For example, increasing the temperature by 20 °C allows to test a device for an effective lifetime of 12 months in only 3 months real time according to the "10-degree rule." However, this is also only valid for first-order chemical processes, and both approaches do not apply in cases where the

Fig. 1.15 Leaked current of planar interdigitated electrode test structures that were coated with either an Al2O3/parylene-C bilayer (A + P) or parylene-C only (P) and soaked in saline solution at various temperatures for an extended period of time. For the parylene-C only devices, the effect of the different temperatures resulting in different failure times and the improved performance of the bilayer are clearly visible. (Reprinted, with permission, from Xie et al. [131])
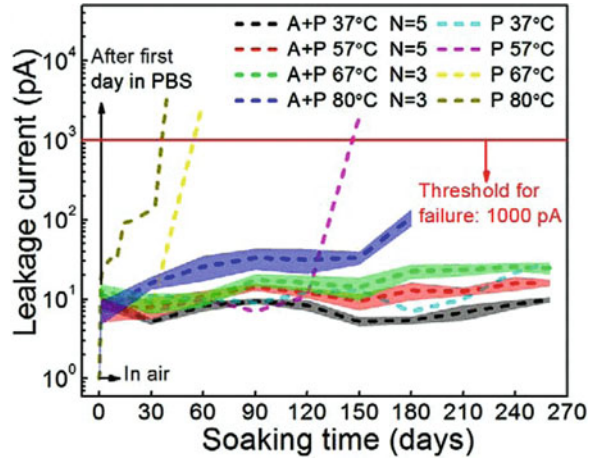
elevated temperature induces processes that are not present in normal aging, such as glass transitions or phase changes [52]. Consequently, any accelerated test protocol has to be designed with great care [46].

The application of either the chemical reaction formula or the "10-degree rule" enables the testing of encapsulation materials in a reduced time frame as this allows to state an effective time the material or device was aged.

However, it would be desirable to always test the whole device in accelerated aging studies. However, in case of complex devices with a high resource cost associated with every sample (like the UEA), this is not economically feasible if entirely new encapsulation materials or processes are studied. Therefore, one can employ more simple test structures as for example planar interdigitated electrodes (IDEs) that are coated with the materials to be studied and monitored with electrochemical impedance spectrometry or leakage current measurements in strongly accelerated aging experiments [131]. Figure 1.15 gives an example of how such test structures have been employed to evaluate the performance of an Al$_2$O$_3$/parylene-C bilayer compared to parylene-C only encapsulation in accelerated aging experiments.

While these simple planar test structures might give a first indication about encapsulation longevity and performance, respective results have to be taken with a grain of salt when generalizing them to the whole device. Even slightly increasing the complexity of the test structures might lead to different results and makes confirmatory accelerated aging testing of the whole device necessary [21].

Of course, the simple approach of evaluating device lifetime by soaking it in heated saline solution does not capture the multitude of possible chemical processes in an in vivo environment that involve the complex composition of body fluids and the immune system's foreign body response. The insufficiency of simple immersion in (heated) saline solution is indicated by the inability to reproduce the failure modes observed on UEAs that were chronically implanted in vivo, as shown in Fig. 1.16.
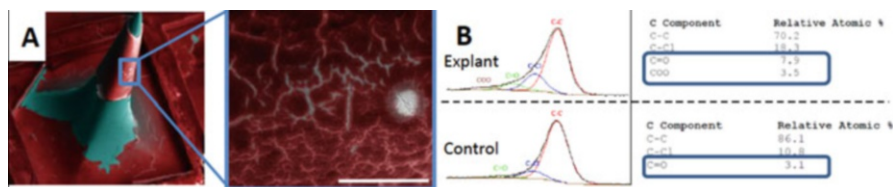
Fig. 1.16 Characterization of explanted UEA. (A) Electrode tine of UEA explanted after 3 years in feline nerve reveals silicon (green) exposed through the damaged parylene-C (red); inset shows detail of parylene-C degradation and cratering over IrO_x (white). Imaging XPS of inset area ("explant") shows evidence of C=O and COO bonds, while identical measurements made on an UEA aged in saline solution ("control") only show nominal levels of C=O binding energies. (Images and data courtesy of Ryan Caldwell)
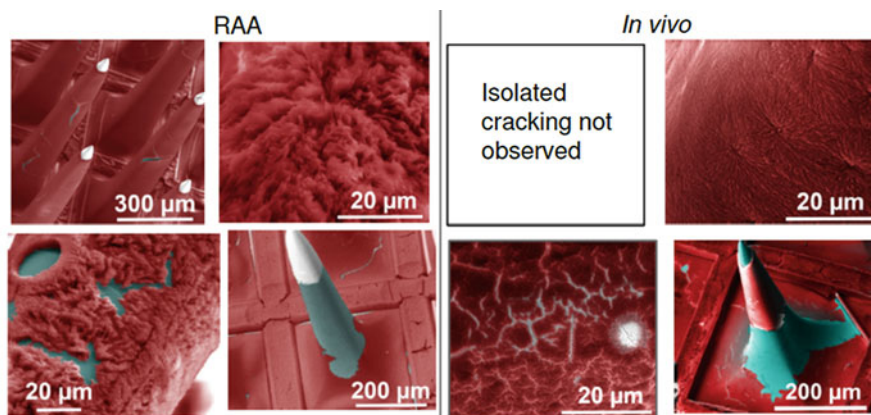
Fig. 1.17 Comparison of Utah electrode array that was subjected to RAA and a device which was explanted after more than 3 years from a feline peripheral nerve. The colors were added to highlight the different materials: red, parylene-C; white, IrO_x; green, Si. (Images and data courtesy of Ryan Caldwell)

In order to improve the predictive capabilities of accelerated aging experiments, it was suggested to use a reactive accelerated aging (RAA) method involving the regular addition of hydrogen peroxide to the saline solution [111]. This method tries to mimic the environment that is created by activated immune cells in response to foreign body intrusion, which includes the release of reactive oxygen species [7, 111].

This RAA method was applied to UEAs, and the damage to the arrays was assessed visually from scanning electron microscopy (SEM) images and chemically from energy dispersive X-ray spectroscopy (EDX) and X-ray photoelectron spectroscopy (XPS) measurements. It was found already from the visual examination that new failure modes had appeared as compared to heated saline solution only devices. Furthermore, comparison to respective measurements on UEAs that were removed after being implanted in a feline peripheral nerve for more than 3 years revealed that the visual damage modes looked very much alike for the explanted and the RAA devices (Fig. 1.17) [20]. This demonstrates the benefit of the RAA method which

enables the evaluation of device and encapsulation performance in a fast and realistic way without requiring in vivo experiments. It allows the reproduction of in vivo damage modes which had not been observed before in aging experiments. However, while promising, the method is still not able to fully emulate in vivo aging. As an example, the chemical analysis showed a difference in both the bulk and the surface composition between in vivo and in vitro aged arrays, hinting that further improvements to the accelerated aging methods may be necessary.

1.4 Wireless Technologies for Use with the UEA

The challenge faced when using a multichannel microelectrode array is how to connect the implanted array to an external signal generator (for stimulation) or data evaluation systems for post processing (in case of recording). Most of the existing neural recording devices use wired connections for data communication. Despite the pioneering and ground-breaking results that tethered studies have produced in the past [31, 47, 48], the wired recording configuration faces limitations with regard to mobility of the subject and a significant inherent risk of infection due to connected mechanical stress induced by the constraining cabling [58]. A straightforward solution to overcome these challenges is the application of wireless technology. This, however, comes with its own obstacles: due to the size and power dissipation limitations of the application, the fabrication of neural recording devices with a high-speed wireless link for reliable wideband neural data transmission at very low power budget is extremely difficult. In device design, a tradeoff between power consumption, noise performance, signal quality, battery life, and size will have to be made. To achieve small device sizes, constraints consist of either limiting the number of recording channels [42] or conceding signal fidelity for increased channel count [99].

Over the years, these issues have been addressed one after another, leading to the development of headstage wireless connectors that are not fully implantable but mark an important milestone as they are already used in animals as well as investigative clinical applications.

Such wireless devices have been developed and tested for various animal species applications, such as insects [44, 94], rodents (Seung Bae [42, 68, 110]), sheep [89], and nonhuman primates (NHPs) [16, 24, 37, 53, 74, 99]. Some of these devices were even advanced beyond the simple headstage concept by employing an enclosure fit for subcutaneous implantation [16, 141]. Additionally, there are efforts to create and utilize application-specific integrated circuits (ASICs) to further advance miniaturization and power efficiency in these kind of devices [12, 33, 75, 136].

In order to advance the general idea of wireless implantable neurodevices even further, efforts have been made in parallel to create fully integrated neural interface (INI) devices. In corresponding developments that were directly tailored for the

Fig. 1.18 Image of an integrated neural interface based on a modified Utah slant electrode array with flip chip bonded ASIC (in this case an INI-R6 chip) for amplification and spike thresholding with AuPd insulated wire coil and SMD capacitors. The device is inductively powered and transmits data wirelessly. (Reprinted, with permission, from Xie et al. [132])
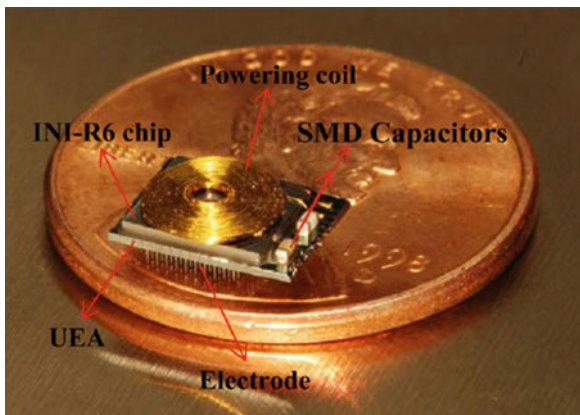
UEA, an ASIC INI chip designed to fit the architecture and 400 μm interelectrode pitch of the UEA was directly flip-chip bonded to a modified array. The modification of the array allowed to use the backplane as a PCB substrate for direct chip mounting of active and passive components such as the ASIC INI chip, a power antenna, and SMD components (Fig. 1.18) [58, 105, 107, 132].

Due to the technical challenges of system miniaturization, power dissipation limits, and, most importantly, establishing a reliable wireless data link with high throughput in situations with a highly active and mobile patient, wireless recording systems have just recently been introduced on the market. Present examples for such systems are the W-Series recording system by Triangle BioSystems International [113]; the Cube2 system by NeuraLynx, Inc. [84]; the Wireless-Systems by Multichannel Systems [76]; and a series of wireless systems by Blackrock Microsystems LLC. The latter include the Brown Wireless Device (BWD), CerePlex W [14], and CerePlex Exilis [13], which are all headstage-based devices. Figure 1.19 depicts the roadmap of the wireless system development from Blackrock Microsystems LLC, with the first device in the series being the BWD.

Although the roadmap in Fig. 1.19 only covers a short time span of 2 years, the requirements and trends for the development are clearly visible. Preferable properties for wireless headstage-type devices are:

1. Small and lightweight (less than 10 g has been demonstrated for the CerePlex Exilis)
2. High-channel count
3. High data transmission rate
4. Range of few meters for reliable wireless transmission
5. Prolonged battery life-time
6. Offering the possibility for practical sterilization.

Reduced weight is ensured by using polymer-based encapsulation materials which not only allow protection of the electronics from mechanical and electrical impact but are also easily sterilizable. A common way to connect the wireless

Key Specs

BWD
- 96 channels, 20 kS/s, 12 bits
- >24 hour battery life
- 50g with battery
- Large animal: NHP/Sheep
- Range: 3m LOS, 2m roaming

CerePlex W 2.0
- 96 channels, 30 kS/s, 12 bits
- ~4 hour battery life
- 33.6g with battery
- Large animal: NHP/Sheep
- Range: 3m LOS, 2m roaming

CerePlex Exilis
- 96 channels, 30 kS/s, 12 bits
- ~2.5 hour battery life
- 9.87g with battery
- Small animal: Rat/Marmoset
- Range: 3m LOS, 1m roaming

CerePlex Exilis	CerePlex W 2.0	CerePlex W 1.0	Brown Wireless
9.87g	33.6g	175g	50g
2017	2016	2015	2015

Timeline
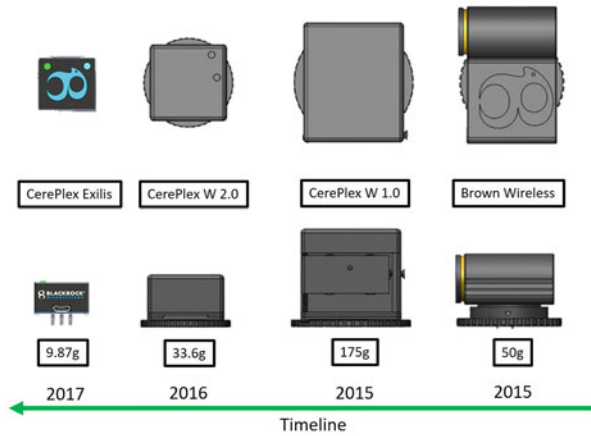
Fig. 1.19 The Roadmap of the 96-channel wireless headstage development at Blackrock Microsystems LLC: from BWD to CerePlex Exilis

transmitter to an implanted microelectrode array is via a "screw-on" attachment to a pedestal connector port on the patient's/subject's skull that is in turn connected to the neural implant. This is illustrated for the BWD from Blackrock Microsystems LLC in Fig. 1.20. The BWD has been extensively tested and is currently actively used in both animal and investigative clinical research.

Figure 1.21 gives an overview of the used wired and wireless components and the recorded neural signals in an experiment with a chair constraint monkey. The comparison clearly shows that the BWD wireless system produced a similar output signal as a typical commercial wired recording system. Other experiments indicated likewise performance. This validates the currently used setup for wireless recording which can be the basis for further developments toward a miniaturized and fully implantable chip.

Although the BWD's performance was promising, there were also drawbacks with regard to design and device performance which needed to be addressed. One of the concerns was that the size and weight of the device was still too big even for large animals and certainly not feasible for small animals such as rodents and marmosets. Motivated by that, the other two devices from the wireless series, CerePlex W and Exilis, were developed and commercialized by Blackrock Microsystems LLC to address these challenges. Compared to the BWD, the CerePlex W and Exilis are much smaller in size and lighter in weight, while providing 1.5 times higher sampling rates and lower noise levels. Furthermore, they both offer the possibility of electrode impedance measurement as an advancement.
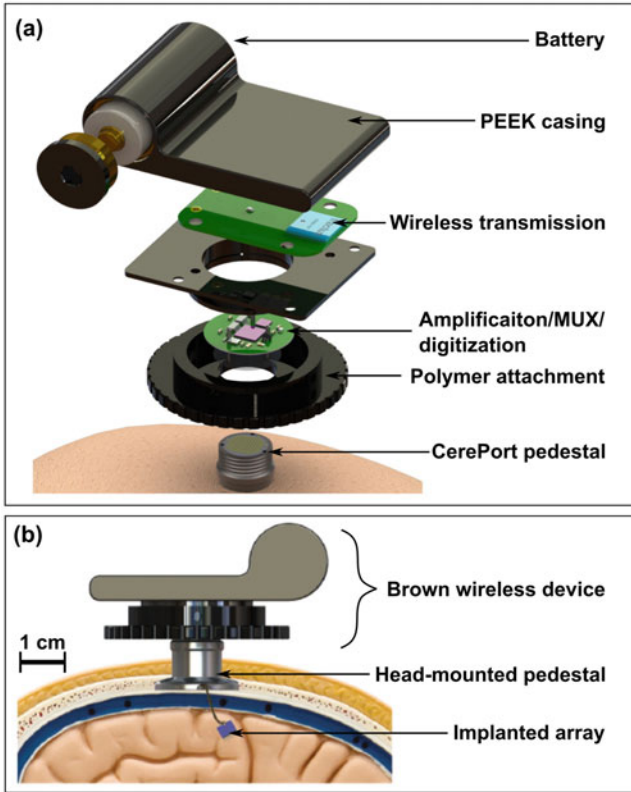
Fig. 1.20 Architecture of the Brown Wireless Device. (**a**) 3D computer-added design (CAD) model showing the complete assembly of the wireless neurosensor. (**b**) 3D CAD model showing the attachment of the wireless neurosensor to a head-mounted pedestal (side view). (Reprinted, with permission, from Yin et al. [137])

1.5 Vision and Concept for Integrated Systems and Implantable Electronics

The ultimate vision for advanced and fully implantable wireless neural interfaces are solutions that integrate the electrode and those electronics necessary to carry out rudimentary signal processing functions, e.g., for amplification and data compression and to facilitate wireless telemetry of data and power. While there is a multitude of options, a potential roadmap, applied to a penetrating electrode such as the UEA, is shown in Fig. 1.22. It has to be noted here that the developmental work on the engineering side is only one side of the medal and that on the other side, regulatory guidelines and constraints have to be met for implantable devices (especially for human use). The stepwise approach depicted in Fig. 1.22 is advantageous to address both parts by successive technological and regulatory iterations of the devices.
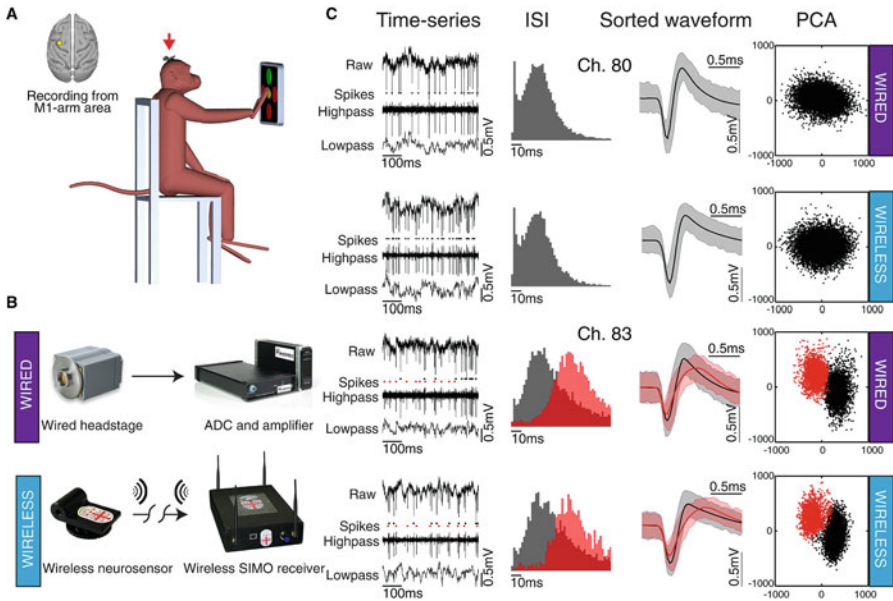
Fig. 1.21 Comparison of recorded neural data from a wired and a wireless setup in an experiment with a monkey. (**a**) Experimental setup and sketch of brain location where the recording took place (primary motor cortex, arm area). The red arrow marks the device location. (**b**) Images of the used devices: the commercial wired system (Cerebus) and the BWD system. (**c**) Recorded neural data for the wired and wireless device. (Reprinted, with permission, from Yin et al. [137])

The neural information system 1 (NIS-1) stage constitutes a conventional passive electrode with percutaneous connector, connected to an external headstage and cable. NIS-2 transfers the headstage function into an implantable device which then generates an amplified, digital signal and allows reduction of the number of wires, independent of the number of electrode channels. An example for this stage is the CerePlex-I system by Blackrock Microsystems LLC. NIS-3 constitutes a passive device with percutaneous connector, attached to a wireless headstage, allowing rigorous testing, market release, and regulatory clearance for a wireless module for high-resolution, high-channel neural data. This is the current development stage for the Utah electrode array by Blackrock Microsystems LLC. NIS-4 provides power through a percutaneous connection but allows data to be transmitted wirelessly from the implant. NIS-5 allows wireless power and data transfer (to a receiver hub in its direct proximity). The NIS-6 stage finally allows wireless power and longer distance transfer directly to, e.g., a beltpack receiver.

The abovementioned CerePlex-I system (Fig. 1.23) is an intermediate step toward a wireless fully integrated system, which transfers part of the headstage functionality to a digitization board which is implanted under the skin on the skull.

The device consists of three main parts: (1) a neural interface such as the UEA for stimulation/recording of neural tissue, (2) a microsystem composed of an
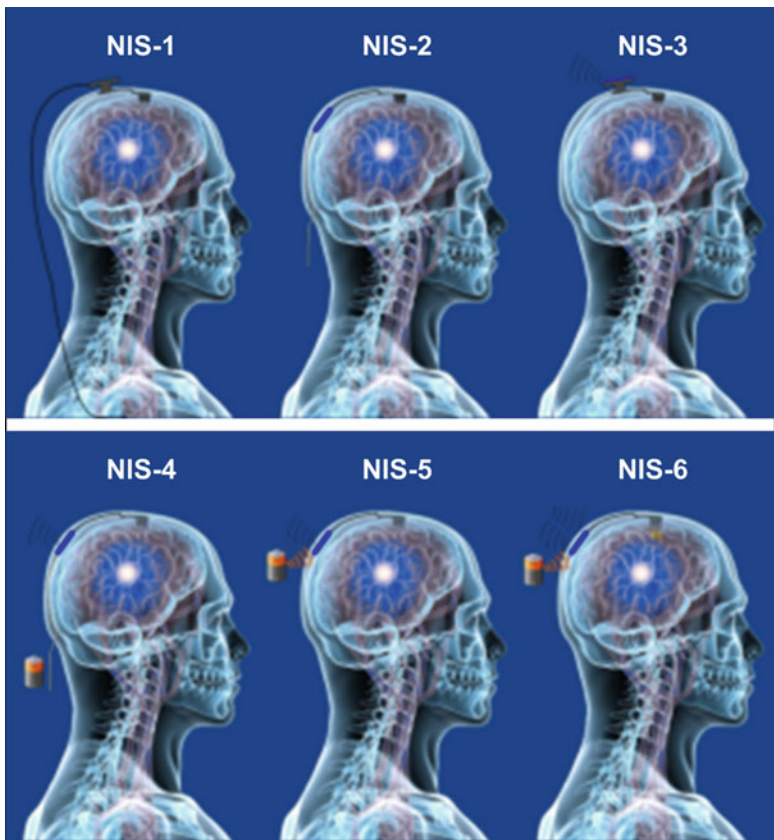
Fig. 1.22 Potential roadmap and concepts for implantable wired and wireless neural interfaces. (Image copyright and courtesy of Blackrock Microsystems LLC)

encapsulated printed circuit board (PCB) containing a 128 channel ASIC implanted under the skin, and (3) an electrode tail connector referred to as the pigtail, connecting the implanted part to the neural signal processing system. A combination of the CerePlex I and multiport approach allows further scaling of channel count.

The vision for the future is the complete miniaturization and integration of all components on the device. A first demonstration toward that goal was given by Sharma et al. [105]. Such a system would allow to fully implant the recording functionality by a microelectrode array in combination with an onboard first data analysis and wireless power and data transmission. Further iterations of the device designed for high-channel count would feature a modular design that amplifies and multiplexes neural signals through an ASIC mounted on the chip but connected with a wired connection to a pedestal connector or a chest-mounted pacemaker style implantable module with rechargeable batteries and wireless data link. With
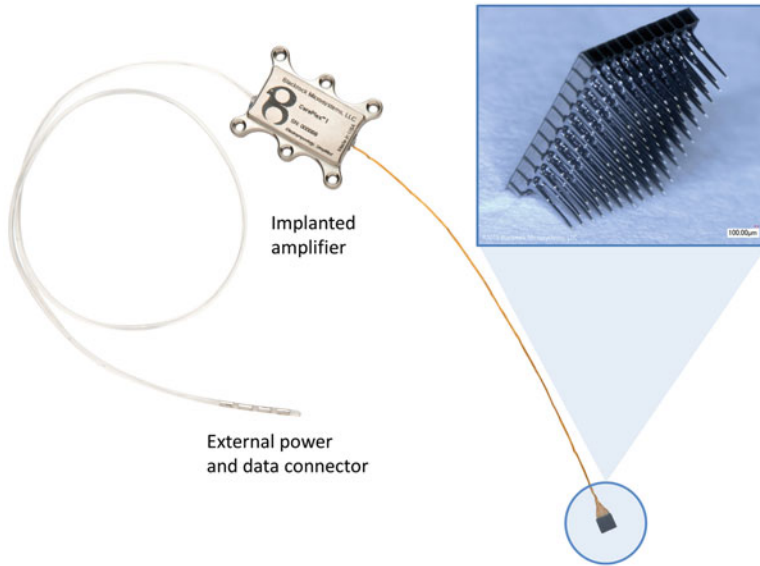
Fig. 1.23 Image of the Blackrock Microsystems LLC CerePlex-I system connected to a UEA. (Image copyright and courtesy of Blackrock Microsystems LLC)

constantly advancing microfabrication leading to decreasing footprint and ultralow power consumption of the necessary electronic components, big steps toward a realization of this vision are expected over the next years.

References

1. Abaya TVF et al (2012) 3D waveguide penetrating arrays for optical neural stimulation. In: 2012 international conference on optical MEMS and nanophotonics. IEEE, pp 216–217
2. Abaya TVF et al (2014) Deep-tissue light delivery via optrode arrays. J Biomed Opt 19 (1):15006
3. Abdo A et al (2011) Floating light-activated microelectrical stimulators tested in the rat spinal cord. J Neural Eng 8(5):56012
4. Abdulagatov AI et al (2011) Al_2O_3 and TiO_2 atomic layer deposition on copper for water corrosion resistance. ACS Appl Mater Interfaces 3(12):4593–4601
5. Adamantidis AR et al (2007) Neural substrates of awakening probed with optogenetic control of hypocretin neurons. Nature 450(7168):420–424
6. Aravanis AM et al (2007) An optical neural interface: *in vivo* control of rodent motor cortex with integrated fiberoptic and optogenetic technology. J Neural Eng 4(3):S143–S156
7. Badwey JA, Karnovsky ML (1980) Active oxygen species and the functions of phagocytic leucocytes. Annu Rev Biochem 49:695–726
8. Bajaj P et al (2007) Ultrananocrystalline diamond film as an optimal cell interface for biomedical applications. Biomed Microdevices 9(6):787–794
9. Barrese JC et al (2013) Failure mode analysis of silicon-based intracortical microelectrode arrays in non-human primates. J Neural Eng 10(6):66014

10. Bhandari R et al (2008) A novel method of fabricating convoluted shaped electrode arrays for neural and retinal prostheses. Sensors Actuators A Phys 145–146:123–130

11. Bhandari R et al (2009) Wafer-scale processed, low impedance, neural arrays with varying length microelectrodes. In: TRANSDUCERS 2009–2009 international solid-state sensors, actuators and microsystems conference. IEEE, pp 1210–1213

12. Biederman W et al (2013) A fully-integrated, miniaturized (0.125 mm^2) 10.5 µW wireless neural sensor. IEEE J Solid State Circuits 48(4):960–970

13. Blackrock Microsystems (2018a) CerePlex Exilis. Available at: http://blackrockmicro.com/cereplex-exilis/. Accessed 27 June 2018

14. Blackrock Microsystems (2018b) Cereplex W. Available at: http://blackrockmicro.com/cereplex-wireless-headstage/. Accessed 27 June 2018

15. Bolzan AE et al (1988) Smooth and rough platinum deposits resulting from the electroreduction of hydrous oxide platinum overlayers—a mechanistic approach. Electrochim Acta 33(12):1743–1751

16. Borton DA et al (2013) An implantable wireless neural interface for recording cortical circuit dynamics in moving primates. J Neural Eng 10(2):26010

17. Boutte RW, Blair S (2016) Maskless wafer-level microfabrication of optical penetrating neural arrays out of soda-lime glass: Utah optrode array. Biomed Microdevices 18(6):115

18. Branner A, Stein RB, Normann RA (2001) Selective stimulation of cat sciatic nerve using an Array of varying-length microelectrodes. J Neurophysiol 85(4):1585–1594

19. Buzsáki G (2004) Large-scale recording of neuronal ensembles. Nat Neurosci 7(5):446–451

20. Caldwell RB (2017) Strategies towards the mitigation of shunting in implanted neural arrays to improve device stability for chronic applications (Order No. 10688653). Available from ProQuest Dissertations & Theses Global. (2189849447)

21. Caldwell R et al (2017) Analysis of Al_2O_3 —parylene C bilayer coatings and impact of microelectrode topography on long term stability of implantable neural arrays. J Neural Eng 14(4):46011

22. Campbell PK et al (1991) A silicon-based, three-dimensional neural interface: manufacturing processes for an intracortical electrode array. IEEE Trans Biomed Eng 38(8):758–768

23. Castagnola E et al (2014) Smaller, softer, lower-impedance electrodes for human neuroprosthesis: a pragmatic approach. Front Neuroeng 7:8

24. Chestek CA et al (2009) HermesC: low-power wireless neural recording system for freely moving Primates. IEEE Trans Neural Syst Rehabil Eng 17(4):330–338

25. Cheung K (2007) Implantable microscale neural interfaces. Biomed Microdevices 9(6):923–938

26. Cho I-J, Baac HW, Yoon E (2010) A 16-site neural probe integrated with a waveguide for optical stimulation. In: 2010 IEEE 23rd international conference on micro electro mechanical systems (MEMS). IEEE, pp 995–998

27. Clark GA et al Selective, high-optrode-count, artifact-free stimulation with infrared light via intrafascicular utah slanted optrode arrays. In Photonic Therapeutics and Diagnostics VIII (Vol. 8207, p. 82075I). International Society for Optics and Photonics

28. Cogan SF (2008) Neural stimulation and recording electrodes. Annu Rev Biomed Eng 10:275–309

29. Cogan SF et al (2003) Plasma-enhanced chemical vapor deposited silicon carbide as an implantable dielectric coating. J Biomed Mater Res 67A(3):856–867

30. Cogan SF et al (2016) Tissue damage thresholds during therapeutic electrical stimulation. J Neural Eng 13(2):21001

31. Collinger JL et al (2013) High-performance neuroprosthetic control by an individual with tetraplegia. Lancet 381(9866):557–564

32. Davis TS et al (2016) Restoring motor control and sensory feedback in people with upper extremity amputations using arrays of 96 microelectrodes implanted in the median and ulnar nerves. J Neural Eng 13(3):36001

33. Denison T et al (2007) A 2 uW 100 nV/rtHz chopper-stabilized instrumentation amplifier for chronic measurement of neural field potentials. IEEE J Solid State Circuits 42(12):2934–2945

34. Drake KL et al (1988) Performance of planar multisite microprobes in recording extracellular single-unit intracortical activity. IEEE Trans Biomed Eng 35(9):719–732

35. Ersen A et al (2015) Chronic tissue response to untethered microelectrode implants in the rat brain and spinal cord. J Neural Eng 12(1):16019

36. Fortin JB, Lu T-M (2004) Chemical vapor deposition polymerization: the growth and properties of parylene thin films. Kluwer Academic Publishers, Boston

37. Foster DJ et al (2014) A freely-moving monkey treadmill model. J Neural Eng 11(4):46020

38. Franks W et al (2005) Impedance characterization and modeling of electrodes for biomedical applications. IEEE Trans Biomed Eng 52(7):1295–1302

39. Gradinaru V et al (2007) Targeting and readout strategies for fast optical neural control in vitro and in vivo. J Neurosci 27(52):14231–14238

40. Green RA et al (2012) Variation in performance of platinum electrodes with size and surface roughness. Sens Mater 24(4):165–180

41. Green RA et al (2014) Laser patterning of platinum electrodes for safe neurostimulation. J Neural Eng 11(5):56017

42. Greenwald E et al (2011) A VLSI neural monitoring system with ultra-wideband telemetry for awake behaving subjects. IEEE Trans Biomed Circuits Syst 5(2):112–119

43. Hämmerle H et al (2002) Biostability of micro-photodiode arrays for subretinal implantation. Biomaterials 23(3):797–804

44. Harrison RR et al (2011) Wireless neural/EMG telemetry Systems for Small Freely Moving Animals. IEEE Trans Biomed Circuits Syst 5(2):103–111

45. Hassler C et al (2010) Characterization of parylene C as an encapsulation material for implanted neural prostheses. J Biomed Mater Res B Appl Biomater 9999B(1):266–274

46. Hemmerich KJ (1998) General aging theory and simplified protocol for accelerated aging of medical devices. Med Plast Biomaterials 5:16–23

47. Hochberg LR et al (2006) Neuronal ensemble control of prosthetic devices by a human with tetraplegia. Nature 442(7099):164–171

48. Hochberg LR et al (2012) Reach and grasp by people with tetraplegia using a neurally controlled robotic arm. Nature 485(7398):372–375

49. Hsu J-M et al (2007) Characterization of a-SiCx:H thin films as an encapsulation material for integrated silicon based neural interface devices. Thin Solid Films 516(1):34–41

50. Hsu JM et al (2008) Effect of thermal and deposition processes on surface morphology, crystallinity, and adhesion of Parylene-C. Sens Mater 20(2):87–102

51. Hsu J-MJ et al (2009) Encapsulation of an integrated neural interface device with Parylene C. IEEE Trans Biomed Eng 56(1):23–29

52. Hukins DWL, Mahomed A, Kukureka SN (2008) Accelerated aging for testing polymeric biomaterials and medical devices. Med Eng Phys 30(10):1270–1274

53. Jackson A, Mavoori J, Fetz EE (2007) Correlations between the same motor cortex cells and arm muscles during a trained task, free behavior, and natural sleep in the macaque monkey. J Neurophysiol 97(1):360–374

54. Janting J, Branebjerg J, Rombach P (2001) Conformal coatings for 3D multichip microsystem encapsulation. Sensors Actuators A Phys 92(1–3):229–234

55. Jiang G, Zhou DD (2010) Technology advances and challenges in hermetic packaging for implantable medical devices. In: Zhou D, Greenbaum E (eds) Implantable neural prostheses 2: techniques and engineering approaches. Springer, New York, pp 27–61

56. Jun JJ et al (2017) Fully integrated silicon probes for high-density recording of neural activity. Nature 551(7679):232–236

57. Keuning W et al (2012) Cathode encapsulation of organic light emitting diodes by atomic layer deposited Al_2O_3 films and Al_2O_3/a-SiN_x:H stacks. J Vac Sci Technol A Vac Surf Films 30(1):01A131

58. Kim S et al (2009) Integrated wireless neural interface based on the Utah electrode array. Biomed Microdevices 11(2):453–466

59. Klein JD, Clauson SL, Cogan SF (1989) Morphology and charge capacity of sputtered iridium oxide films. J Vac Sci Technol A 7(5):3043–3047
60. Kozai TDY et al (2014) Chronic tissue response to carboxymethyl cellulose based dissolvable insertion needle for ultra-small neural probes. Biomaterials 35(34):9255–9268
61. Kuppusami S, Oskouei RH (2015) Parylene coatings in medical devices and implants: a review. Univ J Biomed Eng 3(2):9–14
62. Leach J, Achyuta AKH, Murthy SK (2010) Bridging the divide between neuroprosthetic design, tissue engineering and neurobiology. Front Neuroeng 2:18
63. Leber M (2018) Unpublished (in progress). *unpublished*
64. Leber M et al (2016) Different methods to alter surface morphology of high aspect ratio structures. Appl Surf Sci 365:180
65. Leber M et al (2017) Novel method of fabricating self-dissolvable and freely floating neural array. In 2017 19th international conference on solid-state sensors, actuators and microsystems (TRANSDUCERS). IEEE, pp 1726–1729
66. Ledermann N et al (2000) Sputtered silicon carbide thin films as protective coating for MEMS applications. Surf Coat Technol 125(1–3):246–250
67. Lee H et al (2005) Biomechanical analysis of silicon microelectrode-induced strain in the brain. J Neural Eng 2(4):81–89
68. Lee SB et al (2013) A wideband dual-antenna receiver for wireless recording from animals behaving in large arenas. IEEE Trans Biomed Eng 60(7):1993–2004
69. Limb SJ et al (1998) Growth of fluorocarbon polymer thin films with high CF2 fractions and low dangling bond concentrations by thermal chemical vapor deposition. Appl Phys Lett 68 (20):2810
70. Loeb GE et al (1977) Parylene as a chronically stable, reproducible microelectrode insulator. IEEE Trans Biomed Eng BME-24(2):121–128
71. Marrese CA (1987) Preparation of strongly adherent platinum black coatings. Anal Chem 59 (1):217–218
72. Meyer RD et al (2001) Electrodeposited iridium oxide for neural stimulation and recording electrodes. IEEE Trans Neural Syst Rehabil Eng 9(1):2–11
73. Minnikanti S et al (2014) Lifetime assessment of atomic-layer-deposited Al2O3–Parylene C bilayer coating for neural interfaces using accelerated age testing and electrochemical characterization. Acta Biomater 10(2):960–967
74. Miranda H et al (2010) HermesD: a high-rate long-range wireless transmission system for simultaneous multichannel neural recording applications. IEEE Trans Biomed Circuits Syst 4 (3):181–191
75. Muller R et al (2014) A miniaturized 64-channel 225μW wireless electrocorticographic neural sensor. In: 2014 IEEE international solid-state circuits conference digest of technical papers (ISSCC). IEEE, pp 412–413
76. Multi Channel Systems (2018) Wireless-systems. Available at: https://www.multichannelsystems.com/products/wireless-systems. Accessed 27 June 2018
77. Musallam S et al (2007) A floating metal microelectrode array for chronic implantation. J Neurosci Methods 160(1):122–127
78. Najafi K, Wise KD, Mochizuki T (1985) A high-yield IC-compatible multichannel recording array. IEEE Trans Electron Devices 32(7):1206–1211
79. Nature (2011) Method of the year 2010. Nat Methods 8(1):1–1
80. Negi S et al (2009) Effect of sputtering pressure on pulsed-DC sputtered iridium oxide films. Sensors Actuators B Chem 137(1):370–378
81. Negi S, Bhandari R, Rieth L, Solzbacher F (2010a) In vitro comparison of sputtered iridium oxide and platinum-coated neural implantable microelectrode arrays. Biomed Mater (Bristol, England) 5(1):15007
82. Negi S, Bhandari R, Rieth L, Van Wagenen R et al (2010b) Neural electrode degradation from continuous electrical stimulation: comparison of sputtered and activated iridium oxide. J Neurosci Methods 186(1):8–17

83. Negi S, Bhandari R, Solzbacher F (2012) Morphology and electrochemical properties of activated and sputtered iridium oxide films for functional electrostimulation. J Sensor Technol 2(3):138–147

84. NeuraLynx (2018) Cube2. Available at: https://neuralynx.com/hardware/cube2. Accessed 27 June 2018

85. Park S et al (2010) Nanoporous Pt microelectrode for neural stimulation and recording: in vitro characterization. J Phys Chem C 114(19):8721–8726

86. Pashaie R et al (2014) Optogenetic brain interfaces. IEEE Rev Biomed Eng 7:3–30

87. Prochazka A, Mushahwar VK, McCreery DB (2001) Neural prostheses. J Physiol 533 (1):99–109

88. Richardson RR, Miller JA, Reichert WM (1993) Polyimides as biomaterials: preliminary biocompatibility testing. Biomaterials 14(8):627–635

89. Rizk M et al (2009) A fully implantable 96-channel neural data acquisition system. J Neural Eng 6(2):26002

90. Robblee LS et al (1983a) Electrical stimulation with Pt electrodes. VII. Dissolution of Pt electrodes during electrical stimulation of the cat cerebral cortex. J Neurosci Methods 9 (4):301–308

91. Robblee LS, Lefko JL, Brummer SB (1983b) Activated Ir: an electrode suitable for reversible charge injection in saline solution. J Electrochem Soc 130(3):731

92. Robblee LS et al (1985) Charge injection properties of thermally-prepared iridium oxide films. MRS Proc 55:303

93. Roy RK, Lee K-R (2007) Biomedical applications of diamond-like carbon coatings: a review. J Biomed Mater Res B Appl Biomater 83B(1):72–84

94. Sato H et al (2009) Remote radio control of insect flight. Front Integr Neurosci 3:24

95. Scharf R et al (2016) Depth-specific optogenetic control in vivo with a scalable, high-density µLED neural probe. Sci Rep 6(1):28381

96. Scharf R, Reiche CF, McAlinden N, Cheng Y, Xie E, Sharma R, Tathireddy P, Rieth L, Mathieson K, Blair S (2018) A compact integrated device for spatially selective optogenetic neural stimulation based on the Utah Optrode Array. In Optogenetics and Optical Manipulation 2018 (Vol. 10482, p. 104820M). International Society for Optics and Photonics

97. Schmitt G et al (1999) Passivation and corrosion of microelectrode arrays. Electrochim Acta 44(21–22):3865–3883

98. Schwartz AB et al (2006) Brain-controlled interfaces: movement restoration with neural prosthetics. Neuron 52(1):205–220

99. Schwarz DA et al (2014) Chronic, wireless recordings of large-scale brain activity in freely moving rhesus monkeys. Nat Methods 11(6):670–676

100. Seidl K et al (2011) CMOS-based high-density silicon microprobe arrays for electronic depth control in Intracortical neural recording. J Microelectromech Syst 20(6):1439–1448

101. Selbmann F et al (2016) Deposition of Parylene C and characterization of its hermeticity for the encapsulation of MEMS and medical devices. In: 2016 IEEE 11th annual international conference on nano/micro engineered and molecular systems (NEMS). IEEE, pp 427–432

102. Seymour JP et al (2009) The insulation performance of reactive parylene films in implantable electronic devices. Biomaterials 30(31):6158–6167

103. Shandhi MMH et al (2015) A novel method of fabricating high channel density neural array for large neuronal mapping. In: 2015 Transducers – 2015 18th international conference on solid-state sensors, actuators and microsystems (TRANSDUCERS). IEEE, pp 1759–1762

104. Shandhi MMH et al (2017) Reusable high aspect ratio 3-D nickel shadow mask. J Microelectromech Syst 26(2):376–384

105. Sharma A et al (2010) Long term in vitro stability of fully integrated wireless neural interfaces based on Utah slant electrode array. Appl Phys Lett 96(7):73702

106. Sharma R et al (2011) Application-specific customizable architectures of Utah neural interfaces. Procedia Eng 25:1016–1019

107. Sharma A et al (2012) Evaluation of the packaging and encapsulation reliability in fully integrated, fully wireless 100 channel Utah slant electrode Array (USEA): implications for long term functionality. Sensors Actuators A Phys 188:167–172

108. Stadler S, Ajmera PK (2008) Sensors and materials: an international journal on sensor technology. Scientific Publ. Division of MYU, Tokyo

109. Subbaroyan J, Martin DC, Kipke DR (2005) A finite-element model of the mechanical effects of implantable microelectrodes in the cerebral cortex. J Neural Eng 2(4):103–113

110. Szuts TA et al (2011) A wireless multi-channel neural amplifier for freely moving animals. Nat Neurosci 14(2):263–269

111. Takmakov P et al (2015) Rapid evaluation of the durability of cortical neural implants using accelerated aging with reactive oxygen species. J Neural Eng 12(2):26003

112. Tan X et al (2018) Auditory neural activity in congenitally deaf mice induced by infrared neural stimulation. Sci Rep 8(1):388

113. Triangle Biosystems International (2018) W-Series. Available at: http://www.trianglebiosystems.com/w-series-systems.html. Accessed 27 June 2018

114. Troyk PR, Cogan SF (2005) Sensory neural prostheses. In: Neural engineering. Springer, Boston, pp 1–48

115. Tykocinski M et al (2001) Chronic electrical stimulation of the auditory nerve using high surface area (HiQ) platinum electrodes. Hear Res 159:53–68

116. Vanhoestenberghe A, Donaldson N (2013) Corrosion of silicon integrated circuits and lifetime predictions in implantable electronic devices. J Neural Eng 10(3):31002

117. Wang J et al (2012) Integrated device for combined optical neuromodulation and electrical recording for chronic *in vivo* applications. J Neural Eng 9(1):16001

118. Wark HAC et al (2013) A new high-density (25 electrodes/mm^2) penetrating microelectrode array for recording and stimulating sub-millimeter neuroanatomical structures. J Neural Eng 10(4):45003

119. Wellman SM et al (2017) A materials roadmap to functional neural Interface design. Adv Funct Mater 28(12):1701269

120. Wells J et al (2005) Optical stimulation of neural tissue in vivo. Opt Lett 30(5):504

121. Weremfo A et al (2015) Investigating the interfacial properties of electrochemically roughened platinum electrodes for neural stimulation. Langmuir 31(8):2593–2599

122. Wessling B, Mokwa W, Schnakenberg U (2006) RF-sputtering of iridium oxide to be used as stimulation material in functional medical implants. J Micromech Microeng 16(6):S142–S148

123. Whalen JJ et al (2006) Electrochemical characterization of charge injection at electrodeposited platinum electrodes in phosphate buffered saline. J Electrochem Soc 153(12):C834

124. Wise KD (2005) Silicon microsystems for neuroscience and neural prostheses. IEEE Eng Med Biol Mag 24(5):22–29

125. Wise KD, Angell JB, Starr A (1970) An integrated-circuit approach to extracellular microelectrodes. IEEE Trans Biomed Eng BME-17(3):238–247

126. Wu F et al (2015) Monolithically integrated μLEDs on silicon neural probes for high-resolution Optogenetic studies in behaving animals. Neuron 88(6):1136–1148

127. Xiang Z et al (2014) Ultra-thin flexible polyimide neural probe embedded in a dissolvable maltose-coated microneedle. J Micromech Microeng 24(6):65015

128. Xiao X et al (2006) In vitro andin vivo evaluation of ultrananocrystalline diamond for coating of implantable retinal microchips. J Biomed Mater Res B Appl Biomater 77B(2):273–281

129. Xie X (2013) Atomic layer deposited aluminum oxide and parylene C bi-layer encapsulation for biomedical implantable devices (Order No. 3607382). Available from ProQuest Dissertations & Theses Global. (1492997360)

130. Xie X et al (2012) Plasma-assisted atomic layer deposition of Al_2O_3 and parylene C bi-layer encapsulation for chronic implantable electronics. Appl Phys Lett 101(9):93702

131. Xie X et al (2013) Long-term bilayer encapsulation performance of atomic layer deposited Al2O3 and parylene c for biomedical implantable devices. IEEE Trans Biomed Eng 60 (10):2943–2951

132. Xie X, Rieth L, Williams L et al (2014a) Long-term reliability of Al2O3 and Parylene C bilayer encapsulated Utah electrode array based neural interfaces for chronic implantation. J Neural Eng 11(2):26016
133. Xie X, Rieth L, Negi S et al (2014b) Self aligned tip Deinsulation of atomic layer deposited Al2O3 and Parylene C coated Utah electrode Array based neural interfaces. J Micromech Microeng Struct Devices Syst 24(3):35003
134. Xie W, Kothari V, Terry BS (2015) A bio-inspired attachment mechanism for long-term adhesion to the small intestine. Biomed Microdevices 17(4):68
135. Yao Q et al (1999) Adhesion enhancement of underfill materials by silane additives. In: Proceedings – international symposium on advanced packaging materials: processes, properties and interfaces. IMAPS – International microelectronics assembly and packaging society, pp 27–30
136. Yin M et al (2013) A 100-channel hermetically sealed implantable device for chronic wireless neurosensing applications. IEEE Trans Biomed Circuits Syst 7(2):115–128
137. Yin M et al (2014) Wireless neurosensor for full-spectrum electrophysiology recordings during free behavior. Neuron 84(6):1170–1182
138. Yoo J-M et al (2012) Hybrid laser and reactive ion etching of Parylene-C for deinsulation of a Utah electrode array. J Micromech Microeng 22(10):105036
139. Yoo J-M et al (2013) Excimer laser deinsulation of Parylene-C on iridium for use in an activated iridium oxide film-coated Utah electrode array. J Neurosci Methods 215(1):78–87
140. Yu Q, Deffeyes J, Yasuda H (2001) Engineering the surface and interface of Parylene C coatings by low-temperature plasmas. Prog Org Coat 41(4):247–253
141. Zhang J et al (2009) Integrated device for optical stimulation and spatiotemporal electrical recording of neural activity in light-sensitized brain tissue. J Neural Eng 6(5):055007
142. Zhou D (2007) Platinum electrode surface coating and method for manufacturing the same

Chapter 2
EEG-Based Brain-Computer Interfaces

Yijun Wang, Masaki Nakanishi, and Dan Zhang

Abstract Brain-computer interfaces (BCIs) provide a direct communication channel between human brain and output devices. Due to advantages such as non-invasiveness, ease of use, and low cost, electroencephalography (EEG) is the most popular method for current BCIs. This chapter gives an overview of the current EEG-based BCIs for the main purpose of communication and control. This chapter first provides a taxonomy of the EEG-based BCI systems by categorizing them into three major groups: (1) BCIs based on event-related potentials (ERPs), (2) BCIs based on sensorimotor rhythms, and (3) hybrid BCIs. Next, this chapter describes challenges and potential solutions in developing practical BCI systems toward high communication speed, convenient system use, and low user variation. Then this chapter briefly reviews both medical and non-medical applications of current BCIs. Finally, this chapter concludes with a summary of current stage and future perspectives of the EEG-based BCI technology.

Keywords Brain-computer interfaces · EEG-based BCI · hybrid BCI · ERP · SSVEP

2.1 Introduction

Since Vidal first proposed the term "brain-computer interface (BCI)" in early 1970s [1], BCIs have received increasing attention in the fields of neuroscience, neural engineering, and clinical rehabilitation [2–4]. Especially during the past two

Y. Wang (✉)
Institute of Semiconductors, Chinese Academy of Sciences, Beijing, China
e-mail: wangyj@semi.ac.cn

M. Nakanishi
Institute for Neural Computation, University of California San Diego, San Diego, CA, USA

D. Zhang
Department of Psychology, Tsinghua University, Beijing, China
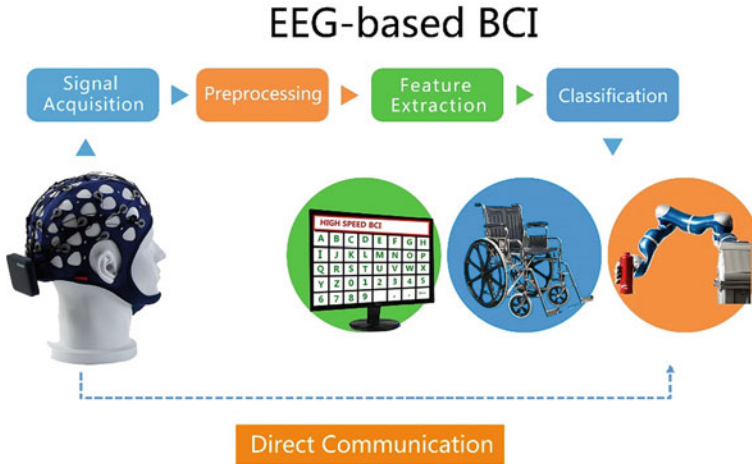
Fig. 2.1 System diagram of a typical EEG-based BCI system for communication and control

decades, BCI has rapidly become a hot topic in both research and practice. The primary goal of BCI research is to provide a non-muscular communication channel to help people with severe motor disabilities to communicate with their environments. Among different brain imaging techniques that have been applied to BCIs, electroencephalography (EEG) has become the most popular method due to its advantages such as non-invasiveness, ease of use, and low cost. Figure 2.1 shows the system diagram of a typical EEG-based BCI system for communication and control, which consists of three major components: signal acquisition, data processing, and device control. Although the scope of application of EEG-based BCIs has been significantly extended in recent years, this chapter mainly focuses on the traditional EEG-based BCIs for the purpose of communication and control.

In the twentieth century, early works by research pioneers laid important groundwork for the BCI field. In the 1970s, Vidal first proposed the term of BCI for the purpose of controlling external apparatus with brain signals and developed a BCI system based on visual event-related potentials (ERPs) [5]. The system converted ERPs corresponding to four retinotopic maps of a checkerboard stimulus into movement control commands to move a mobile through a maze. In 1988, Farwell and Donchin described a mental prosthesis system using the P300 component of ERPs [6]. The system consisting of a six-by-six matrix served as a keyboard and was operated by flash elicited P300 at a speed of ~2 characters per minute. In the early 1990s, BCI systems based on sensorimotor rhythms emerged. Woplaw et al. trained subjects to learn self-control of amplitude of mu rhythm [7]. The system realized one-dimensional cursor control by translating mu rhythm amplitudes into cursor movements. Pfurtscheller et al. performed a BCI system based on event-related desynchronization (ERD) of sensorimotor rhythms [8]. The system was operated by discriminating the spatio-temporal patterns of ERD during imagination of left and right hand movements. During this period, the ERP-based BCI paradigms were

further extended. Sutter developed a brain response interface using pseudo-random sequence modulated visual evoked potentials (VEPs) in 1992 [9]. The eight-by-eight visual keyboard recognized the user's eye gaze direction using VEPs and obtained high communication rates. In the late 1990s, Birbaumer et al. developed a spelling device for the completely paralyzed patients based on slow cortical potentials (SCPs) [10]. The system allowed the subjects to select letters by driving a cursor with their SCPs using an imagery strategy.

Almost two decades into the twenty-first century, BCI research has achieved significant progress and shown promising prospects and applications in various fields. The progress mainly includes the following aspects: signal processing [11, 12], machine learning [13, 14], system paradigm [15, 16], and applications [17, 18]. Advanced EEG signal processing and machine learning algorithms have been applied to significantly improve the performance of the early developed BCI paradigms (e.g., BCIs based on P300 and sensorimotor rhythms). Meanwhile, new BCI paradigms have been proposed and achieved rapid development. Various types of visual and auditory BCIs based on ERPs have been developed and proven highly efficient in terms of information transfer rate (ITR) [19]. A hybrid BCI system that combines a traditional BCI with other physiological signals has shown advantages in BCI performance and system flexibility [20]. Over the past decade, a wide range of BCI applications have emerged, which considerably expanded the original goals. Assistive BCIs and rehabilitative BCIs, which are designed for communication and motor rehabilitation, have been widely investigated in experimental and clinical studies [21]. In addition, the potential applications of BCI go far beyond the medical applications. For example, passive BCIs have been developed for assessing and monitoring mental states in real time [22].

Although the performance of BCI systems has improved significantly in recent years, researchers still face a lot of challenges in promoting wide use of the BCI technology. On one hand, compared to traditional input technologies, the current levels of BCI performance are still very low and do not support fast and complex communication and control. The performance bottleneck is mainly caused by the lack of knowledge of the underlying neural mechanisms of information encoding in EEG signals. Besides, decoding EEG signals requires more efficient computational modeling approaches based on signal processing and machine learning techniques. On the other hand, transitioning BCI systems from a well-controlled laboratory setting to a real-life environment remains challenging due to the complications of EEG measurement [23]. A practical BCI system must meet the requirements of good user experience and robust system performance [24]. At present, there is a great need for a mobile EEG platform with user-friendly electrode technology.

This chapter gives a comprehensive overview of the current EEG-based BCIs for the purpose of communication and control. This chapter first provides a taxonomy of the EEG-based BCI systems by categorizing them into three major groups: (1) BCIs based on ERPs, (2) BCIs based on sensorimotor rhythms, and (3) hybrid BCIs. And then, this chapter describes challenges and potential solutions in developing practical BCI systems for real-life applications toward high communication speed, convenient system use, and low user variation. Next, this chapter briefly reviews both medical

and non-medical applications of current BCIs. Finally, this chapter concludes with a summary of current stage and future perspectives of the EEG-based BCI technology.

2.2 Taxonomy of Current BCIs

Since many brain signals and system paradigms have been applied to BCIs, a taxonomy is useful for providing a summary of the current status of BCIs. A taxonomy not only provides a systematic description of brain signals and modulation methods used in system design but also aids building general frameworks in system implementation. In general, BCI systems can be classified by the brain signals employed in the system (e.g., P300, VEP, or sensorimotor rhythms) [2]. Alternatively, BCIs can be categorized by operation paradigms like dependent/independent BCIs or synchronous/asynchronous BCIs [15]. Recently, a taxonomy of visual and auditory BCIs was proposed according to the multiple target access methods used in information encoding [19]. To give a meaningful overview of the current BCI systems, this chapter provides a simple taxonomy of BCI based on the types of EEG control signals. By jointly considering brain signals summarized in recent reviews [19, 20, 25], this chapter categorizes the current BCI systems into three major groups: (1) BCIs based on ERPs, (2) BCIs based on sensorimotor rhythms, and (3) hybrid BCIs. Figure 2.2 illustrates the proportions of journal papers in ISI Web of Science for these three BCI groups in the last five years (2012–2016). The numbers of papers for the ERP-based BCIs and the sensorimotor BCIs are
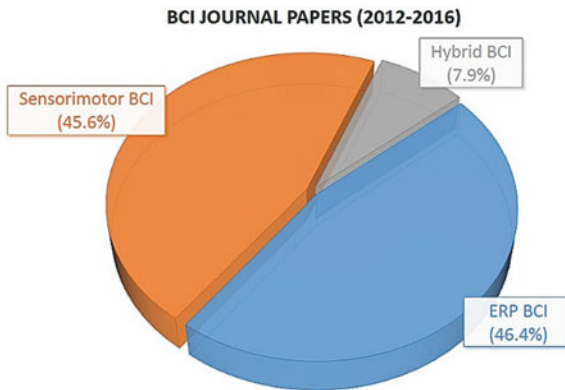
Fig. 2.2 Distribution of major BCI studies including ERP BCI, sensorimotor BCI, and hybrid BCI in recent years.
Notes: Data were obtained from ISI Web of Science using the corresponding topics of journal papers during the last five years (2012–2016). The analysis includes a total of 2658 papers (1234 papers for the ERP BCI, 1213 papers for the sensorimotor BCI, and 211 papers for the hybrid BCI).

comparable (1234 versus 1213, percentage: 46.4% versus 45.6%), which are significantly larger than that of the hybrid BCIs (211, percentage: 7.9%). Note that the hybrid BCIs also include other physiological signals such as electromyogram (EMG) and electrooculogram (EOG) [20]. Without loss of generality, this chapter focuses on the most popular brain signals and system paradigms used in recent BCI studies.

2.2.1   BCIs Based on ERPs

2.2.1.1   ERP Signals for BCI

ERPs, which were originally called evoked potentials (EPs), are measured electrical brain potentials that are evoked by stimuli, which display stable time relationships to a reference event (as opposed to the spontaneous EEG rhythms) [26]. Typically, an ERP waveform consists of multiple peaks and troughs, which are called ERP components. Major ERP components include visual and auditory responses, N2, P3, response-related components, and language-related components. Among these ERP components, two types of signals have been widely used in BCI systems since very early studies in the 1970s and 1980s [5, 6]. The first type is the VEP family, which includes subtypes of transient VEP (TVEP), steady-state VEP (SSVEP), motion VEP (mVEP), and code modulated VEP (cVEP). VEPs are ERPs elicited by visual stimuli, which can be measured with maximum amplitude over the occipital region [27]. Event-related P300 component is another type of commonly used ERP signal. P300, a positive deflection around 300–400 ms after a relevant stimulus, which can be measured over the central and parietal areas, reflects stimulus evaluation, selective attention, and conscious discrimination in an oddball task [28]. In addition to VEP and P300 signals, other types of ERP signals including auditory evoked potential, N2pc, error-related negativity, and N400 have also been investigated in a few BCI studies.

ERP signals are modulated by exogenous stimuli or endogenous mental activities. The exogenous stimuli in BCI systems can be visual or auditory stimuli (e.g., VEPs are elicited by exogenous visual stimuli), while endogenous activities include users' attention or mental tasks (e.g., P300 is an endogenous brain response to an oddball stimulus). In a BCI system, the ERP signals of sensation, perception, or cognition can be modulated by voluntary control (e.g., attention) of the subject. The information encoded in the modulated ERP signals can be decoded by signal processing and classification algorithms. In contrast to spontaneous EEG rhythms that do not require external stimuli, the ERP signals exhibit good characteristics including high signal-to-noise ratio (SNR), reliable spatio-temporal features, and low user variation. With rapid advances of signal modulation and demodulation techniques, ERP-based BCI systems have achieved very high communication speed and therefore become more popular in recent BCI research [19].

2.2.1.2   Modulation of ERP Signals

Signal modulation plays an important role in the ERP-based BCIs. First, to convey the user's intent, ERP signals must be modulated by the user's mental activities in an efficient way so that the modulated ERP signals can be reliably demodulated into the original messages. Second, toward high communication rate, a large bandwidth is required so that the modulated ERP signals corresponding to different intents can be easily discriminated. By introducing the multiple access (MA) techniques in telecommunications [29], the signal modulation approaches in ERP-based BCI systems can be classified by the major MA techniques: time division multiple access (TDMA), frequency division multiple access (FDMA), code division multiple access (CDMA), and space division multiple access (SDMA). This classification can facilitate the understanding of various ERP-based BCI paradigms, which can be considered under a unified signal modulation framework.

First, TDMA allows multiple users to share the same communication channel by dividing the signal into different time slots. In ERP-based BCIs, TDMA is the most popular method for multiple target coding. In these BCI systems, multiple targets appear at different time slots. For example, TDMA has been widely used in the visual P300-based BCI systems [30]. In the standard 'row/column' paradigm, in which each row and column are flashed in a random order, flashing of the row and column of the desired character will elicit P300 signals. Detection of P300 in different time slots can identify the target character. The other single character, checkerboard, and region-based P300 paradigms all follow the principle of TDMA. In addition to P300, the VEP-based BCIs using mVEP [31] and TVEP [32] also employ the TDMA method. Second, FDMA divides the entire bandwidth into multiple individual bands, each for a single user. The SSVEP-based BCI [33] is a typical FDMA system. In a typical frequency coding-based SSVEP BCI, all stimuli flash concurrently at different frequencies, and a target stimulus can be identified by analyzing the frequency of the elicited SSVEP. In ERP-based BCIs, FDMA has higher capacity than TDMA. The SSVEP-based BCIs can discriminate 40 different frequencies within a short stimulus duration (e.g., 500 ms) and thereby achieve very high ITRs [34, 35]. Third, CDMA assigns separate codes to modulate users' signals. The BCIs based on pseudorandom cVEP [9, 36] are typical CDMA systems. The CDMA BCI systems show high performance comparable to FDMA. Last, SDMA divides the geographical space into smaller spaces for multiple users. The SDMA BCI systems use retinotopic mappings of different stimulus locations in the visual field to elicit different spatial patterns of TVEP or SSVEP signals [5, 37]. The number of targets in SDMA is generally limited by the low spatial resolution of EEG-based retinotopic mapping.

2.2.1.3   Demodulation of ERP Signals

In an ERP-based BCI, information embedded in the modulated ERP signals needs to be demodulated and converted into control commands. Due to high trial-to-trial

variability of ERP signals, advanced data analysis methods are required in the demodulation of ERP, especially in signal-trial analysis and classification of ERP [38]. ERP demodulation can be considered an EEG pattern recognition problem, which includes data pre-processing, feature extraction, and classification. Signal processing [11] and machine learning [13] are two major data analysis techniques. The signal processing algorithms have been widely used in the pre-processing and feature extraction procedures. The aim of data pre-processing is to improve the SNR of the ERP signals by removing task-irrelevant noises. Bandpass filtering and spatial filtering are two commonly used pre-processing procedures. Bandpass filtering only allows the frequency range of ERP signals to remain. Spatial filtering further enhances ERP signals by calculating a weighted linear combination of multiple EEG channels [39]. Besides, trial averaging is another efficient way to enhance the SNR of ERPs. After pre-processing, features that reflect the characteristic of ERP signals can be extracted. The features for ERPs generally exploit the spatio-temporal information of the signals (e.g., concatenation of ERP amplitude for all time points and all channels) [38]. In addition to time and space domains, features in the frequency domain (e.g., power spectral density) have also been used in the detection of SSVEP signals [40]. After feature extraction, the machine learning algorithms are applied to classification (e.g., discriminating target and non-target ERPs). Classifiers such as linear discriminant analysis (LDA) and support vector machine (SVM) have been widely used in the classification of ERPs with the extracted spatio-temporal features. In online BCI systems, classifiers are obtained from labelled training data collected in calibration sessions and then applied to predict the label of testing data during the system operation.

2.2.1.4 Dependent and Independent ERP-Based BCIs

EEG-based BCIs are categorized as dependent and independent systems [2]. An independent BCI does not depend on the brain's normal output pathways (i.e., peripheral nerves and muscles) to generate the brain activity that carries the user's intent. In contrast, a dependent BCI requires some activity from peripheral nerves and muscles to modulate the brain activity. The ERP-based BCIs include both dependent and independent systems. In BCIs, ERP signals are generally modulated by eye fixation or attention. BCIs based on visual ERPs majorly depend on the control of the muscles of the eye to gaze at desired targets and fall into the dependent BCI class. Most of VEP and visual P300-based BCIs use gaze-dependent paradigms. Different from direct eye gaze (i.e., overt attention), covert attention mechanisms such as spatial selective attention and feature selective attention have been investigated to develop gaze-independent BCI paradigms. There are three types of independent BCIs based on ERP signals: auditory BCIs, tactile BCIs, and independent visual BCIs [41]. For example, using standard oddball tasks, P300 signals can be elicited by auditory, tactile, or visual stimuli, which do not require gaze control to select a target. In addition, SSVEP BCIs that use spatial or feature selective attention to modulate the amplitude of attended/unattended SSVEPs are independent [42, 43]. Due to a larger number of classes and a higher level of signal modulation,

the dependent BCIs can achieve much higher communication speed than the independent BCIs. However, for totally locked-in patients who even lose extraocular muscle control, only independent BCIs are useful.

2.2.2 BCIs Based on Sensorimotor Rhythms

2.2.2.1 Sensorimotor Rhythms for BCI

BCI systems based on sensorimotor mu/beta rhythms have been developed rapidly in recent years [25]. The neurophysiological studies of the sensorimotor cortex reveal that mu (8–12 Hz) and beta (18–26 Hz) rhythms are modulated by actual movement or preparation of movement. The event-related power change of brain rhythms in a specific frequency band is known as event-related desynchronization and synchronization (ERD/ERS) [44]. Specifically, in the sensorimotor cortex, ERD indicates power decrease of mu/beta rhythms during movement. In contrast, ERS indicates power increase that typically occurs after movement. ERD/ERS of sensorimotor rhythms occur not only with movement, but also with preparation for movement or motor imagery (i.e., imagined movement). During motor imagery, ERD/ERS of mu/beta rhythms display characteristic spatial patterns corresponding to different body parts (e.g., left hand versus right hand). Source imaging studies further show that the ERD sources are located in corresponding cortical areas somatotopically during motor imagery of different body parts. These findings suggest that motor imagery can provide a good way to implement an independent BCI based on self-regulation of the sensorimotor rhythms.

Motor imagery is the basic strategy to operate a sensorimotor BCI. Many studies have demonstrated that people can learn to control (increase or decrease) the amplitude of the sensorimotor rhythms using motor imagery. For example, with the Wadsworth BCI developed by Wolpaw and his colleagues, subjects were trained to learn self-control of mu/beta rhythm amplitude to realized 1-D, 2-D, or 3-D cursor control by translating mu/beta rhythm amplitudes into cursor movements [7, 45, 46]. In the initial training sessions, subjects mostly employed motor imagery (e.g., imagination of hand movements) to control the cursor movement. Instead of continuous movement control, another approach for sensorimotor BCIs is to classify the motor imagery states (e.g., left hand, right hand, feet) using pattern classification techniques. Spatial patterns of ERD/ERS of the mu/beta rhythms are used as features for classification. The Graz BCI developed by Pfurtscheller and his colleagues employed spatial filters and classifiers to train subjects to generate discriminable motor imagery states and therefore built a co-adaptive learning system, which allowed brain learning and machine learning at the same time [8, 47]. The system can discriminate more complex spatio-temporal patterns of ERD/ERS during imagination of movements of different body parts including left and right hands, feet, and tongue [48].

2.2.2.2 Feature Extraction and Classification

The most commonly used features for indexing ERD/ERS of the mu/beta rhythms include band power values, amplitude envelope by the Hilbert transform, and autoregressive model [47]. Time-frequency analysis can provide more detailed features by jointly considering EEG dynamics in frequency and time domains and thereby improve the classification performance [49, 50]. In addition to temporal and spectral features, since ERD/ERS during motor imagery exhibit characteristic spatial patterns, the extraction of spatial features is especially important for the discrimination of motor imagery states. In the space domain, various approaches have been proposed to enhance the extraction of spatial features. First, spatial filtering techniques can significantly enhance the SNR of the mu/beta rhythms by removing the task-irrelevant brain activities. The supervised common spatial pattern (CSP) algorithm and its extensions such as multi-class CSP and filter bank CSP algorithms have been proved highly efficient for extracting discriminative information cross-motor imagery states [51–53]. Unsupervised methods such as independent component analysis (ICA) have also been applied to extract independent sensorimotor components toward a calibration-free system [54]. Second, EEG source imaging methods have been proposed to extract spatial features in the source space, which show improved spatial resolution and specificity than scalp EEG, for classifying motor imagery states in BCIs [55]. Source imaging approaches with a high spatial resolution were able to enhance BCI performance of decoding complex right-hand motor imagery tasks (i.e., flexion, extension, supination, and pronation) [56]. Third, independent from spectral features, amplitude and phase coupling measures such as non-linear regressive coefficients and phase locking value have been applied to extract brain synchrony features that reflect connectivity between multiple cortical regions involved in motor imagery [57]. By enhancing the extraction of spatial features from the sensorimotor areas, these signal processing approaches significantly facilitate the classification of motor imagery states. After feature extraction, the widely used classifiers such as LDA and SVM convert the features to continuous or discrete control commands to operate output devices [14].

2.2.2.3 User Training

User training plays a key role in the sensorimotor BCI. In the BCI system that requires subject to learn self-control of mu/beta rhythm amplitude, subjects usually take multiple training sessions for weeks and months to realize multi-dimensional control of cursor movement [45]. For the system that discriminates motor imagery states, the selection of the kind of motor imagery affects the BCI performance. For example, kinesthetic motor imagery was found to be superior to visual-motor imagery with respect to distinct spatial patterns [58]. Therefore, user training should emphasize kinesthetic experiences instead of visual representations of movements to obtain reliable motor-imagery-based BCI control. In the BCI systems that employ

machine learning approaches, the brain and the machine can adapt to each other simultaneously, leading to a co-adaptive learning paradigm, which can significantly reduce the user training time [59, 60].

In the sensorimotor BCI, "BCI Illiteracy" is a big challenge for user training and system applications [61]. An estimation of 10% of people was found not able to use the motor imagery BCI after a short training session around 10 min [47]. To avoid costly training of participants who might not obtain BCI control, a neurophysiological predictor of BCI performance based on resting state EEG was proposed and achieved a high correlation between the predictor and the BCI performance after online training [62]. Currently, a general concern of researchers is how a naïve user can learn to operate the sensorimotor BCI. There are few BCI studies focusing on the training of naïve users. By adopting advanced signal processing and machine learning algorithms, a motor imagery BCI system achieved accurate performance in naïve subjects even in the first session [63]. In addition, the co-adaptive learning approach was demonstrated helpful for subjects who suffer from the BCI illiteracy problem to successfully gain control of the system [59].

2.2.3 Hybrid BCIs

2.2.3.1 Hybrid Modalities

A hybrid BCI combines a BCI with other physiological or technical signals [20, 64]. The goal of hybrid BCIs is to integrate multiple input signals to improve the performance of normal BCIs, and enlarge the population of end-users. In a hybrid BCI, at least one brain signal should be employed to provide intentional input to the BCI for real-time communication or control. According to the type of the second signal modality, hybrid BCIs can be categorized into pure hybrid BCIs and mixed hybrid BCIs [65]. A pure hybrid BCI typically combines two EEG patterns together toward enhanced BCI performance. The widely used hybrid EEG patterns are the combination of ERPs and sensorimotor rhythms (e.g., SSVEP-motor imagery, P300-motor imagery), and the combination of two ERP signals (e.g., P300-SSVEP, N2pc-SSVEP). In addition to hybrid EEG signals, other types of brain signals can also be employed to build a pure hybrid BCI. For example, a hybrid near-infrared spectroscopy (NIRS)-EEG BCI was developed and significantly improved the classification accuracy of motor imagery [66]. A mixed hybrid BCI combines EEG with other non-neuronal control signals toward more robust and reliable control. The control signals can be physiological signals (e.g., EMG, EOG, or heart rate) or signals from other existing input devices like an eye tracking system. These control signals typically are generated by residual muscle functions. For example, EMG signals, which can be modulated by residual muscle activities of patients, have been used to implement hybrid BCIs with various EEG signals and achieved significantly improved accuracy and ITR [20, 65].

The hybrid BCI processes the multiple input signals simultaneously or sequentially. Accordingly, hybrid BCIs can be divided into these two types (i.e., simultaneous and sequential hybrid BCIs) [64]. Simultaneous hybrid BCIs fuse information from different input signals, which carry the same desired goal for intentional control, to improve the accuracy. For example, in visual ERP-based BCIs, SSVEP and P300 signals have been widely used to detect gaze direction, therefore, a hybrid SSVEP-P300 BCI can significantly enhance the performance of gaze-dependent target identification by combining the two independent EEG signals [67]. Data fusion plays an important role in a simultaneous hybrid BCI [68]. Information fusion of multiple input signals is required in the procedures of feature extraction, feature combination, and classification decision. Sequential hybrid BCIs operate two systems sequentially, typically with one system as a switch or selector and another system for regular BCI control. The input signal for a switch or selector generally requires high accuracy and reliability, but a small number of discriminable conditions. For example, a brain switch based on motor imagery has been widely used in sequential hybrid BCIs [64]. In a sequential hybrid BCI, multiple control signals are processed separately toward different outputs, and therefore data fusion is not required.

2.2.3.2 Hybrid EEG Signals

In hybrid BCIs, the simultaneous pure hybrid BCIs that only employ multiple EEG patterns are of great interest to BCI researchers due to the great challenges in system design and data fusion. There are two different ways to form hybrid EEG signals. The first approach is to design hybrid BCI paradigms with multiple mental tasks, which can be used to elicit different EEG signals for single or multiple dimensional controls. An example is hybrid BCIs based on SSVEP and P300 signals, which have been widely used in visual BCIs [19]. Frequency-coded SSVEP stimuli can be superimposed onto P300 stimuli coded with a standard row/column paradigm. The attended target stimuli can simultaneously evoke P300 and SSVEP, which can facilitate the discrimination between target and non-target stimuli [67]. Another diagram used the SSVEP blocking approach to evoke P300 and block SSVEP at the same time, which also significantly improved target discrimination [69]. The combination of motor imagery task and visual attention tasks was proposed to develop a hybrid BCI, which can be applicable for more users [70]. The concurrent motor imagery (i.e., imagination of left or right hand movements) and visual attention (gazing left or right flickering stimuli) tasks simultaneously produced independent ERD and SSVEP features for enhanced classification performance. In another study, motor imagery and P300 tasks were performed simultaneously and independently to control 2D cursor movement [71]. Subjects obtained independent mu/beta rhythms and P300 for horizontal and vertical movement controls, respectively. The second approach to form hybrid EEG signals only employs a single type of mental tasks, which can elicit multiple EEG signals. The combination of ERPs and oscillatory brain rhythms can improve the discriminability of EEG patterns. For

example, the combination of ERD/ERS and the lateralized readiness potential facilities the classification of motor imagery tasks [72]. In the gaze-independent SSVEP BCI based on visual spatial attention, the combination of SSVEP and the parieto-occipital alpha rhythm resulted in improved classification accuracy [73]. In addition, with appropriate design, multiple ERP signals can be modulated by a common task. For example, hybrid N2pc and SSVEP features were combined to realize fast detection of covert visuospatial attention in a recent study [74].

2.3 Challenges in Developing BCIs for Practical Applications

Although the feasibility of various BCI paradigms has been well demonstrated in the past decade, translating BCI systems from well-controlled laboratories to complicated living environments still poses great challenges [19, 24]. First of all, the BCI performance in terms of ITR is a key factor in building practical applications for communication and control. Due to limits of the EEG technology, the bottleneck problem in communication speed remains unsolved. Especially in the noisy living conditions, the low ITR is still the key obstacle to BCI applications. Second, the usability of the system plays another key role in practical applications for daily routine use. The two major issues regarding user experience include system calibration and asynchronous system design. The third factor is the practicality of the hardware and software platform. Specifically, practical BCI applications require a convenient mobile EEG system with electrodes that are easy to apply. Besides, analysis of mobile EEG signals, which are more easily contaminated by various noises, requires further development on algorithms. These technical issues need to be addressed to develop BCIs that can satisfy requirements for widespread usage in daily life.

2.3.1 Improving Information Transfer Rate

2.3.1.1 ITR in EEG-Based BCIs

Various metrics (e.g., classification accuracy, ITR, sensitivity and specificity, efficiency and utility, and the like) have been proposed for evaluating the performance of BCIs [75]. Among them, the ITR has been the most widely used metric in BCIs for the purpose of communication and control. Currently, the most popular method for calculating ITR based on Shannon channel theory is defined as follows [2]:

$$\text{ITR} = \left(\log_2 M + P\log_2 P + (1 - P)\log_2 \left[\frac{1 - P}{M - 1} \right] \right) * \left(\frac{60}{T} \right) \qquad (2.1)$$

where N is the number of possible choices, P is the classification accuracy, and T (in seconds/selection) is the average time for each selection. Due to its capability to quantify communication speed, ITR in bits/minute (bpm) has been widely used to evaluate the performance of online BCI systems.

According to temporal control paradigm, BCI systems can be divided into synchronous and asynchronous BCIs [15]. Most current BCIs use synchronous control protocols where the system controls are periodically available and the timing of the operation is determined by the system. In general, ITR calculation in Eq. (2.1) can be directly used for synchronous BCIs. In contrast, the system controls are continuously available in the asynchronous control protocols. By discriminating non-control state and intentional control state, the asynchronous BCIs allow users to make self-paced decisions on when to start or stop the operation. Since the timing of system operation may vary dramatically depending on the user's control state, asynchronous BCI systems usually do not report ITR [76].

2.3.1.2 BCIs with High ITRs

In Wolpaw et al.'s review in 2002 [2], the BCIs showed maximum ITRs up to 10–25 bpm [2]. Over the past 15 years, advances in BCI research have dramatically increased the ITRs for BCIs in all categories. First, for the sensorimotor BCIs, the ITRs have been improved by applying efficient signal processing and machine learning algorithms. However, due to the small number of possible choices and the endogenous control property, ITRs reported for the motor imagery BCIs were generally lower than 15 bpm [77]. Second, for the ERP-based BCIs, the ITRs have achieved a number of breakthroughs. With recent advances in information coding and EEG decoding, the current ERP-based BCI systems have achieved multifold increases of ITR compared with the early systems. Notably in recent studies on visual BCI spellers, the ITRs above 100 bpm have been reported in BCIs using P300 [78], cVEP [36], and SSVEP [34, 35, 79–81]. Townsend et al. used temporal constraints to develop an asynchronous presentation paradigm for the P300 BCI and reported an ITR of 120 bpm with a subject using a 72-target matrix [78]. Bin et al. developed a 32-target BCI using cVEP and achieved an average ITR of 108 bpm [36]. In the past several years, the BCIs based on SSVEPs have demonstrated a series of systems with high ITRs. Chen et al. developed a 45-target BCI, which was calibration free, with frequency-based stimulus coding and EEG decoding methods and obtained an ITR of 105 bpm [79]. The ITR was further improved to 151 bpm by adopting a filter bank analysis algorithm [80]. More recently, the combination of advanced SSVEP detection and multi-target coding methods has been proved highly efficient for the SSVEP-based BCIs. Nakanishi et al. proposed to incorporate individual calibration data in SSVEP detection and reported an ITR of 166 bpm using a mixed frequency and phase coding method [81]. Chen et al. reached a spelling speed at 1 character per second by proposing a joint frequency and phase modulation method and pushed the ITR up to 270 bpm [34]. In a recent study, by adopting a new spatial filtering algorithm, Nakanishi et al. achieved an ITR of 325 bpm [35], which was the maximum ITR reported in current

BCIs. Note that, since the spelling speed of 1 character per second is close to the speed limit of human gaze control, there might be little room for improving the practical ITR of BCI spellers [34]. Third, for the simultaneous hybrid BCIs, the ITRs have been significantly increased compared with the single modalities. The ITRs of hybrid BCIs highly depend on the signals employed in system design. For example, the hybrid P300-SSVEP BCIs reported ITRs around 50–60 bpm [67, 82], while the hybrid SSVEP-EMG BCI reached an ITR above 90 bpm [65]. Compared with the ERP-based BCIs, there is still large room for improvement of ITRs in the hybrid BCIs.

2.3.1.3   Approaches for Improving ITR

The performance bottleneck of current BCIs is mostly attributed to the poor SNR of EEG signals. Therefore, approaches for improving ITR generally aim to improve the SNR of EEG by adopting advanced signal processing and machine learning algorithms [11, 13]. However, according to Eq. (2.1), the methods for improving ITR can be considered with respect to number of choices (N), classification accuracy (P), and target selection time (T) separately. Note that, these parameters cannot be considered independently because they always interact with each other in BCI systems. For example, there is always a tradeoff between classification accuracy and target selection time toward an optimal ITR.

Classification accuracy is crucial in ITR estimation. The methods to improve classification accuracy can be summarized into two directions [19]. The first direction is to enhance the SNR of task-related EEG signals. In this direction, advanced signal processing algorithms have been applied to artifact removal, spatial filtering, and feature extraction [11]. For example, in the sensorimotor BCIs, the CSP-based spatial filtering algorithms have been widely used to extract the task-related power change of mu/beta rhythms during motor imagery [52, 53]. In the SSVEP BCIs, the canonical correlation analysis-based spatial filtering algorithms significantly improve the SNR of SSVEPs [80, 81, 83]. Besides, the amplitude and SNR of task-related EEG signal can be enhanced by user training. In the sensorimotor BCIs, users learn to control the amplitude of sensorimotor rhythms through online training with feedbacks [45]. Alpha neurofeedback training has been shown efficient for improving the SNR of SSVEPs [84]. The second direction for improving classification accuracy is to maximize the separability of multiple classes. To this end, machine learning-based classification techniques have been widely used in feature selection, feature combination, and classification [13, 14]. For example, linear classifiers like LDA have shown good performance in the sensorimotor and ERP-based BCIs [38]. In addition, separability of multiple classes can be improved by encoding more informative features in EEG signals. For example, the hybrid frequency and phase coding methods have been applied in the SSVEP-based BCIs [34, 81]. The hybrid EEG signals used in the simultaneous hybrid BCIs can significantly improve the separability of different classes by combining multiple EEG signals.

The number of choices also plays an important role in ITR estimation. In the sensorimotor BCIs, the number of choices are generally very limited due to the low spatial resolution of EEG patterns. The discrete classification of motor imagery tasks typically includes imagination of hands, feet, and tongue movements [48]. The number of choices can be improved by enabling the continuous control of 2D and 3D movements [45, 46]. The ERP-based BCIs show good capability in implementing a large number of choices. For example, a P300 BCI using the method of flashing quasi-random groups of characters realized a 7×12 matrix speller [85]. The BCI system using cVEP could discriminate 64 classes [9]. In these systems, the MA methods from telecommunications facilitate the implementation of a large number of classes [19].

The target selection time requires to be optimized toward high ITRs, especially in the ERP-based BCIs. Due to the non-stationarity of EEG signals, the number of trial repetitions required for target identification should be able to vary over time. In the P300 BCI, the dynamic stopping method has been proposed to reduce the target selection time by adaptively adjusting the number of trial repetitions [86]. In addition, the target selection time can be largely reduced by employing more efficient target coding methods. For example, in the VEP-based BCIs, the FDMA and CDMA methods require a much shorter time duration to code multiple targets than the TDMA method.

2.3.2   Reducing System Calibration Time

The non-stationarity and individual variance of EEG signals pose great challenges to the implementation of BCIs using training-based machine learning algorithms [19]. A calibration session is typically required to collect training data for building a classification model before the operation of the BCI system. In practice, the repetitive calibration procedures could be boring and time-consuming. To facilitate system calibration, different methods have been developed to reduce the calibration time or even realize zero-training paradigms. To reduce the calibration time, the machine learning algorithms need to have good generalization ability and robustness even when the training dataset is small. In recent years, the zero-training methods have obtained increasing attention. These methods aim to transfer information across multiple sessions, subjects, or tasks to obtain generalizable models that can be directly used for operating BCIs. For example, for each individual user, the cross-session transfer of spatial filters and EEG templates was developed for detecting SSVEPs without new calibration [87]. Besides, the cross-subject transfer of models has been demonstrated feasible for SSVEP [88] and P300 [89] detection without individual calibration data. In addition, the cross-task transfer of spatial filters derived from resting EEG data was proposed to implement zero-training classification of EEG in motor imagery tasks [90]. Furthermore, to better address the non-stationarity issues, adaptive classification methods have been developed to automatically update the classifiers during online BCI operations [88, 91]. The

combination of information transfer and adaptive classification methods provides a practical solution to facilitate the calibration procedure of current BCIs.

2.3.3 Asynchronous System

Asynchronous BCIs, in which users make self-paced operations, are more flexible and natural for routine use than synchronous BCIs [15]. In asynchronous BCIs, continuous detection of idle state is required for discriminating the intentional control state and the non-control state. The BCI system only sends control command when an intentional control state is detected. Accurate detection of the idle states is crucial for practical applications; however, it remains a challenging task due to the large variability of idle states, which might involve different mental activities. One way to address the control state detection issue is to design a switch, which can turn on/off the BCI control mode. This method has been applied in SSVEP-based BCIs. For example, the idle state and the control state were switched by selecting an on/off stimulus, which turned on/off the visual stimuli of the SSVEP BCI [92]. To implement a user-initiated asynchronous BCI system, the discrimination of EEG signals between the idle state and the intentional control state is important and of great interest. For example, in a sensorimotor BCI-based brain switch, EEGs corresponding to idle and imaginary movement states were classified sample-by-sample and the averaged results over time were used to control the switch [93]. In the ERP-based BCIs, the method for detecting idle states is generally based on the computational modeling of EEG signals under the idle and control states. In an SSVEP BCI, spontaneous EEG signals under different types of idle states (on-screen, off-screen, eye-closed) and SSVEPs were classified by SVM classifiers [94]. In an N200 BCI, a computational model of the mVEP response patterns, which integrated the spatial profile of the speller matrix, was used to detect the non-control state effectively [95]. In a P300 BCI, computational models for target P300, non-target P300, and non-control EEG signals were proposed for detecting control and non-control states based on likelihood [96].

2.3.4 Developing Mobile BCI System

Despite the significant performance improvement of EEG-based BCIs, real-life BCI applications have still been hindered by the lack of portability and cumbersome system settings such as skin preparation and gel application. Developing a mobile BCI platform enables the movement of BCI systems from well-controlled laboratory settings to real-world environments. To design a mobile BCI system, the following three major challenges need to be addressed.

First, a mobile BCI system requires advanced sensor technologies to facilitate the skin preparation and gel application, which may take around an hour for

conventional high-density EEG systems. Recently, researchers have developed various types of EEG electrodes. For example, dry- and non-contact electrodes showed good performance in an online BCI experiment based on SSVEPs recorded from the occipital area without conductive gels [97]. In another study, a soft, foldable, and ultra-thin electrode constructing fractal mesh geometry was introduced for long-term recording of high-fidelity EEG signals for a persistent BCI [98]. Besides, placing electrodes over non-hair-bearing areas is another way to avoid the interference from hairs. For instance, several studies demonstrated that behind/around-the-ear electrodes can be an alternative solution to measure EEG for BCIs [99, 100]. In addition, the platform for ear-EEG, which can record EEG signals from electrodes placed in-the-ear, has been developed for brain monitoring [101]. Second, a portable platform using mobile hardware for stimulus presentation, signal acquisition, and data processing is required to expand the capability of BCIs. Recent rapid advances in mobile devices like smartphones made it possible to implement a truly portable BCI. For example, a cellphone-based phone-dialing BCI system was demonstrated using SSVEPs [102]. A head-mounted virtual reality (VR) platform also showed great potentials for implementing a mobile BCI system. Nakanishi et al. proposed a portable BCI, which integrated wireless and wearable EEG, dry EEG and EOG sensors, and a head-mounted VR display, for assessing visual field loss in glaucoma patients based on multi-focal SSVEPs [103]. Third, artifact removal techniques are necessary for a robust mobile BCI. In general, subjects are instructed to remain stationary and focus only on their tasks in laboratory experiments, resulting in clean EEG recordings. However, in real-world situations, motion artifacts and ambient noises can be a severe problem since users' behaviors are not restricted. To simulate realistic motion artifacts, dual-task experimental design, in which subjects needed to perform a primary motor task and a secondary cognitive task at the same time, has been proposed. For example, Gramann et al. recorded EEG from subjects standing or walking on a treadmill while performing a visual oddball response task [104]. Although the scalp recordings were contaminated with motion artifacts, source ERP activities decomposed by ICA did not differ across conditions [104]. Lin et al. performed an online SSVEP BCI using a wearable EEG system in human subjects under walking conditions [105]. These results suggest that subjects can use ERP-based BCIs even while moving by combining mobile EEG with efficient de-noising algorithms.

2.4 Applications of BCIs

Facilitated by the rapid development of modern information technology, BCIs are moving beyond laboratories into real-world applications. The majority of the available BCI applications has been focusing on decoding and outputting users' intention, in which the users actively perform certain mental tasks for the purpose of controlling external devices. The devices can be assistive or rehabilitative, used in both medical and non-medical scenarios. BCIs can also be applied to monitor users'

mental states in real time without their active participation. Applications in this direction mainly focus on healthy people in non-medical scenarios. Below we briefly review the state-of-the-art BCI applications and organize them by their design purposes (i.e., medical or non-medical).

2.4.1   BCIs for Medical Use

ERP-based BCIs are probably the most popular BCI systems serving as an assistive tool for severely motor disabled people, for example, patients with amyotrophic lateral sclerosis (ALS) [106, 107]. Compared to sensorimotor BCIs, the major advantage for ERP-based BCIs is its relative ease of acquiring reliable signals with little training required [17]. Using the classical P300 speller, ALS patients have demonstrated the capability of operating necessary software such as word processing, painting, e-mailing, and controlling home appliances, in their home environment for a considerably long time (>2.5 years in [108] and 14 weeks in [109]). Nevertheless, challenges still remain for patients with complete locked-in syndrome, who are speculated to lack the contingency between a voluntary intention and its consequence [110].

Sensorimotor BCIs, by contrast, have been suggested as an effective approach for rehabilitative purposes (see [10, 45] for attempts to implement assistive BCIs). The most widely studied population is the stroke patients, in which rehabilitative BCIs are expected to help them regain the lost motor functions. Sensorimotor BCIs detect and translate patients' movement intentions into actual limb movements, with the help of a prosthesis or a direct functional electrical stimulation. Such rehabilitation training is believed to induce reorganization of neural circuits, thus facilitating motor function recovery [111].

2.4.2   BCIs for Non-medical Use

Both ERP-based and sensorimotor BCIs can be used in non-medical scenarios, as a novel human-computer interaction (HCI) approach, especially in gaming industry [112, 113]. BCIs are considered as an additional input modality (along with keyboard, speech, gestures, and so on) to control a game or a general HCI application (e.g., in VR environments), providing a unique and possibly useful way for interaction.

An emerging but more important BCI application direction for healthy users is real-time monitoring of critical mental states, such as attention, stress, cognitive load, emotion, and the like. Most of these BCIs, recently termed as 'passive BCIs'

[22], usually take the form of hybrid BCIs, in which other physiological or environmental signals are also included when necessary, with the aim of having a more comprehensive overview of the users' states. Passive BCIs provide an objective evaluation in the fields of driving safety [114, 115], education [116], user experience, or neuro-marketing [117]. Although still at an early stage, BCI development in this direction is believed to benefit a much larger population, beyond the scope of clinical population.

2.5 Summary

The past 20 years have witnessed unprecedented progress in the BCI technology. In addition to the original purpose to help the patients with motor disabilities to communicate with their environments, current BCI applications have been extended to various fields including brain state monitoring, neuro-rehabilitation, and human performance improvement in the last few years. More generally, BCI can be defined as a real-time platform that uses online brain signal analysis to influence human interactions with their environments. In the field of communication and control, beyond the initial definition of interface, the current BCI technology places more emphasis on the interaction between human brain and the output devices. The practical BCI applications will allow researchers to study the mutual interference between brain and devices in long-term interaction.

Despite significant progress in performance improvement, low communication rates remain key obstacles to BCI-based communication and control. The improvement of communication speed will continue to be a main challenge in BCI research. The following efforts can be made in this direction. First, by increasing our understanding of how sensation, perception, and cognition are encoded in brain signals, new BCI paradigms with wider communication bandwidths can be developed. Second, by considering BCI as a communication system, advanced technologies from telecommunications can be employed to improve information modulation and demodulation in BCIs. Third, more efficient signal processing and machine learning algorithms can facilitate the decoding of EEG. Fourth, brain stimulation methods such as electrical and magnetic stimulation can be employed to enhance the brain signals. Furthermore, the future performance breakthroughs of BCI require the collaboration between neuroscience, artificial intelligence (AI), and engineering. In the near future, the combination of BCI with AI can lead to new hybrid intelligence systems that can effectively fuse human and machine intelligence.

References

1. Vidal JJ (1973) Toward direct brain-computer communication. Annu Rev Riophys Bioeng 2:157–180
2. Wolpaw JR, Birbaumer N, McFarland DJ, Pfurtscheller G, Vaughan TM (2002) Brain computer interfaces for communication and control. Clin Neurophysiol 113(6):767–791
3. Birbaumer N (2006) Brain-computer-interface research: coming of age. Clin Neurophysiol 117(3):479–483
4. Lebedev MA, Nicolelis MAL (2017) Brain-machine interfaces: from basic science to neuroprostheses and neurorehabilitation. Physiol Rev 97(2):767–837
5. Vidal JJ (1977) Real-time detection of brain events in EEG. Proc IEEE 65(5):633–664
6. Farwell LA, Donchin E (1988) Talking off the top of your head – toward a mental prosthesis utilizing event-related brain potentials. Electroencephalogr Clin Neurophysiol 70(6):510–523
7. Wolpaw JR, McFarland DJ, Neat GW, Forneris CA (1991) An EEG-based brain-computer interface for cursor control. Electroencephalogr Clin Neurophysiol 78(3):252–259
8. Pfurtscheller G, Flotzinger D, Kalcher J (1993) Brain-computer interface – a new communication device for handicapped persons. J Microcomput Appl 16(3):293–299
9. Sutter EE (1992) The brain response interface: communication through visually-induced electrical brain responses. J Microcomput Appl 15(1):31–45
10. Birbaumer N, Ghanayim N, Hinterberger T, Iversen I, Kotchoubey B, Kubler A, Perelmouter J, Taub E, Flor H (1999) A spelling device for the paralyzed. Nature 398:297–298
11. Bashashati A, Fatourechi M, Ward RK, Birch GE (2007) A survey of signal processing algorithms in brain-computer interfaces based on electrical brain signals. J Neural Eng 4(2):R32–R57
12. Makeig S, Kothe C, Mullen T, Bigdely-Shamlo N, Zhang Z, Kreutz-Delgado K (2012) Evolving signal processing for brain–computer interfaces. Proc IEEE 100:1567–1584
13. Müller KR, Krauledat M, Dornhege G, Curio G, Blankertz B (2004) Machine learning techniques for brain-computer interfaces. Biomed Tech 49(1):11–22
14. Lotte F, Congedo M, Lecuyer A, Lamarche F, Arnaldi B (2007) A review of classification algorithms for EEG-based brain-computer interfaces. J Neural Eng 4(2):R1–R13
15. Mason SG, Bashashati A, Fatourechi M, Navarro KF, Birch GE (2007) A comprehensive survey of brain interface technology designs. Ann Biomed Eng 35(2):137–169
16. Lance BJ, Kerick SE, Ries AJ, Oie KS, McDowell K (2012) Brain computer interface technologies in the coming decades. Proc IEEE 100:1585–1599
17. Mak JN, Wolpaw JR (2009) Clinical applications of brain-computer interfaces: current state and future prospects. IEEE Rev Biomed Eng 2:187–199
18. Van Erp J, Lotte F, Tangermann M (2012) Brain-computer interfaces: beyond medical applications. Computer 45(4):26–34
19. Gao S, Wang Y, Gao X, Hong B (2014) Visual and auditory brain-computer interfaces. IEEE Trans Biomed Eng 61(5):1436–1447
20. Müller-Putz G, Leeb R, Tangermann M, Höhne J, Kübler A, Cincotti F, Mattia D, Rupp R, Müller KR, Millan JR (2015) Towards noninvasive hybrid brain–computer interfaces: framework, practice, clinical application, and beyond. Proc IEEE 103(6):926–943
21. Chaudhary U, Birbaumer N, Ramos-Murguialday A (2016) Brain–computer interfaces for communication and rehabilitation. Nat Rev Neurol 12(9):513–525
22. Zander TO, Kothe C (2011) Towards passive brain–computer interfaces: applying brain–computer interface technology to human–machine systems in general. J Neural Eng 8(2):025005
23. Millán JR, Rupp R, Müller-Putz GR, Murray-Smith R, Giugliemma C, Tangermann M, Vidaurre C, Cincotti F, Kübler A, Leeb R, Neuper C, Müller KR, Mattia D (2010) Combining brain–computer interfaces and assistive technologies: state-of-the-art and challenges. Front Neurosci 4:161

24. Wang Y, Gao X, Hong B, Gao S (2010) Practical designs of brain–computer interfaces based on the modulation of EEG rhythms. In: Graimann B, Allison B, Pfurtscheller G (eds) Brain–computer interfaces. Springer, Heidelberg, pp 137–154
25. Yuan H, He B (2014) Brain–computer interfaces using sensorimotor rhythms: current state and future perspectives. IEEE Trans Biomed Eng 61(5):1425–1435
26. Luck SJ (2005) An introduction to the event-related potential technique. MIT Press, Cambridge
27. Regan D (1989) Human brain electrophysiology: evoked potentials and evoked magnetic fields in science and medicine. Elsevier, New York
28. Patel SH, Azzam PN (2005) Characterization of N200 and P300: selected studies of the event-related potential. Int J Med Sci 2(4):47–154
29. Rappaport TS (2001) Wireless communication, principle and practice, 2nd edn. Prentice-Hall, Englewood Cliffs
30. Fazel-Rezai R, Allison BZ, Guger C, Sellers EW, Kleih SC, Kübler A (2012) P300 brain computer interface: current challenges and emerging trends. Front Neuroeng 5:14
31. Guo F, Hong B, Gao X, Gao S (2008) A brain–computer interface using motion-onset visual evoked potential. J Neural Eng 5(4):477–485
32. Lee PL, Hsieh JC, Wu CH, Shyu KK, Chen SS, Yeh TC, Wu YT (2006) The brain computer interface using flash visual evoked potential and independent component analysis. Ann Biomed Eng 34(10):1641–1654
33. Vialatte FB, Maurice M, Dauwels J, Cichocki A (2010) Steady-state visually evoked potentials: focus on essential paradigms and future perspectives. Prog Neurobiol 90(4):418–438
34. Chen X, Wang Y, Nakanishi M, Gao X, Jung TP, Gao S (2015) High-speed spelling with a noninvasive brain-computer interface. Proc Natl Acad Sci U S A 112(44):E6058–E6067
35. Nakanishi M, Wang Y, Chen X, Wang YW, Gao X, Jung TP (2017) Enhancing detection of SSVEPs for a high-speed brain speller using task-related component analysis. IEEE Trans Biomed Eng. (in press)
36. Bin G, Gao X, Wang Y, Li Y, Hong B, Gao S (2011) A high-speed BCI based on code modulation VEP. J Neural Eng 8(2):025015
37. Maye A, Zhang D, Engel AK (2017) Utilizing retinotopic mapping for a multi-target SSVEP BCI with a single flicker frequency. IEEE Trans Neural Syst Rehabil Eng. (in press)
38. Blankertz B, Lemm S, Treder M, Haufe S, Müller KR (2011) Single trial analysis and classification of ERP components—a tutorial. NeuroImage 56(2):814–825
39. Parra LC, Spence CD, Gerson AD, Sajda P (2005) Recipes for the linear analysis of EEG. NeuroImage 28(2):326–341
40. Wang Y, Gao X, Hong B, Jia C, Gao S (2008) Brain–computer interfaces based on visual evoked potentials-feasibility of practical system designs. IEEE Eng Med Biol Mag 27 (5):64–71
41. Riccio A, Mattia D, Simione L, Olivetti M, Cincotti F (2012) Eye-gaze independent EEG-based brain–computer interfaces for communication. J Neural Eng 9(4):045001
42. Kelly SP, Lalor EC, Finucane C, McDarby G, Reilly RB (2005) Visual spatial attention control in an independent brain–computer interface. IEEE Trans Biomed Eng 52 (9):1588–1596
43. Zhang D, Maye A, Gao X, Hong B, Engel AK, Gao S (2010) An independent brain–computer interface using covert non-spatial visual selective attention. J Neural Eng 7(1):016010
44. Pfurtscheller G, Lopes da Silva FH (1999) Event-related EEG/MEG synchronization and desynchronization: basic principles. Clin Neurophysiol 110(11):1842–1857
45. Wolpaw JR, McFarland DJ (2004) Control of a two-dimensional movement signal by a noninvasive brain-computer interface in humans. Proc Natl Acad Sci U S A 101 (51):17849–17854
46. McFarland DJ, Sarnacki WA, Wolpaw JR (2010) Electroencephalographic (EEG) control of three-dimensional movement. J Neural Eng 7(3):036007

47. Pfurtscheller G, Neuper C (2001) Motor imagery and direct brain-computer communication. Proc IEEE 89(7):1123–1134
48. Pfurtscheller G, Brunner C, Schlogl A, Lopes da Silva FH (2006) Mu rhythm (de)synchronization and EEG single-trial classification of different motor imagery tasks. NeuroImage 31 (1):153–159
49. Wang T, Deng J, He B (2004) Classifying EEG-based motor imagery tasks by means of time-frequency synthesized spatial patterns. Clin Neurophysiol 115(12):2744–2753
50. Li J, Wang Y, Zhang L, Cichocki A, Jung TP (2016) Decoding EEG in cognitive tasks with time-frequency and connectivity masks. IEEE Trans Cogn Dev Syst 8(4):298–308
51. Ramoser H, Müller-Gerking J, Pfurtscheller G (2000) Optimal spatial filtering of single trial EEG during imagined hand movement. IEEE Trans Neural Syst Rehabil Eng 8(4):441–446
52. Blankertz B, Tomioka R, Lemm S, Kawanabe M, Müller KR (2008) Optimizing spatial filters for robust EEG single-trial analysis. IEEE Signal Process Mag 25(1):41–56
53. Ang KK, Chin ZY, Wang C, Guan C, Zhang H (2012) Filter bank common spatial pattern algorithm on BCI competition IV datasets 2a and 2b. Front Neurosci 6:39
54. Wang Y, Jung TP (2013) Improving brain-computer interfaces using independent component analysis. In: Allison B, Dunne S, Leeb R, Millan JR, Nijholt A (eds) Towards practical brain-computer interfaces: bridging the gap from research to real-world applications. Springer, Heidelberg, pp 67–83
55. Qin L, Ding L, He B (2005) Motor imagery classification by means of source analysis for brain-computer interface applications. J Neural Eng 2(4):65–72
56. Edelman BJ, Baxter B, He B (2016) EEG source imaging enhances the decoding of complex right-hand motor imagery tasks. IEEE Trans Biomed Eng 63(1):4–14
57. Wei Q, Wang Y, Gao X, Gao S (2007) Amplitude and phase coupling measures for feature extraction in an EEG-based brain-computer interface. J Neural Eng 4(2):120–129
58. Neuper C, Scherer R, Reiner M, Pfurtscheller G (2005) Imagery of motor actions: differential effects of kinesthetic and visual-motor mode of imagery in single-trial EEG. Brain Res Cogn Brain Res 25(3):668–677
59. Vidaurre C, Sannelli C, Müller KR, Blankertz B (2011) Machine-learning-based coadaptive calibration for brain-computer interfaces. Neural Comput 23(3):791–816
60. Acqualagna L, Botrel L, Vidaurre C, Kübler A, Blankertz B (2016) Large-scale assessment of a fully automatic co-adaptive motor imagery-based brain computer interface. PLoS ONE 11 (2):e0148886
61. Kübler A, Neumann N, Wilhelm B, Hinterberger T, Birbaumer N (2004) Predictability of brain-computer communication. J Psychophysiol 18:121–129
62. Blankertz B, Sannelli C, Halder S, Hammer EM, Kübler A, Müller KR, Curio G, Dickhaus T (2010) Neurophysiological predictor of SMR-based BCI performance. NeuroImage 51 (4):1303–1309
63. Blankertz B, Losch F, Krauledat M, Dornhege G, Curio G (2008) The Berlin brain-computer interface: accurate performance from first-session in BCI-naïve subjects. IEEE Trans Biomed Eng 55(10):2452–2462
64. Pfurtscheller G, Allison BZ, Bauernfeind G, Brunner C, Solis Escalante T, Scherer R, Zander TO, Müller-Putz G, Neuper C, Birbaumer N (2010) The hybrid BCI. Front Neurosci 4:30
65. Lin K, Cinetto A, Wang Y, Chen X, Gao S, Gao X (2016) An online hybrid BCI system based on SSVEP and EMG. J Neural Eng 13(2):026020
66. Fazli S, Mehnert J, Steinbrink J, Curio G, Villringer A, Müller KR, Blankertz B (2012) Enhanced performance by a hybrid NIRS–EEG brain computer interface. NeuroImage 59 (1):519–529
67. Yin E, Zhou Z, Jiang J, Chen F, Liu Y, Hu D (2013) A novel hybrid BCI speller based on the incorporation of SSVEP into the P300 paradigm. J Neural Eng 10(2):026012
68. Li Y, Pan J, Long J, Yu T, Wang F, Yu Z, Wu W (2016) Multimodal bcis: target detection, multidimensional control, and awareness evaluation in patients with disorder of consciousness. Proc IEEE 104(2):332–352

69. Xu M, Qi H, Wan B, Yin T, Liu Z, Ming D (2013) A hybrid BCI speller paradigm combining P300 potential and the SSVEP blocking feature. J Neural Eng 10(2):026001

70. Allison BZ, Brunner C, Kaiser V, Müller-Putz GR, Neuper C, Pfurtscheller G (2010) Toward a hybrid brain–computer interface based on imagined movement and visualattention. J Neural Eng 7(2):26007

71. Li Y, Long J, Yu T, Yu Z, Wang C, Zhang H, Guan C (2010) An EEG-based BCI system for 2-D cursor control by combining Mu/Beta rhythm and P300 potential. IEEE Trans Biomed Eng 57(10):2495–2505

72. Höhne J, Holz E, Staiger-Sälzer P, Müller KR, Kübler A, Tangermann M (2014) Motor imagery for severely motor-impaired patients: evidence for brain-computer interfacing as superior control solution. PLoS ONE 9(8):e104854

73. Kelly SP, Lalor EC, Reilly RB, Foxe JJ (2005) Visual spatial attention tracking using high-density SSVEP data for independent brain-computer communication. IEEE Trans Neural Syst Rehabil Eng 13(2):172–178

74. Xu M, Wang Y, Nakanishi M, Wang YT, Qi H, Jung TP, Ming D (2016) Fast detection of covert visuospatial attention using hybrid N2pc and SSVEP features. J Neural Eng 13 (6):066003

75. Billinger M, Daly I, Kaiser V, Jin J, Allison BZ, Müller-Putz GR, Brunner R (2013) Is it significant? Guidelines for reporting BCI performance. In: Allison B, Dunne S, Leeb R, Millan JR, Nijholt A (eds) Towards practical brain-computer interfaces: bridging the gap from research to real-world applications. Springer, Heidelberg, pp 333–354

76. Yuan P, Gao X, Allison B, Wang Y, Bin G, Gao S (2013) A study of the existing problems of estimating the information transfer rate in online brain–computer interfaces. J Neural Eng 10 (2):026014

77. Müller KR, Tangermann M, Dornhege G, Krauledat M, Curio G, Blankertz B (2008) Machine learning for real-time single-trial EEG-analysis: from brain – computer interfacing to mental state monitoring. J Neurosci Methods 167(1):82–90

78. Townsend G, Platsko V (2016) Pushing the P300-based brain-computer interface beyond 100 bpm: extending performance guided constraints into the temporal domain. J Neural Eng 13(2):026024

79. Chen X, Chen Z, Gao S, Gao X (2014) A high-ITR SSVEP-based BCI speller. Brain-Comp Interfaces 1(3–4):181–191

80. Chen X, Wang Y, Gao S, Jung TP, Gao X (2015) Filter bank canonical correlation analysis for implementing a high-speed SSVEP-based brain-computer interface. J Neural Eng 12 (4):046008

81. Nakanishi M, Wang Y, Wang YT, Mitsukura Y, Jung TP (2014) A high-speed brain speller using steady-state visual evoked potentials. Int J Neural Syst 24(6):1450019

82. Xu M, Chen L, Zhang L, Qi H, Ma L, Tang J, Wan B, Ming D (2014) A visual parallel-BCI speller based on the time–frequency coding strategy. J Neural Eng 11(2):026014

83. Lin Z, Zhang C, Wu W, Gao X (2007) Frequency recognition based on canonical correlation analysis for SSVEP-based BCIs. IEEE Trans Biomed Eng 54(6):1172–1176

84. Wan F, Da Cruz JN, Nan W, Wong CM, Vai MI, Rosa A (2016) Alpha neurofeedback training improves SSVEP-based BCI performance. J Neural Eng 13(3):036019

85. Jin J, Allison BZ, Sellers EW, Brunner C, Horki P, Wang X, Neuper C (2011) Optimized stimulus presentation patterns for an event-related potential EEG-based brain-computer interface. Med Biol Eng Comput 49(2):181–191

86. Schreuder M, Höhne J, Blankertz B, Haufe S, Dickhaus T, Tangermann M (2013) Optimizing event-related potential based brain–computer interfaces: a systematic evaluation of dynamic stopping methods. J Neural Eng 10(3):036025

87. Nakanishi M, Wang Y, Jung TP (2016) Session-to-session transfer in detecting SSVEPs with individual calibration data. In: Schmorrow DD, Fidopiastis CM (eds) Foundations of augmented cognition: neuroergonomics and operational neuroscience. Springer International Publishing, Cham, pp 253–260

88. Yuan P, Chen X, Wang Y, Gao X, Gao S (2015) Enhancing performances of SSVEP-based brain-computer interfaces via exploiting inter-subject information. J Neural Eng 12(4):046006

89. Xu M, Liu J, Chen L, Qi H, He F, Zhou P, Wan B, Ming D (2016) Incorporation of inter-subject information to improve the accuracy of subject-specific P300 classifiers. Int J Neural Syst 26(3):1650010

90. Wang Y, Wang YT, Jung TP (2012) Translation of EEG spatial filters from resting to motor imagery using independent component analysis. PLoS ONE 7(5):e37665

91. Vidaurre C, Sannelli C, Müller KR, Blankertz B (2010) Machine-learning-based coadaptive calibration for brain-computer interfaces. Neural Comput 23(3):791–816

92. Cheng M, Gao X, Gao S, Xu D (2002) Design and implementation of a brain-computer interface with high transfer rates. IEEE Trans Biomed Eng 49(10):1181–1186

93. Mason SG, Birch GE (2000) A brain-controlled switch for asynchronous control applications. IEEE Trans Biomed Eng 47(10):1297–1307

94. Zhang D, Huang B, Wu W, Li S (2015) An idle-state detection algorithm for SSVEP-based brain-computer interfaces using a maximum evoked response spatial filter. Int J Neural Syst 25 (7):1550030

95. Zhang D, Song H, Xu H, Wu W, Gao S, Hong B (2012) An N200 speller integrating the spatial profile for the detection of the non-control state. J Neural Eng 9(2):026016

96. Zhang H, Guan C, Wang C (2008) Asynchronous P300-based brain-computer interfaces: a computational approach with statistical models. IEEE Trans Biomed Eng 55(6):1754–1763

97. Chi YW, Wang YT, Wang Y, Maier C, Jung TP, Cauwenberghs G (2012) Dry and non-contact EEG sensors for mobile brain-computer interfaces. IEEE Trans Neural Syst Rehabil Eng 20 (2):228–235

98. Norton JJ, Lee DS, Lee JW, Lee W, Kwon O, Won P, Jung SY, Cheng H, Jeong JW, Akce A, Umunna S, Na I, Kwon YH, Wang XQ, Liu Z, Paik U, Huang Y, Bretl T, Yeo WH, Rogers JA (2015) Soft, curved electrode systems capable of integration on the auricle as a persistent brain-computer interface. Proc Natl Acad Sci U S A 112(13):3920–3925

99. Wang YT, Nakanishi M, Wang Y, Wei CS, Cheng CK, Jung TP (2017) An online brain-computer interface based on SSVEPs measured from non-hair-bearing areas. IEEE Trans Neural Syst Rehabil Eng 25(1):11–18

100. Pacharra M, Debener S, Wascher E (2017) Concealed around-the-ear EEG captures cognitive processing in a visual Simon task. Front Hum Neurosci 11:290

101. Looney D, Kidmose P, Park C, Ungstrup M, Rank ML, Rosenkranz K, Mandic DP (2012) The in-the-ear recording concept: use-centered and wearable brain monitoring. IEEE Pulse 3 (6):32–42

102. Wang YT, Wang Y, Jung TP (2011) A cell-phone based brain-computer interface for com-munication in daily life. J Neural Eng 8(2):025018

103. Nakanishi M, Wang YT, Jung TP, Zao JK, Chien YY, Diniz-Filho A, Daga FB, Lin YP, Wang Y, Medeiros FA (2017) Detecting glaucoma with a portable brain-computer interface for objective assessment of visual function loss. JAMA Ophthalmol 135(6):550–557

104. Gramann K, Gwin JT, Bigdely-Shamlo N, Ferris DP, Makeig S (2010) Visual evoked re-sponses during standing and walking. Front Hum Neurosci 4:202

105. Lin YP, Wang Y, Jung TP (2014) Assessing the feasibility of online SSVEP decoding for moving humans using a consumer EEG headset. J Neuroeng Rehabil 11:119

106. Sellers EW, Donchin E (2006) A P300-based brain-computer interface: initial tests by ALS patients. Clin Neurophysiol 117(3):538–548

107. Nijboer F, Sellers EW, Mellinger J, Jordan MA, Matuz T, Furdea A, Kübler A (2008) A P300-based brain–computer interface for people with amyotrophic lateral sclerosis. Clin Neurophysiol 119(8):1909–1916

108. Sellers EW, Vaughan TM, Wolpaw JR (2010) A brain-computer interface for long-term independent home use. Amyotroph Lateral Scler 11(5):449–455

109. Holz EM, Botrel L, Kaufmann T, Kübler A (2015) Long-term independent brain-computer interface home use improves quality of life of a patient in the locked-in state: a case study. Arch Phys Med Rehabil 96(3):S16–S26
110. Birbaumer N, Piccione F, Silvoni S, Wildgruber M (2012) Ideomotor silence: the case of complete paralysis and brain-computer interfaces (BCI). Psychol Res 76(2):183–191
111. Van Dokkum L, Ward T, Laffont I (2015) Brain computer interfaces for neurorehabilitation-its current status as a rehabilitation strategy post-stroke. Ann Phys Rehabil Med 58(1):3–8
112. Bos DPO, Reuderink B, van de Laar B, Gürkök H, Mühl C, Poel M, Heylen D (2010) Brain-computer interfacing and games. In: Tan DS, Nijholt A (eds) Brain-computer interfaces. Springer, London, pp 149–178
113. Ahn M, Lee M, Choi J, Jun SC (2014) A review of brain-computer interface games and an opinion survey from researchers, developers and users. Sensors 14(8):14601–14633
114. Lal SK, Craig A (2002) Driver fatigue: electroencephalography and psychological assessment. Psychophysiology 39(3):313–321
115. Healey J, Picard RW (2005) Detecting stress during real-world driving tasks using physiological sensors. IEEE Trans Intell Transp Syst 6(2):156–166
116. Poulsen AT, Kamronn S, Dmochowski J, Parra LC, Hansen LK (2017) EEG in the classroom: synchronised neural recordings during video presentation. Sci Rep 7:43916
117. Khushaba RN, Wise C, Kodagoda S, Louviere J, Kahn BE, Townsend C (2013) Consumer neuroscience: assessing the brain response to marketing stimuli using electroencephalogram (EEG) and eye tracking. Expert Syst Appl 40(9):3803–3812

Chapter 3
Invasive Brain Machine Interface System

**Yile Jin, Junjun Chen, Shaomin Zhang, Weidong Chen,
and Xiaoxiang Zheng**

Abstract Because of high spatial-temporal resolution of neural signals obtained by invasive recording, the invasive brain-machine interfaces (BMI) have achieved great progress in the past two decades. With success in animal research, BMI technology is transferring to clinical trials for helping paralyzed people to restore their lost motor functions. This chapter gives a brief review of BMI development from animal experiments to human clinical studies in the following aspects: (1) BMIs based on rodent animals; (2) BMI based on non-human primates; and (3) pilot BMIs studies in clinical trials. In the end, the chapter concludes with a summary of potential opportunities and future challenges in BMI technology.

Keywords Brain-machine interfaces · Neural ensemble recording · Neural decoding · Neural stimulation · Electrocorticogram

3.1 Introduction

Spinal cord and limb nerve injury, amyotrophic lateral sclerosis, and other neuro-muscular degeneration are common neurological disorders that cause hemiplegia and paraplegia. There are 130,000 new paralyzed patients due to spinal cord injury (SCI) per year in the world [1]. About half of these patients are injured above the sixth section of the cervical vertebra. Thus, the movement of the limbs will be affected. Except for spinal cord injury, some other diseases can cause a loss of motor

Y. Jin · J. Chen · S. Zhang (✉) · X. Zheng
Qiushi Academy for Advanced Studies, Zhejiang University, Hangzhou, China

Department of Biomedical Engineering, Zhejiang University, Hangzhou, China
e-mail: shaomin@zju.edu.cn

W. Chen
Qiushi Academy for Advanced Studies, Zhejiang University, Hangzhou, China

College of Computer Science, Zhejiang University, Hangzhou, China

function, when patients deeply appreciate how important the motor function is. Most of these patients are unable to take care of themselves and have a poor quality of life. Meanwhile, the drug is not effective in their cases.

Brain-Machine interfaces (BMIs) establish a direct pathway for communication and control between the brain and external devices, which means utilizing neural signals to control external devices to accomplish the desired action [2–4]. This pathway enables direct interaction between the brain and external devices independent of spinal cord/peripheral neuromuscular system. Not only does it assist and enhance the interaction between the human and outside world, but also repair the sensory, motor, and other cognitive dysfunction, providing a new means of rehabilitation for the disabled.

BMI is mainly composed of signal acquisition, signal processing, signal decoding, and external device control module [3, 4]. Signal acquisition module utilizes various sensor brain signal acquisition to collect electroencephalogram (EEG), magnetic signals, image signals, and others which can reflect neural activities in the brain. Signal processing refers to amplifying and filtering the original signal, consequently enhancing the effective signals and inhibiting the invalid signals like noise. Signal decoding is a process mapping the neural activities to motion parameters, which can be further converted to commands to control external devices. External devices aim at assisting or enhancing the motor function of subjects. Some common ones are a computer mouse, electric wheelchair, robotic arm, and so on.

BMIs are divided into non-invasive BMIs and invasive BMIs according to whether the signal acquisition equipment invades the organism of subjects [2]. Invasive BMIs based on cortical neural signals can directly obtain spike and field potentials with the features of being an informative and high temporal-spatial resolution, so as to predict the subjects' behavior intention and achieve real-time and precise control of external devices in multiple degrees of freedom. Since this century, scientific journals such as Nature and Science have reported a number of significant research achievements about invasive BMIs. The related research also promotes people's awareness of the nervous system and establishes a large number of methods to process complex information, which greatly helps computer improve comprehension to complex perceptual information and increase the efficiency of processing mass heterogeneous information.

From the point of view of the development of BMIs studies, the current trend of development of BMI is gradually transformed from laboratory to clinical application. Experimental study of BMI is more and more advanced, from rodent animals gradually shifted to non-human primates, and has carried out preliminary clinical studies; The paradigms in studies are getting more complex, from the two-dimensional (2-D) cursor control to the development of multi-degree of freedom prosthesis for performing reach-to-grasp movements. The clinical study of these invasive BMI will provide a solid foundation for its clinical applications.

3.2   BMIs on Rodents

With the deepening understanding of the encoding rules of the cerebral motor cortex in the rodent and the continuous improvement of the accuracy of the off-line decoding algorithms, researchers try to bypass the natural neural pathway and establish the artificial information transmission pathways, which means direct extraction of neural signals of cerebral motor cortex and real-time control of external device. According to the difference of the direction of information transmission, the rodent BMI can be classified into one-way BMI and two-way BMI.

3.2.1   Neural Decoding Studies in Rodents

One-way BMI refers to the extraction of neural signal from the cerebral cortex of animals, the translation of neural signals into motion commands according to the mapping between them and controlling external device to complete the task. In one-way BMI, information is transmitted from the nervous system to the external device on the artificial pathway. The animal can only receive the feedback of external device through its natural sensory system, such as vision, audition, touch, etc. One-way BMI is the earliest brain-machine interface system.

According to whether the animal gets the feedback of external device in real time, one-way BMI is classified into open-loop BMI and closed-loop BMI. The world's first open-loop BMI system was built by Chapin in 1999, in which the rat pressed the lever by its neural signals [5]. As shown in Fig. 3.1, the rat was first trained to learn to press the lever with its forelimb (Fig. 3.1b). The displacement of the lever was proportional to that of a robot arm which delivers water to rats (Fig. 3.1c). Once the displacement exceeded the threshold, the rat could get the water reward. During the experiment, multi-channel neural signals of the primary motor cortex (MI) and the ventrolateral (VL) thalamus were recorded simultaneously. In behavioral control mode, the rat drank water by pressing the lever. In the BMI mode, the connection between the lever and the robot was cut off, and the displacement of the robot was controlled by control commands decoded from the 32-channel neural signals. Then, the control mode switches to BMI mode. In the early stage of BMI mode, the rat still tried to press the lever to get the reward. As time went on, the rat completed the task only by modulating its neural activity, and the association between the forelimb's displacement and neural activity was weaker and weaker. Finally, the rat drank water only by modulating neural signals without moving its forearm. The experiment first proved the feasibility of an online BMI system and opened the door to the BMI field.

In 2009, Lee et al. built a rat BMI system to control turntables [6]. In behavioral training, the rat was trained to control the direction and magnitude of a turntable to obtain water. The motion set C_q consisted of seven elements $\{-3, -2, -1, 0, 1, 2, 3\}$, where the sign of the element represented the rotation direction and the
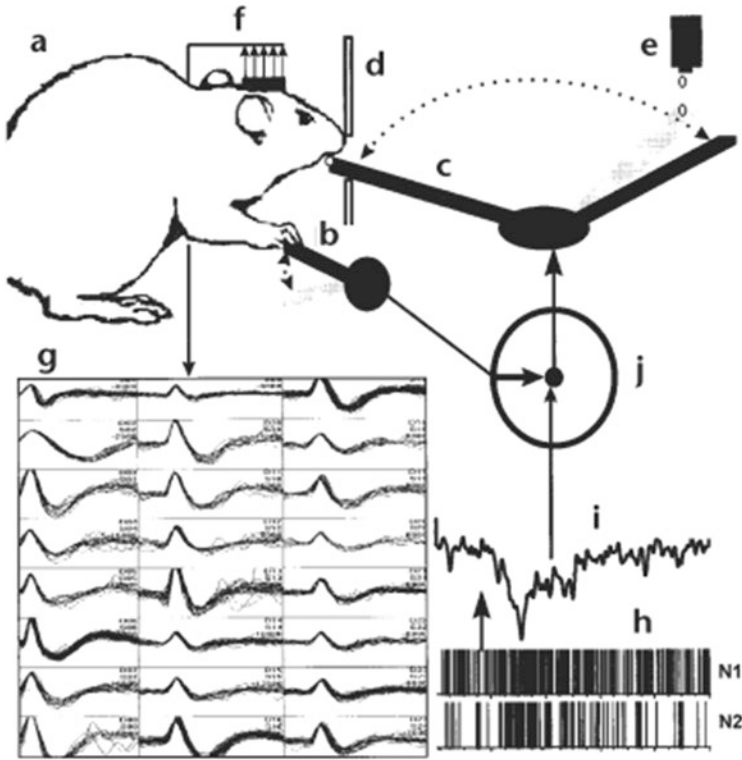
Fig. 3.1 The first BMI study in rodents [5]

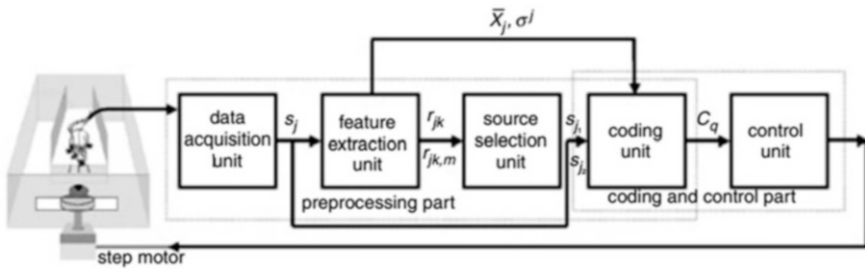**Fig. 3.2** A turning table paradigm in rodent BMI study [6]

magnitude represented the rotation amplitude. After behavioral training, multi-electrodes were implanted in the SI vibrissae area. As shown in Fig. 3.2, multi-channel spike train was sent into feature extraction and channel selection units which selected two channels s_{j1}, s_{j2} as decoding channels according to correlation. The

coding unit obtained the mapping between the relative deviation of s_{j1}, s_{j2} and the motion data $C_q = f(s_{j1}, s_{j2})$. According to the mapping obtained above, the decoder generates the control command every 200 ms to make the turntable rotation.

In 2012, Manohar et al. built the BMI system of the rat hindlimb pressing lever under three different conditions [7]. The rat was trained to press the lever to get the reward in the behavioral control mode, which was followed by three neural control modes (NC). In the first mode, the mechanical connection between the lever and the reward delivery was cut off, but the rat could still press the lever. In the second mode, the lever was removed and the rat got the reward purely by modulating its neural signals. In the third mode, the spinal cord of the rat was completely transected and the rat relearned to modulate the BMI system. They compared the performance and neural firing pattern in the behavior control mode and three neural control modes. When the control mode was switched from the behavior control mode to the neural control mode, the response of the direct population was significantly enhanced, and the decoded information was significantly increased. When the lever was removed, the control performance was similar but the neural response changed significantly. When the spinal cord completely transected, the decoded information decreased by 40%. With a period of learning, the control performance gradually recovered, but still worse than before. The experiment demonstrated that the animals' state, such as the limitation of movement and the integrity of neural pathways, had a large influence on the BMI performance and the firing pattern of a neural population.

For some paralyzed patients, such as those with spinal cord injury, their cerebral motor cortex and effector (such as the arm) are intact and the lesion is located on the neural pathway, which breaks the transmission of information. For these patients, the best way to repair the motor function is to build an artificial neural pathway between the cerebral motor cortex and the effector. So researchers tried to combine traditional BMI with muscle electrical stimulation technique and put forward a new repairing technique of neural pathway. In 2014, Alam et al. reconstructed the neural pathway between the primary motor cortex and the hind limb of the rat with spinal cord transection [8]. They recorded the neural activity from the primary motor cortex of running rats before and after spinal cord transection in rats running tasks. The results showed that the association between neural activity and motion states decreased significantly after the transaction, but the stationary state and moving state could be still distinguished by decoding. After transection of the spinal cord, action potentials of the motor cortex were used to stimulate the muscles of the hindlimb. When the smoothed firing rate exceeds the threshold for the five consecutive time windows, the neural stimulator stimulated the hind limb muscle with a bidirectional pulse (biphasic pulse), which resulted in the synchronization movement between the hind legs and forelimb

The traditional BMI has to acquire a section of neural signal and movement data to train the decoder before translating the neural signals into control commands. However, for paralyzed patients, it is difficult to get the training data. A solution is based on motor imagination in which the paralyzed patients observe the automatic movement of external device while imagining themselves controlling the device. Then, the neural signals and the movement data are used to train decoder. With the

in-depth study of brain plasticity, researchers try to set the mapping between the neural signal and motion states arbitrarily without a training set. Relying on the neural plasticity, the brain modulates its firing pattern to adapt to the artificial mapping and finally control the external device.

In 2005, without the advanced training and neural data for animals, Kipke et al. made use of the brain plasticity and adaptive decoder to build a rat BMI system to control an auditory cursor [9]. In each trial, the rat was given a target tone (10 Hz) and then required to control the auditory cursor to match the target tone. A Kalman decoder was used to translate the multi-channel neural signals into the pitch of an auditory cursor which was fed back to the rat in real time. The initial parameters of the decoder were randomly generated. A block estimation adaptive strategy was used to update the decoder parameters. Each block contained 10 trials. After each block, the pool of the neural signals and pitch of the auditory cursor during the previous 10 trials served as the training set to retrain the decoder. The new decoder was then used in the next block of trials. As the training went on, the success rate increased gradually from the random level.

The experiment carried by Kipke et al. harnessed the plasticity of the brain and adaptive strategy of the decoder to converge the encoding rules of both natural neural system and decoder. Thus, the final neural mapping was based on natural mapping, but not exactly the same. Considering the great role of neural plasticity in the BMI system, researchers have tried to build some BMI systems entirely relying on the plasticity of the neural system. In 2012, Carnema et al. proposed the operative conditioning experiment based on neurons, which artificially set new neuronal encoding rules which are completely different from natural ones. Then, the rat was trained to modulate the activities of neurons to control an auditory cursor [10]. The researchers successfully achieved the two-way control of the auditory cursor with this method and studied the functional coherence and plasticity of cortex and striatum. Specifically, two groups of primary motor cortex (MI) neurons were selected as conditioned neurons, and the rat was trained to control the auditory cursor to reach the high or low threshold by modulating neural firing patterns. The relationship between the pitch of the auditory cursor and the response of the two groups of neurons was opposite: the increased response of the first neural population increased the pitch of the auditory cursor while that of the second neural population reduced the pitch. Therefore, to reach the high pitch target, the rat had to activate the first neural population while suppressing the second one; to reach the low pitch target, the modulation was opposite. The results indicated that the firing patterns of striatal neurons changed as the rat learned to control the auditory cursor and gradually matched the preset encoding rules. Furthermore, the firing pattern of the motor cortex and striatum become more and more similar. The experiment further extended our understanding of neural plasticity and proved that through training the animal could master a new encoding rule which was completely different from natural ones and achieved control of the external device.

In 2014, Widge et al. made a similar operant conditioning experiment to control an auditory cursor [11]. Different from the Carnema's experiment, they only extracted one neuron from the prefrontal cortex (PFC) as the conditioned neuron, and its firing rate was positively related to the pitch of the auditory cursor. The experiment trained the rat to move the auditory cursor to the target within a period of time to and maintain for 500 ms. After training, all rats were able to complete the BMI tasks successfully. The results demonstrated the feasibility of a single neuron in the operant conditioning control of BMI. In 2013, Arduin et al. achieved to train rat to self-drink by modulating single neuron in the motor cortex to control the one-way movement of the water bottle [12]. In the same year, he further improved his experiment and achieved two-way continuous brain control [13].

3.2.2 Bidirectional Recording and Stimulating System for Free Moving Rats

Just as described before, the information pathway of the one-way BMI is from the brain to the external device whose feedback is transmitted back by natural sense such as vision, audition, or touch. The development of intracranial microstimulation (ICMS) provides a new approach to transmit information directly to the brain independent of the natural neural feedback pathways. Recently, the technique of guiding the animal to conduct a specific task by ICMS has become more and more mature. Therefore, researchers tried to build the two-way information interaction between the neural system and the external device, e.g., bidirectional BMI.

The first bidirectional BMI is a hybrid neuro-robotic system connecting the brainstem tissue of lamprey *in vitro* and a moving robot, which was built in Northwest University in 2003 [14]. After that, the bidirectional BMIs based on animal tissue *in vitro* have been widely studied.

In 2012, Vato et al. built a bidirectional BMI *in vivo* on an aesthetic rat. 16-channel microwire arrays were implanted into the primary motor cortex (M1) and primary sensory cortex (S1), respectively [15]. On the "read-out" pathway, the first two principal components of the M1 neural response were used to form a two-dimensional force vector (Fig. 3.3b, c), which drive a simulated point-mass moving in a viscous medium (Fig. 3.3d). On the "write-in" pathway, the position of the point-mass was transformed into one of four stimulus pattern by "Sensory Interface," and each stimulus pattern was produced by a pair of channels of S1 microwire array (Fig. 3.3a). The rat was trained to modulate its M1 neurons firing according to the stimulus feedback to move the point-mass from an arbitrary starting location to the selected equilibrium point.

In 2010, Kipke et al. built a bidirectional BMI based on the awake rat [16]. An abstract task was designed that required the rat to modulate its neural activity and gave the feedback by ICMS. The motor cortex and the visual cortex of the untrained
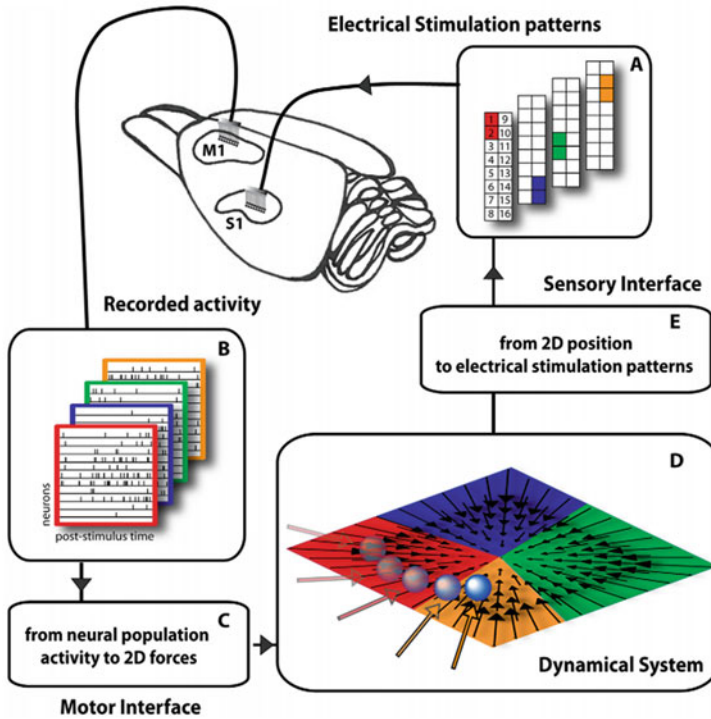
Fig. 3.3 A bidirectional BMI *in vivo* on an aesthetic rat [15]

rat was implanted with multi-channel electrodes. In each trial, the rat maintained its motor cortex ensemble baseline firing rates for 450 ms to begin a trial. Then, the "go" cue was given by ICMS and the rat had to modulate its motor cortex for 450 ms within the 4 s response period in order to receive the food reward. The rat was given continuous feedback via visual cortex ICMS during the response periods that was representative of the motor cortex ensemble dynamics. The results indicated that the rat could master an open-loop control task and build the association between the stimulus and the firing pattern of the motor cortex through a period of training.

Gage et al. designed a more systematic BMI to transform neurons in rats into sounds of different frequencies [9]. For a successful trial, rats need to regulate neuronal activity to reach the target frequency and maintain a certain time. DiGiovanna et al. proposed another BMI adaptation paradigm based on enhanced learning [17]. The goal of the intelligent system was to maximize the final reward after making the action in the intelligent system. The brain cortex uses the intrinsic reinforcement learning mechanism to regulate the relevant neurons, and the machine needs to simulate the corresponding reinforcement learning process. Mahmoudi et al. proposed the concept of symbiotic BMI, which obtained the reward information directly from the NAcc region of the rat brain as feedback to machine enhanced learning [18].

3.2.3 New Exploration of BMIs Researches in Rodent Animals

The BMI technique based on the neural signal recording, encoding, decoding, and ICMS could not only build the artificial open-loop information pathway between the brain and the external device and rebuild or repair some damaged motor function but also achieve the direct communication between the brain and external devices. In 2013, Nicolelis's team in Duke University built a brain-to-brain interface (BTBI) between two rats, which transmitted information from the brain of encoder rat to that of decoder rat [19]. Specifically, the two rats were placed in two separated boxes, and the encoder rat was trained to press one of two levels according to the visual stimulus to receive the water reward. Meanwhile, M1 neural activity was recorded from the encoder rat and transmitted to the decoder rat by ICMS. The decoder rat had to select the same lever pressed by the encoder to get the water reward. Once the decoder rat completed the trial successfully, the encoder rat got an extra reward. This suggested that BTBIs could enable networks of animal's brains to exchange, process, and store information and, hence, serve as the basis for studies of novel types of social interaction and for biological computing devices (Fig. 3.4).

Traditional BMI technique is based on electrophysiology, i.e., neural signal collecting and ICMS. Apart from this, researchers have tried to make use of other techniques to build BMIs. In 2014, Carnema's team in UC Berkley used two-photon imaging to perform a conditional operant experiment on awake rats and control an auditory cursor [20]. The fluorescence value was binned by 200 ms time windows and transmitted to the decoder to get the pitch of auditory cursor. The increase of the first neural ensemble (E1) increased the pitch while the increase of the second neural ensemble (E2) decreased the pitch. The rat was trained to modulate the activity of both E1 and E2 population to maintain the cursor within a baseline range to start a
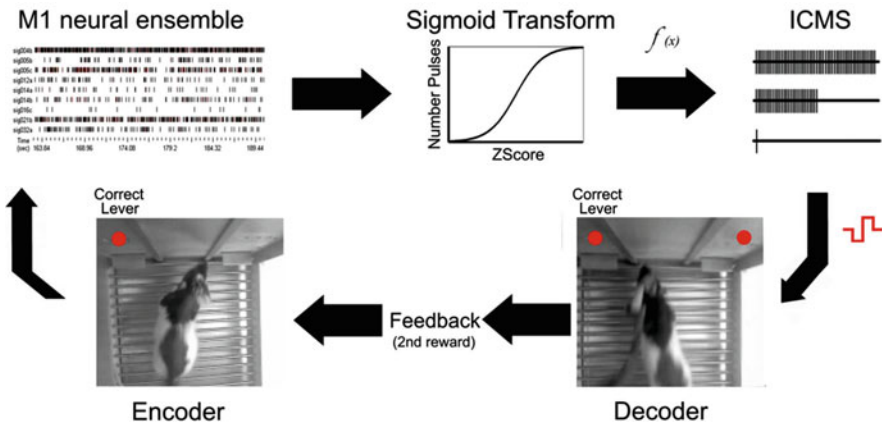

Fig. 3.4 A brain-to-brain interface (BTBI) system demonstrated on animal studies [19]

trial and then moved it to a high threshold within 30 s to complete a trial. This experiment expanded the technique of BMI further.

3.3   BMIs on Non-human Primates

3.3.1   Neural Signal Processing and Neural Decoding

- Neural signal processing

Carmena et al. started studying invasive BMIs in non-human primates (macaques) in 2003, which promoted the rapid development of this technology [21]. Researchers parsed a variety of movement-related parameters from recorded neural signals to control a robotic arm and accomplish reaching and grasp with the visual feedback.

In 2008, Schwartz and his colleagues implemented that the monkey could perform self-feeding in three-dimensional space with its arm fixed [22]. Researchers sent the food to a monkey by equipment during the experiment. While the neural signals of the monkey were decoded to control a robotic arm, the monkey could learn to grip the food and feed itself. The research was of great significance in that it reconstructed the motor function of arms in three-dimensional space.

The recording quality of neural activities is very important for neural signal analysis. The collecting and recording of neural signals are becoming more accurate with the development of the microelectrodes or probes. Nowadays, there exist commercial electrodes that were approved by the Food and Drug Administration (FDA) to be utilized even on human beings. The microelectrodes can be implanted into several brain cortex to collect multi-channel neural activities. One of the key questions in BMI is to decode the multi-channel neural activities efficiently and accurately.

Neural signals contain some noises that are irrelative to the task, which raises the difficulty of analyzing the model parameters, the complex of information learning models, and real-time decoding. So it is essential to decrease the scale of neural activities and extract the valid part of neural activities.

Chapin et al. utilized the principal component analysis (PCA) to reduce the dimensionality of the neural activities to one. They established an analytical model to predict the trajectory of the forearm [5]. The PCA reduces the dimensionality by eliminating the correlation between the signals, and the dimensionality reduction process might miss some useful information. Wessberg et al. used the Neuron-Dropping Analysis to achieve information reduction [23]. This method is target oriented with high computational complexity.

- Neural signal decoding

The studies on the neural population decoding in BMI can be divided into two categories. The first method assumes that the relationship between neural activities and movement conforms to the linear model, such as population vector and related

algorithm [22, 24, 25], Wiener filter-based analysis method [21, 26, 27], Kalman filter-based analysis method [28–30], Fisher linear discriminant based method, and maximum likelihood estimation method. Although the linear analytic model has achieved good results in relatively simple decoding applications, recent studies have found that the nonlinear method has a more reasonable analogy to the real nervous system. In recent years, many attempts have been made to use non-linear methods for neural decodings, such as particle filter [31, 32] and unscented Kalman filters [33, 34].

The above researches have established a good foundation for neural population decoding. However, on account of the complexity of the brain system, it is necessary to achieve efficient and accurate neural population decoding. First, the brain cortex is a plastic system, so the time-varying neural activities raise great challenges to the traditional static information processing method; second, the neural activities show similar features in both time domain and frequency domain. Neural activities from limited brain cortex and frequency band can hardly represent the whole brain system. So the exploration of efficient, dynamic, and joint analytic models and algorithms is still an open question for BMI.

3.3.2 Closed-Loop Decoding for Online Control

The ideal BMI aims to achieve bi-directional information interaction between the brain and the external devices. In recent years, with the development of neural signal analysis technology and neural stimulation technology, researchers have focused their attention on bi-directional closed-loop BMI system research.

Novellino et al. combined *in vitro* cultured rat neurons and embedded signal processing platform to build a bi-directional BMI system prototype. The system used the signals of the neurons to control the movement of a car. There is stimulus feedback to the neurons when the car hits the obstacle. So the bi-directional interaction between neurons and the external environment was established [35]. Doherty et al. gave monkey direction instruction by electrical stimulation on the sensory cortex. Then, the direction selection task was achieved by real-time decoding of the motor cortex. The results showed that the monkey could obtain external information and output control sequences to the external devices [36]. In addition, Ye, Rolston, and Venkatraman et al. developed a number of stimulated neural signal acquisition systems that combine both neural stimulation and recording techniques to achieve a preliminary bi-directional communication system. Above studies showed that the bi-directional BMI has great application potential in developing disease treatment and understanding brain network mechanism [37–39].

Intracortical electrical stimulation, as a somatosensory information input, not only establishes a new information transfer path between brain cortex and external environment but may also improve the performance of the vision-based feedback BMI by information integration. Preliminary studies have shown that the electrical

stimulation can not only instruct the movement of animals but also feedback the movement information to the brain cortex.

O'Doherty et al. trained monkeys to finish the movement direction selection task with tactile feedback and electrical stimulation [36, 40]. After two weeks, the result showed that the natural tactile feedback in the experiment and cortical electrical stimulation provide almost the same amount of information. At the same time, a considerable number of studies have confirmed that multi-modal feedback can provide more information and improve the performance of BMI. Nicoliles et al. found that visual feedback is very important for the motor control BMI and visual feedback coupled with tactile feedback can further improve the overall performance of the system; [4] Suminski et al. studied the natural somatosensory feedback and the mechanism of visual and found that somatosensory feedback is more likely to affect the neural activity of the motor cortex than visual feedback, and more importantly, the combination of two different modes of feedback can provide more information [41]. Further results showed that the dual-mode feedback could significantly improve the control performance of the BMI when the feedback of the two modes is consistent.

Several studies have shown that the plasticity of the brain cortex is closely related to BMI. In the process of neural decoding, neural activity is a dynamic learning process, and the mapping between the output signal (usually the neural signals) and the input signal (usually the kinematic data of the limb) is changing over time. In previous BMI studies, results have shown that the activity of a single neuron may change with the decoding algorithm. Ganguly et al. conducted a preliminary exploration of the adaptability and plasticity of the neural population in the context of BMI. Their findings suggest that the cerebral cortex has a very prominent learning ability and can quickly adapt to mutations in the decoding model [42].

Other researchers also found that cortical electrical stimulation can also affect the plasticity of the cortex. Moritz et al. have shown that functional connectivity can be established between the two neurons by cortical electrical stimulation, which provides a new idea for nerve repair [43]. Rebesco et al. have shown that cortical electrical stimulation can not only serve as an information input, but also can effectively enhance the functional connection of nerve, and eventually lead to behavioral changes, and this plasticity may be associated with natural stimulus caused by Hebby learning mechanism [44].

The study of the changes of the neuron population under the condition of invasive BMI would help us understand the plastic mechanism of the brain and construct the bi-directional closed-loop interaction. The use of the plasticity of the brain, combined with machine learning, can improve the performance of BMI. Taylor et al. used a mutual adaptation algorithm on the rhesus monkey's three-dimensional cursor control task and updated the mapping of neuronal activity to the movement of the cursor by iterating the changes in neuron during the learning process [24].

3.4   Pilot BMIs Studies in Clinic Researches

3.4.1   Invasive BMI System Based on Spike Signals from Human Brain

The ultimate goal of brain-machine interface development is to realize the practical application of clinical patients. Currently, there are mainly two types of invasive BMIs clinical studies. One type of BMIs employed fully implantable microelectrode arrays to collect the spike signals of neuron populations. This method has the advantage of acquiring high spatial and temporal resolution signals that contain rich information of movement and can be used to realize the high-precision motion control. However, due to the need of microelectrode array implanted directly into the cerebral cortex, the damage induced by implantation makes it difficult to achieve long-term application; the other type is a semi-invasive BMIs, which mainly used the electrodes placed on the surface of the cortex, collecting field potential signals from the cerebral cortex. Its damage to the brain is relatively small, but the spatial resolution of this type of signal is relatively lower than that of the invasive microelectrode array. Each method has its advantages and disadvantages.

In the past two decades, many BMI system has also been developed for clinical transformations. In 1998, Philip Kennedy and Roy Bakay from Emory University started their researcher invasive BMIs [45]. Their study implanted a neurotrophic electrode into a patient who had severe amyotrophic lateral sclerosis (ALS) for 2.5 years prior to the implantation and was ventilator-dependent for 1.5 years. The electrode consists of a hollow glass conical tip about 1.5 mm in length which contains two gold recording wires. They recorded action potentials in the patient's brain over several months. By decoding the action potential, the patient ultimately was able to control the clicking of a computer mouse. This study was the first clinical study of invasive BMI which achieve the high-quality neural signal recording and movement output decoding, which laid the foundation for the development of invasive BMI.

With the development of the electrode technology, many researchers began to study the clinical BMI experiments based on the microelectrode arrays. In 2006, the group of Donoghue achieved a BMI for movement intent decoding for a tetraplegic patient [29]. The patient in this study was a 25-year-old male who had sustained knife wound, the spinal cord between cervical vertebrae C3–C4 of the patient was transected, which results in complete tetraplegia. During the research, a 96-ch microelectrode array was implanted in the arm area of the primary motor cortex of the patient for neural signal recording. The BMI system decoded the different direction movement imagination and was finally used to control a computer mouse in a two-dimensional plane. By making use of this BMI system, the patient was able to open the e-mail, draw figures using a paint program, play video games, and even adjusted the volume, channel, and power to his television. This study was the first attempt to make use of microelectrode arrays in clinical BMI use, which provides valuable research experience for the clinical transformation of invasive BMI. Then,

the group further study the long-term stability performance of the BMI system in chronic application [46]. They found that the BMI system still kept a high system performance even 1000 days after the microelectrode arrays implantation. Though there were still many problems such as electrode aging and signal attenuation which may affect the long-term use of BMI system, this study proved that the BMI based on microelectrode array could keep a stable system performance for 2–3 years. In 2008, other two subjects participated in the BMI experiment. One participant was a 54-year-old woman who had thrombosis of the basilar artery and extensive pontine infarction 9 years prior to trial recruitment while another participant was a 37-year-old man who had been diagnosed with ALS for about 6 years. The two participants successfully achieved the online control of a computer mouse by using the BMI system after some training sessions. This result proved that the BMI system might be a benefit to the patients who suffer long-term motor dysfunction. Then, the further study of robot hand control by BMI was carried out in 2012 [29]. A stroke patient and the 54-year-old woman described above participated in this study. The system successfully decoded the three-dimensional trajectory of the hand movement. The brain activity of M1 was extracted to control the movement and grasp of a robot hand. The 54-year-old woman successfully used the robot hand to grasp a coffee cup and move to her own mouth to drink the coffee by absolutely brain control. This study shows us the prospects of invasive BMI system in daily life application.

The group of Andrew B Schwartz also had some research on clinical invasive BMI. They set up a clinical BMI system based on the microelectrode array in 2013 [46]. A 52-year-old woman who was tetraplegic participant in this study. Two 96-ch microelectrode arrays were implanted in her arm area of premotor cortex (PM), and the participant had to control a prosthesis using her brain signals by the BMI system after a 13-weeks' training. The participant had to perform a seven-dimensional sequence task including three-dimensional position, rotating the palm in one of six directions (possible orientations included pronation–supination $\pm45°$, ulnar-radial deviation $\pm20°$, and flexion-extension $\pm45°$ of the wrist), or a grasp target (open or closed hand). The participant used the prosthesis under full brain control to do nine tasks (selected from 19 possible tasks) on the action research arm test (ARAT), which is an assessment of the unilateral upper limb function used commonly in patients who have had a stroke. This study showed a high-performance BMI system with multi-degree of freedom, which was difficult to achieve by non-invasive BMI. Then in 2015, the group of Schwartz further achieved the ten-dimensional anthropomorphic arm control in human BMI [47]. The ten dimensions contain translation (x,y,z), orientation ($\theta x, \theta y, \theta z$), pinch (p), scoop (s), finger ab/adduction (f), and thumb opposition/extension (t). This study found that individual motor cortical neurons encode many parameters of movement and that high-dimensional operation of prosthetic devices can be achieved with simple decoding algorithms, which shows the invasive BMI has the potential to control high-degree freedom prosthetic devices.

In recent years, more and more fully invasive BMI system has been studied. Richard A. Andersen et al. set up a BMI system based on the signals in posterior parietal cortex (PCC) [48]. PCC is regarded as being responsible for the process of

high-level movement planning. This study implanted a microelectrode array to the PCC and successfully decoded the different object and trajectory of motor imagination. Bouton et al. study the hand motor function rehabilitation based on invasive BMI [49]. The study participant was a 24-year-old male with quadriplegia from cervical spinal cord injury sustained in a diving accident. The researcher decoded the neuronal activity and control activation of the participant's forearm muscles through a high-resolution neuromuscular electrical stimulation system. Through the system, the participant complete a Grasp-pour-and-stir functional movement task, which need the participant to opening his hand (a), grasping the glass bottle (b), pouring its contents (dice) into a jar (c), grasping a stir stick from another jar (d), transferring the stir stick without dropping it (e), and using it to stir the dice in the jar (f). These results have significant implications in advancing neuroprosthetic technology for people worldwide living with the effects of paralysis, which extended the application of BMI.

3.4.2   Invasive BMI System Based on Clinic ECoG Signals

We can obtain high temporal-spatial resolution brain signals by implanting microelectrode array to decode higher degrees of freedom and finer arm motion and achieve more natural and complex arm movement, which is the goal and direction of BMI. However, the fully implantable microelectrode arrays may cause damage to the blood-brain barrier, inflammatory response, and immune reaction, which may produce a series of biological and non-biological effects, leading to the attenuation and loss of the brain signals. It limits the application of implantable microelectrode array in the clinical BMI studies. On the contrary, the electrocorticogram (ECoG) electrode is located under the subdural and on the surface of cortical, which does not cause damage to the cerebral cortex. The neuronal damage can be completely avoided. Although the spatial resolution of the ECoG signal is slightly lower than that of the microelectrode array, the ECoG has a fewer surgical risk and better long-term stability of the signal. So the ECoG is relatively more meaningful for the clinical application of BMI. In the past few years, the study of clinical BMI based on ECoG signals had made great progress.

As early as in 2004, Gerwin Schalk, Eric C Leuthardt, Daniel W Moran ,and Jeffrey G Ojemann started the study of ECoG-based clinical BMI [49]. All the participants in the study were clinical epilepsy patients in whom subdural electrode arrays were implanted for three to eight days in preparation for surgery to remove an epileptic focus. The ECoG arrays located in sensorimotor cortex. Over brief training, the four participants then used these signals to master closed-loop control and to achieve success rates of 74–100% in a one-dimensional (1-D) binary task. Further analysis showed that ECoG also has a correlation with the direction of the two-dimensional joystick movement. Then in 2006, the same group set up a closed-loop BMI in paralyzed patients [50]. There are four participants, and the electrode covered their sensorimotor cortex and some speech cortex areas. In order

to identify brain signals used for BCI control, the subjects were asked to perform paired blocks of repetitive hand/tongue, foot/shoulder movements, or repetitive speaking of the word "move" (screening procedure). From the spectral analysis, the researchers identified the locations and frequency bands in which amplitude was different between the task and rest, which will be selected in the subsequent closed-loop BMI. The participants received online feedback that consisted of the 1-D cursor movement that had shown correlation with tasks during the screening procedure. Their study showed that visual cursor feedback could effectively improve the success rate of the task. The work of Schalk was the first attempt to set up ECoG-based clinical BMI, which proved that ECoG was an available signal source in clinical BMI use.

The group of Schalk then used the ECoG signal to decode the trajectory of the cursor in two-dimensional plane [51]. The study included five patients with intractable epilepsy. The subjects were asked to use a joystick to move a white cursor in two dimensions to track a green target. By decoding the kinematic parameters from ECoG, the study showed that the correlation coefficients (r) between the actual and decoded kinematic parameters were as high as 0.7, which proved that ECoG-based BMI was feasible in two-dimensional trajectory decoding. Carsten Mehring et al. did similar work in 2008 [56]. Six patients suffering from intractable pharmaco-resistant epilepsy were included in their study, and the electrical stimulation through the electrode grid was performed to identify the functional mapping of the cortex. A Kalman filter was applied to decode the two-dimensional trajectory of the arm, and their result showed that the low-frequency component of ECoG has better performance for the two-dimensional trajectory decoding. In 2013, Yasuhiko Nakanishi and Takufumi Yanagisawa from Japan successfully decoded the three-dimensional trajectory of arm movement using ECoG signals [52]. There were three participants in this study; two of them had spastic paresis and weakness due to stroke, and the other was diagnosed with intractable epilepsy. The participants were asked to reposition three blocks one by one and clockwise at the corners of a square table, and an optical motion capture system was used to record the arm movement. Their work successfully predicted three-dimensional arm trajectories in time series from ECoG signals, which proved that we could extract the motion parameters of three-dimensional arm movement from ECoG signals.

In addition to continuous arm movement trajectory decoding, some teams have used ECoG signals to decode different finger movement and gestures. In 2009, Schalk et al. proved that it is possible to decode the flexion of individual fingers using ECoG signals [53]. A data glove (5DT) was used to record the flexion of each finger in this study. Their result showed that there was a different spatial pattern of ECoG signals for different finger movement and the LMP, and high gamma component of ECoG could decode the flexion of each finger with best decoding performance. Then in 2010, Nitish V. Thakor et al. found that ECoG signals correlated with finger positions [54]. Their study indicated that when the subjects engaged in slow and deliberate grasping motions, the amplitudes of the low-pass ECoG (LMP) over specific electrodes were correlated with the position of individual fingers. The work of Mehring and Shenoy both showed that ECoG signals could be

used to decode different gestures [55–58]. Mehring's experiment requires subjects to grasp different objects with different gestures; and in Shenoy's experiment, the subject was asked to perform several specific gestures, which require different fingers to bend and stretch. Both experiments proved that ECoG signal was able to decode different gestures.

For that ECoG signals could be used to decode different motion parameters, some studies have implemented prosthesis control based on ECoG signals. In 2013, Matthew S. Fifer et al. trained two human subjects to achieve simultaneous neural control of reaching and grasping movements with a dexterous robotic prosthetic arm [59]. The group of Toshiki Yoshimine from Japan also used human ECoG signal to real-time control of a prosthetic hand [60]. Two decoders were trained to control the prosthetic hand. The first decoder was trained to classify the movement state R or M, and the second was trained to predict the types of performed movement with the state M. Based on the two decoders, the subject could asynchronously control of the prosthetic hand to perform three types of hand movement. In a further study, the subject could control the prosthetic hand to perform more tasks such as grasping, thumb flexion, elbow flexion, pinching, hand-opening, elbow flexion, and elbow extension [61]. This study tested the clinical BMI in a large number of subjects (12 subjects included) and achieved prosthetic hand control for multiple types of gestures. Wei Wang et al. used ECoG signals to control of 3-D cursor movement and 3-D prosthetic arm movement [62]. The participant in this study was a 30-year-old man with tetraplegia; he was asked to observe hand and arm movements of a virtual character on an LCD screen and simultaneously attempted the same movement. The participant successfully controlled the prosthetic arm hitting physical targets. This study indicated that we could extract the information of motion intent from ECoG signals. Another application of clinical BMI was a brain-control typing system. Ramsey et al. set up a BMI-based computer typing program for a locked-in patient with ALS [63]. The ALS patient was a 58 years old woman, and four subdural electrode strips were implanted in her brain motor cortex. The signal recording, conversion, and transmission devices of the typing system were fully implanted, which make the BMI system more simple and convenient for use. Portability and simplification have gradually become a key factor in the clinical transformation of the BMI system.

The key factor in invasive BMI is to improve the decoding performance of the system as much as possible. ECoG arrays usually cover a wide range, and ECoG signals have a wide frequency range, so it's meaningful to set up a BMI of ECoG based on multi-frequency band and multi-brain area. Ramsey et al. set up a BMI to decode gesture and compared the decoding performance of M1, S1, and whole sensorimotor cortex (M1 + S1) [63]. The result showed that decoding performance of M1 and S1 was similar, while the decoding performance of the whole sensori-motor cortex was significantly better, which means that the BMI of ECoG based on the multi-brain area may improve the system performance. Hotson et al. study the decoding performance of different frequency component of ECoG [64]. They divided the ECoG signal to seven frequency band, 0–4 Hz, 4–8 Hz, 7–13 Hz, 14–30 Hz, 30–50 Hz, 70–110 Hz, and 130–200 Hz, and used the signals of the

seven single frequency band and multi-frequency band to decode the arm trajectory, respectively. Their result showed that multi-frequency band has the best decoding performance for all subjects. The above studies showed that take advantage of the ECoG signals of different brain area and different frequency band was of great benefit to improve the decoding performance.

3.5 Opportunities and Challenges

3.5.1 Opportunities

- Restoration of motor function in the paralyzed

One of the most important applications of BMIs is the restoration of motor function in the paralyzed. Two main reasons that lead to paralysis are descending corticospinal tract injury caused by spinal cord injury and neuromuscular dysfunction. The paralyzed suffer great physical and psychological trauma. One of the reasons for the rise of the technology of BMIs exactly is to help the paralyzed restore motor function. Researchers have conducted a series of experiments on non-human primates and human and have made some progress, laying a good foundation for the clinical practice of BMIs.

Capogross and his colleagues alleviated gait deficits after a spinal cord injury in non-human primates in 2016 [65]. First, unilateral spinal cord injury model was established by the side cutting the middle section of the monkey's spinal cord. Second, the monkeys were implanted with a microelectrode array into the leg area of the left motor cortex and with electrical stimulators into the lower spinal cord segment and the spinal cord segment associated with motion control of lower limbs. During the movement of monkeys, neural signals were used to decode the movement of lower limbs. Decoding results were then sent to control electrical stimulators to simulate spinal cord, consequently alleviating gait deficits of lower limbs.

- BMIs as a potential therapy for nerve recovery

Since the 1990s, BMIs have been mainly focused on two aspects: (1) The field of neuroscience, in which the physiological characteristics of the neural circuits are studied by designing new experimental paradigms. (2) The field of neural engineering, in which technologies and means of restoring motor function for the paralyzed are studied. Recent clinical studies have found that the BMIs used as one of the potential tools for neurorehabilitation. The results have shown that long-term BMIs training combined with physical therapy has a significant effect on the recovery of motor function. So does BMIs training combined with virtual reality system.

In 2016, Donati conducted 12 months training with a multi-stage BMI-based gait neurorehabilitation paradigm aimed at restoring locomotion in eight paraplegic patients [66]. This paradigm combined intense, immersive virtual reality training, enriched visual-tactile feedback, and walking with two EEG-controlled robotic

actuators, including a custom-designed lower limb exoskeleton capable of delivering tactile feedback to subjects. Following 12 months of training with this paradigm, all eight patients experienced neurological improvements in somatic sensation. Patients also regained voluntary motor control in key muscles below the SCI level. As a result, 50% of these patients were upgraded to an incomplete paraplegia classification. Donati and his colleagues hypothesized that this unprecedented neurological recovery results from both cortical and spinal cord plasticity triggered by long-term BMI usage.

3.5.2 Challenges

- Biocompatibility and long-term stability of electrodes

Biocompatibility and long-term stability of electrodes is the key that determines whether BMIs technology can be widely applied to the clinic. Biocompatibility of electrodes is closely related to the long-term stability of recording. Currently, the biocompatibility of implanted microelectrodes is poor. And with the increase of implant time, it's easy to induce the rejection of biological tissue. The hyperplastic tissue covers the surface of the electrode, resulting in a reduction in the quality of the signal recorded by the electrodes. Simultaneously, the impedance variations caused by the corrosion and degradation of the electrode materials will also influence the long-term stability of recording.

Researchers have proposed some relevant strategies to enhance the stability of electrode recording, including electrode improvement in size, geometry, shape, coating, and materials. The results of the study confirm that smaller electrode size can achieve a relatively long signal recording time. At present, researchers have focused on the feasibility of extracellular or intracellular neural recording with carbon nanotube electrodes in that they have low impedance, and are capable of recording the activities of a single unit. Another focus is a bioactive coating, which has the effect of slowing the rejection and enhancing the stability of the signal recording. In addition, the bioactive coating can reduce the response of glial cells and increase the survival rate of peripheral nerve cells.

- The portability of BMIs system

In real life, a BMI operator may not carry a large number of signal cables and signal acquisition equipment. It is important to study how to simplify the BMI system or make it more portable. Ramsey et al. developed a highly integrated BMI system which could be fully implanted into a patient with late-stage amyotrophic lateral sclerosis (ALS) [63]. The patient could accurately and independently controlled a computer typing program with the assistance from this fully implanted BMI system. The future BMI system could be further integrated wireless communication and power. Another critical factor in the clinical application of invasive BMI is the decoding performance of the system. In practical applications, there might be no

fault tolerant space so that we have to improve the decoding performance of a BMI system and minimize the decoding error rate as much as possible. The studies of Ramsey and Hotson et al. have proved that combining the neural signals from different brain regions and frequency components is of great significance to improve the decoding performance of a BMI system [63, 64]. In addition, looking for a better feature, exploring the neural mechanism underlying movement control, and developing decoding algorithm more in line with the neural characteristics will play a key role to improve the performance of the BMI system.

Clinical translation of invasive BMI is an essential process before a BMI system could be brought into clinical application and even real-life application. We still need to solve some critical issues when translating the BMI system from the lab to the bed of patients and form a stable and mature application system. When the BMI system could be applied to reallife application, the brain control as Avatar will no longer be fantasy.

References

1. Andersen RA et al (2014) Toward more versatile and intuitive cortical brain–machine interfaces. Curr Biol 24(18):R885–R897
2. Donoghue JP (2008) Bridging the brain to the world: a perspective on neural interface systems. Neuron 60(3):511–521
3. Hatsopoulos NG, Donoghue JP (2009) The science of neural interface systems. Annu Rev Neurosci 32:249–266
4. Lebedev MA, Nicolelis MAL (2006) Brain-machine interfaces: past, present and future. Trends Neurosci 29(9):536–546
5. Chapin JK et al (1999) Real-time control of a robot arm using simultaneously recorded neurons in the motor cortex. Nat Neurosci 2(7):664–670
6. Lee Y et al (2009) Classification of BMI control commands from rat's neural signals using extreme learning machine. Biomed Eng Online 8:29
7. Manohar A et al (2012) Decoding hindlimb movement for a brain machine interface after a complete spinal transection. PLoS One 7(12):e52173
8. Alam M et al (2014) A brain-machine-muscle interface for restoring hindlimb locomotion after complete spinal transection in rats. PLoS One 9(8):e103764
9. Gage GJ et al (2005) Naive coadaptive cortical control. J Neural Eng 2(2):52–63
10. Koralek AC et al (2012) Corticostriatal plasticity is necessary for learning intentional neuroprosthetic skills. Nature 483(7389):331–335
11. Widge AS, Moritz CT (2014) Pre-frontal control of closed-loop limbic neurostimulation by rodents using a brain-computer interface. J Neural Eng 11(2):024001
12. Arduin PJ et al (2013) "Master" neurons induced by operant conditioning in rat motor cortex during a brain-machine interface task. J Neurosci 33(19):8308–8320
13. Arduin PJ et al (2014) Bidirectional control of a one-dimensional robotic actuator by operant conditioning of a single unit in rat motor cortex. Front Neurosci 8:206
14. Kositsky M et al (2003) Dynamical dimension of a hybrid neurorobotic system. IEEE Trans Neural Syst Rehabil Eng 11(2):155–159
15. Vato A et al (2012) Shaping the dynamics of a bidirectional neural interface. PLoS Comput Biol 8(7):e1002578

16. Marzullo TC et al (2010) Development of closed-loop neural interface technology in a rat model: combining motor cortex operant conditioning with visual cortex microstimulation. IEEE Trans Neural Syst Rehabil Eng 18(2):117–126
17. DiGiovanna J et al (2009) Coadaptive brain-machine interface via reinforcement learning. IEEE Trans Biomed Eng 56(1):54–64
18. Mahmoudi B, Sanchez JC (2011) A symbiotic brain-machine interface through value-based decision making. PLoS One 6(3):e14760
19. Pais-Vieira M et al (2013) A brain-to-brain interface for real-time sharing of sensorimotor information. Sci Rep 3:1319
20. Clancy KB et al (2014) Volitional modulation of optically recorded calcium signals during neuroprosthetic learning. Nat Neurosci 17(6):807–809
21. Carmena JM et al (2003) Learning to control a brain-machine interface for reaching and grasping by primates. PLoS Biol 1(2):E42
22. Velliste M et al (2008) Cortical control of a prosthetic arm for self-feeding. Nature 453 (7198):1098–1101
23. Wessberg J et al (2000) Real-time prediction of hand trajectory by ensembles of cortical neurons in primates. Nature 408(6810):361–365
24. Taylor DM, Tillery SIH, Schwartz AB (2002) Direct cortical control of 3D neuroprosthetic devices. Science 296(5574):1829–1832
25. Wahnoun R, He J, Helms TS (2006) Selection and parameterization of cortical neurons for neuroprosthetic control. J Neural Eng 3(2):162–171
26. Kim S et al (2008) Neural control of computer cursor velocity by decoding motor cortical spiking activity in humans with tetraplegia. J Neural Eng 5(4):455–476
27. Hochberg LR et al (2006) Neuronal ensemble control of prosthetic devices by a human with tetraplegia. Nature 442(7099):164–171
28. Wu W et al (2003) Neural decoding of cursor motion using a Kalman filter
29. Hochberg LR et al (2012) Reach and grasp by people with tetraplegia using a neurally controlled robotic arm. Nature 485(7398):372–375
30. Gilja V et al (2012) A high-performance neural prosthesis enabled by control algorithm design. Nat Neurosci 15(12):1752–1757
31. Brockwell AE, Rojas AL, Kass RE (2004) Recursive bayesian decoding of motor cortical signals by particle filtering. J Neurophysiol 91(4):1899–1907
32. Shoham S et al (2005) Statistical encoding model for a primary motor cortical brain-machine interface. IEEE Trans Biomed Eng 52(7):1312–1322
33. Li S, Li J, Li Z (2016) An improved unscented Kalman filter based decoder for cortical brain-machine interfaces. Front Neurosci 10:587
34. Li Z et al (2009) Unscented Kalman filter for brain-machine interfaces. PLoS One 4(7):e6243
35. Novellino A et al (2007) Connecting neurons to a mobile robot: an *in vitro* bidirectional neural interface. Comput Intell Neurosci 2007:12725
36. O'Doherty JE et al (2011) Active tactile exploration using a brain-machine-brain interface. Nature 479(7372):228–U106
37. Ye X et al (2008) A portable telemetry system for brain stimulation and neuronal activity recording in freely behaving small animals. J Neurosci Methods 174(2):186–193
38. Rolston JD, Gross RE and Potter SM (2009) NeuroRighter: closed-loop multielectrode stimulation and recording for freely moving animals and cell cultures. Conf Proc IEEE Eng Med Biol Soc, 2009:6489–6492
39. Venkatraman S and Carmena JM (2011) Active sensing of target location encoded by cortical microstimulation. IEEE Trans Neural Syst Rehabil Eng, 19(3):317–324
40. O'Doherty JE et al (2011) Active tactile exploration using a brain-machine-brain interface. Nature, 479(7372):228–231
41. Suminski AJ et al (2010) Incorporating Feedback from Multiple Sensory Modalities Enhances Brain-Machine Interface Control. Journal of Neuroscience 30 (50):16777–16787

42. Karunesh Ganguly, Jose M. Carmena and James Ashe (2009) Emergence of a Stable Cortical Map for Neuroprosthetic Control. PLoS Biology 7(7):e1000153
43. Chet T Moritz and Eberhard E Fetz (2011) Volitional control of single cortical neurons in a brain–machine interface. Journal of Neural Engineering 8(2):025017
44. James M Rebesco and Lee E Miller (2011) Enhanced detection threshold for cortical stimulation produced by Hebbian conditioning . Journal of Neural Engineering 8(1):016011
45. P.R. Kennedy et al (2000) Direct control of a computer from the human central nervous system. IEEE Transactions on Rehabilitation Engineering 8(2):198–202
46. Collinger JL, Wodlinger B, Downey JE, Wang W, Tyler-Kabara EC, Weber DJ, McMorland AJC, Velliste M, Boninger ML, Schwartz AB (2013) High-performance neuroprosthetic control by an individual with tetraplegia. Lancet 381(9866):557–564
47. Wodlinger B, Downey JE, Tyler-Kabara EC, Schwartz AB, Boninger ML, Collinger JL (2015) Ten-dimensional anthropomorphic arm control in a human brain−machine interface: difficulties, solutions, and limitations. J Neural Eng 12(1):016011
48. T. Aflalo et al (2015) Decoding motor imagery from the posterior parietal cortex of a tetraplegic human. Science 348(6237):906–910
49. Eric C Leuthardt et al (2004) A brain–computer interface using electrocorticographic signals in humans. Journal of Neural Engineering 1(2):63–71
50. E.C. Leuthardt et al (2006) Electrocorticography-Based Brain Computer Interface—The Seattle Experience. IEEE Transactions on Neural Systems and Rehabilitation Engineering 14(2):194–198
51. G Schalk et al (2007) Decoding two-dimensional movement trajectories using electrocorticographic signals in humans. Journal of Neural Engineering 4(3):264–275
52. Yasuhiko Nakanishi et al (2013) Prediction of Three-Dimensional Arm Trajectories Based on ECoG Signals Recorded from Human Sensorimotor Cortex. PLoS ONE 8(8):e72085
53. J Kubánek et al (2009) Decoding flexion of individual fingers using electrocorticographic signals in humans. Journal of Neural Engineering 6(6):066001
54. Acharya S et al (2010) Electrocorticographic amplitude predicts finger positions during slow grasping motions of the hand. J Neural Eng 7(4):046002
55. Pistohl T et al (2008) Prediction of arm movement trajectories from ECoG-recordings in humans. J Neurosci Methods 167(1):105–114
56. Pistohl T et al (2012) Decoding natural grasp types from human ECoG. NeuroImage 59(1):248–260
57. Pistohl T et al (2013) Grasp detection from human ECoG during natural reach-to-grasp movements. PLoS One 8(1):e54658
58. Chestek CA et al (2013) Hand posture classification using electrocorticography signals in the gamma band over human sensorimotor brain areas. J Neural Eng 10(2):026002
59. Fifer MS et al (2014) Simultaneous neural control of simple reaching and grasping with the modular prosthetic limb using intracranial EEG. IEEE Trans Neural Syst Rehabil Eng 22(3):695–705
60. Yanagisawa T et al (2011) Real-time control of a prosthetic hand using human electrocorticography signals. J Neurosurg 114(6):1715–1722
61. Yanagisawa T et al (2012) Electrocorticographic control of a prosthetic arm in paralyzed patients. Ann Neurol 71(3):353–361
62. Wang W et al (2013) An Electrocorticographic brain Interface in an individual with tetraplegia. PLoS One 8(2):e55344
63. Vansteensel MJ et al (2016) Fully implanted brain–computer Interface in a locked-in patient with ALS. N Engl J Med 375(21):2060–2066
64. Hotson G, Fifer MS, Acharya S, Benz HL, Anderson WS, Thakor NV, Crone NE, Robin DA (2014) Coarse Electrocorticographic decoding of Ipsilateral reach in patients with brain lesions. PLoS One 9(12):e115236
65. Capogrosso M, Milekovic T, Borton D, Wagner F, Moraud EM, Mignardot J-B, Buse N, Gandar J, Barraud Q, Xing D, Rey E, Duis S, Jianzhong Y, Ko WKD, Li Q, Detemple P,

Denison T, Micera S, Bezard E, Bloch J, Courtine G (2016) A brain–spine interface alleviating gait deficits after spinal cord injury in primates. Nature 539(7628):284–288

66. Donati AR et al (2016) Long-term training with a brain-machine Interface-based gait protocol induces partial neurological recovery in paraplegic patients. Sci Rep 6:30383

Chapter 4
Peripheral Neural Interface

Peng Zhang, Xiao Li, Dingyin Hu, Qiuxia Lai, Yuanyuan Wang, Xuan Ma, Qi Xu, Wei Li, Jian Huang, and Jiping He

Abstract Peripheral nervous system, widely spread in the whole body, is the important bridge for the transmission of neural signals. Signals from the central nervous system (brain and spinal cord) are transmitted to different parts of the body by the peripheral nerves, while along the way they also feedback all kinds of sensory information. Certain level of information integration and processing also occurs in the system. It has been shown that neural signals could be extracted from the distal end of the stump, indicating that the bridge is still effective after limb damage or amputation, which is the neurophysiological basis for the research and development of peripheral nerve interface for the prosthetic system.

Keywords Peripheral nervous · Motor information · Sensory information · Nerve regeneration and repair

4.1 Introduction

The physical disability can be caused by many factors such as accidents, wars, and natural disasters besides the primary malignant tumors in the limb, such as thromboangiitis obliterans, diabetes, and other diseases caused by tissue infection

P. Zhang · X. Li · D. Hu · Q. Lai · Y. Wang · X. Ma · Q. Xu · W. Li · J. Huang
Neural Interface and Rehabilitation Technology Research Center, School of Automation, Huazhong University of Science and Technology, Wuhan, China

J. He (✉)
Neural Interface and Rehabilitation Technology Research Center, School of Automation, Huazhong University of Science and Technology, Wuhan, China

Beijing Advanced Innovation Center for Intelligent Robot and System, School of Mechatronical Engineering, Beijing Institute of Technology, Beijing, China

Center for Neural Interface Design, School of Biological and Health Systems Engineering, Arizona State University, Tempe, AZ, USA
e-mail: Jiping.He@asu.edu

necrosis, which may also lead to amputation. According to the data from the National Bureau of Statistics in 2006, there are 24.12 million people with various physical disabilities in China, accounting for 29.07% of the total number of disabled people. For these persons with physical disability, the movement function restoration of hand and upper limb is particularly important. Developing novel intelligent prostheses and corresponding control methods can help them fetch food, grasp different objects, and restore important motor functions in their daily life, thus improving their life quality and even helping them return to work, which is of great significance to social development and stability.

Many amputees are not willing to wear and use traditional prostheses because of their limited functions and degrees of freedom (DoF). In recent years, some intelligent prostheses with excellent and reliable performance and high DoF have been developed, such as DLR/HIT prosthetic manipulator developed by the German Aerospace Center and Harbin Institute of Technology [1]; the i-limb prosthetic hand with multiple DoF made by British Touch Bionics; the SmartHand, dexterity prosthetic hand, developed in Italy; and so on. However, the outstanding performance of these prostheses will not be fully realized until the methods enabling the amputees to control the prosthesis with multiple DoF accurately and easily have been developed.

Extracting motor commands from neural signals to control the prosthesis by amputees' intention is a key breakthrough for improving the prosthesis performance and is also an interdisciplinary research focus. Electromyogram (EMG), electroencephalogram (EEG), cortical neural signal (CNS), or peripheral neural signal (PNS) all can be used as the source of prosthetic control instructions. However, they have different characteristics in signal acquisition technique and quality, and actual control performance while constructing interfaces with different degrees of invasiveness and feasibility, details are described in Table 4.1.

EMG can be recorded easily and noninvasively, and there are commercial EMG prosthetic products. However, limited control instructions can be extracted from EMG signals while a sufficient number of muscles without atrophy in the residual limb are required, which is not applicable for patients with high amputation and muscular atrophy. The target muscle rehabilitation technology (target muscle reconstruction, TMR), created by the American Chicago Rehabilitation Center, can effectively solve the problem of controlling in high limb amputation. To a certain extent, the DoF and flexibility of controlling can be improved by TMR, but its clinical application is limited for the complexity in implementation [2].

EEG can also be recorded noninvasively and has high temporal resolution. Brain computer interface (BCI) based on EEG has been widely applied in rehabilitation training and prostheses control. However, prosthesis control based on EEG requires users to concentrate on movement imagery without other actions (like talking or other movements and so on); otherwise, correct movement intentions cannot be extracted. In daily life, people always performed more than one action at the same time. So, this method is unnatural and is not consistent with user habits while having bottlenecks in rate of information transmission, control accuracy, and control commands decoding [3].

Table 4.1 Characteristic comparison among different prosthetic control interfaces

Interface type			Advantages	Disadvantages
EMG	Surface EMG (sEMG)	Normal sEMG	Noninvasive, simple procedure and convenient adjustment	Low DOF, unnatural
			High real-time in controlling	Sufficient normal muscles in residual limb
			Existing commercial products, mature technology	Not suitable for high level amputation
				Electrode movements, channel crosstalk, Low long term stability
		TMR	Suitable for high level amputation	Not suitable for distal amputation
			Higher flexibility of control	
			Some sensory feedback can be restored by functional electrical stimulation	Complexity and a large number of electrodes are required
	Invasive EMG (iEMG)		High signal quality	A lot of electrodes are required
			Small channel crosstalk	
			High selectivity	
EEG			High temporal resolution	Electrode placement is complex
			Noninvasive	Unnatural
			Have been widely used in disease detection and rehabilitation treatment	Low information transfer rate
				Low control command type
				Susceptible to interference
CNS (Local field potential and spike)			Directly decode the high-level control command	Large invasive
PNS			Natural	Special electrode is required
			More commands can be decoded from one electrode channel	Lack of decoding method
			High reliability	Immature technology

A large amount of movement and sensory information can be accurately extracted from cortical neural signals in particular cortex areas for controlling assistive devices precisely. However, electrode implantation in the cortex has to be performed via craniotomy, and this surgery has relatively larger risk. Moreover, long-term reliability and biocompatibility of the electrodes are also a problem because the patient can only undergo such electrode implantation surgery once [4].

Comprehensive consideration of invasiveness, expected effects, and ease of implementation, the best way for constructing interface for prosthesis control, is based on PNS. G. S. Dhillon et al. in the University of Utah have demonstrated that residual peripheral nerve keeps the original function and can transmit control commands for the amputated limb even after amputation for a long time [5]. Making

full use of the signals from the residual peripheral nerve, amputees may use the prosthesis freely as with their own arms. PNS can be acquired from special electrodes implanted into the peripheral nerve with relatively simple surgery, while CNS recording requires craniotomy and is more complex with greater risk. In addition, both movement commands and sensory information are transmitted in the peripheral nerve and make closed-loop neural interface with sensory feedback possible.

There are three important research topics about PNS which will be presented in this chapter. Sections 4.2 and 4.3 present the research about PNS decoding and sensory feedback, respectively. Movement signals decoding and sensory signal feedback construct a closed-loop system, while nerve regeneration and repair in Sect. 4.4 provide the foundation for this closed-loop system. How to acquire peripheral neural signals, which were transmitted from the central nervous system, from residual peripheral nerve will be introduced in Sect. 4.2; how to provide sensory feedback by peripheral neural interface will be introduced in Sect. 4.3; some findings in neural cell culture and artificial stretch will be presented in Sect. 4.4.

4.2 Peripheral Neural Signal Acquisition

PNS has captured wide attention from international research community. As early as 2007, Chen et al. of Zhongshan Hospital affiliated to Fudan University conducted an experimental study on the control of electronic prostheses by the amputee for the first time in China [6]. They inserted the intrafascicular electrodes directly into the three main nerve bundles of the upper arm, and the electrodes were connected to a prosthetic device at the distal end. It was found that the signal derived from the radial nerve (simple motor nerve bundle) could trigger the prosthetic simulation device reaching out the fingers when the patient imagined the movement of the hand, but the fingers could not be closed. On the other hand, signals from other nerves (mixed nerve bundles) couldn't effectively drive the prosthetic device. This study validates the possibility of using PNS to control prostheses in a further step; however, the neural signals are only used as a control switch for prosthetics other than being fully analyzed. In 2010, PM Rossini and S. Micera et al. implanted four intrafascicular electrodes into the ulnar nerve and the median nerve of an amputee to perform a long track recording [7]. Slight hold, tight hold, and flexion and extension of little thumb are extracted from the recording signals to develop commands for the robotic arm's performing online. However, there is still a lack of research on the use of PNS to control prosthesis to complete more complex reaching and grasping tasks. For peripheral neural electrode, S. Micera et al. developed a variety of recording or stimulation electrodes, such as cuff electrode, the flat interface nerve electrode (FINE), longitudinal intrafascicular electrode (LIFE), etc. As to the PNS processing, they applied wavelet denoising method for preprocessing and the support vector machine (SVM) or artificial neural network (ANN) for classification corresponding to different tasks. Clinical trials have been conducted to verify the feasibility of the PNS on controlling the external machines. S. Micera pointed out that their future PNS research would focus on decoding more control instructions from the electrode

recordings to achieve a higher degree of freedom for prosthesis control; higher user autonomy; developing bio-PNS interface by providing the users with the sense of feedback; and artificial limb control algorithm with higher robustness and adaptability.

Overall, the earlier carried-out research on EMG and EEG identification and analysis comes out with many practical applications. The modeling research on neural signals in the cerebral cortex and the corresponding limb motor function gained much progress, which provides lots of references for the study of PNS. In recent years, PNS shows the unique advantages and great promotion potential in the field of brain machine interface, thus attracting great interest from international research groups. However, great breakthroughs are expected in the PNS identification and other issues, as with the specialized analysis software and practical algorithms. Although the use of PNS to control robots is already realized by some teams, there is still a long walk to achieve flexible movement patterns with more degrees of freedom by accurate control. Before applying the neural interface constructed by PNS to clinical practice, a large number of animal studies are needed. Primates (such as macaques) become ideal animal test subjects since the anatomical and physiological functions of the nervous system as well as the motor system are the closest to humans. Moreover, PNS animal experiments are related to some key techniques such as the implantation of multichannel nerve electrodes, neural signal acquisition, and monkeys' training, which are challenges for the research institutions.

4.2.1   Surgery and Data Collection

There are mainly three peripheral nerves involved in the transmission of control commands and sensory signals for upper limb, including the ulnar nerve, the radial nerve, and the median nerve. In order to acquire meaningful neural information and to perform electrical stimulation for sensory feedback, we implanted special designed electrodes into these nerves of the monkey. All surgery and data recording procedures were strictly in compliance with the guidelines for the care and use of laboratory animals and were approved by the Institutional Animal Care and Use Committee in Huazhong University of Science and Technology.

4.2.1.1   Electrode Implantation

The electrodes we used in this experiment included floating microelectrode arrays (FMAs), which can be inserted into the nerve fasciculus and cuff electrode, which wrapped the nerves. One of the key concerns for electrode implantation is to meet the requirements for stable recording while allowing monkeys to perform various behavior tasks. To prevent the monkey scratching the connectors or the wires, the connectors must be mounted on its skull firmly. Since the electrodes were implanted into the nerves in the arm, long wires had to be used for linking the electrodes and the connector. Here
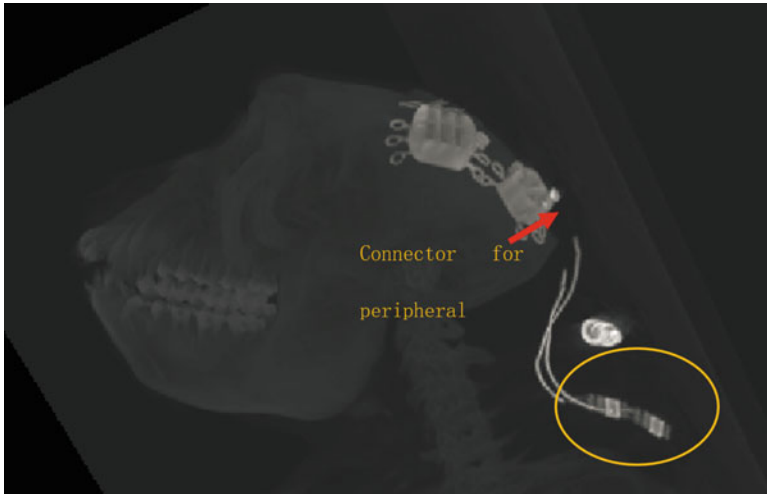
Fig. 4.1 The CT image of the monkey with peripheral neural electrodes implantation. The electrodes were implanted into the median nerve and ulnar nerve of the monkey and the electrodes were connected to the connector with wire through a subcutaneous tunnel. The connector was fixed on the skull with a custom-made pedestal

the wires we adopted in this experiment had a length of 30 cm, as shown in Fig. 4.1, which were connected with the connector and electrode through a subcutaneous tunnel.

The surgery procedures are shown in Fig. 4.2. The first step was to incise the muscles and expose the nerves. According to the relative positions of the nerves, different nerves can be identified clearly, mainly were median nerve, ulnar nerve and radial nerve. For FMA implantation, the array was held by an inserter, which can generate negative pressure, and then inserted fast into the target nerve. For firm fixing, a silicone film was used to wrap the array and sewed up with medical sutures. The surgery was finished after sewing the cuttings, and the total surgery time expended was about 3–5 h.

One FMA electrode and one cuff electrode were implanted in the median nerve and ulnar nerve of a monkey. The two electrodes implantation was achieved through a single surgical site at the elbow. The FMA electrode was inserted into the median nerve with its pins and the cuff electrode wrapped on the ulnar nerve. Moreover, the FMA electrode and that part of the nerve were wrapped by a silicone film.

4.2.1.2 Acute Electrode Implantation test

Movements like hand grasping can be generated by current pulse stimulation on given electrodes after peripheral neural electrode implantation, as shown in
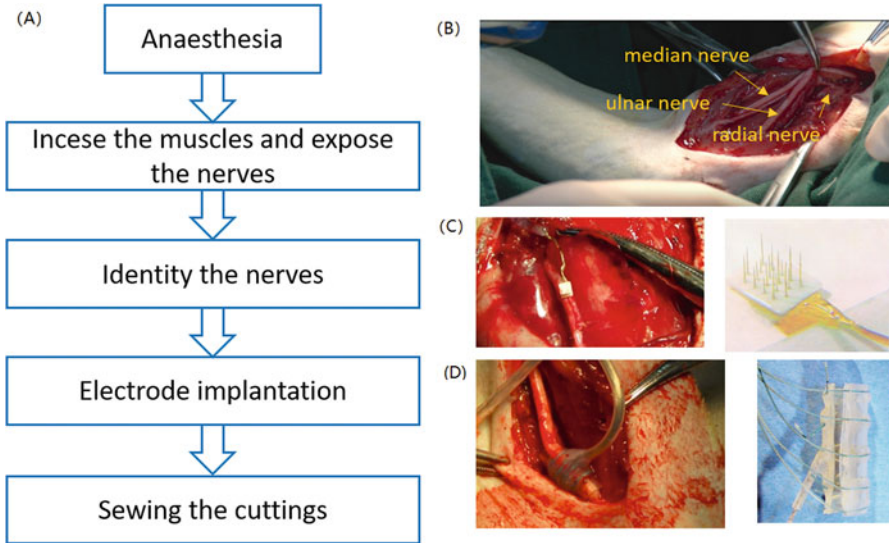
Fig. 4.2 Procedure of the surgery for peripheral electrode implantation. (A) is the flow chart of the surgery. (B) shows the surgical stie and these three exposed nerves, median nerve, ulnar nerve and radial nerve. (C) shows the implantation of the FMA electrode. (D) shows the implantation of the cuff electrode

Fig. 4.3 [8]. The hand shape at static state, when no current pulses were delivered to the electrodes, was shown in Fig. 4.3a. At the beginning phase of electrical stimulation, clear movement tendency could be observed, as indicated in Fig. 4.3b, c. The termination of a movement induced by current pulse was shown in Fig. 4.3d. The experiments described here demonstrate the feasibility of recruiting motor units to generate certain movements by electrical stimulation. However, the details about the patterns of stimulation parameters require further researches.

4.2.2 Experiment

4.2.2.1 Experimental Protocols

When performing the tasks, the animal was comfortably seated in a primate chair with its left arm restricted. The monkey was required to reach and grasp one of the three target objects indicated by the target LED in each trial, as shown in Fig. 4.4. For investigating the neuronal activity corresponding to different grasping gestures, three types of target objects were used, including cylinder, plate, and ring. It is obvious in Fig. 4.4b that the monkey adopted three kinds of hand shapes with large discrepancy with regard to the three types of target objects.
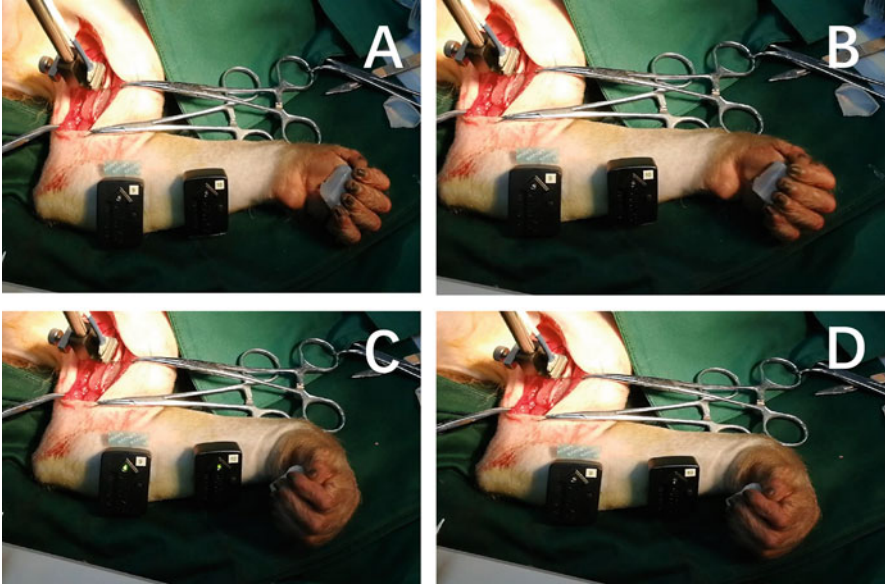
Fig. 4.3 Stimulation of median nerve recruits specific digit and wrist movements. A microelectrode array was implanted into the median nerve of the monkey and pulse-trian was delivered by a electrical stimulator (Plexstim, Plexon, Inc.), meanwhile sEMGs of the forearm were recorded by the Delsys surface EMG system (Delsys, Inc.) to evaluate the electrical stimulation performance. Hand grasping can be generated with specific electrical stimulation parameters and different parameters can evoke different movements

The procedures of the task in Fig. 4.4c show a typical successful trial. One successful experimental trial began with the center LED lighting (center on); then the monkey rapidly put its hand on the center pad and kept for 500 ms at least. Then, one of the three target LEDs was on (target on), cueing the monkey to release from the center pad (center release) and reach to the target indicated by that LED. The monkey should maintain a proper hand gesture according to the shape of the object and made a powerful grasp so as to trigger the FSRs (target hit). After keeping a firm grasping for about 200 ms, it was allowed to release the hand (target release) and then received several drops of water as reward. After an inter-trial interval of about 5–10 s, the monkey returned its hand to the center pad and waited for the beginning of the next trial.

The definition about several important periods during the tasks, are the baseline, the reaction period, and the moving period. During the reaction period, the monkey was in preparation for the future movements, but no movement occurred. During the early stage of the moving period (0–200 ms), hand grasping gestures have not been fully formed.
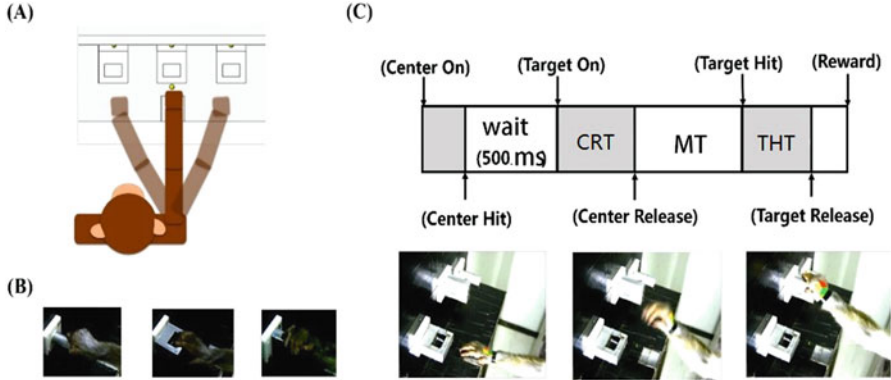
Fig. 4.4 Paradigm design of grasping multiple targets. (A) is the schematic diagram of monkey behavioral experiment. The monkey was guided to reach and grasp three different target objects. (B) is the pictures that the monkey was grasping these three target objects, cylinder, plate, and ring. (C) shows the sequence of the behavioral task. Each trial began with a cueing of center light on, instructing the monkey to fixate on the center pad. After a center holding time of 500ms, the center light went out meanwhile one arbitrary target light went on, cueing the monkey to reach for the corresponding target and make a whole-hand grasp movement. After a target holding time (THT), the target light went out. The monkey would return the hand and a reward of a few drops of water would be delivered

4.2.2.2 Peripheral Neural Data

The acquisition and recordings of neural data were finished by the OmniPlex system (Plexon, USA). The field potentials acquired by the cuff and the FMA on the median nerve were shown in Figs. 4.5 and 4.6 correspondingly.

4.2.3 Neural Decoding Algorithms

Over the decades, various practical decoding algorithms have been developed to analyze neural signals, with continuous improvement in their applicability to neural experimental data (see [9, 10] for recent reviews). A typical Bayesian framework of recursive estimation is introduced here [11], known as a Bayes filter, where the EMG signals from each muscle and the limb kinematics from the lower limb movement were regarded as hidden states of a dynamic network system, while neuronal spiking signals were recorded from motor cortical cortex using the implanted microelectrode arrays as the measurements of the dynamic system, in which the value updates constantly (see [12] for more details about the experiment).

In our experimental data analysis, the x_n denoted the hidden state x value at the n-th time instant. In EMG signal decoding, x_n is given by $x_n = [u_1(n), u_2(n), \ldots, u_M(n)]^T$, where $u_m(n)$, $m = 1, \ldots, M$ is the value of EMG signal from m-th muscle
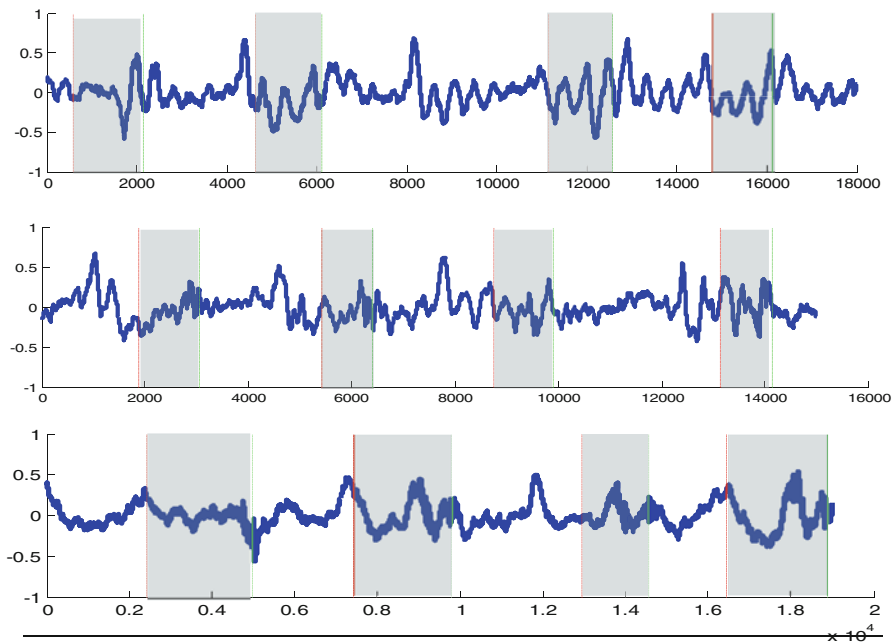
Fig. 4.5 The field potentials acquired by the cuff electrode
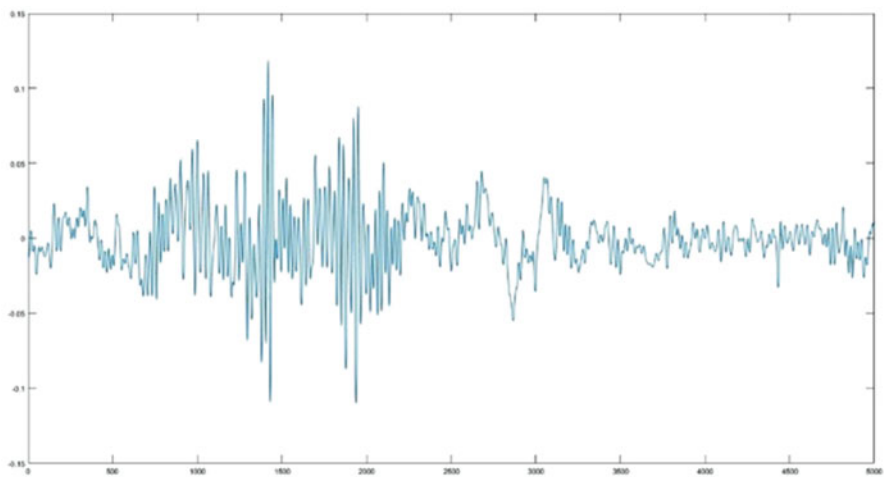
Fig. 4.6 The field potentials acquired by the FMA

activity at the time n and M denotes the total number of muscles where we implanted EMG recording electrodes. When decoding lower limb kinematics, the x_n given by $x_n = [Z(n), V(n), A(n)]^T$, where the $Z(n)$, $V(n)$, $A(n)$ separately respect the position, the velocity, and the acceleration of the marker at the time n. At the same time, the y_n denotes the constantly updated measurement values of the dynamic system at the time n, which is a vector data containing the spike counts of neurons in the n-th time bin.

The estimation process consists of two steps: (i) prediction and (ii) update. In the prediction step, the prior distribution of x_n is estimated from the previous states, then use a Markov model to generate x_n, so we have:

$$p(x_n|y_{1:n-1}) = \int p(x_n|x_{n-1})p(x_{n-1}|y_{n-1})dx_{n-1} \qquad (4.1)$$

where $p(x_n|x_{n-1})$ represents the state of dynamic system changed from current time instant to the next moment and $p(x_{n-1}|y_{n-1})$ corresponds to the posterior probability value for the previous states.

The update step, the posterior prediction $p(x_n|y_{1:n})$ is calculated by updating the prior prediction with the new measurement values y_n:

$$p(x_n|y_{1:n}) = \frac{p(y_n|x_n)p(x_n|y_{1:n-1})}{p(y_n|y_{1:n-1})} = \alpha p(y_n|x_n)p(x_n|y_{1:n-1}) \qquad (4.2)$$

where $p(y_n|x_n)$ represents the mapping relation between the dynamic system and the spike measurements and the normalization constant α in the formula can usually be ignored. Utilizing Eqs. (4.1) and (4.2), we can calculate the $p(x_n|y_{1:n})$ recursively. For practical data process, there are two widely used algorithms, the Kalman filter method [13] and the unscented Kalman filter method [14], that could be used to estimate the EMG signals and kinematics recursively from the neuronal signals recorded from motor cortex; for more detailed information, refer to [15].

4.3 Sensory Signal Feedback

For people who lost a limb after amputation, the concomitant loss of motor and sensory functions results in enormous inconvenience in activities of daily living and deterioration in quality of life [16–19]. To regain ability for grasping and manipulating objects requires appropriate tactile information in addition to motor-driven grippers [20–22]. To better restore amputees' limb function and enable them to better manipulate delicate objects in daily life, adequate sensory feedback is necessary, especially tactile information.

Open-loop myoelectric control via surface EMG once was the most sophisticated bio-control strategy clinically available since powered limb prostheses were

developed to functionally restore arm/hand function in 1960s. However, this kind of control approach did not improve significantly grasping/manipulation due to lack of intuitive user interaction and/or sensory feedback involved in task control [23]. In order to achieve closed-loop control in grasping tasks, several feedback approaches have been proposed in the development of neural interface. For example, force feedback is often used in the hierarchical manner of shared-control for the manipulation tasks involving grasp [24]. Visual and/or auditory feedback has frequently been introduced to assist users in the control of prosthetic limb for reaching and grasping [25]. For sensory substitution, vibrotactile or electrotactile stimulations play a crucial role in providing sensory perception as feedback [26–29]. More recently direct stimulation of the peripheral nerves becomes more focused research corresponding to signals generated by the artificial sensor systems on the prosthetic limb [30–32].

As the complexity of the prosthetic hardware advanced significantly over the last decade, effective control strategies utilizing such high degrees of freedom in more dexterous prosthetic limbs become notably inadequate. For example, the sophisticated prosthesis, SmartHand [33–35], contains so many degrees of freedom, yet it is difficult for a patient to control it naturally. Furthermore, versatile sensors on new prostheses provide much valuable feedback information that substitute naturally the missing sensory information, and if transmitted to patient in a more natural or intuitive way [36], such feedback can be perceived as originating from the missing limb while without overwhelming the concentration of the user [37].

Recently, a study [38] has presented an evident improvement in the quality of sensation and showed that experience of stable touch perceptions can lead to more precise and reliable control of the prosthetic limb. While too many afferents are synchronously stimulated through these electrodes, it will be feasible to achieve more selective stimulation in order to generate more naturalistic tactile sensations. This is important to make the conversion of the prosthetic sensor outputs into patterns of electrical stimulation on peripheral sensory nerves [39].

In this section, we describe a neural prosthesis based on electrical stimulation to provide sensory feedback for closed-loop control. A Schunk Dexterous Hand (SDH) with array sensors on every segment of its fingers provides sensory feedback through a fully implantable electrical stimulation device, which can generate time-variant stimulation parameters according to the sensor measurements and is promising for the generation of natural, graded intensity of grasp force perception [38]. Particularly, the implanted part of this stimulation device is wirelessly powered via magnetically resonant coupling so that there's no need for an internal battery [40].

4.3.1   Materials and Method

The prosthetic part of the experimental neural prosthetic system consists of a 6-degree-of-freedom (DoF) Schunk Powerball Lightweight Arm 4P (LWA 4P), with a 7-DoF three-fingered SDH attached as its end effector. Each finger is
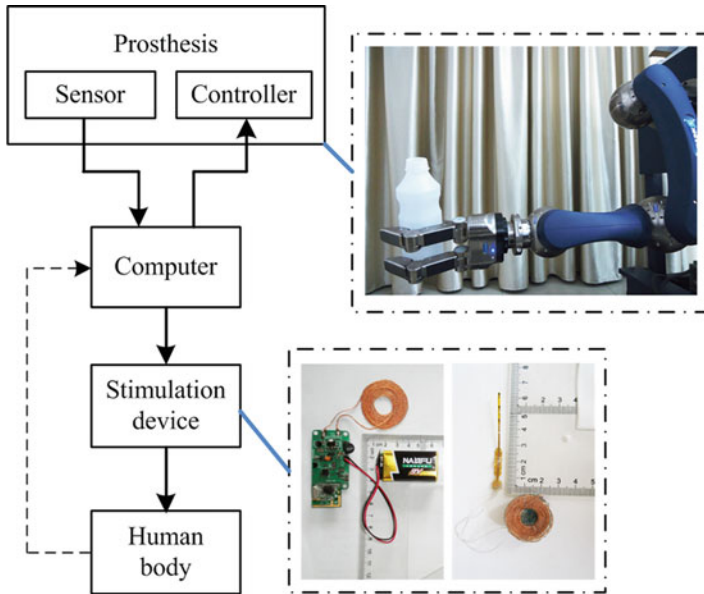
Fig. 4.7 The prosthesis is a combination of a LWA 4P and a SDH, which can provide sensory feedback information as well as moving according to the commands delivered by the computer. The stimulation device consists of the external controller, the implantable pulse generator (IPG), the lead extension and electrode. (Adapted from Qiuxia Lai; Dingyin Hu; Ang Ke; Jiping He, Providing Sensory Feedback Using Electrical Stimulation for Neural Prosthesis, Neuroscience and Biomedical Engineering, 2014. Spring, 2: 99~104)

equipped with two tactile array sensors to provide primitive contact pressure distribution as well as the synthetic force information for the calculation of the parameters needed for electrical stimulation, namely, the pulse width, the pulse amplitude, and the stimulation frequency. The robotic arm and hand communicate with a computer through CAN (controller area network) bus, and the tactile sensors are connected through serial port.

The stimulation system is based on wireless power transfer technology and contains the external controller, the implantable pulse generator (IPG), the lead extension, and electrode, as shown in Fig. 4.7. The controller receives stimulation parameters from the computer via a USB port after the real-time processing of the sensor data and then delivers the parameters to the IPG via wireless communication. The IPG generates time-variant stimulation pulses and delivers them to the bipolar electrode by the lead extension to elicit continuous "natural" sensations on the human body according to the stimulation patterns. Due to its tiny size and wireless power transfer this stimulation system is easily suited for implant operation.

We intend to provide sensory feedback signals that mimic the body's original biological sensors according to the tactile sensor data via the electrical stimulation

device. The improvement in quality of sensation and the closed-loop control strategy is promising to lead to more precise, reliable, and natural control of the prosthetic limbs in daily life tasks.

4.3.2 Experiment

At current preliminary stage, we conducted two separate experiments. One aimed at collecting sensor data to be analyzed later for the generation of electrical stimulation patterns, and the other focused on the functional testing of the stimulation device. In the near future, the integrated complete experiment combining these two parts will be conducted, first in animal models for safety and reliability verification before into clinical trial having patients' participation.

4.3.2.1 Sensor Data Acquisition

In daily life, drinking water from a bottle is a simple but frequent behavior, yet most current prostheses cannot provide satisfactory assistance due to their innate shortage in utilizing natural sensory information.

In order to study the sensory information and regulation in this daily life activity as well as to find out a general research approach for similar issues, we conducted the experiment to collect the outputs of these array sensors during the task execution process when the prosthesis took up a bottle of water, moved to another place, poured water out, held the bottle upright again, and then put down the emptied bottle.

The recorded contact sensor data were visualized using pseudo-coloring scheme to present intuitive information of the pressure distribution and its dynamic variation during the experiment, as shown in Fig. 4.8. Detailed explanation is presented next.

In Fig. 4.8 four phases of the water bottle grasp and take-up, tilting for water-pouring procedure in the experiment task, are shown on the top panel, and the corresponding visualized contact pressure presentations are placed below. The water level is indicated by dash line on the bottle. The meaning of pseudo-color picture used to visualize the acquired contact pressure data is illustrated by the color bar and the unit of sensor readouts is millivolt. Each of the three fingers contains two tactile array sensors consisting of 78 and 86 tactile cells, respectively, and each cell can perceive the pressure applied on it.

All sensor data were delivered to the computer and recorded for offline analyses. In the pseudo-color picture, each figure under the representing bottle orientation shows three dynamic pressure distributions for the three fingers: the left color column represents the right-lower finger seen in the real object picture, the middle column represents the left (opposing) finger, and the right represents the right-upper finger. The primitive readouts are the voltages measured on each cell.
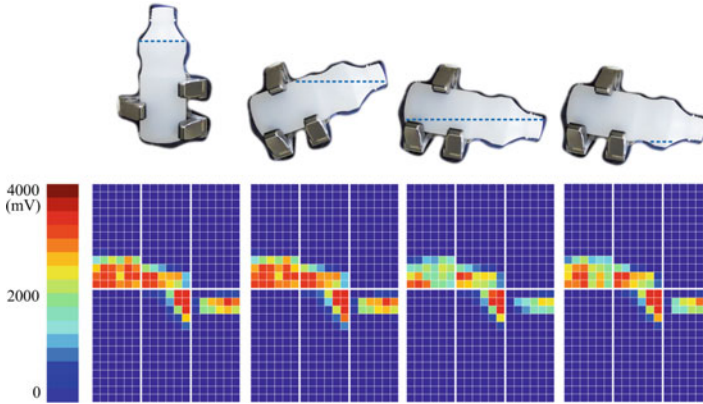
Fig. 4.8 Several typical time phases during the water-pouring procedure in the experiment task. The top panel shows the real scenes and the bottom panel shows the corresponding pseudo-color picture drawn according to the sensor readouts. The dash line indicates the water level inside the bottle, while the water outside isn't shown. The color bar demonstrates the meaning of the pseudo-color picture. Each of the color square in the pseudo-color picture represents a cell in the array sensor and its color demonstrates the voltage value which reflects the force strength exerted on it at that time point. Qiuxia Lai; Dingyin Hu; Ang Ke; Jiping He, Providing Sensory Feedback Using Electrical Stimulation for Neural Prosthesis, Neuroscience and Biomedical Engineering, 2014. Spring, 2: 99~104

4.3.2.2 Stimulation Pattern Generation

The stimulation device was designed to be capable of altering stimulation parameters in real time during its working procedure. The external controller receives commands from a computer via a USB port connection [41]. Then the external controller transmits the stimulation parameters to the IPG by radio frequency telemetry. The IPG generates pulses through the electrode to elicit certain neural responses [42].

In order to prevent corrosion and irreversible electrolyte reactions, the waveforms used in clinical stimulation should be charge-balanced, while compared with biphasic charge-balanced waveforms, asymmetric charge-balanced waveforms can provide better control of electrochemical reactions and may suppress undesired reactions [43].

To ensure charge balance at the electrode site, we monitored the raw output signals applied to a pair of electrode contacts under different specified stimulation parameters with the active electrodes immersed in 0.9% saline. Two waveforms from each electrode contact form together and generate the final stimulation pulse, as shown in Fig. 4.9.

We also altered the stimulation parameters during voltage observing procedure in order to test the capability of our stimulation device to generate different stimulation waveforms real time according to the computer commands. The voltage waveforms were recorded via the oscilloscope, as well. Some examples are demonstrated in Fig. 4.9. The stimulation parameters tested in the experiment were 50 Hz, 2.64 V, and 1200 μs and 10 Hz, 1.32 V, and 400 μs, respectively.

Fig. 4.9 Voltage waveforms observed on the oscilloscope. The active electrodes were immersed in 0.9% saline. The specified stimulation parameters are (**a**) 50 Hz, 2.64 V, 1200 μs and (**b**) 10 Hz, 1.32 V, 400 μs, respectively
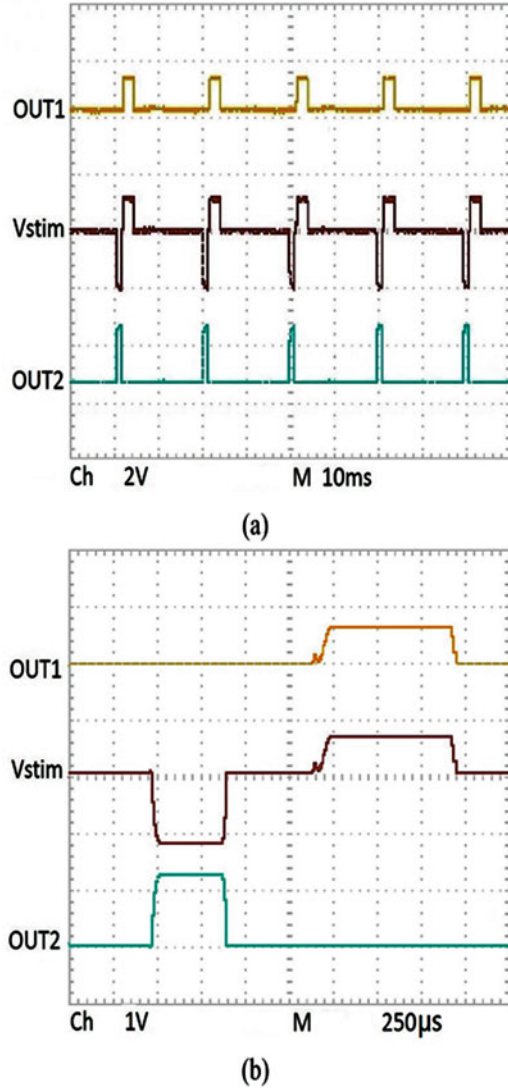
4.3.3 Results and Discussions

4.3.3.1 Sensor Data Analysis

In the sensor data acquisition experiment, we observed an evident variation of the measured voltage. The pressure remained zero before the SDH touched the water bottle, and as can be seen in Fig. 4.8, the pressure later reached its desired maximum value when the fingers firmly held the bottle without squeezing hard to break it, and
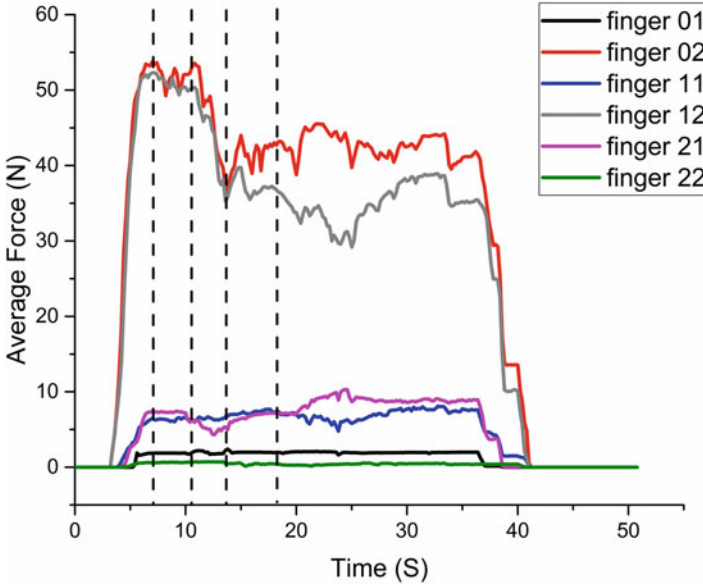
Fig. 4.10 Average forces of the 6 array sensors averaged from 12 experiments. In the "finger xy," x with the value 0–2 represents the three fingers from left to right in the bottom panel of Fig. 4.8, and y with value 1 represents the proximal part, and 2 represents the distal part of the finger

then decreased when water flowed out of the bottle. Finally, it returned to zero after putting down the bottle. We can also find out that each array sensor experienced different amounts of pressure, and this pressure distribution may result from the relative position and contact area between the bottle and the SDH, i.e., the holding posture affected the sensor output value. However, the variation rules of the pressure values on all six array sensors are similar during the experiment.

The array sensor data are initially in the form of voltage, and we calibrated the voltage into pressure using the formula:

$$p = v \, P^*/V^*. \tag{4.3}$$

where the $P* = 0.000473$ N/(mm $\times$ mm) and the $V^* = 592.1$ mV according to the documentation of SDH.

After acquiring the pressure value on each cell, the average force on every array sensor can be calculated. The calculated force of the 6 array sensors averaged from 12 experiments is displayed in Fig. 4.10, and the time points corresponding to the given phases in Fig. 4.8 are marked by the dash lines. In Fig. 4.10, the "finger xy" indicates the six tactile array sensors embedded in the SDH, in which x ranging from 0 to 2 indicates the finger and y with values 1 and 2 indicates whether the sensor is proximal or distal.

We can see that there exists high-frequency jiggering in the force curves, indicating that the bottle slid a little during the whole experiment procedure. The distal

part of the right-lower finger and the proximal part of the right-upper finger, i.e. "finger 01" and "finger 22," have the smallest average force during the 12 experiments, and as can be seen from the original data, the pressure of each cell stays 0 in most of the 12 experiments, resulting in the equal-zero average values. The distal parts of the left finger and the right-upper finger, i.e., "finger 11" and "finger 21," have the second largest average force, and the sum of the two values seems to remain the same. The remaining two finger patches, i.e., "finger 02" and "finger 12," have the largest average force, which then diminished to a smaller value when water started to flow out of the bottle. From the analysis above we can conclude that as for the holding posture in the experiments, only four finger patches played the main role, which form two interaction force pairs and keep the bottle balanced. When water was flowing out of the bottle, the average force measured on "finger 02" and "finger 21" increased a little, which may be due to that the water at bottom of the bottle flowed to the bottle neck. So there was more water need to be supported by these two fingers at that moment.

However, the analysis above is only for the averaged results. As for the data acquired in each single experiment, we discover that there often exist certain finger patches that didn't experience any pressure during the whole procedure. This phenomenon may not be ideal for shared load of fingers, but it is not unusually seen in real life because of the uneven surface or shape when grasping an object. This observation suggests that, for larger, heavier or irregular shaped/structured objects, grasping postures may need pre-planning to distribute pressure more evenly among all fingers of a robotic hand to prevent slippery or damage of robot hand or weak parts of the objects.

In further research, we plan to extract more information from these sensor data to generate proper electrical stimulation parameters and elicit sensations in human body real time. The type of stimulation represents the objects' contact properties detected by the array sensors on the robotic hand and is promising to contribute a lot in the control of neural prosthesis because the sensory feedback information provided can help to reach a closed-loop control effect and will greatly improve the performance of the neural prosthesis when carrying out daily life tasks. What we need to do next is to propose more effective algorithms and make better use of these force data to acquire motor-related information and apply it to the controller designing.

4.3.3.2 Stimulation Pattern Generation

In the stimulation pattern generation experiment, we observed a charge-balanced waveform between the bipolar electrodes from oscilloscope. The active electrodes were immersed in 0.9% saline and the raw output signals were monitored under different specified stimulation parameters. As illustrated in Fig. 4.9, stimulation parameters are 50 Hz, 2.64 V, and 1200 μs (a) and 10 Hz, 1.32 V, and 400 μs (b), respectively. One channel of the electrode contact outputs a square pulse OUT1 and the other electrode contact outputs a delayed square pulse OUT2 whose amplitude is

one-half and the duration is double of the OUT1 waveform. The charge-balanced biphasic stimulation waveforms Vsim are formed by these two square pulses and have a negative phase followed by a positive phase with an inter-pulse delay. We can observe a significant difference when stimulation parameters changed.

We conclude that both changes in the pulse width and the stimulation frequency can result in different stimulation waveforms, demonstrating the capability of the stimulation device to provide different stimulation patterns for eliciting variable sensations.

In future research, we will utilize the calculated force information to generate corresponding stimulation parameters (pulse width, amplitude, and frequency) that are promising to elicit natural sensory responses. The sensation elicited on sensory nerves can provide sensory feedback different from other kinds of feedback such as visual and vibratory feedback, and can induce users' intuitive response in the control of neural prosthesis, which is destined to realize a more natural control performance. Currently the exact relationship between the stimulation parameters and the elicited sensations is still unclear; we need to do further carefully designed research to investigate and acquire this kind of information and find out the proper way to provide users with natural sensations.

In this section, we report a novel experiment to measure the tactile sensor information during the process of taking up a bottle or cup of water, moving to a designated location while holding the bottle/cup upright, pouring the water out, returning the bottle back to upright position again and then putting down the empty bottle, and monitored the output stimulation waveforms of the stimulation device under specific stimulation parameters. These are preliminary experiments to explore approaches to restore the motor function for paralyzed people or amputees by introducing sensory feedback via electrical stimulation on peripheral nerves and controlling the motion of prostheses according to the motor intention decoded from user consciousness.

We now have successful access to acquire the data used for sensory feedback as well as the approach to generate various stimulation patterns; what we need to do in successive stages include conducting more experiments combining these two sub-systems and developing an effective algorithm to convert the output of tactile array sensors on the prosthesis into patterns of electrical stimulation of sensory nerve. Moreover, we will also do investigative work to use decoded motor intention into real-time control commands to directly manipulate the prosthetic limbs as the natural sensory feedback are elicited via electrical stimulation synchronically, thus reaching a natural closed-loop control performance.

There are many scientific and technical challenges to be conquered before we can achieve the ultimate research goal. Along the way, the development effort should bring significant medical benefits to the patients and society. If the natural sensory feedback is achieved, the amputees will be able to perform naturally functional control on the prostheses as if they were just extension parts of their body.

4.4   Neural Regeneration and Repair

Autologous nerve grafts remain the "gold standard" for repair of peripheral nerve lesions. However, this approach is plagued by permanent loss of harvested nerve function and the potential formation of painful neuromas. Furthermore, there are obvious limitations in the supply of donor nerves, making autografts can only be used to repair short nerve lesions. Neural repair technology based on tissue engineering has shown promising prospects in the treatment of nerve injury. However, this treatment needs autologous nerve to stimulate axonal regeneration and extension into target tissues. Therefore, how to produce plenty of living nerve constructs in a short time is full of significance.

Fine-motor control of an artificial arm will ultimately require a different kind of link between living tissue and the prosthesis. Except for muscles, nerve fibers can also be the intermediary between the severed axons in a stump and the electrical wiring of a prosthetic device. D. Kacy Cullen and Douglas H. Smith believed this kind of neural interface has some advantages, such as low invasion, high sensitivity, convenient for signal separation, and short rehabilitation period [44]. To create such a neural bridge, we firstly have to figure out how to grow nerve fibers that are long enough to span the gap between the host axons and the electronics.

Although it has been well known that axon growth can be guided by chemical cues and electrical stimulation, both of these two methods couldn't produce regular neural tissues. In nature, the actual growth of the axon also appears to be dependent on mechanical stimuli. By the proper stretch speed, we can achieve regular nerve constructs. The nervous tissue constructs consisting of living axons, which provides an enticing target for host axon ingrowth and synaptic integration. Compared with original neural interface, our method shows some advantages. Firstly, living axonal constructs can provide regenerative support for the proximal stump where target is cut off. Secondly, the array and neurons can make stable connection in vitro. Thirdly, most host nerves will never connect directly with the electrical devices which usually cause damage to the respective tissue. Finally, the process of mechanical stretch can produce more regular nerve fascicles (details in Table 4.2).

Table 4.2 Comparison of different methods for the directed nerve growth

| Methods	Advantages	Disadvantages
Chemical	The inherent characteristics of the organisms	Long period
	The growth speed and direction are controllable	Unquantifiable
	Both direction: Attraction and rejection	Irregular
	Kinds of neurotrophic factors for varied nerves	
Electrical	The growth speed and direction are controllable	Unquantifiable
	Noninvasive	Irregular
	Neural regulation and functional reconstruction	
Mechanical	The inherent characteristics of the organisms	Easily cause nerve damage
	The growth speed and direction are controllable	
	Regular nerve fibers	Few studies
	Quantifiable	

4.4.1 Axon Stretch Growth

In the past, a few reported studies have attempted gradually lengthening the axons by towing growth cone. In 1984, Bray successfully stretched the growth cones of individual chick sensory axons more than 100 μm within a few hours by a micro-electrode [45]. In 1993, Heidemann et al. performed a series of studies. The growth cones of single axons were lengthened at precise increments via stretching glass pipettes using an external device. The rate of towed growth showed a linear dependence of growth rate with applied tensions between 25 and 560 micro dynes. He found the axons could be towed at a maximal limit of 1 mm every day without thinning down [46]. In 1977, S. Chada found the elongation rate and magnitude of applied tension have linear relationship in both central and peripheral neurons [47].

When the stretch time is too long or the speed too fast, the axon will be disconnected. Therefore, we can't produce long neural tissues by stretch growth cone. Actually, integrated axon tracts without growth cones could also undergo a form of more rapid and sustained growth under stretch. The majority of cell types in nature increase their volumes by division during development. However, neurons are non-mitotic, so the expansion of nervous tissue depends on another process. For example, during development of blue whale, the spinal axons need to undergo continuous mechanical tension as their spinal cord grows in length. Although without growth cones, these integrated axons could reach 30 m in the end.

However, the elongation of integrated axon tracts was not experimentally demonstrated until 2001 [47]. Smith et al. found integrated axon tracts without growth cones could be stretched at a faster rate. Two large populations of neurons were seeded on adjacent membranes within a bioreactor, and then the top membrane was slided across the bottom membrane at set rates by a programmable microstepper motor system. When the microstepper motor moved the top membrane, the axonal bundles crossing between the two membranes were stretched to a new length. In the end, the axons had grown up to 1 cm after 10 days of stretch. In the following years, they optimized the stretch growth paradigm, and dorsal root ganglion (DRG) axon tracts initially only 100 μm in length could be extended up to 10 cm by stretch for 2 weeks [48]. Despite this rapid stretching, sodium channel activation, inactivation, and recovery or potassium channel activation were demonstrated no change according to the whole cell patch clamp technique.

4.4.1.1 Principles of Axon Stretch Growth

In order to stretch axon bundles, as depicted in Fig. 4.11, one stationary substrate membrane as the bottom of the culture chamber. Another towing membrane made by the same material was positioned over the bottom membrane. Both of the two membranes would need to be thin and transparent enough so that adherent cells on their surfaces could still be within the working distance of a high magnification microscope objective. The towing membrane was fixed to a machined plastic block
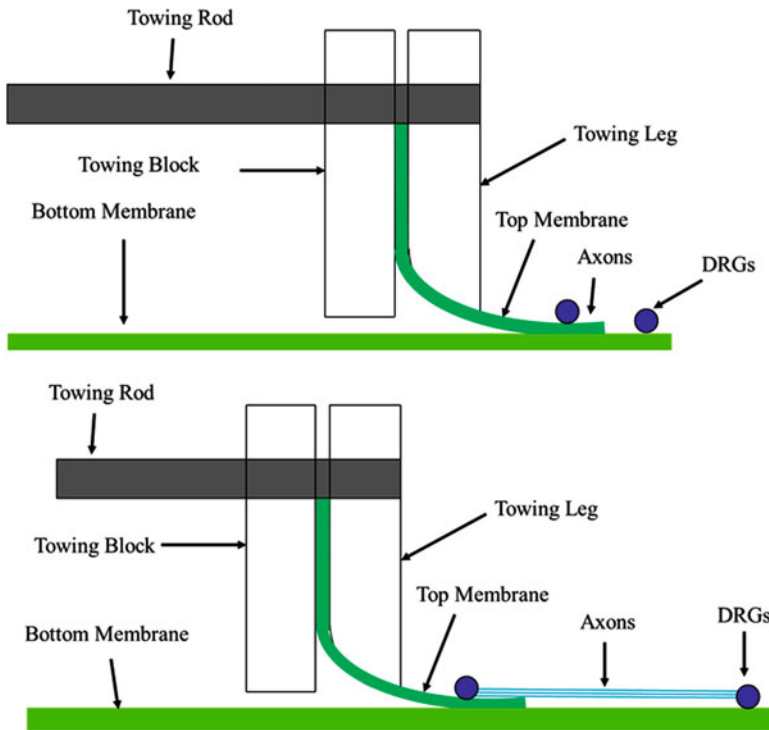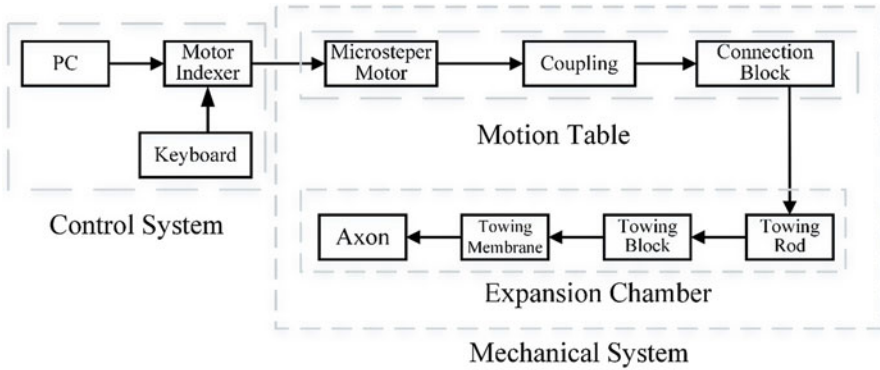
Fig. 4.11 Schematic diagram of axon stretch-growth

so that it could be moved over the bottom membrane by a microstepper motor system. First, the neurons were placed on the two adjoining substrates and formed new synaptic connections between each other over 5 days. Then, the axon bundles across the border between the top and bottom membranes were stretched in a stepwise fashion. After several days' stretch, the axon tracts could reach several centimeters in length.

4.4.1.2 Fabrication of Bioreactor

In order to stretch neural cells, axon expansion chamber will not only need to culture cells like a common culture vessel, but also need to stretch axons. The design needs to meet the following requirements:

1. Conditions for culture of neural cells in vitro. A. It can store and replace culture medium. B. It can be sterilized and maintained in a sterile environment. C. To exchange gas and maintain appropriate pH value medium. D. The material used in the incubator has no toxic gas under special temperature and humidity conditions. E. The bottom and top are transparent to facilitate observation during culture.

Fig. 4.12 Control structure diagram of axon stretch system
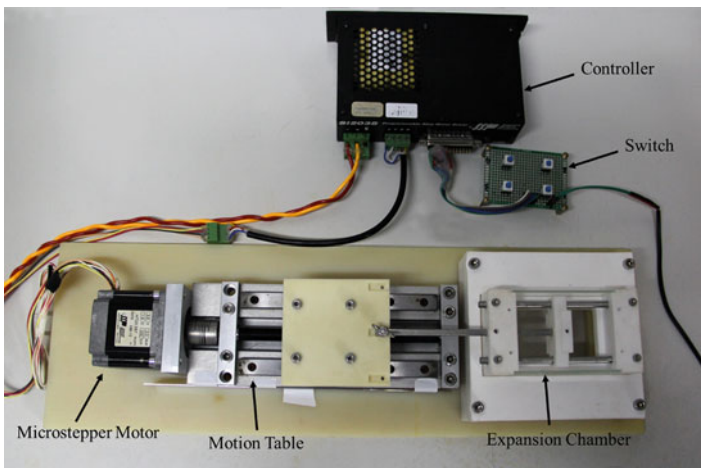
Fig. 4.13 Axon stretch growth bioreactor system. (Adapted from Li, Xiao, et al. "Development of a new miniaturized bioreactor for axon stretch growth." Journal of integrative neuroscience 15.03 (2016): 365–380)

2. Conditions for axon stretch growth. A. The materials used under special temperature and humidity conditions of the incubator will not deform and ensure the stability and accuracy during stretch growth. B. Stepper motor needs to work well in the incubator; each displacement distance is small enough to not affect the cell growth. C. The wire passes through the incubator, but does not destroy the air pressure and the sterile environment in the incubator.

   A miniaturized bioreactor (Fig. 4.12) was engineered to gradually apply tension to axon bundles spanning two separate membranes. As showed in Fig. 4.13, the axon
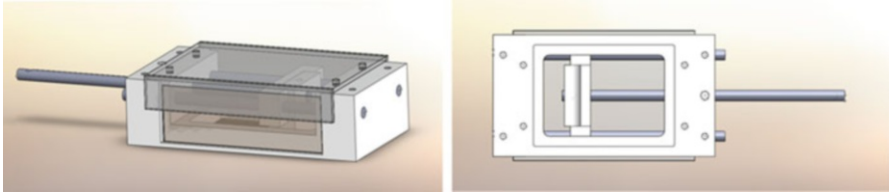
Fig. 4.14 Axon expansion chamber

stretch growth bioreactor system was composed of axon expansion chamber, linear motion table, microstepper motor, and controller. Aside from the motor indexer, the bioreactor was located in a CO_2 incubator during neural culture and axon stretch growth experiments. The axon expansion chamber was seated within the chassis underlying the linear motion table, meanwhile the towing rod extending from the axon expansion chamber was fastened to the table using an acrylonitrile-butadiene-styrene (ABS) adaptor.

As is shown in Fig. 4.14, the axon expansion chamber is composed of the stretching frame, towing block, towing leg, and so on.

4.4.2 Axon Stretch Growth

When the axons sprouted from their cell body and formed synaptic connections with target cells, the axon stretch growth will begin. As the distance between the neuronal somata and the target cells increased, the axons will undergo the continuous tension. These forces increased axons' growth rate by stimulating axons to add cytoskeleton, axolemma, and other cellular building materials somewhere along their central length to minimize strain.

4.4.2.1 Key Factors in Axon Stretch Growth

1. Traction Mode.

Small and frequent stretches are important to the survival of axons undergoing stretch growth, particularly at the start of stretching. As shown in Fig. 4.15, if high elongation rates are applied early, growth cannot be sustained, and axons will rupture within the first 24 h. But if the rate increases slowly, the cell can accommodate the rate and grow healthily. Moreover, if the stretch rate increased

Fig. 4.15 Graphic representation of stretching conditions that define the boundaries of axon growth or disconnection
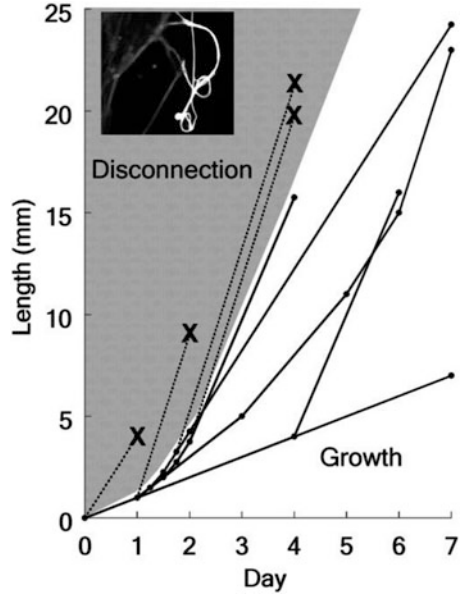
faster than the neuron, the tension will accumulate and cause the axons rupture. Therefore, two sequential factors that defined the boundaries of long-term stretch growth of integrated axons: strain and acclimation.

2. Substrate Attachment.

Another key factor is the neuronal adhesion with the substrate. The elongator substrates coated by both PDL and rattail collagen had been proved it was the best coating method. PLL had been widely used in the cell culture experiment. However, it could be taken in through adsorptive endocytosis by neurons which may provoke inflammatory responses either directly or indirectly through its necrosis-inducing abilities, most of axons had not grown out from the DRGs. Although collagen could provide an optimal condition for cell adhesion, it will rehydrate in the culture medium, which would often cause axon stretch growth experiments to fail. The axons grew very well after 3 days' culture, while they were seemed to be ill at the sixth day. High-molecular-weight PDL could provide enough adhesive force during axon stretch growth, but some residual PDL could not be digested by lysosome which would cause inflammatory responses when the nervous tissue constructs comprised of stretch-grown axons were used to repair nerve damage. By combining soluble PDL and collagen, we can get the most ideal result.

3. Slope Substrate.

In 1911, Harrison cultured cells on a spider web and found the cells grew along the fibers of the web [49]. Since then, with the development of micro- and nano-fabrication techniques, a large number of studies have shown that cells react strongly to topography. Rajnicek et al. reported that central nervous system neurites could be guided by shallow grooves with 14 nm deep and 1 mm wide [50]. Stepien grew chicken DRG neurons on single scratches. He found that direction often increases with increasing depth, but decreases with increasing groove width. If the grooves are >20 mm, most cell types will lose guide [51]. Goldner et al. describe an unusual capability of a subpopulation of DRG neurons could span across the grooves with 200 mm width, even with no underlying solid support [52]. Fricke et al. designed a variety of gradient patterns with slight changes in slope to control axon directionality. They found that reduction in the slope of structure from 0.04 (0.3 mm/7.5 mm) to 0.01 (0.1 mm/7.5 mm) strongly influence neurite growth. Actin and microtubules align along walls and edges, the microtubules being the first element to be aligned, followed by actin. Grooved surfaces also induce changes in transcription and the up and down regulation of several genes, but the explicit mechanism for cell guidance has yet to be clarified [53].

In the axon stretch growth system, there is a topography between the top membrane and the bottom membrane, which will affect the growth direction of the axons. The top membrane need to be polished on one edge to create gradual slope to the border of the exposed underlying membrane.

#### 4.4.2.2   Experimental Design of Axon Stretch Growth

1. Modification of the Membranes.

DRG were isolated from 1 day-old infant Sprague–Dawley rats. The culture surfaces were respectively treated with high-molecular-weight PDL and collagen.

2. The Process of Axon Stretch Growth.

The neurons are placed on the two adjoining substrates and formed new synaptic connections between each other over 5 days. When the axon bundles are across the border between the top and bottom membranes, we can begin to stretch. The following axon stretch growth began at a rate of 0.864 mm/day by taking 1-μm steps every 100 s over 864 iterations. Alternatively, in order to achieve several centimeters' axon tracts rapidly, the stretch rate could begin slowly and gradually accelerate to the desired rate. As is shown in the Fig. 4.16, the important steps are as follows:

Fig. 4.16 Flowchart of
axon stretch growth
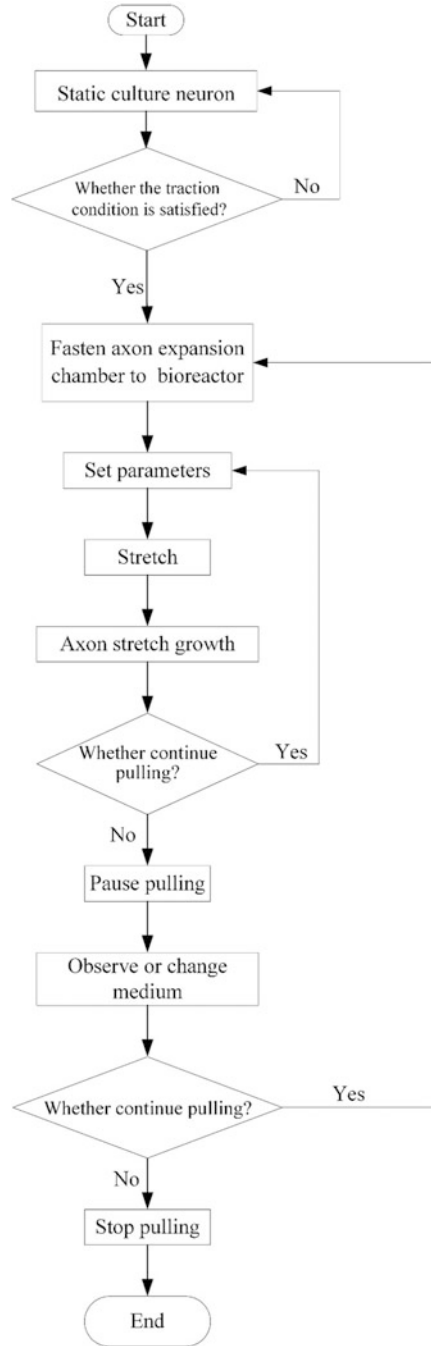
1. Traction condition determination: a large number of axon bundles are across the border between the top and bottom membranes.
2. Install axon expansion chamber: fasten the culture chamber within the chassis underlying the linear motion table, whereas the towing rods extending from the culture chambers were fastened to the table using an ABS adaptor.
3. Set parameters: first of all, in the PC machine, set the traction parameters such as: step length and waiting time, and then downloaded to the controller, you can use the keyboard to achieve the stepper motor to start, pause, positive rotation, negative rotation and other operations.
4. Medium replacement: after 1 week's culture, replace the medium. When the liquid is replaced, the utility model is firstly suspended by the keyboard, and the towing rod is fixed by the nut to prevent the towing rod from moving. After that, loosen the nut between the towing rod and the connecting block, and move axon expansion chamber into the super clean table. Finally, the axon expansion chamber is moved back to the incubator, and the towing rod is fixed with nuts. Connect the block, and then loosen the nut on the pull link, you can restart the pull.

4.4.2.3 Axon Stretch Growth

In order to increase the density of elongating axons in each culture, the elongator substrates were first treated by PDL and then followed by rattail collagen coating. After DRG explants were plated, cultures were maintained for 10 days in the incubator so that axons could grow across the interface of the two adjoining substrates. Before stretching, the total diameter of the axon bundles was about 100 μm, with about 100 axons (Fig. 4.17b). According to the above test, 1 μm step was the better choice. In addition, the axons need sufficient acclimation time to decrease the residual stress after stretching. Therefore, the stretch growth rate was programmed into the motion control system by implementing a displacement step and a resting time in a circular manner, about 1 μm every 100 s. These bridging axons adapted to the stretch by increasing their length from 500 μm to become 5.94 mm long over 7 days of stretch growth (Fig. 4.17h). Because the neighboring axon bundles preferred to join together during stretch-induced growth, the number of axon bundles in the end looked fewer. The neural tracts were stained with β-tubulin antibodies to confirm which were real axons. The entire length of stretch-growing axons labeled positive for β-tubulin protein (Fig. 4.18).

Our work has obtained some successful experience in verifying that mechanical stretch could promote the directional growth of axons, and demonstrating the possibility of repairing nerve injury. Some recent reports highlight the necessary of synergistic training for axons and myelin. This will be our next research goal.
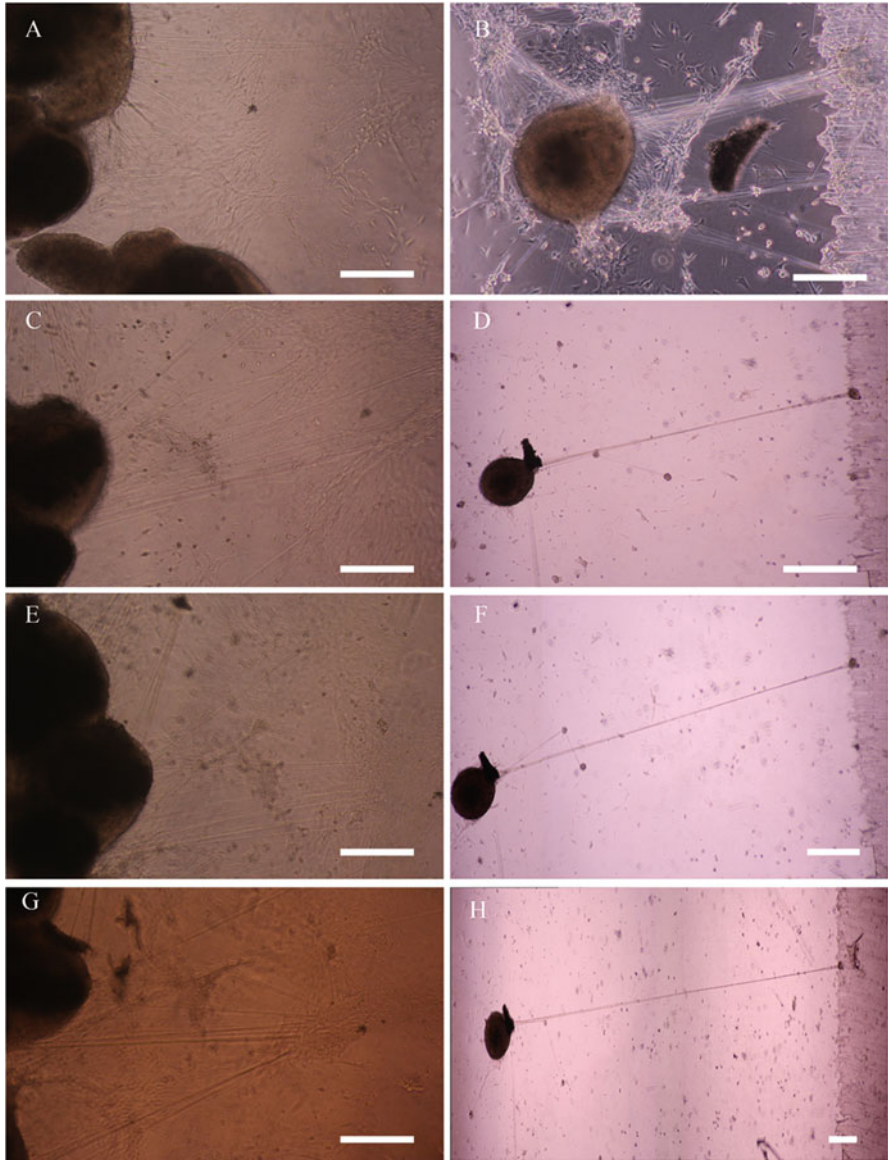
Fig. 4.17 Comparison of DRGs static culture group (left) and stretch-grown group (right) in the axon stretch growth bioreactor. (**a**) DRGs were cultured 3 days. (**b**) DRGs were cultured 10 days. (**c**) DRGs were cultured 10 days. (**d**) DRGs were stretched growth 3 days. (**e**) DRGs were cultured 13 days. (**f**) DRGs were stretched growth 5 days. (**g**) DRGs were cultured 17 days. (**h**) DRGs were stretched growth 7 days. Scale bars: (**a**)–(**c**), (**e**), and (**g**) 200 μm; (**d**), (**f**), and (**h**) 500 μm. (Adapted from Li, Xiao, et al. "Development of a new miniaturized bioreactor for axon stretch growth." Journal of integrative neuroscience 15.03 (2016): 365–380)
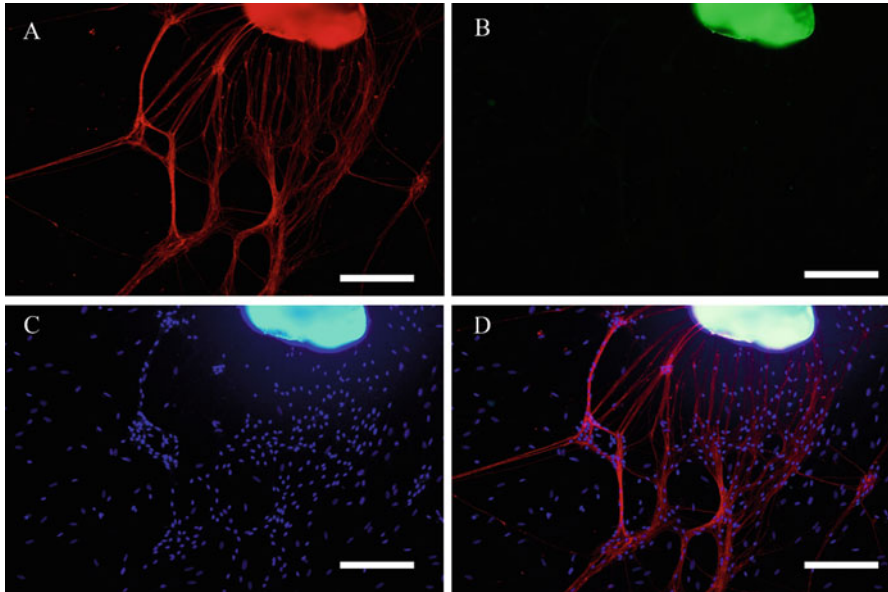
Fig. 4.18 Immunohistochemistry analysis of axon. (**a**) Antibodies against β-tubulin (red) were utilized to determine that elongating processes were axons. (**b**) Antibodies against myelin basic protein (green) were utilized to determine whether there was myelin around the axons. (**c**) Cell nuclei were labelled with DAPI (blue). (**e**) overlay. Scale bars: 100 μm. (Adapted from Li, Xiao, et al. "Development of a new miniaturized bioreactor for axon stretch growth." Journal of integrative neuroscience 15.03 (2016): 365–380)

References

1. Liu H et al (2008) Multisensory five-finger dexterous hand: the DLR/HIT hand II. IEEE/RSJ international conference on intelligent robots and systems, 22–26 September 2008, Nice, France
2. Micera S, Carpaneto J, Raspopovic S (2010) Control of hand prostheses using peripheral information. IEEE Rev Biomed Eng 3:48–68
3. Reuderink B, Poel M, Nijholt A (2011) The impact of loss of control on movement BCIs. IEEE Trans Neural Syst Rehabil Eng 19(6):628–637
4. McFarland DJ, Wolpaw JR (2008) Brain-computer Interface operation of robotic and prosthetic devices. Computer 41(10):52–56
5. Dhillon GS et al (2005) Effects of short-term training on sensory and motor function in severed nerves of long-term human amputees. J Neurophysiol 93(5):2625–2633
6. Xiaofeng Jia, Matthew A. Koenig, Xiaowen Zhang, Jian Zhang, Tongyi Chen, Zhongwei Chen (2007) Residual motor signal in long-term human severed peripheral nerves and feasibility of neural signal-controlled artificial limb. J Hand Surg Am 32(5):657–666
7. Rossini PM et al (2010) Double nerve intraneural interface implant on a human amputee for robotic hand control. Clin Neurophysiol 121(5):777–783
8. Ledbetter NM et al (2013) Intrafascicular stimulation of monkey arm nerves evokes coordinated grasp and sensory responses. J Neurophysiol 109(2):580–590
9. Quian Quiroga R, Panzeri S (2009) Extracting information from neuronal populations: information theory and decoding approaches. Nat Rev Neurosci 10(3):173–185

10. Rolls ET, Treves A (2011) The neuronal encoding of information in the brain. Prog Neurobiol 95(3):448–490
11. Bergman N (1999) Recursive Bayesian estimation, Doctoral dissertation, Department of Electrical Engineering, Linköping University
12. Chaolin Ma XM, Zhang H, Jiang X, He J (2015) Neuronal representation of stand and squat in the primary motor cortex of monkeys. Behav Brain Funct 11:15
13. Grewal MS (2011) Kalman filtering. Springer, Berlin
14. Julier SJ, Uhlmann JK, Durrant-Whyte HF (1995) A new approach for filtering nonlinear systems. In: Proceedings of the American control conference, 21–23 June 1995, Seattle, WA, USA
15. Ma X et al (2017) Decoding lower limb muscle activity and kinematics from cortical neural spike trains during monkey performing stand and squat movements. Front Neurosci 11:44
16. Antfolk C et al (2013) Sensory feedback in upper limb prosthetics. Expert Rev Med Devices 10 (1):45–54
17. Deans SA, McFadyen AK, Rowe PJ (2008) Physical activity and quality of life: a study of a lower-limb amputee population. Prosthetics Orthot Int 32(2):186–200
18. Whitehouse F, Jurgensen C, Block MA (1968) The later life of the diabetic amputee: another look at fate of the second leg. Diabetes 17(8):520–521
19. Østlie K, Magnus P, Skjeldal OH, Garfelt B, Tambs K (2011) Mental health and satisfaction with life among upper limb amputees: a Norwegian population-based survey comparing adult acquired major upper limb amputees with a control group. Disabil Rehabil 33:17–18, 1594–1607. https://doi.org/10.3109/09638288.2010.540293
20. Johansson RS, Flanagan JR (2009) Coding and use of tactile signals from the fingertips in object manipulation tasks. Nat Rev Neurosci 10(5):345–359
21. Campbell CS et al (1999) What you feel must be what you see: adding tactile feedback to the trackpoint. In: Proceedings of IFIP INTERACT'99, p 383–390
22. Mugge W et al (2009) Sensory weighting of force and position feedback in human motor control tasks. J Neurosci 29(17):5476–5482
23. Ortiz-Catalan M, Hakansson B, Branemark R (2014) An osseointegrated human-machine gateway for long-term sensory feedback and motor control of artificial limbs. Sci Transl Med 6(257):257re6
24. Cipriani C et al (2008) On the shared control of an EMG-controlled prosthetic hand: analysis of user-prosthesis interaction. IEEE Trans Robot 24(1):170–184
25. Childress DS (1980) Closed-loop control in prosthetic systems: historical perspective. Ann Biomed Eng 8(4–6):293–303
26. Pylatiuk C et al (2004) Progress in the development of a multifunctional hand prosthesis. Conference on engineering in medicine and biology society, 1–5 September 2004, San Francisco, CA, USA
27. Sasaki Y, Nakayama Y, Yoshida M (2002) Sensory feedback system using interferential current for EMG prosthetic hand. Conference proceedings of second joint Embs-Bmes conference, 23–26 October 2002, Houston, TX, USA
28. Kaczmarek KA et al (1991) Electrotactile and vibrotactile displays for sensory substitution systems. IEEE Trans Biomed Eng 38(1):1–16
29. Riso RR, Ignagni AR, Keith MW (1991) Cognitive feedback for use with FES upper extremity neuroprostheses. IEEE Trans Biomed Eng 38(1):29–38
30. Navarro X et al (2005) A critical review of interfaces with the peripheral nervous system for the control of neuroprostheses and hybrid bionic systems. J Peripher Nerv Syst 10(3):229–258
31. Micera S et al (2006) Hybrid bionic systems for the replacement of hand function. Proc IEEE 94 (9):1752–1762
32. Dhillon GS, Horch KW (2005) Direct neural sensory feedback and control of a prosthetic arm. IEEE Trans Neural Syst Rehabil Eng 13(4):468–472
33. Cipriani C, Controzzi M, Carrozza MC (2011) The SmartHand transradial prosthesis. J Neuroeng Rehabil 8(1):29

34. Cipriani C, Controzzi M, Carrozza MC (2010) Objectives, criteria and methods for the design of the SmartHand transradial prosthesis. Robotica 28(06):919–927
35. Antfolk C et al (2010) SmartHand tactile display: a new concept for providing sensory feedback in hand prostheses. J Plast Surg Hand Surg 44(1):50–53
36. Micera S, Carpaneto J, Raspopovic S (2010) Control of hand prostheses using peripheral information. IEEE Rev Biomed Eng 3:48–68
37. Almström C, Herberts P, Körner L (1981) Experience with Swedish multifunctional prosthetic hands controlled by pattern recognition of multiple myoelectric signals. Int Orthop 5(1):15–21
38. Tan DW et al (2014) A neural interface provides long-term stable natural touch perception. Sci Transl Med 6(257):257ra138
39. Talan J (2014) Neural Interface activates a sense of touch in prosthetic limbs. Neurol Today 14 (21):10–11
40. Xu Q et al (2013) A novel mat-based system for position-varying wireless power transfer to biomedical implants. IEEE Trans Magn 49(8):4774–4779
41. Zhou H et al (2012) A fully implanted programmable stimulator based on wireless communication for epidural spinal cord stimulation in rats. J Neurosci Methods 204(2):341–348
42. Xu Q et al (2011) A fully implantable stimulator with wireless power and data transmission for experimental use in epidural spinal cord stimulation. Annual international conference of the Ieee engineering in medicine and biology society, 30 August to 3 September 2011, Boston, MA, USA
43. Qi X et al (2005) A versatile microprocessor-based multichannel stimulator for experimental use in epidural spinal cord stimulation. In: IEEE proceedings of first international conference on neural Interface and control, 28–26 May 2005, Wuhan, China
44. Cullen DK, Smith DH (2013) Bionic connections. Sci Am 308(1):52–57
45. Bray D (1984) Axonal growth in response to experimentally applied mechanical tension. Dev Biol 102(2):379–389
46. Heidemann SR, Buxbaum RE (1994) Mechanical tension as a regulator of axonal development. Neurotoxicology 13(1):95–107
47. Smith DH, Smith DH, Wolf JA, Meaney DF (2004) A new strategy to produce sustained growth of central nervous system axons: continuous mechanical tension. Tissue Eng 7(2):131–139
48. Pfister BJ et al (2004) Extreme stretch growth of integrated axons. J Neurosci 24 (36):7978–7983
49. Harrison RG (1911) On the stereotropism of embryonic cells. Science 34(870):279–281
50. Rajnicek A, Britland S, McCaig C (1997) Contact guidance of CNS neurites on grooved quartz: influence of groove dimensions, neuronal age and cell type. J Cell Sci 110(23):2905–2913
51. StEpieŃ E, Stanisz J, Korohoda W (1999) Contact guidance of chick embryo neurons on single scratches in glass and on underlying aligned human skin fibroblasts. Cell Biol Int 23 (2):105–116
52. Goldner JS et al (2006) Neurite bridging across micropatterned grooves. Biomaterials 27 (3):460–472
53. Fricke R et al (2011) Axon guidance of rat cortical neurons by microcontact printed gradients. Biomaterials 32(8):2070–2076

Chapter 5
Brain-Machine Interface-Based Rat-Robot Behavior Control

Jiacheng Zhang, Kedi Xu, Shaomin Zhang, Yueming Wang, Nenggan Zheng, Gang Pan, Weidong Chen, Zhaohui Wu, and Xiaoxiang Zheng

Abstract Brain-machine interface (BMI) provides a bidirectional pathway between the brain and external facilities. The machine-to-brain pathway makes it possible to send artificial information back into the biological brain, interfering neural activities and generating sensations. The idea of the BMI-assisted bio-robotic animal system is accomplished by stimulations on specific sites of the nervous system. With the technology of BMI, animals' locomotion behavior can be precisely controlled as robots, which made the animal turning into bio-robot. In this chapter, we reviewed our lab works focused on rat-robot navigation. The principles of rat-robot system

J. Zhang · K. Xu (✉) · S. Zhang · X. Zheng
Qiushi Academy for Advanced Studies (QAAS), Zhejiang University, Hangzhou, People's Republic of China

Department of Biomedical Engineering, Key Laboratory of Ministry of Education Ministry, Zhejiang University, Hangzhou, People's Republic of China

Zhejiang Provincial Key Laboratory of Cardio-Cerebral Vascular Detection Technology and Medicinal Effectiveness Appraisal, Zhejiang University, Hangzhou, People's Republic of China
e-mail: xukd@zju.edu.cn

Y. Wang · N. Zheng
Qiushi Academy for Advanced Studies (QAAS), Zhejiang University, Hangzhou, People's Republic of China

College of Computer Science and Technology, Zhejiang University, Hangzhou, People's Republic of China

G. Pan · Z. Wu
College of Computer Science and Technology, Zhejiang University, Hangzhou, People's Republic of China

W. Chen
Qiushi Academy for Advanced Studies (QAAS), Zhejiang University, Hangzhou, People's Republic of China

Department of Biomedical Engineering, Key Laboratory of Ministry of Education Ministry, Zhejiang University, Hangzhou, People's Republic of China

College of Computer Science and Technology, Zhejiang University, Hangzhou, People's Republic of China

have been briefly described first, including the target brain sites chosen for locomotion control and the design of remote control system. Some methodological advances made by optogenetic technologies for better modulation control have then been introduced. Besides, we also introduced our implementation of "mind-controlled" rat navigation system. Moreover, we have presented our efforts made on combining biological intelligence with artificial intelligence, with developments of automatic control and training system assisted with images or voices inputs. We concluded this chapter by discussing further developments to acquire environmental information as well as promising applications with write-in BMIs.

Keywords Brain-machine interface · Rat-robot · Behavior control · Brain stimulation

5.1   Introduction

Brain-machine interface (BMI) is a bidirectional pathway between the brain and external facilities. Besides its ability to read out information from the brain, providing an available communication method for the disabled, the BMI also has further applications in "writing" information into the brain. With encoded stimulations, researchers can send artificial information into targeted brain area, interfering neural activities and even generating sensations.

The using of physical stimulation to affect the brain function, mainly by applying electrical current into the brain, has been applied for clinical treatments for more than a century. Since electrical stimulation targeted at motor cortex can elicit limb movements [1], it was well adopted for improving neurosurgical procedures from early times [2]. More recently, deep brain stimulation (DBS) has become a common therapy to alleviate symptoms of some brain disorders such as chronic pain [3, 4] and the Parkinson's disease [5, 6]. Besides, electrical stimulation was also introduced as a tool for regenerating sensory feedback. Cochlear implants [7, 8] and retinal prostheses [9, 10] are two of such applications, replacing the impaired peripheral nerves with artificial devices. Moreover, recent works have shown that intracortical micro-stimulation in primary somatosensory system can generate discriminable tactile percepts from lab animals [11, 12] to human beings [13]. These approaches draw bright prospects of the "write-in" BMI applications.

However, it is not until the mid-1990s that this therapeutic stimulation application had found a new potential in the field of BMIs, when the concept of "bio-robot" first appeared. The idea of the BMI-assisted robotic animal system is accomplished by stimulations on specific sites of the nervous system. Studies in functional mechanisms of the nervous system gave rise to the potential of this animal locomotion control system with focal brain stimulations. Taking advantages of the artificial-evoked locomotion changes, researchers attempted to control animals with virtual perception cues elicited by electrical stimulations. Compared to traditional robot or

biomimetic robot, robotic animals have shown superior performances due to their flexibility, self-sufficient energy supply, and adaptability to complex environments.

One of the earliest attempts on direct animal controlling was made by a Japanese group. In their experiment, an American cockroach was successfully controlled to follow the forward and/or turning commands with electrical stimulations on the antenna [14]. Since the advent of the remarkable work, the researches on robotic animals, or bio-robots, have been developing rapidly in the following decades. Winged insects were one of the most interesting subjects. Artificial stimulation-controlled insects were thought to be an alternative to the insect-mimetic micro-air vehicles (MAVs) for their fascinating flight performances. An expanded variety of insects have been engaged in this cyborg insects study, including months [15, 16], beetles [17], and honeybees [18]. By implanting microelectrodes into antenna and optic lobes, the insects can be controlled to fly according to preset routes or even switch the wing oscillations.

Another hot spot in the field of bio-robot is behavior control of vertebrates [19–22]. Compared to insects, vertebrates have much more complicated brain structural and functional divisions and thus can be controlled to finish more complex tasks. Among various animals, rodents are always elusive with high agility, indicating the possibility of utilizing them for investigations and rescues. Furthermore, the rodents have an acute sense of smell, which exceeds most of the man-made sensors in both sensitivity and accuracy, making it a promising subject for explosive or drug detections. However, these small mammals are hard to be tamed with traditional training protocols. With the help of electrical stimulations, locomotion commands can be directly "written" into the animal's brain, saving training time and simplifying training paradigms at the same time. The initial idea of rat-robot control was accomplished by evoking virtual reward stimulation and whisker touching feelings to indicate moving forward or provide turning cues, respectively. Encouraged by this work, some other groups have made advances in control improvements.

In this chapter, we firstly introduced how rat-robot be controlled with write-in BMI. We then described some methodological advances developed for better locomotion modulation, such as optogenetic modulation methods. We also introduced our implementation of combining "write-in" BMI with "readout" BMI, as mind-controlled rat navigation system. Besides, we presented our efforts made on optimizing control strategies for automatic control and combining machine intelligence with biological intelligence for cognition enhancements. We concluded this chapter by discussing further developments to acquire environment information as well as promising applications with write-in BMIs.

5.2 Basis of Rat Navigation System

In 2002, Dr. Chapin and his colleagues managed to navigate rats through a complex field with electrical stimuli instead of external turning cues and rewards used in operant learning paradigms [23]. To accomplish the locomotion control, the rats
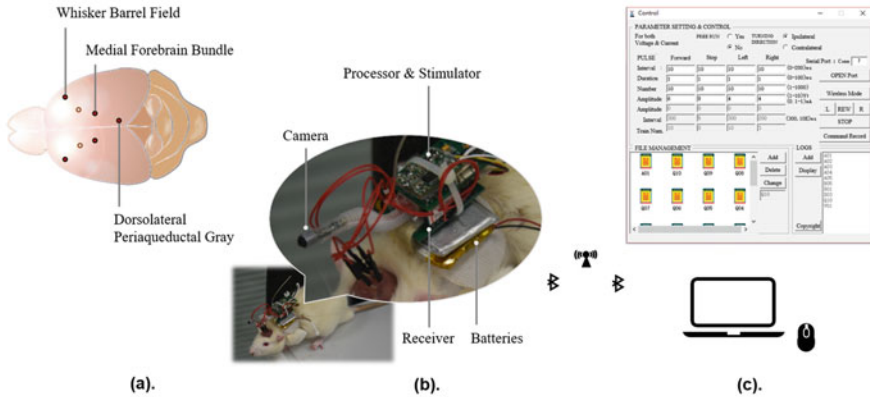
Fig. 5.1 Overview of the rat navigation system. The whole system is consisted of three parts: animal preparation, stimulator backpack, and remote control system. (**a**) Target brain sites for rat locomotion control, including turning cues (whisker barrel field/ventral posterior medial nucleus of thalamus, indicated in black dots and red circles, respectively), reward stimulation (medial forebrain bundle), and force holding (dorsolateral periaqueductal gray). (**b**) The stimulation backpack equipped with a video camera, which turning the received commands into electrical stimulations into corresponding brain sites and relaying captured videos back to operators at the same time. (**c**) GUI for operators to adjust stimulation parameters and deliver locomotion commands. The rat-robot can be controlled with a wireless mouse, and the information is exchanged wirelessly with Bluetooth

were firstly implanted with bipolar microelectrodes. After a period of training for the rats to correlate the electrical stimulation commands and corresponding behaviors, the rat's locomotor behavior can be controlled by the operators. In this model, electrical stimulations in different sites of the brain evoked different behavioral responses in rats, enabling accurate movement control in real time. Besides stimulation electrodes implantation, a backpack containing microprocessor and microstimulator needs to be mounted onto the rat for electrical stimuli delivering. The commands are then transferred wirelessly between computer and backpack. Figure 5.1 shows an overview of the whole rat-robot navigation system.

5.2.1 Principles of Rat-Robot Control

The BMI-assisted rat-robot locomotion control is mainly managed by evoking sensations and perceptions that lead to behavior changes caused by habits or reflections rather than directly activating targeted muscles. For movement control strategy design, the most classical method is to use electrical stimulation-evoked reward mechanism as an alternative for operant conditioning training. Other methods based on fear or punishment were also brought up as training-free solutions for rat-robot system improvement.

5.2.1.1   Virtual Reward-Based Training Method

To navigate a robot, at least two commands are needed for basic movement control: moving forward and turning left or right. Similarly, for typical rat-robot navigation control system, electrical stimulations are delivered into medial forebrain bundle (MFB) and somatosensory cortex (barrel field, S1BF) as virtual reward and turning cues, respectively, for movement control.

Medial forebrain bundle (MFB) has been proved to be involved in study and reward mechanisms. Electrical stimulation of MFB not only reinforces forward locomotion but also motivates further locomotion. Thus, MFB stimulation can be served as a virtual reward cue for rats to move forwards [24]. The effects of MFB stimulation can be tested and evaluated by behavioral tasks. Two typical behavioral designs are free-roaming task and lever-pressing task. The free-roaming task takes place in circular field or eight-arm maze. Rats receiving electrode implantation in MFB are allowed free roaming in the field. MFB stimulation with appropriate intensity will increase long-term locomotor activity of rats, inducing the rats to approach toward centered regions more often. In lever-pressing task, the rats are trained for a self-stimulation reward task. Once the lever is pressed by rat, a train of MFB stimulation will be delivered immediately to the rat as virtual reward. In the beginning of the first training session, the rats may touch the lever accidentally. After several tries, the rats learn the rule of self-reward stimulation and start pressing the lever frequently for reward seeking. After several days of reward training, the rats will show active movements with MFB reward stimulation.

The turning cues are induced by stimulating bilateral somatosensory cortex. Rat's somatosensory cortex barrel field (S1BF) is related to whisker sensing process. Stimulations in S1BF produce virtual whisker "touch" perceptions, inducing head movements and turning behaviors [25]. With this strategy, the rats need to receive a reinforcement training section of about 5–7 days. During this section, the animals are trained to link electrical cues with appropriate turning directions. At the beginning of each training session, the rats are motivated to keep running forwards in an eight-arm maze with MFB stimulations. Either left or right turning cues will be given when the rats entering the central area of the maze. Once the animal turns correctly after turning cue delivers, the rat will receive a train of MFB stimulation as reward. By associating MFB rewards to each correct turn, the rats can learn to perform highly accurate turning behavior following electrical stimulations. Generally, the initial turning directions are not uniform across untrained rats. While some animals would turn ipsilateral to the stimulated site, others show contralateral turning behavior. As the training procedure associated turning cues with rewards, the rats could finally turn to consistent direction according to turning instructions. Particularly, the turning direction is largely depended on the association of MFB rewards, especially in those initial trainings. When MFB rewards are given upon ipsilateral turns, the rat could learn to turn ipsilaterally to the S1BF stimulation, and vice versa [26].

5.2.1.2 Optimization of the Turning Behavior

With the combination of MFB reward and S1BF turning cues, the rats can be navigated over three-dimensional structures by operators. Motivated by MFB rewards, the animals are able to run forwards and even climb or descend steps. However, the control of turning behavior of the reported rat-robot exhibits a large variability in the results produced. Although the training procedure ensures a high success rate of turning behavior in rats after corresponding stimulation cue, the trained rats are observed to have no response to the electrical stimuli occasionally. Recent studies suggested that deep brain stimulation in thalamus might elicit more stable sensations in animals [27]. In rat's whisker sensing pathway, deflections of whiskers first activate neural responses in the brainstem. The information is then transferred into ventral posteromedial (VPM) nuclei of thalamus before it finally projected to the somatosensory cortex (S1BF).

We have tested the effects of VPM stimulation for turning behavior control [28]. The behavioral study showed robust turning reactions following VPM stimulation without training (see Fig. 5.2a). Parameter modulation tests display a near-linear relationship between the turning angle of the rat and stimulation intensity, suggesting the possibility of quantitative control of turning behavior [29]. A later micro-PET imaging study has shown that stimulation in VPM induces significant glucose uptake changes in S1 [30]. Further optical imaging studies display a larger activated area in S1BF with stimulation in VPM thalamus rather than directly in S1BF area (see Fig. 5.3), suggesting an amplifying effect through thalamocortical pathway. These behavioral and imaging results indicated that VPM stimulation may provide a more efficient alternative method for turning control in rat-robot system.
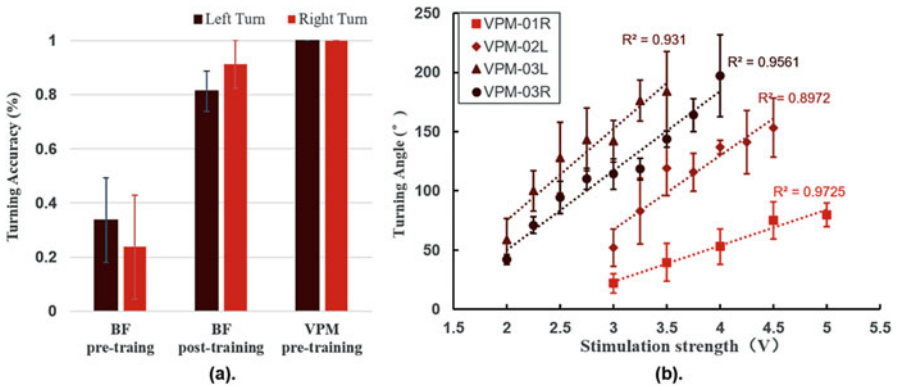

Fig. 5.2 Performances of turning behavior with VPM stimulations. (**a**) Turning accuracies calculated from both S1BF stimulation group and VPM stimulation group. VPM stimulation resulted in highly successful turning behavior without training. (**b**) The effect of stimulation strength on rat's turning angle. With the increase of stimulation voltage, the turning angle of rat showed near-linear trends. (**a** and **b** are modified from [28], Table 1 and Fig. 2A, respectively.)
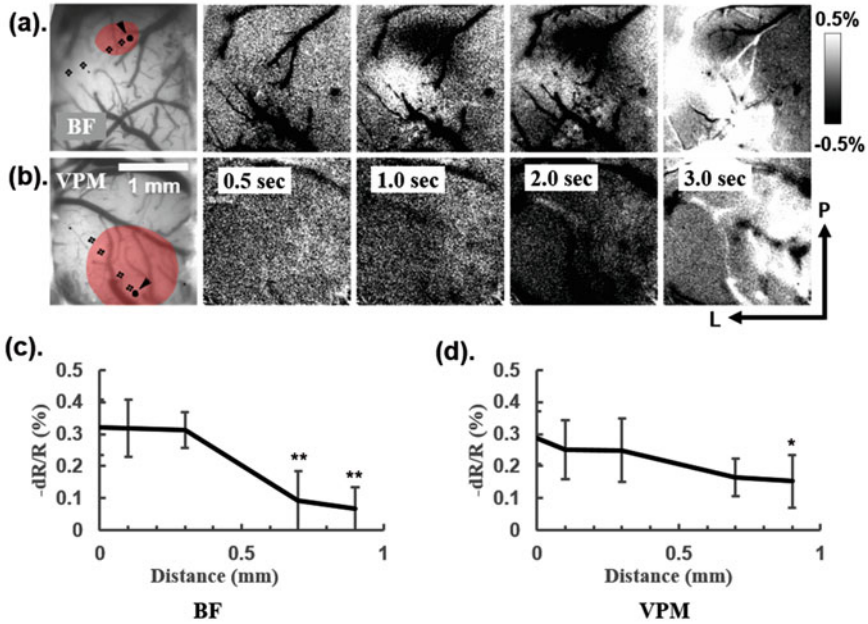
Fig. 5.3 Optical imaging responses to electrical stimulations. (**a** and **b**) Intrinsic optical imaging responses to S1BF stimulation and VPM stimulation, respectively. The darkened area indicated cortical activation spread. After a 500 ms stimulation (between 0.5 s and 1.0 s illustrated), the cortical area imaged over time responded differently to the two stimulation methods. The red-colored areas in the vessel maps illustrated significance ($p < 0.01$, t-test) between stimulation trials and control trials. *P* posterior, *L* lateral. (**c** and **d**) The corresponding response magnitudes as function of distance from the arrowed ROIs (regions of interest). S1BF stimulation resulted in a quicker drop of response magnitudes at distant spots. (Student's t-test, $*$, $p < 0.05$; $**$, $p < 0.01$). (**b** and **d** are modified from [29], Fig. 2.)

5.2.1.3   Punishment-Driven Behavior Control

With a combination of forward and turning commands, the rat can be controlled to move in a complex environment. Unlikely to traditional mechanical robots, one of the limitations of this intelligent robot is that the rats can hardly stay still without commands. Therefore, it is important to find a way to keep the rat immobile. One of the solutions is to utilize the distinct feel of fear and defense. Researches have shown that electrical stimulation in dorsolateral periaqueductal gray (dlPAG) induces defensive behaviors [31]. With the increase of stimulation strength, the animals show series of behavioral changes from alertness to freezing and finally escape [32]. In order to maintain immobility, stimuli should be carefully controlled in a certain range. We have tested the impacts of stimulation parameters and found that variation of both stimulation frequency and pulse train duration is efficient in
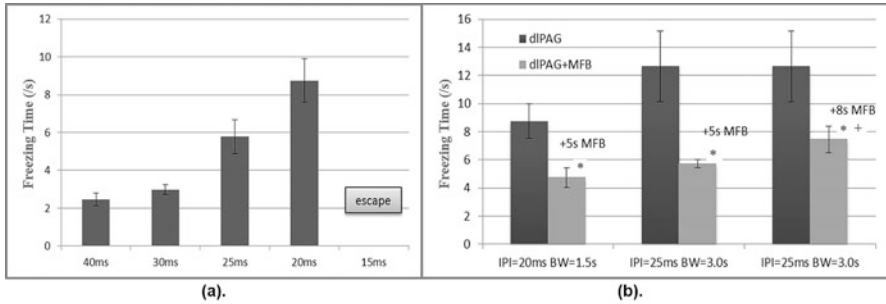
Fig. 5.4 Freezing behavior evoked by dlPAG stimulations. (**a**) Rat's freezing time changes resulted from different stimulation inter-pulse intervals (IPI). Rats showed longer freezing time with shorter pulse intervals and even start escape at the inter-pulse interval of 15 ms. (**b**) Reward stimulation effects on freezing behavior evoked by dlPAG stimulations. The MFB reward can remarkably reduce the freezing time durations at varying combination of inter-pulse interval (IPI) and burst width (BW). ∗, P < 0.01 different from dlPAG stimulation and dlPAG +MFB stimulation; +, P < 0.01 different from dlPAG+5 s MFB stimulation and dlPAG +8 s MFB stimulation. (Modified from [29], Figs. 1 and 3, respectively)

modulation of freezing time of the animal [33]. Furthermore, since MFB stimulation has reward effects, an MFB stimulation following dlPAG stimulation can remarkably reduce the freezing time, bringing the animal back from the holding state more quickly (as illustrated in Fig. 5.4b). Hence, by stimulating dlPAG or MFB, the rat's behavior can be switched between hold still and move on, like a real robot.

This "fear-caused" freezing reaction is more instinctive and can be evoked directly without any training. Similarly, a new method was proposed as a "virtual punishment"-driven solution to rat-robot navigation control [34]. This study investigated the responses of rats with stimulations in amygdale nucleus (AMY) and thalamic ventral posterolateral (VPL) as the alternatives to forward and turning cues, respectively. These two sites are involved in nociception or fear/anxiety information transmitting, providing a potential for learning-free rat-robot developments. More lately, another team also reported a direct turning behavior control method accomplished by stimulating nigrostriatal pathway [35]. This newly adopted brain site exhibits an immediate contralateral turning behavior in response to a single stimulation.

5.2.2 The Remote Control System

During locomotion control of rat-robot, cable connections for stimulation delivery may be a major limitation for animal's movements while roaming in large area. Thus, telemetry systems have been designed to overcome this problem. Feng et al. have designed a remote control stimulation system for controlling free-roaming animals [26]. The control system includes a remote-controlled micro-stimulator, a

control program, and the Bluetooth modules for wireless communication between stimulator and control program. The control program firstly initiates the hardware and opens a protocol file for a specific rat. When user orders an instruction such as move forward or turn left/right, the program sends commands to the transmitter with preset stimulation parameters. The commands are finally translated by the receiver, and corresponding stimulations are delivered into the corresponding brain sites through electrodes implanted.

The stimulator is designed to be mounted on the rats for commands receiving and stimulation delivering. To fit small animals, the remote-controlled micro-stimulator should be kept small and light. At this point, one of the main concerns is the power consumption of the micro-stimulator. Thanks to the development of microelectronics, microprogrammed control unit (MCU) with high speed and low power consumption can be adopted as the main processor for control of receiving commands and delivering stimulations. The whole backpack mounted on controlled rat contains a receiver and a stimulator and weights only 20 g, with a total size of 36 mm × 22 mm × 15 mm. The stimulation commands received are translated by the MCU and then electrical pulses are delivered into corresponding sites of the rat's brain. Generally, the electrical stimuli are trains of biphasic, charge-balanced pulse trains. The stimuli delivered are effective with either constant voltage or constant current.

The control program is designed for navigation orders delivering as well as stimulation parameter setting. A basic instruction set for rat-robot navigation includes "Forward", "Left", and "Right", corresponding to the virtual reward and turning cues. For some cases, the "Stop" command can be added for the holding behavior control. With preset communication protocols, the instructions made by operators can then be transmitted to the stimulator and be finally translated into electrical stimulation pulses. For convenience, a wireless mouse or other portable devices can be employed as remote controller, providing a real mobile solution to working in complicated circumstances. As to optimize the animal locomotion control, the stimulation parameters are adjusted individually and can be saved and retrieved for reuse or edition in file management panel.

A Bluetooth module is applied for wireless communication in this system. The module can work properly within a range of 100 m with communication speed up to 70 kb/s, which is even sufficient for multi-channel bidirectional communication. Therefore, an improved version has been developed realizing a bidirectional telemetry system with both electrical stimulation and signal recording for free-roaming rats [36]. In this version, besides producing four-channel stimulus, the system can also acquire two-channel neural signals in real time. The recording module is capable of recording both neural action potentials (APs) and local field potentials (LFPs). This bidirectional communication system takes step towards the final goal of developing a closed-loop BMI. By analyzing neural signals in real time, stimulations can be triggered when necessary, forming a closed-loop brain-machine interface. Such closed-loop system is flexible in stimulation time, providing better treatment effects in clinical therapy with deep brain stimulation (DBS).

5.2.3   Rat Navigation Guided by Remote Control

After a few days of adaptation and training, the rats can learn to link the S1BF turning cues with MFB stimulation rewards, showing the feasibility of electrical stimulation-evoked "virtual" learning. With proper combinations of these two stimulation commands, the rats can be well steered towards targeted locations by operators. Notably, during navigation control, the MFB stimulation not simply acts as a reward feedback whenever the rat responding to turning cue correctly but also serves as a driving force to keep the rats moving continuously. In fact, frequent MFB stimulations during rats' locomotion reinforce their motivation of moving forward. Free-roaming rats with MFB stimulations show an increased locomotion activity and take more approaches toward the central area of the field. Therefore, with the help of this "virtual reward" stimulation, the rats can be induced to climb or descend from ladders/stairs and steep ramps or even jump off platforms.

Together with turning cues, well-trained rat-robots can then be adapted to complex three-dimensional obstacle courses quickly. As shown in Fig. 5.5, with the
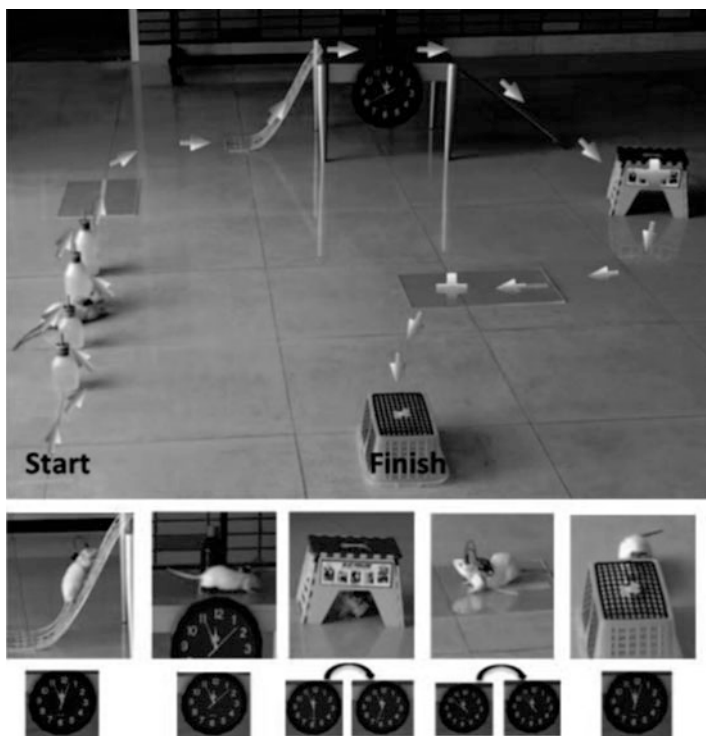
Fig. 5.5 An example of guided rat navigation using brain micro-stimulation. Well-trained rat-robot can be guided to pass through slalom courses, climb steep ramps, and even hold still for 3–5 s at target spots. (From [33], Fig. 4.)

"holding" command of dPAG stimulation, the rats can even be controlled to stay still for several seconds at any locations that be instructed to. Moreover, we have managed to guide the rats in some real conditions, such as passing through offices and corridors, crossing narrow pipelines and clumps of grass, and circumventing obstacles. While configuring the rat's backpack with a wireless micro-camera, the environmental images can be captured in real time, enabling the operators to navigate the rat-robots at beyond-visual ranges.

5.3 Novel Rat-Robot Control Method Based on Optogenetics

Optogenetics is one of the newly developed neural modulation techniques in recent years. By genetically expressing light-sensitive channel protein on specific type of neural population, targeted opsin-transduced neurons can be activated via optical stimulations with certain wavelengths. Compared with traditional electrical stimulation, optogenetic technique has the advantage of activating specific types of neurons, thus narrowing the activated range to desired areas. Besides, it also provides an opportunity to record neural electrophysiological activities during stimulation. For precise locomotion control, we developed a rat-robot system based on optical modulation.

5.3.1 Model of Optogenetics-Based Rat-Robot

The basic idea of optogenetic technique is to utilize the light-sensitive membrane ion channels to selectively activate neural populations. Different opsin channels can be activated with stimulation lights at different wavelengths, enabling either excitation or inhibition of the selected neural populations. Neural modulation by optogenetic technique requires transduction of light-sensitive opsin, optical stimulus with specific wavelengths, and proper stimulation intensities. In our current optical modulated rat-robot model, opsin gene of channelrhodopsin-2 (ChR2) is chosen for exciting neural populations. This opsin carried by adeno-associated virus (AAV) is transduced into excitatory neurons under the guidance of calcium-calmodulin-dependent kinase II type-FC; (CaMKIIFC;) promoters. After 3–4 weeks of recovery and ChR2 expression, the targeted areas in the rat's brain can then be activated by delivering blue light at a wavelength of 473 nm.

Similar to electrical stimulation control, optogenetic modulation of locomotion is also based on evoking virtual reward and defense behavior. For the "holding" behavioral modulation, optical stimulation is targeted at dPAG, the same brain area as used in electrical stimulation model. However, as to reward delivery, MFB
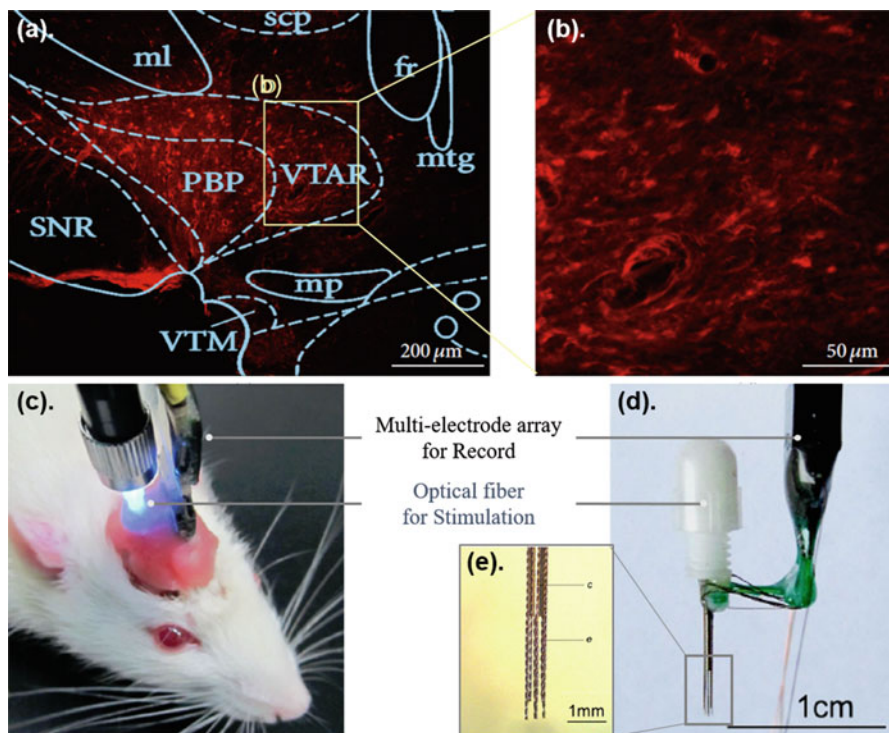
Fig. 5.6 Setup of the optogenetic model. (**a**) A typical view of the ChR2-mCherry expression on the neurons expressing CaMKIIα in and around the region of VTA (ventral tegmental area). An enlarged region of interest (ROI, squared in **a**) is illustrated in (**b**). (**c**) ChR2-transduced rat with implanted devices for optogenetic modulation. (**d**) The implanted device ("optrodes") with both optogenetic stimulations and electrophysiological recordings. (**e**) Enlargement of the electrode tips. The centered guide cannula is prepared for virus injection and fiber implantation, and the surrounded electrodes are for neural signal recording, with two different depths. (**a** and **b** are modified from [37], and Fig. 1. (**c–e**) is modified from [38], Figs. 1 and 3.)

is not an ideal target for optogenetic model since this bypassing axon bundle is lacking of cell bodies to be transduced with opsin genes and activated by light. Actually, MFB is one of the projections from the ventral tegmental area (VTA) with ventral striatum. VTA is believed to be involved in natural reward circuitry and motor activity, as well as drug addictions, providing an ideal site for opsin gene expression.

Successful expression of opsin genes can be verified by histological studies. The ChR2-mCherry expression traces can be observed on frozen brain slices with fluorescent images taken under a microscope. Figure 5.6a and b shows a typical view of the ChR2-mCherry expression image captured with fluorescent microscope, revealing a high density of transduced neural populations in the targeted brain regions with normal cell morphologies [37].

5.3.2 Optical Stimulation and Electrophysiology

Similar to electrical stimulations, during optical stimulations, the light intensity is of crucial importance. Previous researches showed that light intensity lower than the threshold of 1 mW·mm^{-2} can hardly activate ChR2-transduced neurons [39, 40], while overlarge stimulation intensity may damage the brain tissue around the stimulation site. Therefore, to activate enough range of brain tissue safely and efficiently, the appropriate stimulation intensity needs to be carefully calculated. Besides, due to diffusion and scattering, the light transmission distance in brain tissue is limited. According to the Kubelka-Munk model for diffuse scattering media [39], the light transmission fraction of an ideal model expresses relationships with both light penetration in the brain and scatter coefficient of penetration distance. For rats we have used in rat-robot control model, the appropriate distance for light delivery over the targeted brain area is 0.5 mm [38].

Besides the main advantage of activating neural populations selectively and precisely, the optical stimulation also enjoys the benefit of being free from stimulation artifacts. We have designed a multi-electrode array coupled with fiberoptic for simultaneous optical stimulation and electrophysiological recording [38]. As shown in Fig. 5.6c–e, this integrated optrode array device is consisted of a centered fiber guide cannula and 16 surrounding recording electrodes with 2 layers for different recording depths. In vivo electrophysiological recording demonstrates that optical stimulation can successfully evoke an increased neuronal activity with time specificity. Figure 5.7a and b illustrates the electrophysiological responses to optical stimulation [37]. During optical stimulation, neural spike firing activities show obvious increases in recorded area. At the end of optical stimulation, neural activities drop back to normal background level. Similar changes are also observed in local field potential signals, where the magnitude recorded increases during optical stimulation period. With the help of simultaneous electrophysiological recording, we have further tested the effects of stimulation parameters. As shown in Fig. 5.7c, optical stimulation with low frequency (5 Hz) can hardly induce significant increase in neuronal activities. While stimulated with higher frequencies, the spike firing rates recorded display significant increases from background level. The spike firing rate changes can be modulated by both frequency and stimulation intensity, showing increasing firing activities with higher frequency or intensity.

5.3.3 Behavioral Modulation of Optogenetic Rat-Robots

Optical stimulation with proper parameters also exhibits stable behavioral modulation effects on optogenetic rats. Optical stimulation in dPAG area can induce typical freezing and escape responses in rats, similar to that observed on electrically induced behavior change of rats. Track navigation tests showed precise freezing
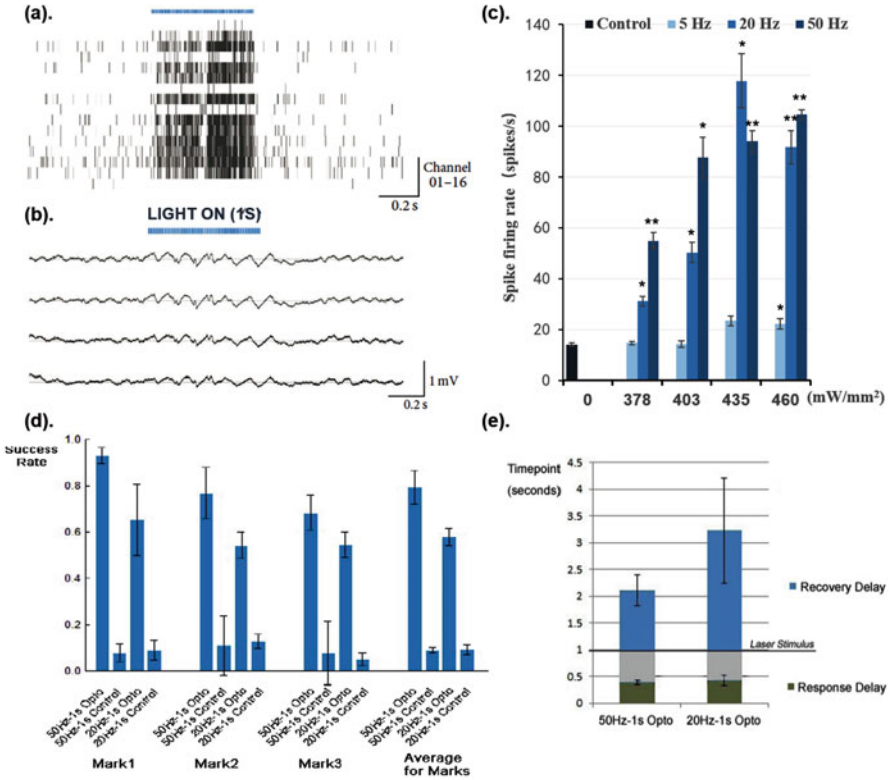
Fig. 5.7 Optogenetic modulation effects on rat-robots. (**a** and **b**) Typical in vivo spike and LFP signals recorded from the implanted optrode device, respectively. The blue bars indicate the onset of stimulation light, a train of 1.0 s pulses, with 15 ms pulse width and 50 Hz frequency. (**c**) The optical modulation effects on electrophysiological recordings. Both stimulation intensity and frequency have modulation effects on spiking firing rates (∗, $p < 0.05$; ∗∗, $p < 0.01$; one-way ANOVA, between stimulation and control group). (**d** and **e**) The modulation effects on rat holding behaviors. The optical simulations have obvious and stable modulation impacts on rat's behaviors at different mark points. (**a** and **b** are modified from [37], Fig. 1c is modified from [41], Fig. 4, and (**d**) and (**f**) are modified from [42], Fig. 1.)

behavior modulation both temporally and spatially. The optogenetic rats can be modulated to hold on any location along the trace, with short response delays (to start freezing) as well as recovery delays (to end freezing after stimulation) [42]. In accordance with electrophysiological recordings, stimulations with higher frequency display better modulation performances on both success rate and response delays (shown in Fig. 5.7d and e). Compared with electrical stimulation, this optical stimulation in dPAG induces more stable and moderate defensive responses, exhibiting shorter recovery periods after stimulation [41]. These results show the superiority of optogenetics over the traditional electrical stimulations.

As to stimulation in VTA, the optogenetic rats exhibit conditionings on reward learning. With optical stimulation, the optogenetic rats exhibit an increased, long-term locomotion activity in a free-roaming task. Further self-reward lever-pressing task shows an ascending tendency of lever presses over training sessions, demonstrating the "virtual reward" effect induced by optical stimulation in VTA neurons [37]. These results indicate that optical stimulation in VTA is an alternative way to induce reward-seeking behavior in rats rather than electrical stimulation in MFB. Taken together, the technique of optogenetics provides a novel method to regulate rat's locomotion switching between move and stop more precisely than traditional electrical stimulations both spatially and temporally.

5.4 Rat-Robot Navigation System Controlled by Human Brain

As mentioned above, the BMIs are bidirectional communication pathways which are able to modulate brain activities as well as to interpret thoughts in living brains through computers. Therefore, by combining the two directional BMI pathways, a "Brain-to-Brain Interface" (BBI) can be established where neural activities of two or more individual brains can be linked by external devices [43]. Experiments have proved that BBIs have the ability to translate locomotor intentions in real-time among brains [44–48] and even across species [49]. The application of BBI may augment the mutual coupling of brains, coupling neural processes of one brain to another, and thus may have a positive impact on human social behavior. Another potential application of BBI system is to implement locomotor control of cyborgs directly with human thoughts. Zhang's group has demonstrated a cyborg cockroach navigation system controlled by steady-state visual evoked potential (SSVEP) with a noninvasive BMI device. Since the SSVEP-based BMI decoding relies on visual stimulations, the operator's attention may be distracted from cyborg's location feedback by real-time images. To overcome this shortage, we have explored the utilization of motor imagery as an alternative solution. Here, we will briefly introduce our efforts made on motor imagery-based "mind control" of our rat-robots system [50].

5.4.1 Configuration of the BBI System

The BBI system is comprised of an electroencephalography (EEG)-based noninvasive BMI device, a host computer, the rat-robot navigation control system, and a video camera-based visual feedback system. The EEG-based BMI device is applied for motor imagery signal acquisition from human operators. The signals are sent to the host computer through Bluetooth, where motor intentions are recognized and
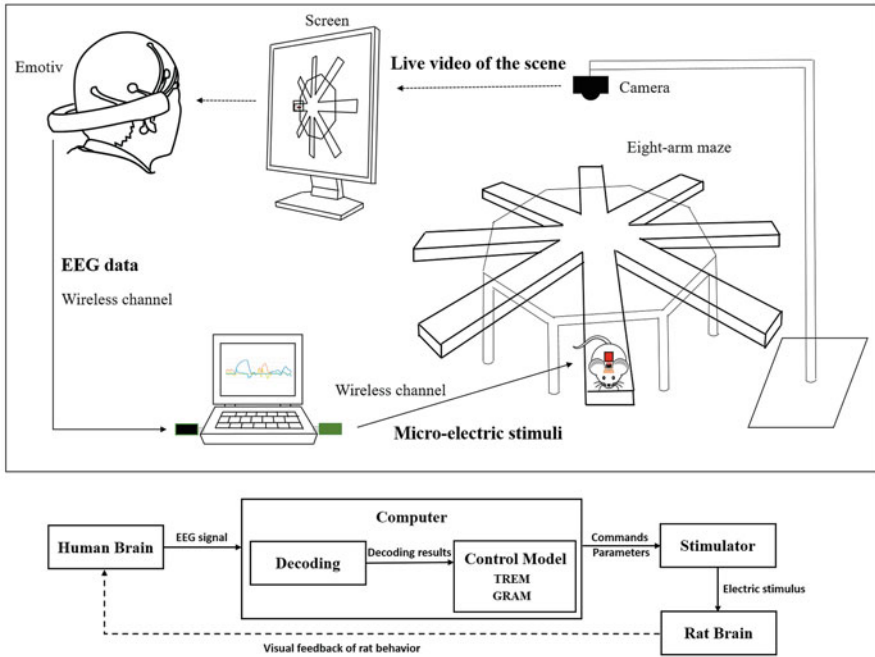
Fig. 5.8 The framework of mind-controlled rat-robot system. (From [50], Fig.1)

classified. The decoding results of motor imagery signals are then translated into locomotion control commands of the rat-robots. With the help of the remote control system, the navigation commands from the operators can finally be applied on rats through stimulator backpack.

To form a closed-loop control system, we have chosen video information as feedback signals. The visual feedback information is provided by a bird's-eye camera, with which the entire experimental field is supervised. The recorded images are sent back to an LCD screen and presented in front of the operator; thus the rat's location can be traced by an operator in real time. Figure 5.8 shows the framework of a complete BBI system.

5.4.2 Implementation of Motor Imagery-Based BMI

Different from typical manual control model, the mind control signals need to be detected and deciphered before controlling stimulations delivered to rat-robot. The operator's "thoughts" are recorded by noninvasive EEG devices. In our current BBI system, the Emotiv EPOC Neuroheadset (Emotiv Company) [51] is employed

for EEG signal recording, providing up to 14 recording channels and wireless information transmission in real time. The neural signal obtained is transmitted to the host computer for further processing. As the SSVEP signals are liable to distract the operator's attention from the visual feedback of rat-robot's locomotion states, we tried a combination of nictation signals and motor imagery signals as mind control signal sources, where the nictation signal is used for reward control and motor imagery as turning cues. The eye blinks are detected by amplitude changes from raw data recorded with the frontopolar channel of the Emotiv device. And the turning cues are decoded from motor intent of left and/or right arm movement of the operator. This imagination signal requires the operators to modulate their oscillation rhythms of sensorimotor cortex into the upper mu frequency band (10–14 Hz). The power spectrum of the imagination raw data is calculated as the main character for motor intent decoding. After several sessions of signal decoding training, motor intents can be detected and evaluated by classification algorithms.

To eliminate the noises from real motor intent signals, thresholds are set as criteria for corresponding control stimulation delivering. Decoding results are detected as real intentions only when the resulting values are above the thresholds, while subliminal ones are considered as noises. However, the threshold needs to be determined carefully, since higher thresholds can efficiently reduce false alarm rate while increasing the miss rate at the same time. During rat-robot navigation control, either the increasing of fake control stimulations or the missing of key turning commands may cause failures in rat's locomotion control, resulting in lowered control efficiency. One of the feasible alternatives is to use changing gradients as the evaluation criteria. Recorded data shows that compared to background noises, the real intention signals display a larger gradient at the beginning. By calculating the changing gradients of the values decoded, the control efficiency can be significantly improved while ensuring a low false alarm rate as well.

Open-field tasks show that the system performs a mean delay of 158 ms between the detection of motor intents and the delivering of electrical stimulations, which is sufficient for stable control of rat's locomotion. Further eight-armed maze tasks also show an overall success rate above 80%. These control results suggest that our BBI system realizes a high-performance mind-controlled rat-robot navigation model.

5.5   Optimized Solutions for Control Strategy

In previous sections we have demonstrated a navigation system manipulated by human operators with hand or even by the mind. However, for mass preparations, human training seems to be inefficient, since experiences and concentrations are required for the training sessions. Besides, lack of information feedback is another main drawback of current rat-robot model. These restrictions hold the rat-robot technique back in demonstration stage rather than real practical applications. One

of the solutions is to employ artificial intelligence as controlling assistant. In this section, we will demonstrate our attempts made on automatic control systems and other artificial equipment assisted control strategies.

5.5.1 Automatic Control System Designed for Rat Navigation

Machine learning gives computers artificial intelligence in many aspects. With the help of this technology, robots can be controlled automatically by computers. Thus, it is natural to expect an automatic controlled rat-robot system. However, unlike traditional mechanical robots, there are several challenges of controlling these living creatures. Self-consciousness and biological intelligence are the major differences between bio-robots and traditional robots. To rat-robots, stimulations are more like "cues" to induce proper movements rather than force driven, resulting in uncertainties of reactions to the same command. It makes the decision logic hard to be modeled with explicitness and preciseness. In addition, the body of rat-robot is variable among individuals and not rigid while moving, making it difficult to extract locomotion information of the animal. Without precise locomotion parameters, it is impossible to evaluate the feedback of control command and thus difficult to make the following decisions.

To solve the problem of locomotion parameters, an extra bird's-eye camera is employed to supervise the entire experimental scene for real-time movement capture of the rat. The rat's locomotion information including body position and head orientation is tracked and extracted with imaging processing techniques [52]. A decision algorithm based on state machines can then be used to choose proper command to induce rat-robot to accomplish a preset navigation task. The schematics of the navigation system are illustrated in Fig. 5.9.

As to individual variations, we borrow experiences from human navigating operations and propose a new method to learn and imitate this process [53]. Different from the traditional methods that try to describe controlling logic explicitly, the new model regards the navigation as a whole procedure and learns to make controlling decision based on the operations made by human operators. In this model, a General Regression Neural Network (GRNN) is applied as the mathematical model for control decision learning. A total of two steps are included in this model. During the first training stage, the control commands made by human operators and the corresponding locomotion information of rat-robot (including body position and head orientation) are extracted and synchronized as the labels and inputs to the model. During this short training session, the GRNN configures the network with the instances. After the training sessions, the GRNN model is able to generate controlling instructions automatically and thereby takes place of human operators to navigate the rat-robot. This newly proposed method displays comparable performance to human operators with high accuracy and reasonable stimulation instructions quantities, indicating that the basic locomotion as position and
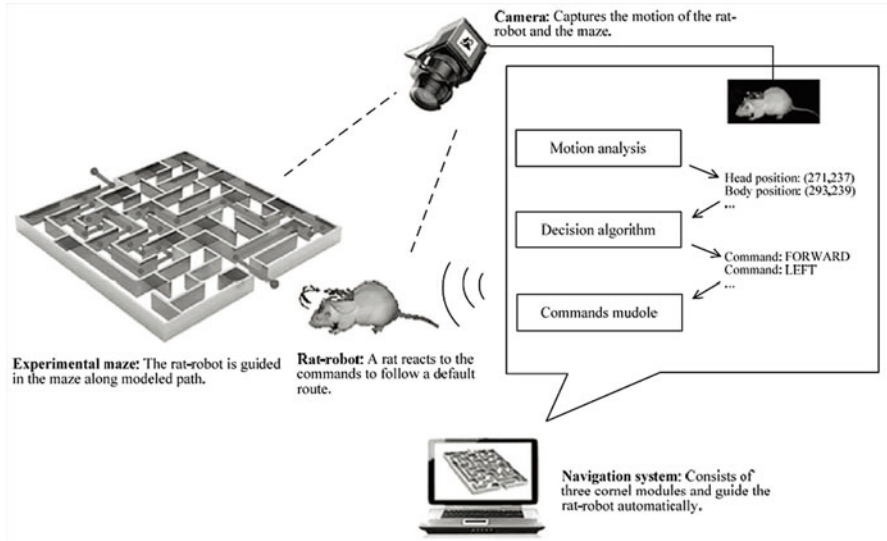
Fig. 5.9 The framework of automatic navigation system for rat-robot. (From [54], Fig. 5)

orientation can provide enough evidences for controlling decision-making [54]. This conclusion is essential for further studies of bio-robots.

5.5.2   A Reward-Driven Control System

The control strategy mentioned above mainly focuses on simplifying the decision logic by mimic the controlling principles conducted by human operators as a whole. In this process, three directional commands are needed to be classified from loco-motion information. In fact, thanks to its biological intelligence, the rat-robots have shown the capabilities of reward seeking during daily training. It is well known that rats have remarkable ability in navigation [55]. In spatial learning studies, the rats are trained to seek for rewards and correct their behaviors whenever the rewards are deprived [56]. Therefore, it is feasible to use single reward command to guide the rat-robot, further reducing the decision-making procedure of the automatic control-ling strategy.

According to this idea, we have designed a new automatic controlling strategy by applying reward-only commands [57]. This method simplifies the automatic navi-gation algorithm largely by taking full advantage of the rats' learning capabilities. A schematic diagram of control strategy is illustrated in Fig. 5.10. Before the naviga-tion test, the destination of the task is preset, and the corresponding navigation route is yielded by path planning algorithm. During navigation task, the rat-robot receives rewards frequently when it performs ideal behaviors as walking along the right route. If it walks into incorrect direction, the rewards are cut off as a cue. The rat-robot
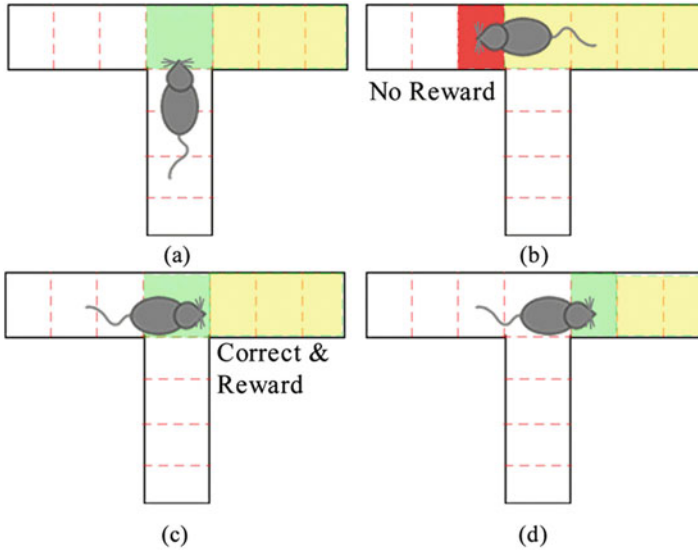
Fig. 5.10 Schematic of the reward-only automatic control model for rat-robot navigation. The green grids indicate current correct locations of the rat, the yellow grids denote the ideal route toward destinations, and the red ones represent the wrong route. (**a**) The rat-robot enters the crossing area of the maze following reward stimulation without turning cues. (**b**) The rat turns into one of the arms at its own will. As entering a wrong grid, no reward is given, and the ideal route is re-computed. (**c**) The rat turns back seeking for reward and enters the correct direction. As the route is reset, the rat gets reward again. (**d**) The rat moves forward following the reward stimulation toward the targeted end. (From [57], Fig. 1)

would realize its error and correct to proper direction for rewards. After several days of training with the automatic control system, the rat-robots show high performances in simple T-maze tasks, with their turning directional preferences dropping along with the training session. These results indicate a successful attempt at combining biological intelligence with artificial intelligence, providing new ideas for further studies on bio-robot controlling and intelligence hybrid.

Furthermore, to enhance the capability of exploring un-configured environment, we propose another reinforcement learning process-involved graded reward-generating algorithm [58]. Q-learning procedure, one of the classical reinforcement learning methods, is introduced in this method, to generate an incremental sequence of electrical reward according to the distance from the preset destination. During navigation task, the rat-robot receives higher reward stimulations when it approaches closer to the given destination. After the initial trial-and-error test, the animal learns to seek the maximum reward spots in an unknown environment. Since the rat has excellent spatial recognition, the rat-robot and the reinforcement learning algorithm can convergent to an optimal route by co-learning. This work has significant inspiration for the practical development of bio-robot navigation with hybrid intelligence.

5.5.3 Cognition Enhancement of Rat-Robotics with Visual/ Audio Cue

Another advantage of hybrid intelligence is that we can balance biological intelligence with artificial intelligence. Utilizing of animals instead of mechanics overcomes difficulties faced by traditional robotics such as motion flexibility and stability, and meanwhile, external devices can be a compensation for rat's own limitations. For example, it is broadly known that rats communicate with ultrasound band (higher than 20 kHz) [55], which is far beyond human speech wavelength range (300–3400 Hz). It seems impossible for rats to understand or even hear voice commands from human beings. Nevertheless, with the help of speech recognition module, computers can directly translate vocal navigation commands into electrical stimulations without hand operations [59].

In addition, when the rats are equipped with sensory devices, environmental information can be acquired and analyzed by computers remotely. This equipment upgrade may encourage the rat-robot to move further into larger areas. Considering the poor vision of rats, one of the most intuitive approaches is taking images. With miniature cameras mounted on backpack, environmental imaging information can be captured and transferred back to a host computer. Operators can then guide the rat-robot from far beyond visual range. Furthermore, with the technology of image recognition, objects of interest can be detected efficiently by algorithms. The object detection results can in turn be taken as guidance on adjusting the moving directions of rat-robot toward the object. Incorporated with object detection methods, this closed-loop model can accomplish beyond visual range control of rat robotics automatically, which is of great significance for remote searching tasks [60].

5.6 Conclusions and Future Perspectives

For decades, great progress has been made in locomotion control of rat-robots. Commands "written" into the rat's brain have become more and more efficient. The main idea of locomotion control is to use electrical stimulation to mimic natural perceptions and feelings that result in corresponding behaviors of rats. By carefully selecting stimulation sites and parameters, rats can be guided in complex environments. Integrated with artificial intelligence, rats can even be controlled automatically by computers to reach a preset destination. On the contrary, there are also many limitations to what has so far been accomplished with rat navigation system. The major problem is the lack of feedback information of the environment surroundings. Without efficient information feedback, operators can hardly control the rats to avoid obstacles or adjust heading direction towards targets. Video cameras with image stabilization technique mentioned in Sect. 5.2 are one of the solutions. However, the angle of view restricts the ranges of information obtainment. Besides, weights of bear load also limit quantity and dimension of equipment that can be carried by rats.

In actual situations, odor information is always of great importance. In fact, rodents have excellent sense of smells. Given their small sizes and light body weights, rodents are more suitable for demining than traditional canine. APOPO (Anti-Personnel Landmines Detection Product Development), a non-governmental organization, has been developing technologies for landmine detection using African Giant Pouched rats (*Cricetomys gambianus*) since 1996. Although the trained rats showed a relatively high average indication rate of 76%, the score was varied among individuals while taking a long period of training as well. When taking advantage of BMI technology, the training paradigms are simplified. The electrical stimulation can provide more stable control of rat's locomotion, and the virtual reward stimulation may accelerate combination learning between target odor and reward. Moreover, with a bidirectional BMI, odor information might be read out straightly from the rat's brain, and more information could then be decoded including odorant components and concentrations. These readouts might largely enrich operator's knowledge of environmental information, leading to more precise navigation control of rat-robots.

Clinically, BMIs are designed for movement assistance and rehabilitation therapy of paralyzed patients. An ideal BMI system requires bidirectional, closed-loop information communication. Besides reading out motion intentions through brain-to-machine pathway to drive prosthetics, sensory information feedback is of equal importance. Compared to neural signal decoding, this recoding process through machine-to-brain pathway still needs a long way to go deep into. To write in sensory information properly, stimulation modes, target sites, and stimulation parameters are all needed to be taken into consideration carefully. As our rat-robot model is based on virtual sensation generation, studies on locomotion control also shed lights on stimulation targets and parameter determinations. Through behavioral and imaging tests, stimulation parameters can be optimized for more natural sensation regeneration. Inspiringly, researchers from Pittsburgh have recently succeeded in restoring tactile sensation through intracortical micro-stimulation upon human being [13]. By delivering electrical micro-stimulation into corresponding representation locations in somatosensory cortex, stable sensations can be evoked naturally. Similar to the relationship between somatosensory cortex and thalamus in rodents, some study suggested more stable encoding in thalamus than in cortex with nonhuman primates [61]. As to stimulation methods, for clinical consideration, researchers are making great efforts on seeking for possible noninvasive stimulation approaches. Transcranial direct current stimulation (tDCS) and transcranial magnetic stimulation (TMS) are two of the most commonly used noninvasive stimulation methods for neural activity modulation. Both tDCS and TMS are considered safe and painless for human use; nonetheless, lacking spatial specificity, these two stimulation methods are not suitable for localized stimulations. Ultrasound has recently been shown to be capable of inducing reversible changes of neural activity noninvasively. Unlike tDCS and TMS, focused ultrasound can be applied to deep brain structures and hit the target specifically with greater spatial precision [62]. Though it still needs to be assessed before clinical trials, this technique and other new ones will have impacts on neural modulations.

References

1. Fritsch G, Hitzig E (1870) Uber die elektrische Erregbarkeit des Grossihirns. Arch Anat Physiol Wissen Med 37:300–332
2. Gildenberg PL (2005) Evolution of neuromodulation. Stereotact Funct Neurosurg 83 (2–3):71–79
3. Owen SL, Green AL, Stein JF et al (2006) Deep brain stimulation for the alleviation of post-stroke neuropathic pain. Pain 120(1–2):202–206
4. Marchand S, Kupers RC, Bushnell MC et al (2003) Analgesic and placebo effects of thalamic stimulation. Pain 105(3):481–488
5. Krack P, Batir A, Van Blercom N et al (2003) Five-year follow-up of bilateral stimulation of the subthalamic nucleus in advanced Parkinson's disease. N Engl J Med 349(20):1925–1934
6. Bittar RG, Burn SC, Bain PG et al (2005) Deep brain stimulation for movement disorders and pain. J Clin Neurosci 12(4):457–463
7. Wilson BS, Dorman MF (2008) Cochlear implants: a remarkable past and a brilliant future. Hear Res 242(1–2):3–21
8. Shannon RV (2012) Advances in auditory prostheses. Curr Opin Neurol 25(1):61–66
9. Chow AY, Chow VY, Packo KH et al (2004) The artificial silicon retina microchip for the treatment of vision loss from retinitis pigmentosa. Arch Ophthalmol 122(4):460–469
10. Yanai D, Weiland JD, Mahadevappa M et al (2007) Visual performance using a retinal prosthesis in three subjects with retinitis pigmentosa. Am J Ophthalmol 143(5):820–827
11. Romo R, Hernandez A, Zainos A et al (2000) Sensing without touching: psychophysical performance based on cortical microstimulation. Neuron 26(1):273–278
12. Houweling AR, Brecht M (2007) Behavioural report of single neuron stimulation in somato-sensory cortex. Nature 451(7174):65–68
13. Flesher SN, Collinger JL, Foldes ST et al (2016) Intracortical microstimulation of human somatosensory cortex. Sci Transl Med 8(361):141r–361r
14. Holzer R, Shimoyama I (1997) Locomotion control of a bio-robotic system via electric stimulation. In: Intelligent robots and systems, 1997. IROS'97., Proceedings of the 1997 IEEE/RSJ international conference on IEEE, pp 1514–1519
15. Bozkurt A, Gilmour R, Stern D et al (2008) MEMS based bioelectronic neuromuscular interfaces for insect cyborg flight control. In: Proceedings IEEE micro electro mechanical systems IEEE, p 160
16. Bozkurt A, Gilmour RF Jr, Lal A (2009) Balloon-assisted flight of radio-controlled insect biobots. IEEE Trans Biomed Eng 56(9):2304–2307
17. Sato H, Berry CW, Peeri Y et al (2009) Remote radio control of insect flight. Front Integr Neurosci 3:24
18. Bao L, Zheng N, Zhao H et al (2011) Flight control of tethered honeybees using neural electrical stimulation. In: International IEEE EMBS conference on neural engineering IEEE, pp 558–561
19. Talwar SK, Xu S, Hawley ES et al (2002) Direct brain stimulation enables training of complex behaviors in freely roaming animals. In: Proceedings of annual international conference of the IEEE engineering in medicine and biology society IEEE, pp 2076–2077
20. Gomes W, Perez D, Catipovic J (2006) Autonomous shark tag with neural reading and stimulation capability for open-ocean experiments. EOS Trans Am Geophys Union 87:36
21. Brown S (2006) Stealth sharks to patrol the high seas. New Sci 189(2541):30–31
22. Wang W, Guo C, Sun J et al (2009) Locomotion elicited by electrical stimulation in the midbrain of the Lizard Gekko gecko. In: Budiyono A, Riyanto B, Joelianto E (eds) Studies in computational intelligence. Springer, Berlin, p 145
23. Talwar SK, Xu S, Hawley ES et al (2002) Rat navigation guided by remote control. Nature 417 (6884):37–38
24. Hermer-Vazquez L, Hermer-Vazquez R, Rybinnik I et al (2005) Rapid learning and flexible memory in "habit" tasks in rats trained with brain stimulation reward. Physiol Behav 84 (5):753–759

25. Doty RW (1969) Electrical stimulation of the brain in behavioral context. Annu Rev Psychol 20:289–320
26. Feng Z, Chen W, Ye X et al (2007) A remote control training system for rat navigation in complicated environment. J Zheijang Univ Sci A 8(2):323–330
27. Francis JT, Xu S, Chapin JK (2008) Proprioceptive and cutaneous representations in the rat ventral Posterolateral thalamus. J Neurophysiol 99(5):2291–2304
28. Xu K, Zhang J, Zhou H et al (2016) A novel turning behavior control method for rat-robot through the stimulation of ventral posteromedial thalamic nucleus. Behav Brain Res 298 (Pt B):150–157
29. Zhang J, Zhang S, Yu C et al (2018) Intrinsic optical imaging study on cortical responses to electrical stimulation in ventral posterior medial nucleus of thalamus. Brain Res 1684:40–49
30. Zhu Y, Xu K, Xu C et al (2016) PET mapping for brain-computer Interface stimulation of the Ventroposterior medial nucleus of the thalamus in rats with implanted electrodes. J Nucl Med 57(7):1141–1145
31. Keay KA, Bandler R (2001) Parallel circuits mediating distinct emotional coping reactions to different types of stress. Neurosci Biobehav Rev 25(7):669–678
32. Brandao ML, Troncoso AC, Silva M et al (2003) The relevance of neuronal substrates of defense in the midbrain tectum to anxiety and stress: empirical and conceptual considerations. Eur J Pharmacol 463(1–3):225–233
33. Lin J, Yu C, Jia J et al (2010) Using dlPAG-evoked immobile behavior in animal-robotics navigation. 2010 5th international conference on computer science & education, (iccse 2010) - hefei, china, 1295–1298
34. Huai R, Yang J and Wang H et al (2009) A new robo-animals navigation method guided by the remote control. In: Shi R, Fu WJ, Wang YQ, Wang HB(eds) International conference on biomedical engineering and informatics. IEEE, pp 1170–1173
35. Koo B, Koh CS, Park HY et al (2017) Manipulation of rat movement via Nigrostriatal stimulation controlled by human visually evoked potentials. Sci Rep 7(1):2340
36. Ye X, Wang P, Liu J et al (2008) A portable telemetry system for brain stimulation and neuronal activity recording in freely behaving small animals. J Neurosci Methods 174(2):186–193
37. Guo S, Chen S, Zhang Q et al (2014) Optogenetic activation of the excitatory neurons expressing CaMKIIFC; in the ventral tegmental area upregulates the locomotor activity of free behaving rats. Biomed Res Int 2014:687469
38. Guo S, Zhou H, Zhang J et al (2013) A multi-electrode array coupled with fiberoptic for deep-brain optical neuromodulation and electrical recording. In: Engineering in medicine and biology society (EMBC), 2013 35th annual international conference of the IEEE, pp 2752–2755
39. Aravanis AM, Wang LP, Zhang F et al (2007) An optical neural interface: in vivo control of rodent motor cortex with integrated fiberoptic and optogenetic technology. J Neural Eng 4(3): S143–S156
40. Wang J, Wagner F, Borton DA et al (2012) Integrated device for combined optical neuromodulation and electrical recording for chronic in vivo applications. J Neural Eng 9 (1):16001
41. Chen S, Zhou H, Guo S et al (2015) Optogenetics based rat-robot control: optical stimulation encodes "stop" and "escape" commands. Ann Biomed Eng 43(8):1851–1864
42. Guo S, Zhou H, Wang Y et al (2014) A rat-robot control system based on optogenetics. In: Ren L, Wang H, Dai Z (eds) Applied mechanics and materials, pp 848–852
43. Min BK, Marzelli MJ, Yoo SS (2010) Neuroimaging-based approaches in the brain-computer interface. Trends Biotechnol 28(11):552–560
44. Pais-Vieira M, Lebedev M, Kunicki C et al (2013) A brain-to-brain interface for real-time sharing of sensorimotor information. Sci Rep 3:1319
45. Deadwyler SA, Berger TW, Sweatt AJ et al (2013) Donor/recipient enhancement of memory in rat hippocampus. Front Syst Neurosci 7:120
46. Pais-Vieira M, Chiuffa G, Lebedev M et al (2015) Building an organic computing device with multiple interconnected brains. Sci Rep 5:11869

47. Grau C, Ginhoux R, Riera A et al (2014) Conscious brain-to-brain communication in humans using non-invasive technologies. PLoS One 9(8):e105225
48. Rao RP, Stocco A, Bryan M et al (2014) A direct brain-to-brain interface in humans. PLoS One 9(11):e111332
49. Yoo SS, Kim H, Filandrianos E et al (2013) Non-invasive brain-to-brain interface (BBI): establishing functional links between two brains. PLoS One 8(4):e60410
50. Zhang S, Yuan S, Huang L, Zheng X, Wu W, Xu K, Pan G (2019) Human mind control of rat cyborg's continuous locomotion with wireless brain-to-brain interface. Sci Rep 9:1321. https://doi.org/10.1038/s41598-018-36885-0
51. Martinez-Leon J, Cano-Izquierdo J, Ibarrola J (2016) Are low cost brain computer Interface headsets ready for motor imagery applications? Expert Syst Appl 49:136–144
52. Zhang Y, Sun C, Zheng N, et al (2010) An Automatic Control System for Ratbot Navigation [C]// 2010 IEEE/ACM International Conference on Green Computing and Communications & 2010 IEEE/ACM International Conference on Cyber, Physical and Social Computing. IEEE Computer Society, 2010, Hangzhou, China
53. Sun C, Zheng N, Zhang X et al (2011) An automatic control model for rat-robot. In: Engineering in medicine and biology society, EMBC, 2011 Annual international conference of the IEEE, Boston, USA
54. Sun C, Zheng N, Zhang X et al (2013) Automatic navigation for rat-robots with Modeling of the human guidance. J Bionic Eng 10(1):46–56
55. Whishaw IQ, Kolb B (2004) The behavior of the laboratory rat: a handbook with tests. Oxford University Press, Oxford
56. Hull CL, Spence KW (1938) "Correction" vs "non-correction" method of trial-and-error learning in rats. J Comp Psychol 25(1):127–145
57. Sun C, Zhang X, Zheng N et al (2012) Bio-robots automatic navigation with electrical reward stimulation. Engineering in medicine and biology society (EMBC), 2012 annual international conference of the IEEE,San Diego, California, USA
58. Zhang C, Sun C, Gao L et al (2013) Bio-robots automatic navigation with graded electric reward stimulation based on reinforcement learning. Conf Proc IEEE Eng Med Biol Soc 2013:6901–6904
59. Wu Z, Yang Y, Xia B et al (2014) Speech interaction with a rat. Chin Sci Bull 59 (28):3579–3584
60. Wang Y, Lu M, Wu Z et al (2015) Visual Cue-guided rat cyborg for automatic navigation. IEEE Comput Intel Mag 10(2):42–52
61. Song W, Semework M (2015) Tactile representation in somatosensory thalamus (VPL) and cortex (S1) of awake primate and the plasticity induced by VPL neuroprosthetic stimulation. Brain Res 1625:301–313
62. Yoo SS, Bystritsky A, Lee JH et al (2011) Focused ultrasound modulates region-specific brain activity. NeuroImage 56(3):1267–1275

Chapter 6
Realizing Efficient EMG-Based Prosthetic Control Strategy

Guanglin Li, Oluwarotimi Williams Samuel, Chuang Lin, Mojisola Grace Asogbon, Peng Fang, and Paul Oluwagbengba Idowu

Abstract As an integral part of the body, the limb poses dexterous and fine motor grasping and sensing capabilities that enable humans to effectively communicate with their environment during activities of daily living (ADL). Hence, limb loss severely limits individuals' ability especially when they need to perform tasks requiring their limb functions during ADL, thus leading to decreased quality of life. To effectively restore limb functions in amputees, the advanced prostheses that are controlled by electromyography (EMG) signal have been widely investigated and used. Since EMG signals reflect neural activity, they would contain information on the muscle activation related to limb motions. Pattern recognition-based myoelectric control is an important branch of the EMG-based prosthetic control. And the EMG-based prosthetic control theoretically supports multiple degrees of freedom movements that allows amputees to intuitively manipulate the device. This chapter focuses on EMG-based prosthetic control strategy that involves utilizing intelligent computational technique to decode upper limb movement intentions from which control commands are derived. Additionally, different techniques/methods for improving the overall performance of EMG-based prostheses control strategy were introduced and discussed in this chapter.

G. Li (✉) · O. W. Samuel · C. Lin · P. Fang
CAS Key Laboratory of Human-Machine Intelligence-Synergy Systems, Shenzhen Institutes of Advanced Technology (SIAT), Chinese Academy of Science (CAS), Shenzhen, China

Institute of Advanced Integration Technology, SIAT, Shenzhen, China
e-mail: gl.li@siat.ac.cn

M. G. Asogbon · P. O. Idowu
CAS Key Laboratory of Human-Machine Intelligence-Synergy Systems, Shenzhen Institutes of Advanced Technology (SIAT), Chinese Academy of Science (CAS), Shenzhen, China

Institute of Advanced Integration Technology, SIAT, Shenzhen, China

Shenzhen College of Advanced Technology, University of Chinese Academy of Sciences, Shenzhen, China

149

6.1 Introduction

Human upper limb represent an integral part of the body that provides incredible array of functionalities during activities of daily living (ADL). In addition to possessing dexterous and fine motor grasping/sensing capabilities, the upper limb enables individuals to freely and effectively communicate with their natural environments through artistic expressions, sign languages, and greetings (handshake/hand gesture), among others. Therefore, the loss of one or both arms severely limits individuals' ability especially when they need to perform tasks requiring their arm functions during ADL, thus leading to decreased quality of life [1]. Limb loss also has profound negative impact on amputees including stump pain or phantom limb pain, or perhaps even both, depression, changes in body image, and psychological burden [1–5]. Under certain circumstance, upper limb loss may also affect amputees' stability (dis-balance) during mobility, thus making them prone to falls or collisions with other individuals/objects. To this end, limb loss causes a devastating experience necessitating the need for proper psychological and physical rehabilitation strategy for arm amputees.

A large number of the commercially available upper limb prostheses are either mechanically (body-powered) or electrically (motorized) driven. Meanwhile, body-powered upper limb prosthetic devices were primarily developed as alternative to aid amputees in carrying out ADL requiring their arm functions [6]. Fundamentally, these prostheses operate by using cables to link the movement of the body to the device and thus actuating simple hand tasks such as opening or closing of the hook/gripper. To achieve simple hand grasp tasks, the amputee would need to possess a significant amount control over his/her shoulder, chest, and even the residual limb which should be long enough to support the motion. Although body-powered prostheses have fine cosmetic appearances that are comparable to the human natural arm [7], they are nonintuitive and require significant amount of efforts (burdensome) to perform simple hand tasks and as well support only single degree of freedom (DOF) movement per time [7]. With these limitations, motorized upper limb prostheses are considered as viable alternative for intuitive restoration of multiple DOF arm functions in amputees. At the forefront of this technology are the prostheses that utilize electromyography (EMG) recordings to characterize upper limb movement intentions of the amputees [8–12]. Thus, the properties of the EMG signals are encoded in form of control commands to the prosthetic controller which then actuates the device accordingly. It is noteworthy that in the last two to three decades, the motorized upper limb prosthetic technology has progressively advanced leading to the development of better control methods as well as designs. Hence, this article focuses on the EMG-based prosthetic control with emphases on methods/technologies that could help improve the overall performance and acceptability of the prostheses system.

The remaining part of the chapter is organized as follows: Section 6.2 discusses different EMG-based prosthetic control methods; Section 6.3 introduces some potential techniques for improving the performance of EMG-based prosthetic control; Section 6.4 presents the concluding remarks.
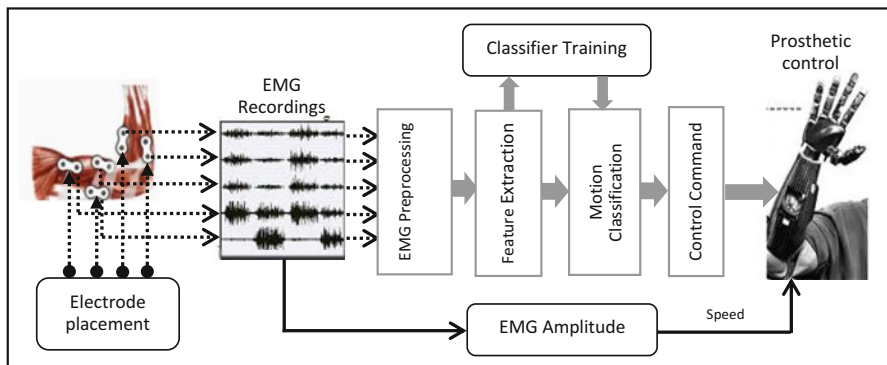
6.2   EMG-Based Prosthetic Control Methods

6.2.1   Background

Fundamentally, EMG signals represent electrical manifestation of neuromuscular activation associated with a contracting muscle. Such signals have been proven to contain rich set of neural information from which different types of upper limb movements could be accurately decoded, thus making them useful control input to prosthetic devices as well as other forms of rehabilitation robots [8, 13]. Additionally, EMG signals carry significant information for diagnosis of neuromuscular disorders and other muscle-related diseases. It has been established that EMG signal patterns for a specific limb movement are repeatable over time and distinct from the patterns of other limb movements. By exploring this phenomenon, researchers have been able to decode a range of arm movements from EMG recordings using intelligent computational methods. To this end, dozens of previous studies have reiterated the potential of EMG-based method in the control of multifunctional prostheses [14–16]. Thus, the following section will focus on discussing the currently applied EMG-based prosthetic control schemes including: pattern recognition (PR) control method and the simultaneous and proportional control (SPC) method.

6.2.2   Pattern Recognition-Based Prosthetic Control

Although the concept of EMG pattern recognition (EMG-PR) is by no means new, it has been proven over time to be promising especially for improving the dexterity of control in upper limb prosthetic devices in comparison with the conventional amplitude-based methods. It is noteworthy that the first generation of pattern recognition-driven prosthetic controllers was built in the late 1960s/early 1970s [17–19]. Since then, advancement in signal processing, multichannel recording, and microprocessor technology has expedited implementation of EMG-PR method in embedded control systems. Also, with a lot of synergistic efforts from the academia and industries, EMG-PR-based prosthetic arms have been recently made available for commercial use.

EMG-PR prosthetic control method is primarily based on the assumption that EMG signal patterns corresponding to a particular class of limb movement are consistently repeatable across trials and as well distinct from EMG signal patterns of the other classes. Due to the promising nature of this control method, it has been

Fig. 6.1 Schematic diagram of EMG-PR-based prosthetic control system

widely explored in the last two to three decades with significant progress reported in terms of its robustness. The control schemes as a whole consist of a sequence of steps beginning with: EMG signal acquisition, preprocessing of the recorded signals, extraction of feature set, classification of the extracted features, and issuing of control commands to drive prosthesis. Figure 6.1 shows the schematic diagram of a typical EMG-PR-based prosthetic control system.

In the above represented control scheme, myoelectric signals are collected via electrodes placed on the skin surface underlying the arm muscles. Often times, the electrodes are integrated with miniaturized amplifier to improve the quality of the recorded signals through standard amplification and filtering procedures. Afterwards, the acquired EMG recordings are subjected to preprocessing procedure, so as to attenuate inherent interferences. In this regard, the 50/60 Hz notch filter is usually applied to the raw acquired signals to minimize interferences resulting from power line noise. In addition to the notch filter, a band-pass filter with cut of frequency between 10/20 Hz and 500 Hz is often applied to the EMG signals to obtain the most useful spectrum with high motor information content.

EMG signals recorded during targeted limb movements are continuous in nature, thus for a specific length of recording, a decision corresponding to a subset of the observed limb movements may be required to actuate the prosthesis. Therefore, the use of data segmentation technique in handling the preprocessed data prior to feature extraction is necessary. This step helps increase the probability of the prosthetic control system achieving high accuracy as well as quick response time. Ideally in real life applications, a response time of no more than 300 ms is required [20]. Note that the response time (which is a function of the *segment length* and the *processing time*) is the time required to produce the control commands that drive the prostheses. In a study conducted by Englehart and Hudgins [21], it was shown that by adopting continuous segmentation on a *steady-state* EMG signal, the segment length can be reduced to about 128 ms without a significant reduction in classification accuracy.

Also, it has been shown previously that segmented *steady-state* EMG signals achieved better accuracy compared to segmented *transient* EMG signals, and less degradation were recorded with shorter segments of the *steady-state* EMG data. After considering the segment length and the state of the data, the third important data segmentation factor is the windowing technique adopted. Data segmentation is often achieved via either of the following windowing techniques: *sliding analyses windowing* and *adjacent windowing* method [20]. The adjacent windowing method uses disjoint segments of predefined length for its feature extraction; and the intended limb movement is classified after a certain processing delay. Because the processing time often denotes a small fraction of segment length, the processor is found to be mostly idle during the remaining time of the segment length. Meanwhile, in the sliding windowing method, the new window segment slides over the current window segment, with an increment time less than the segment length. In comparison, this sliding windowing method takes advantage of the processor's idle time in adjacent windowing method to produce more classified outputs. Thus, the sliding windowing technique has been widely applied to *steady-state* EMG signals for enhanced feature extraction process in most recent studies on EMG-PR-based prosthetic control.

Aside from the feature extraction stage, the choice of classification algorithm has been reported to be another important factor in EMG-PR-based prosthetic control systems. Thus, choosing an efficient classifier becomes necessary to ensure accurate and consistent classification performance. In this regard, a number of classification schemes have been examined with respect to their performance in identifying different upper limb movements. For instance, classification schemes based on Bayesian statistics [22], adaptive neural networks (ANN) [23], fuzzy logic [24], support vector machine [25], and linear discriminant analysis (LDA) [11–26] were previously studied. The ANN-based classifier and the LDA classifier were found to be more accurate for the prediction of limb movement intention. However, the LDA has been widely applied because it is relatively less complex in terms of implementation and performs well in comparison with the ANN and other complex classification Schemes [26].

After reaching a decision on the classification scheme to adopt, a classifier is developed by utilizing part of extracted EMG feature vector. Afterwards, the performance of the built classifier in identifying multiple classes of limb movement intent is evaluated using the testing set as obtained from the remaining part of the feature vector. The performance of the EMG-PR-driven prostheses in terms of its controllability is mostly examined in both off-line and real-time metrics. In general, metrics including recognition rate (classification accuracy) of limb movements/subjects, the time taken to complete a motion (motion completion time), number of successfully completed motion (motion completion rate), and the time taken to select the target motion (motion selection time) are often considered. Also, the performance of the device could be assessed based on the number success recording reaching and grasping tasks.

6.2.3   Simultaneous and Proportional EMG-Based Prosthetic Control

Multiple DOF pattern recognition-based prostheses control schemes have recently been implemented to enable upper limb amputees perform the usual arm function tasks during ADL. Even with this remarkable achievement, the available EMG-PR-based controlled prostheses do not support simultaneous control of multiple DOFs [27, 28]. This limitation prevents upper limb prostheses users from having the natural feel of the coordinated joint control often associated with an intact limb. Although advanced prosthetic arms [29, 30], including multiple DOF wrists, offer the mechanical means to restore arm movements, there is still a significant need for systems that enable simultaneous control of such devices.

To develop a simultaneous prosthetic control scheme which offers multiple DOF movements, different approaches have been proposed in the recent years. These approaches include the use of artificial neural networks for joint kinematics predictions during upper limb movements [31], analysis of the muscle synergies underlying a range of upper limb movements [32], and the utilization of joint kinetics [33]. While these methods have been reported to be promising toward clinical realization of upper limb prostheses, they however mostly focus on providing control for limited classes of limb movements such as wrist without hand or have imposed identical velocities on all active degrees of freedom movements and thus do not provide independent proportional control of individual degrees of freedom.

Additionally, toward achieving simultaneous and proportional control scheme, some investigators developed a model of muscle synergy driven by nonnegative matrix factorization (NMF) method to resolve myoelectric signal factorization issue that is capable of hindering continuous control [32, 34]. The NMF technique often utilizes a DOF-wise training approach, based on which simultaneous control of multi-DOF is achieved via linearly combined single degree of freedom. This kind of strategy supports simultaneous and proportional myoelectric-based control [32, 34]. Despite the promising results of this scheme, there are still some shortcomings that have hindered its real life implementation. The most critical disadvantage of the NMF-driven EMG-based prostheses is that it needs a DOF-wise calibration during which requires a user to activate precisely single DOF in a specific manner, e.g., firstly, trigger DOF1 for several trials followed by DOF2. Besides the inconvenience and the time needed for the execution of this phase, more notably, if the prostheses users are unable to trigger an individual DOF (i.e., the activation patterns during the training session are not exactly of single DOF), the DOF-wise-driven NMF approach will produce inadequate muscle synergy matrix that may result in poor control outcome. This behavior could be attributed to the fact that the classical NMF-based scheme lacks the ability to produce a factorization that is sparse enough for efficient control of multiple DOF [35, 36]. Hence, we proposed an

alternative approach to the classical NMF that identifies the factorization which separates the generated basis functions robustly and concurrently in a quasi-unsupervised way to simultaneously and proportionally control the prostheses.

In the proposed approach, the subject does not need to follow a predefined sequence to activate single DOF in the calibration phase, and can even activate more than one DOF simultaneously in the training stage, which is not allowed in the classical NMF method. Nevertheless, the idea of the synergy matrix could be realized in one step, which is contrary to the conventional NMF approach that attempts to sequentially extract the bases for each DOF. For this reason, constraints were included in the factorization method and the method is at maximizing the sparseness of the resulting control outcome. The constraints associated with the sparseness limits the space of possible NMF solutions. Precisely, the solution with bases functions associated to single DOF, which is the target solution, represents the sparsest of the other solutions. In this regard, the factorization with constraints usually does not need prior calibrations/activations of single DOF and could be utilized to any set of target tasks carried out by the user with no any form of strict labeling. The proposed sparse nonnegative matrix factorization (SNMF)-based simultaneous and proportional myo-control scheme is presented mathematically as follows.

In myoelectric control, multiple DOF limb movements could be re-represented as a linearly combined individual DOFs, and the synergy basis and control input are nonnegative [34]. Suppose we represent the root mean square (RMS) values of an N-channel with T-length surface myoelectric signal as $\mathbf{Z}$, in which the t-th column is the myoelectric signal at a given time t and m represents the number of DOFs. Thus, the multichannel observation can be approximated by the product of a $N \times 2m$ latent nonnegative synergy matrix $\mathbf{W}$ and a $2m \times T$ latent nonnegative control signal matrix.

$\mathbf{F}$ is expressed in the following equation:

$$\mathbf{Z}_{N \times T} \approx \mathbf{W}_{N \times 2m}\mathbf{F}_{2m \times T} \tag{6.1}$$

While the sparseness of the solution is obtained by imposing a specific single DOF activation sequence for calibration, the above factorization problem can be solved in a semi-supervised way with the summation property of DOFs in the muscle signal domain.

A mathematical way to generate a sparse solution without the need for the specific set of calibration data for individual DOF activation is utilized. Meanwhile, this is achieved by imposing a sparseness constraint on the control signals, which leads to the proposed SNMF Scheme [37].

Mathematically, the extent (degree) of sparseness could be controlled by utilizing either l1-norm or l0-norm. To build a computationally efficient system, we chose the l1-norm-based sparse NMF scheme, SNMF [37]. Meanwhile, the objective function of the SNMF method is expressed mathematically as follows:

$$\min_{\mathbf{W,F}} \ \frac{1}{2}\|\mathbf{Z} - \mathbf{WF}\|_{Fro}^2 + \lambda\sum_{t=1}^{T}\|\mathbf{F}(:,t)\|_1^2 \quad s.t. \ \mathbf{W,F} \geq \mathbf{0},$$

$$\Leftrightarrow \min_{\mathbf{W,F}} \ \frac{1}{2}\left\|\mathbf{Z} - \left[W_1^+, W_1^-, \cdots W_m^+, W_m^-\right]\begin{bmatrix} F_1^+ \\ F_1^- \\ \vdots \\ F_m^+ \\ F_m^- \end{bmatrix}\right\|_{Fro}^2 + \lambda\sum_{t=1}^{T}\left\|\begin{bmatrix} F(:,t)_1^+ \\ F(:,t)_1^- \\ \vdots \\ F(:,t)_m^+ \\ F(:,t)_m^- \end{bmatrix}\right\|_1^2$$

$$s.t. \ W_{ij}, F_{ij} \geq \mathbf{0}$$

$$(6.2)$$

where $\mathbf{F}\,(:,t)$ is the t-th column vector of $\mathbf{F}$ [Eq. (6.1)], Fro is the Frobenius norm, and $\lambda > 0$ is a regularization parameter to balance the accuracy of the factorization and the degree of sparseness of $\mathbf{F}$. In the experiment, we choose the optimal λ through cross-validation with the value of $m = 2$. The superscripts "+" and "–" denote the positive and negative direction of each DOF, respectively. The above formulation can be rewritten as:

$$\min_{\mathbf{W, F}} \left\|\begin{pmatrix} \mathbf{W} \\ \sqrt{\lambda}\mathbf{e}_{1\times 2m} \end{pmatrix}\mathbf{F} - \begin{pmatrix} \mathbf{Z} \\ \mathbf{0}_{1\times T} \end{pmatrix}\right\|_{Fro}^2 \quad s.t. \ \mathbf{W,F} \geq \mathbf{0}, \qquad (6.3)$$

where $\mathbf{e}_{1\times 2m}$ represent a row vector that contains values equal to 1 and $\mathbf{0}_{1\times T}$ represent entries with values equal to 0. Equation (6.3) could be adequately solved via the alternating nonnegative least squares (ANLS) approach. Meanwhile, for the ANLS method, $\mathbf{F}$ and $\mathbf{W}$ are iteratively updated by adjusting the other one:

$$\mathbf{F}^{(k+1)} = \underset{\mathbf{F}}{\mathrm{argmin}} \left\|\begin{pmatrix} \mathbf{W}^{(k)} \\ \sqrt{\lambda}\mathbf{e}_{1\times 2m} \end{pmatrix}\mathbf{F} - \begin{pmatrix} \mathbf{Z} \\ \mathbf{0}_{1\times T} \end{pmatrix}\right\|_{Fro}^2 \qquad (6.4)$$

$$\mathbf{W}^{(k+1)} = \underset{\mathbf{F}}{\mathrm{argmin}} \left\|\mathbf{WF}^{(k+1)} - \mathbf{Z}\right\|_{Fro}^2 \qquad (6.5)$$

It could be seen that Eqs. (6.4) and (6.5) represent the classical least square problem, and either of the equation has a closed-form solution. Meanwhile, the derivation in [37] reveals that the SNMF method could converge to a stationary point. The SNMF method can equally extract all the basis functions in a single step from the EMG recordings produced via arbitrary combinations of DOFs per user. Only the ordering of the control input signals (basis functions) would be undetermined using this method, but this issue could be simply addressed. In practice, the labels of the first two single DOFs need to be recorded in order to decide the sequence of the basis in the matrix ($\mathbf{F}$) from which control signal is obtained, thus making the method quasi-unsupervised instead of completely unsupervised.

Having computed the synergy basis matrix $\mathbf{W}$ from the recorded myoelectric signals, it is assumed to be a constant (at least over the period of the test experiments). To estimate the control input signal associated with the intended DOF activation level, a pseudo inverse of W (represented as W+) is applied, and it was multiplied with the newly obtained surface myoelectric signals $\left(\widetilde{\mathbf{Z}} \right)$. Thus, the estimated control input signal $\left(\tilde{\mathbf{F}} \right)$ is defined as follows:

$$\tilde{\mathbf{F}} = \mathbf{W}^{+}\tilde{\mathbf{Z}} \tag{6.6}$$

where

$$\tilde{\mathbf{F}} = \left[\tilde{F}_1^+ ; \tilde{F}_1^- ; \tilde{F}_2^+ ; \tilde{F}_2^- ; \right] \tag{6.7}$$

Toward ensuring that no components are surpassed by the others, the individual component of $\tilde{\mathbf{F}}$ in (6.7) is subject to a normalization process based on its maximum value. An estimate of the control input signal in (6.7) is thus scaled by the scalar correction factors τ_{ij} that are utilized to account for the indetermination of the signal power (range of control signals) during the factorization process:

$$\begin{cases} \tilde{F}_1 = \tau_{11}\tilde{F}_1^+ - \tau_{12}\tilde{F}_1^- \\ \tilde{F}_2 = \tau_{21}\tilde{F}_2^+ - \tau_{22}\tilde{F}_2^- \end{cases} \tag{6.8}$$

where we name $\tilde{F}_1$ and $\tilde{F}_2$ the control signals for DOF1 and DOF2, respectively. The multiplicative factors τ_{ij} are determined for each subject so that the final control signals, $\tilde{\mathbf{F}} = \left[\tilde{F}_1 ; \tilde{F}_2 \right]$ match the range of joint angles in the respective DOFs. The tau-s parameters are manually set before operating online tasks according to different subjects. The obtained control signals, low-pass filtered at 6 Hz (kinematic bandwidth), are then used by the subjects for controlling the DOFs.

It is noteworthy that the proposed SNMF scheme is aimed at robust and concurrent extraction of basis functions for myo-control in upper limb prostheses with a quasi-unsupervised scheme. This factorization scheme shown in our study has merits compared to the classical NMF because it selects the sparsest solution among infinite feasible solutions. To that end, there is no need for pre-calibration of the constraint tasks by users but rather the constraint on the solution. The method has been compared in similar conditions to the NMF and linear regression with results proving it to be superior over these methods even when a single DOF activation was used for the factorization which is an ideal condition for the NMF. Furthermore, the approach could be used by factorizing the myoelectric signals from arbitrary tasks by combining individual DOFs. The proposed factorization algorithm allows robust simultaneous and proportional control and is superior to previous supervised algorithms, and its minimal supervision characteristic paves the way to online adaptation in myoelectric control.

## 6.3   Neural Interfaces for Improvement of EMG-Based Prosthetic Control

6.3.1   Background

The previously described sections show that EMG-based prostheses control method could potentially allow amputees to intuitively manipulate the prosthetic arm with high level of dexterity and as well achieve multiple DOF controls. Developing EMG-based prostheses with these characteristics mainly depends on whether the users have enough residual muscles which act as source of EMG control signals. For instance, individuals with below the elbow amputation (transradial amputees) generally have enough residual muscles for the control of wrist functions such as wrist flexion/extension, wrist pronation/supination, and so on. Also, these category of amputees could provide enough EMG signals from their residual forearm muscles to control hand and even finger movements as reported in a number of previous studies [7]. On the other hand, individuals with high-level amputations (transhumeral or shoulder disarticulation) usually do not have enough residual muscles to provide myoelectric signals for the successful control of the wrist and hand movements although they can produce enough EMG signals for the control of elbow functions (elbow flexion/extension). Thus, intuitively controlling multiple DOF hand/wrist movements becomes a major challenge for these categories of amputees. One possible means of addressing the issue of insufficient generation of myoelectric control signals for these users would be to consider neural machine interfaces approaches such as targeted muscle reinnervation (TMR) and targeted nerve function replacement (TNFR). The theoretical background is that muscles can be considered as the bio-amplifier of the neural signals.

6.3.2   Targeted Muscle Reinnervation Technology

Toward enabling high-level upper limb amputees producing sufficient myoelectric control signals again, a neural machine interface technology known as TMR was proposed by Todd Kuiken et al. [28]. TMR is a surgical procedure that involves the transfer of residual nerves from an amputated limb unto alternative muscle group usually located around the chest region. During the surgery, brachial plexus nerves that provide motor control and sensory feedback prior to amputation are transferred to the arm or chest muscles that are biomechanically nonfunctional. Afterward, a functional link is established between the implanted nerves and the targeted muscles, thereby inducing the contractility of targeted muscles and enabling the generation of additional myoelectric signals. Importantly, this surgical technique is aimed at restoring the peripheral nerve functions in amputees thus enabling the provision of sufficient myoelectric control signals again. A schematic diagram of the TMR surgical procedure is conceptualized in Fig. 6.2a. For the subject shown in
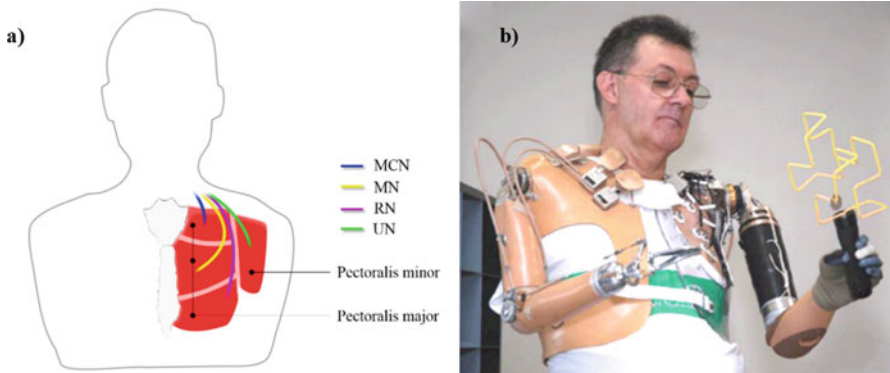
Fig. 6.2 The schematic representation of the TMR technology. (**a**) TMR surgical procedure for shoulder disarticulation amputee. (**b**) A bilateral amputee with successful TMR surgery controlling a prosthetic arm [28]

Fig. 6.2b, the surgery was performed on his right chest region, and it involves transferring the median, ulnar, radial, and musculocutaneous nerves to the subject's pectoralis major muscle segmented into four parts, respectively.

The above described neural machine interface technology for upper limb prostheses control has been implemented and tested on a number of human subjects. The test sessions conducted with a bilateral amputee (Fig. 6.2b) shows that the high-level amputee could efficiently perform additional hand function tasks such as drinking and eating which could not be achieved prior to the TMR surgery. Importantly, the success of performing additional tasks was objectively linked to the realization of more EMG control signals after the TMR surgery.

6.3.3   Targeted Nerve Function Reconstruction Technology

Despite the success recorded by the TMR technology, it still has some limitations which have slowed down its widespread adoption. For instance, TMR surgery involves establishing functional links between the nerves and targeted muscles leading to two major challenges: First, the targeted muscle would atrophy with time because it has been denied of the required nutrients provided by the original nerve which has been replaced with the implanted nerve. Second, intramuscular nerve distribution (a key indicator of the motor function recovery) will also degenerate after a while due to the lack of nutrients from the surrounding cell body.

Peripheral nerves which play an important role after TMR surgery have been reported to have a slow growth rate. That is, it takes about 3~6 months or even more after TMR for proper redistribution of the implanted nerve into the targeted muscle, thus leading to atrophy of the targeted muscle. Aside the slow growth rate, the absence of nerve supplements is another factor responsible for atrophy of the
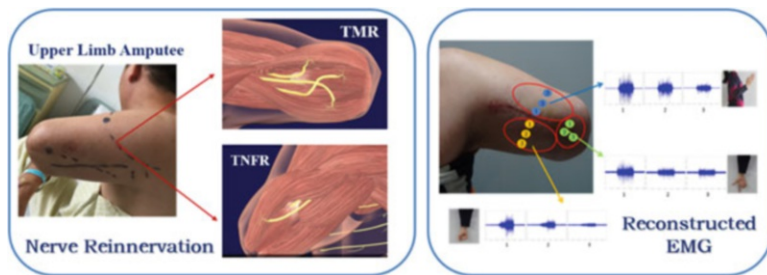
Fig. 6.3 A representation of the TMR/TNFR technology. (**a**) TMR/TNFR surgical procedure for a transhumeral amputee, (**b**) EMG recordings after undergoing a TNFR surgery when the subject was doing different arm movements

targeted muscle [38–40]. In such a situation, high-level upper limb amputees would need training and treatment over an extended period for new functional connections to be established between the targeted muscle and the implanted nerves. It is worth noting that end-to-end anastomosis has been proven to be the best approach for restoring the functions of injured nerves in patients [41]. Thus based on this principle, targeted nerve function reconstruction (TNFR) technology is considered to address the abovementioned problems associated with TMR. This is because TNFR has the potential to better restore the motor functions associated with multiple degrees of freedom upper limb movements. Aiming at improving intramuscular nerve distribution as well as preventing muscle atrophy, TNFR establishes functional links between the nerves of the targeted muscles and nerves from the amputated region/arm of the individual. A schematic representation of the TNFR technology is shown in Fig. 6.3.

Shown in Fig. 6.3 is a male transhumeral amputee that underwent a TNFR surgery. He actually got his left limb amputated in 2012 as a result of injury sustained from a rolling machine. At the time of the surgery (2015), the amputee was approximately 48 years old. Prior to the TNFR surgery, his residual limb was subjected to a number of assessments to ensure that he meets up with the requirement. From the assessments, we found that the residual limb has a length of 22 cm and has not been infected. In addition, the results of an MRI scan show that the musculus biceps brachii and musculus triceps brachii of the residual limb were intact with neuroma tissue formed at median nerve, ulnar nerve, and musculospiral nerve terminals. Afterward, the TNFR surgery was performed on the subject by transecting the MCN, MN, RN, and UN from the residual limb and implanting them into the corresponding MCN, MN, RN, and UN on the amputee's chest region.

About 7 days after the surgery, the operation regions were observed twice a week for 8 consecutive weeks. Indexes, such as status of the incision (healing rate), skin color and temperature, and limb peripheral circumference, were closely monitored. The pre-surgery and post-surgery experiences of the subject were also utilized to assess the limb status. These experiences include the subject's feelings of missing fingers, hand, and arm as well as his experience during observing different

movements (finger, wrist, hand, and elbow). Subsequently, a TNFR testing environment was setup to demonstrate the feasibility of our proposed technology. In the testing environment shown in Fig. 6.3b, the amputee was able to control the virtual prostheses reliably across a range of upper limb movements compared to his pre-TNFR experience. It is noteworthy that the TNFR technology is proposed by our research group and we hope it will revolutionize prostheses control technology and other related EMG-based rehabilitation device technologies in the future.

We further built a number of animal models recently to compare the performance of proposed TNFR technology with that of TMR and found the TNFR model obviously demonstrates better intramuscular nerve distribution compared to the TMR model. Additionally, we found out that bicep brachii muscles on the operational sides of the TNFR model achieved better wet mass compared to that of the TMR model.

6.3.4   Restoration of Sensory Feedback

Tactile sensation is an essential element for a dexterous hand manipulation. In an ideal bidirectional hand prostheses, the user's intentions are first decoded through the efferent pathway, and then a nearly "natural" sensory feedback is delivered through the remnant afferent pathways, simultaneously in real time, as illustrated in Fig. 6.4.

The lack of proper sensory feedback mechanism limits prostheses users in grasping and manipulating objects, which makes the use of prostheses cumbersome and uncomfortable, leading to prosthetic abandonment. In fact, lack of sensory feedback schemes in the currently available multiple-DOF upper-limb prostheses have slowed down its clinical and commercial success [42]. Improper feedback of tactile perception may also lead to "over-grasp" causing damage to an object or "under-grasp" causing slip of object. Report from previous survey indicated that about 95% of male amputees desire to have force feedback in their prostheses and 88% placed more emphasis on grip force and proprioceptive information of prosthesis position and movement. With the rejection rate of upper limb prostheses reaching 39% and the increasing rate of people living with the loss of a limb projected to be doubled by the year 2050 [43], the need for integrating efficient sensory feedback mechanism into the prostheses becomes more necessary.

To restore the lost sensory feedback, Raspopovic et al. [44] were able to stimulate the median and ulnar nerve fascicles using transversal multi-channel intrafascicular electrodes (TIMEs) connected to the artificial hand sensors. The subject was able to control the prosthesis through information provided by the artificial sensors. This feedback enabled users to effectively control the grasping force of the prosthesis with no visual or auditory feedback. To restore a sense of touch that is close to the natural perception, the artificial receptors known as sensors need to first register the characteristics of the sensed object/environment [45], which works in a similar way to the receptor organs in humans. These sensory
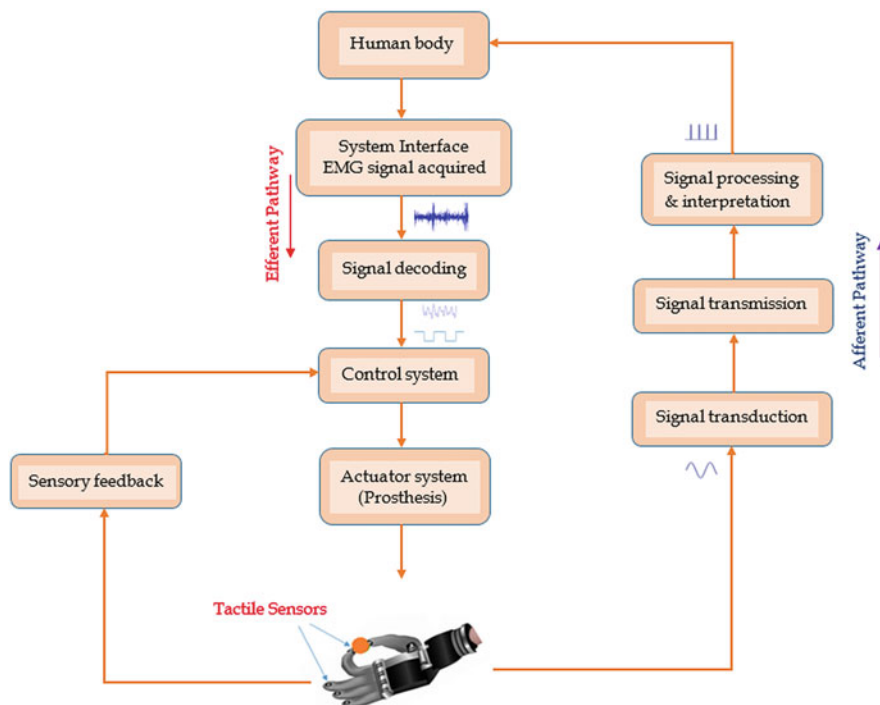
Fig. 6.4 Closed loop architecture for restoring sensory feedback

receptors are broadly classified into pain receptors, cold receptors, warm receptors, and four mechanoreceptors. Then, the receptors encode information into trains of action potentials and also possess characteristic innocuous temperature variation evoked by different afferents between ~5 and 48 °C [46]. The mechanoreceptors are grouped into slow-adapting receptors (SA-I and SA-II) and fast-adapting receptors (FA-I and FA-II) having different receptive fields to which they respond to mechanical stimulus, as well as different rates of adaptation. Also, tactile stimuli are transferred from the artificial receptors to the intact skin through the actuators. At this stage, signals are transported from receptors through nerve fibers to the brain where complex information are interpreted. The time taken for the signal to get to the brain is less than tens of milliseconds [47]. And lastly, a learning process is initiated by the central nervous system to adapt to the new type of afferent signals. A closed loop architecture for restoring a sensory feedback is described in Fig. 6.4. This figure shows the transduction and interfacing system which transmit the electronic signals and the control system which performs signal processing and interpretation.

To provide a sensory feedback mechanism, data are firstly acquired through the use of tactile sensors that come in contact with the target object (Fig. 6.4). Secondly, the analog-to-digital converter digitizes the signal at the signal transduction stage

prior to further analysis. Before further signal processing, unwanted signal distur-
bances called artifact are removed by applying a wavelet transform and empirical
mode decomposition strategies to reduce the noise in the signal [48]. At the last
stage, the transmitted signal which mimics the real signal (action potential) is then
sent to the brain for interpretation.

With the invasive mechanism, action potentials traveling in the form of electrical
signals through the nervous systems could possibly regain all somatic sensory
information with modality matching by implanting neural electrodes in the periph-
eral nerves [49]. This approach is able to restore the sense of touch by means of
implantable nerve interfaces but always associated with risk of surgical procedure,
and their long-term usability needs to be fully investigated [50]. There are three
major approaches for invasive sensory feedback which are peripheral nervous
system (PNS) stimulation, targeted sensory reinnervation (TSR), and central nervous
system (CNS) stimulation. On the other hand, the promising noninvasive mechanism
could be realized through techniques such as mechanotactile, vibrotactile, or
electrotactile stimulations. To achieve any of these stimulation techniques, the
characteristics of the actuator (weight, size, and power consumption) would need
to be considered. Importantly, more research focus has been shifted toward the
noninvasive sensory feedback mechanism in the recent years with a lot of work
currently ongoing in this area.

In summary, integrating an efficient noninvasive sensory feedback mechanism
into the currently available multifunctional upper limb prostheses will not only
improve the control performance of the prostheses but also give users a feel of
their true natural environment during ADL.

6.4   Conclusion

The human upper limb is an important part of the body that enables the accomplish-
ment of a range of tasks in workplace, at home, and in social gathering during ADL.
The loss of this part of the body severely limits the capability of amputees while
undergoing ADL. In this regard, prosthetic device driven by different control
methods have been built to restore the lost limb functions in amputees. At the
forefront of these prostheses, control method is the EMG-based control which has
attracted considerable attention in both the academia and industry in the recent years.
Hence, this chapter focuses on EMG-based prostheses control methods with empha-
ses on pattern recognition-based control as well as simultaneous and proportional
control techniques, with details on the fundamental procedure of decoding limb
movement intents. Also, a number of techniques for improving the overall perfor-
mance of EMG-based prosthetic system were discussed with emphases on the
advantages and limitations.

References

 1. Holzer LA, Sevelda F, Fraberger G, Bluder O, Kickinger W, Holzer G (2014) Body image and self-esteem in lower-limb amputees. PLoS One 9(3):e92943
 2. Geertzen J et al (2015) Dutch evidence-based guidelines for amputation and prosthetics of the lower extremity: amputation surgery and postoperative management Part 1. Prosthetics Orthot Int 39(5):351–360
 3. Mckechnie PS, John A (2014) Anxiety and depression following traumatic limb amputation: a systematic review. Injury 45(12):1859–1866
 4. Physical and Emotional effects of limb amputation: http://www.seriousinjurylaw.co.uk/other-serious-claims/amputation/effects-of-amputation/Date. Last accessed 26 Sept 2017
 5. Đurović A, Ilić D, Brdareski Z, Plavšić A, Đurđević S (2007) Pain, functional status, social function and conditions of habitation in elderly unilaterally lower limb amputees. Vojnosanit Pregl 64(12):837–843
 6. Muilenburg AL, LeBlanc MA (1989) Body-powered upper-limb components. In: Comprehensive management of the upper-limb amputee. Springer, New York, NY, pp 28–38
 7. Li G (2011) Chapter 6: Electromyography pattern-recognition-based control of powered multifunctional upper-limb prostheses. In: Mizrahi J (ed) Advances in applied electromyography, IntechOpen (IntechOpen Limited), London, pp 99–117. ISBN: 978-953-307-382-8
 8. Samuel OW, Li X, Geng Y, Asogbon MG, Fang P, Huang Z, Li G (2017) Resolving the adverse impact of mobility on myoelectric pattern recognition in upper-limb multifunctional prostheses. Comput Biol Med 90:76–87
 9. Scheme E, Englehart K (2011) Electromyogram pattern recognition for control of powered upper-limb prostheses: state of the art and challenges for clinical use. J Rehabil Res Dev 48:643–660
10. Smith LH, Hargrove LJ, Lock BA, Kuiken TA (2011) Determining the optimal window length for pattern recognition-based myoelectric control: balancing the competing effects of classification error and controller delay. IEEE Trans Neural Syst Rehabil Eng 19(2):186–192
11. Li G, Schultz AE, Kuiken TA (2010) Quantifying pattern recognition-based myoelectric control of multifunctional transradial prostheses. IEEE Trans Neural Syst Rehabil Eng 18(2):185–192
12. Li G, Li Y, Yu L, Geng Y (2011) Conditioning and sampling issues of EMG signals in motion recognition of multifunctional myoelectric prostheses. Ann Biomed Eng 39(6):1779–1787
13. Samuel OW, Zhou H, Li X, Wang H, Zhang H, Sangaiah AK, Li G (2017) Pattern recognition of electromyography signals based on novel time domain features for amputees' limb motion classification. Comput Electr Eng 2017:1–10
14. Adewuyi AA, Hargrove LJ, Kuiken TA (2016) An analysis of intrinsic and extrinsic hand muscle EMG for improved pattern recognition control. IEEE Trans Neural Syst Rehabil Eng 24(4):485–494
15. Li X, Samuel OW, Zhang X, Wang H, Fang P, Li G (2017) A motion-classification strategy based on sEMG-EEG signal combination for upper-limb amputees. J Neuroeng Rehabil 14(1):2
16. Geng Y, Samuel OW, Wei Y, Li G (2017) Improving the robustness of real-time myoelectric pattern recognition against arm position changes in Transradial amputees. Biomed Res Int 2017:5090454
17. Finley FR, Wirta RW (1967) Myocoder studies of multiple myopotential response. Arch Phys Med Rehabil 48(11):598–601. [PMID: 6060789]

18. Lawrence P, Herberts P, Kadefors R (1973) Experiences with a multifunctional hand prosthesis controlled by myoelectric patterns. In: Gav rilovic MM, Wilson AB Jr (eds) Advances in external control of human extremities. Etan, Belgrade, pp 47–65
19. Lyman JH, Freedy A, Prior R (1976) Fundamental and applied research related to the design and development of upper-limb externally powered prostheses. Bull Prosthet Res 13:184–195
20. Oskoei MA, Hu H (2007) Myoelectric control systems—a survey. Biomed Signal Process Control 2(4):275–294
21. Englehart K, Hudgins B (2003) A robust, real-time control scheme for multifunction myoelectric control. IEEE Trans Biomed Eng 50(7):848–854
21. Khushaba RN, Al-Timemy A, Kodagoda S, Nazarpour K (2016) Combined influence of forearm orientation and muscular contraction on EMG pattern recognition. Expert Syst Appl 61:154–161
22. Huang YH, Englehart K, Hudgins B, Chan AD (2005) A Gaussian mixture model based classification scheme for myoelectric control of powered upper limb prostheses. IEEE Trans Biomed Eng 52:1801–1811
23. Hudgins B, Parker P, Scott RN (1993) A new strategy for multifunction myoelectric control. IEEE Trans Biomed Eng 40(1):82–94
24. Ajiboye AB, Weir RF (2005) A heuristic fuzzy logic approach to EMG pattern recognition for multifunctional prosthesis control. IEEE Trans Neural Syst Rehabil Eng 13:280–291
25. Oskoei MA, Hu H (2008) Support vector machine-based classification scheme for myoelectric control applied to upper limb. IEEE Trans Biomed Eng 55(8):1956–1965
26. Hargrove L, Englehart K, Hudgins B (2007) A comparison of surface and intramuscular myoelectric signal classification. IEEE Trans Biomed Eng 54:847–853
27. Coapt (2013) Available: http://coaptengineering.com/
28. Kuiken TA, Li G, Lock BA, Lipschutz RD, Miller LA, Stubblefield KA, Englehart KB (2009) Targeted muscle reinnervation for real-time myoelectric control of multifunction artificial arms. JAMA 301:619–628
29. Harris A, Katyal K, Para M, Thomas J (2011) Revolutionizing prosthetics software technology. In: Systems, man, and cybernetics (SMC), 2011 IEEE international conference on, October, IEEE, pp 2877–2884
30. Samuel OW, Asogbon MG, Geng Y, Chen S, Fang P, Lin C, Wang L, Li G (2018) A novel time-domain descriptor for improved prediction of upper limb movement intent in EMG-PR system. In: Engineering in medicine and biology society (EMBC), 40th annual international conference of the IEEE, 2018, July 17–21, 2018, Honolulu, Hawaii, USA
31. Muceli S, Farina D (2012) Simultaneous and proportional estimation of hand kinematics from EMG during mirrored movements at multiple degrees-of-freedom. IEEE Trans Neural Syst Rehabil Eng 20:371–378
32. Jiang N, Englehart KB, Parker PA (2009) Extracting simultaneous and proportional neural control information for multiple-DOF prostheses from the surface Electromyographic signal. IEEE Trans Biomed Eng 56:1070–1080
33. Samuel OW et al (2016) Examining the effect of subjects' mobility on upper-limb motion identification based on EMG-pattern recognition. In: Intelligent robot systems (ACIRS), Asia-Pacific conference, IEEE, 137–14
34. Jiang N, Rehbaum H, Vujaklija I, Graimann B, Farina D (2014) Intuitive, online, simultaneous, and proportional myoelectric control over two degrees-of-freedom in upper limb amputees. IEEE Trans Neural Syst Rehabil Eng 22(3):501–510
35. Lee DD, Seung HS (2001) Algorithms for non-negative matrix factorization. In: Advances in neural information processing systems. MIT Press, Cambridge, MA, pp 556–562
36. Lee DD, Seung HS (1999) Learning the parts of objects by non-negative matrix factorization. Nature 401(6755):788–791
37. Kim H, Park H (2007) Sparse non-negative matrix factorizations via alternating non-negativity-constrained least squares for microarray data analysis. Bioinformatics 23(12):1495–1502
38. Kuiken TA, Childress DS, Rymer WZ (1995) The hyper-reinnervation of rat skeletal muscle. Brain Res 676:113–123

39. Williams HB (1996) The value of continuous electrical muscle stimulation using a completely implantable system in the preservation of muscle function following motor nerve injury and repair: an experimental study. Microsurgery 17:589–596
40. Nicolaidis SC, Williams HB (2001) Muscle preservation using an implantable electrical system after nerve injury and repair. Microsurgery 21:241–247
41. Grinsell D, Keating CP (2014) Peripheral nerve reconstruction after injury: a review of clinical and experimental therapies. J Biomed Res Int 2014:698256
42. Samuel OW, Asogbon MG, Geng Y, Al-Timemy AH, Pirbhulal S, Ji N et al (2019) Intelligent EMG pattern recognition control method for upper-limb multifunctional prostheses: advances, current challenges, and future prospects. IEEE Access 7:10150–10165
43. Ziegler-Graham K, MacKenzie J, Ephraim P, Travison T, Brookmeyer R (2008) Estimating the prevalence of limb loss in the United States: 2005 to 2050. Arch Phys Med Rehabil 89(3):422–429
44. Raspopovic S, Capogrosso M, Petrini FM, Bonizzato M, Rigosa J, DiPino G, Carpaneto J, Controzzi M, Boretius T, Fernandez E, Granata G, Oddo CM, Citi L, Ciancio AL, Cipriani C, Carrozza MC, Jensen W, Guglielmelli E, Stieglitz T, Rossini PM, Micera S (2014) Restoring natural sensory feedback in real-time bidirectional hand prostheses. Sci Transl Med 6:222ra19
45. Christian A, Anders B, Sven-Olof F, Fredik S, Goran L, Birgitta R (2012) Sensory feedback from a prosthetic hand based on air-mediated pressure from the hand to the forearm skin. J Rehabil Med 44:702–707
46. Chortos A, Liu J, Bao Z (2016) Pursuing prosthetic electronic skin. Nat Mater 15(9):937–950
47. Zou L, Ge C, Wang ZJ, Cretu E, Li X (2017) Novel tactile sensor technology and smart tactile sensing systems: a review. Sensors 17(11):2653
48. Saal HP, Bensmaia SJ (2015) Biomimetic approaches to bionic touch through a peripheral nerve interface. Neuropsychologia 79:344–353
49. D'anna E, Petrini FM, Artoni F, Popovic I, Simanić I, Raspopovic S, Micera S (2017) A somatotopic bidirectional hand prosthesis with transcutaneous electrical nerve stimulation based sensory feedback. Sci Rep 7(1):10930
50. Micera S (2016) Staying in touch: toward the restoration of sensory feedback in hand prostheses using peripheral neural stimulation. IEEE Pulse 7(3):16–19

Chapter 7
Neural Interface: Frontiers and Applications

Cochlear Implants

Xiaoan Sun, Sui Huang, and Ningyuan Wang

Abstract The theory and implementation of modern cochlear implant are presented in this chapter. Major signal processing strategies of cochlear implants are discussed in detail. Hardware implementation including wireless signal transmission circuit, integrated circuit design of implant circuit, and neural response measurement circuit are provided in the latter part of the chapter. Finally, new technologies that are likely to improve the performance of current cochlear implants are introduced.

Keywords Cochlear implant · Signal processing strategy · Neural response measurement

7.1 Introduction of Cochlear Implant

A cochlear implant is a surgically implanted electronic device that provides functional hearing to a person with severe to profound sensorineural hearing loss. It bypasses a non-functional inner ear and stimulates the auditory nerve directly with patterns of electrical currents derived from incoming sounds. A cochlear implant system usually consists of an external sound processor and an implanted current stimulator. Cochlear implant is widely accepted as the only effective way to restore functional hearing for deaf people in daily clinical practice and is the most successful neural prosthesis in current world. Up to date, about 450,000 people worldwide have received cochlear implants; half of them are pediatric users who were able to develop near normal language skills and merged seamlessly into mainstream schools and society. As the technology of cochlear implant improves, and the risk associated with the device and the surgery decrease over the years, more and more people

X. Sun (✉) · S. Huang · N. Wang
Nurotron Biotechnology Inc., Irvine, CA, USA
e-mail: xsun@nurotron.com

benefit from the device each year. The clinical threshold to be considered as a cochlear implant candidate has been dropped from 100 dB hearing loss in 1980s and 1990s to 85 dB hearing loss in current years. Therefore, the boundary between hearing aids user and cochlear implant candidate becomes obscure and interleaved.

According to census by World Health Organization in 2010, there are about 360 million hearing-impaired people worldwide, representing the second largest group of handicapped people. This number grows annually as a result of 0.1–0.2% rate of congenital deaf among newborns. In addition, consequential deaf from disease, medicine intoxication, trauma, environmental noise, and genetic disorders also contribute to the increase of deaf population. Traditionally, large amount of resource is required to set up rehabilitation facilities for deaf people, yet the effectiveness of these rehabilitations is very limited. They still live within the deaf society and find it hard to communicate with the outside world. The appearance of cochlear implants changes the situation fundamentally. Most modern cochlear implant recipients can carry a normal conversation in a quite environment, although they still find it challenging to communicate in a noisy environment.

The development of modern cochlear implant is a long and interesting journey, including joint efforts from physiologists, physicians, and engineers. In 1957, French physician Djourno and his colleagues induced successful hearing with electrical stimulation in two totally deaf patients. The news spurred an intensive level of research activities worldwide to restore hearing to deaf people. In 1961, William House in Los Angeles, California, implanted a single-channel cochlear implant in the scalar tympani of two deaf people. Both subjects report useful hearing from electrical stimulation although the initial devices only lasted 2 weeks. In 1978, Graeme Clark in Australia developed a multi-channel cochlear implant and implanted in two deaf people. Although single-channel cochlear implant won the first round as the first FDA-approved device for clinical use, multi-channel device is the standard for modern cochlear implants because of its superior performance.

A cochlear implant usually includes an internal implant device and an external sound processor, as shown in Fig. 7.1. The external sound processor (1) powered by battery pack (2) picks up sound through microphone and processes and encodes sound signal, which is then transmitted wirelessly by transmission coil (3) to the receiver coil (4) of internal device. The current stimulator (5) of internal device converts the received signals into electrical impulses and sends the impulses through electrode body (6) to an electrode array (7). The electrical impulses from the electrode array (7) stimulate the auditory nerves (8), allowing the brain to perceive sound.

Now there are four major cochlear implant providers in the world: Cochlear Corporation in Australia (www.cochlear.com), Med-El Corporation in Austria (www.medel.com), Advanced Bionics Corporation in the United States (www.advancedbionics.com), and Nurotron Biotechnology Inc. in China (www.nurotron.com). There are a couple of smaller cochlear implant companies with no significant market shares. They all provide multi-channel devices with 12–24 electrodes, while Nurotron device has the most intra-cochlear electrodes of 24. Functions like virtual channel, electrode impedance measurement, and neural response telemetry also become standard for modern cochlear implant devices. The recognition rate of short sentences in quiet is around 80% for the products of all four major manufactures.
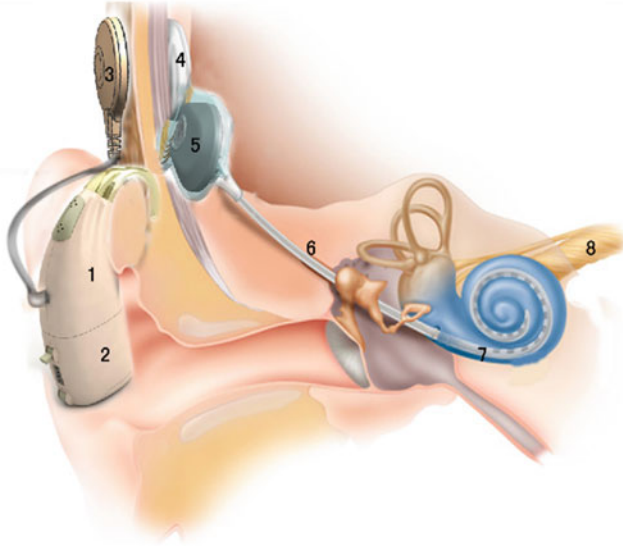
Fig. 7.1 External device of cochlear implant system includes (1) sound processor, (2) battery pack, (3) transmission coil. Internal device of cochlear implant system includes (4) receiver coil, (5) current stimulator, (6) body of electrode, (7) electrode array, which stimulator auditory nerves (8) with current pulses

7.2 System Specification

The ultimate goal of cochlear implant is to restore effective hearing for severe to profound hearing-impaired people through safe electrical stimulation of auditory nerve. To this end, the design and manufacture of a cochlear implant system should satisfy requirements in three aspects. First, the material of the implant device should be safe for long-term implantation. Second, the circuit of the implant should be able to deliver safe, reliable, and accurate current stimulation. And last, the structure of the implant should consider surgical requirement and provide enough protection for electronic components. The architecture of a modern cochlear implant system is shown in Fig. 7.2, consisting of a speech processor, a RF unit, an internal unit, an electrode array, a remote controller, and a fitting unit [76].

7.2.1 Speech Processor

The speech processor shown in Fig. 7.3 is the core of the external part of the cochlear implant system. The entire speech processor is powered by a battery block. The clock block provides clock signal to all blocks except the power amplifier and the reverse telemetry decoder. The audio signal from natural environment or other
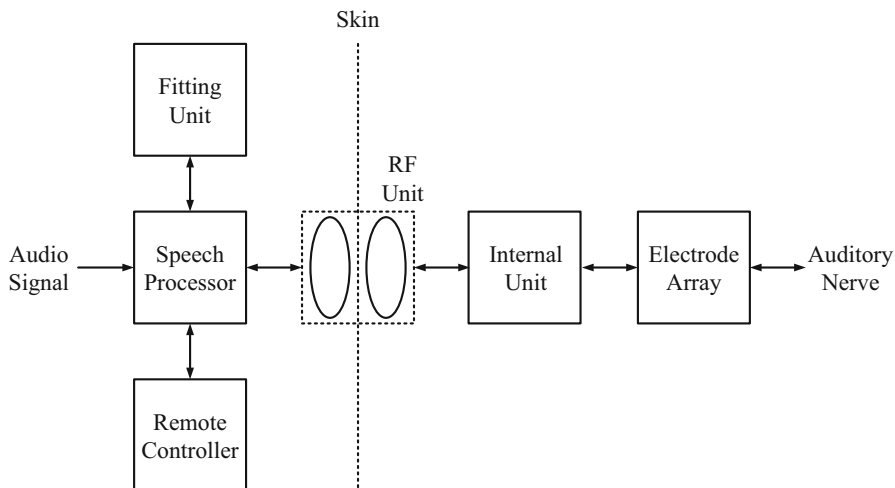
Fig. 7.2 Typical architecture of a modern cochlear implant system
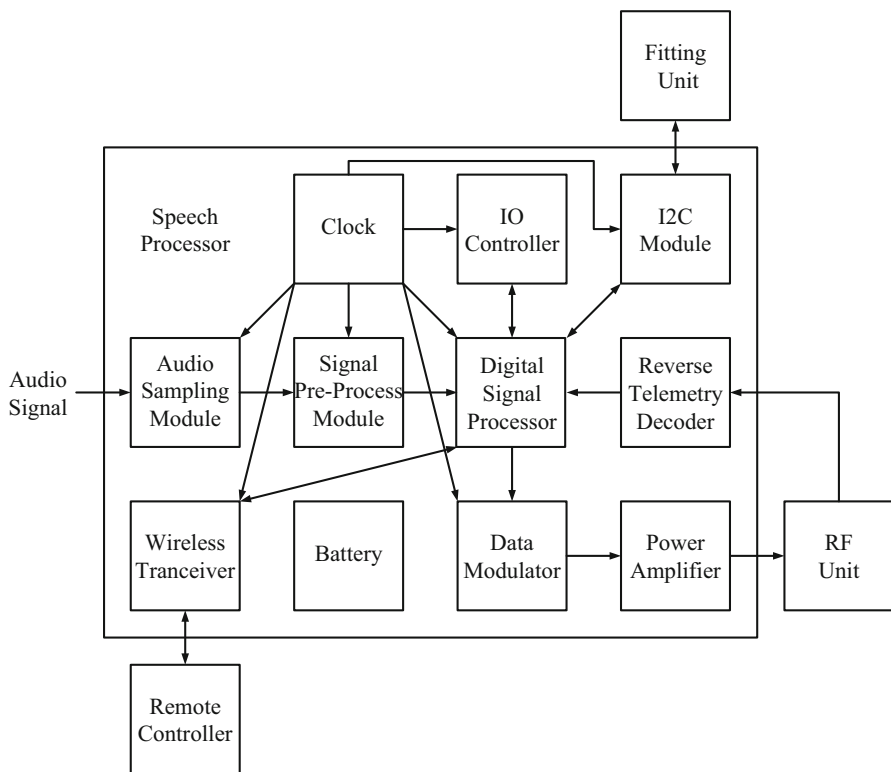
Fig. 7.3 Block diagram of speech processor

electrical devices (TV, radio, tele-coil, etc.) is first sampled, digitized, and synchronized in audio sampling module. Processed by signal pre-processing module and digital signal processor (DSP) based on certain encoding strategies, the output of audio sampling module is converted to data that contains stimulation information. Then the data are modulated at data modulation block by radio frequency (RF) carrier signal and sent to power amplifier (PA). The amplified signal is eventually sent to RF unit. The reverse telemetry decoder detects and modulates the signal from the RF unit when the system is in the status of reverse telemetry. The decoded signal goes into the DSP for further operation. The I2C module and wireless transceiver, which are both controlled by the DSP, are used to communicate with the fitting unit and remote controller, respectively. The IO controller controls indication lights and buttons on the speech processor.

7.2.2 RF Unit

The RF unit is composed of a transmitter coil and a receiver coil connected with their resonant circuits, which are on the outside and inside of human body, respectively. Through this inductive link, the stimulating information as well as power is transmitted into the internal unit to control the unit to stimulate the auditory nerve. More interestingly, using the reverse telemetry technique, the data from the implant can be sent back to the speech processor with the same link.

7.2.3 Remote Controller

The remote controller is used to execute some regular operation, for example, turning on and off the system, adjusting the sound volume, changing fitting maps, and so on. In some applications, it could also be used to check the status of the speech processor and the internal unit. Most of the recent cochlear implant products favor this wireless control unit because it is much more convenient for users or guardians of users to manipulate the device instead of pushing buttons on the speech processors.

7.2.4 Fitting Unit

The fitting unit, which is not worn by users, is only used by clinicians for clinical uses, e.g., impedance test, neural response measurement, fitting program, etc. The fitting unit can bi-directionally communicate with the speech processor. On one hand, when clinicians want to optimize performance of devices, different stimulating

information can be sent to speech processors from fitting programs. On the other hand, when they need to detect the condition of implants, the internal data from implants can also be sent back to the unit.

7.2.5 Internal Unit

The block diagram of the internal unit is shown in Fig. 7.4. The RF signal from the RF unit is divided into two paths. One goes into the power generator to provide a high voltage for the stimulating circuit and power supply for all other internal circuits. The other path goes to RF signal demodulator. If the RF signal is a command signal, the demodulator sends the signal to the command decoder, which stores the decoded information in the setting register. If the RF signal is a data signal, the data decoder is activated, and the stimulating data is sent to the data distributor. The output of the demodulator is also the source of the clock generator, which is basically a clock recovery circuit to provide a stable clock signal for other blocks. The stimulating circuit is controlled by data distributor that decides current amplitude and electrode address and by the timing controller that controls the stimulating time. The stimulating current finally flows from the stimulating circuit to the electrode array. The recording circuit is used to record the voltage signal in the electrode, which is converted to the digital signal and transmitted back to RF unit through the reverse telemetry modulator.

7.2.6 Electrode Array

The electrode array is a major part of the implant, which is inserted into the cochlea. The stimulating current pulse goes out from the stimulating electrode to activate the neurons and flows back to the return electrode in the end. To avoid the DC voltage shift accumulation, normally the current pulse has two phases with positive and negative current as shown in Fig. 7.5.

7.3 Signal Processing Strategies

7.3.1 Introduction

Speech processor can be described as the brain of a cochlear implant. Acoustic signals are processed and encoded into specific parameters of electric pulses using particular signal processing methods, termed as "signal coding strategy".

In the CI system, the signal coding strategy plays an extremely important role in generating auditory perception of CI recipients (e.g., [72, 74]), which determines
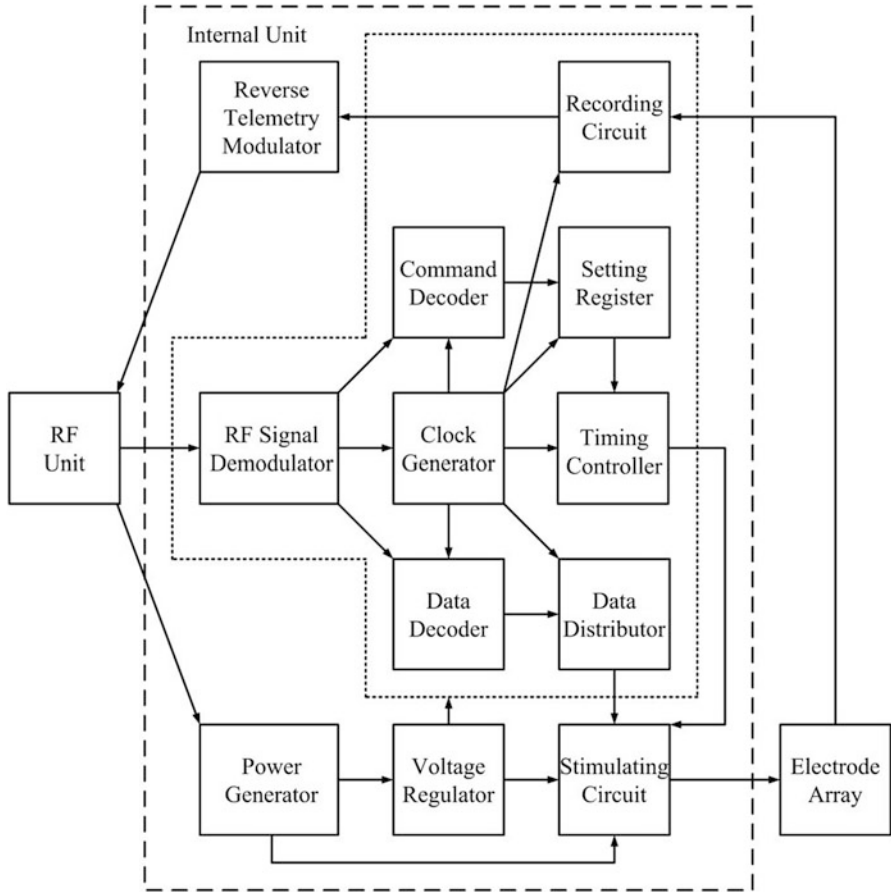
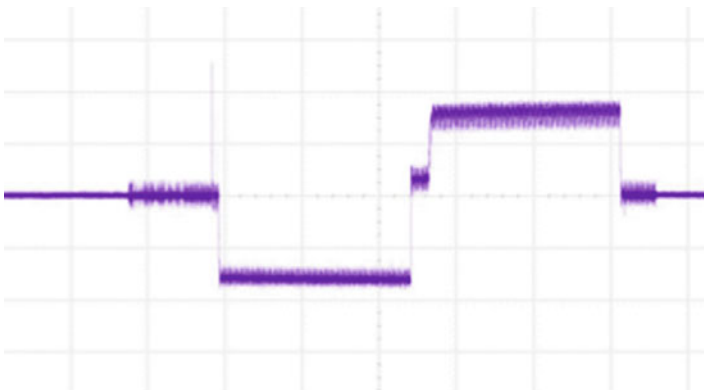**Fig. 7.4** Block diagram of internal unit

Fig. 7.5 A typical biphasic stimulating pulse using the return electrode as reference

which electrodes should be activated in each cycle according to the input acoustic signals. Many stimulating strategies have been developed over the past two decades. An ideal stimulating strategy is one that allows a CI user to perceive sounds clearly and accurately.

All modern multi-electrode CIs have been developed to take advantage of the so-called tonotopic organization in the cochlea that the apical part and the basal part of the cochlea encode low-frequency and high-frequency sounds, respectively. In these types of CIs, a bank of filters is employed to divide speech into different frequency bands, but they differ in processing and encoding acoustic signals into electric pulses.

7.3.2 Formant-Based Strategies

One group of coding strategies was based on the idea of speech production and perception, in which spectral peaks or formants are extracted and delivered to different electrodes. The F0/F2 strategy was first developed and implemented in the Nucleus Wearable Speech Processor [16]. In this strategy, the fundamental frequency (F0) and the second formant (F2) are extracted from the speech signal in each frame. One zero-crossing detector is used to estimate F0 from the output of a low-pass filter, which has a cutoff frequency of 270 Hz, and another zero-crossing detector is used to estimate F2 from the output of a 1000–4000 Hz band-pass filter. The amplitude of F2 is then estimated by rectifying and low-pass filtering the output signal. The schematic diagram is shown in Fig. 7.6.

The addition of the first formant (F1) information was found to improve the speech recognition performance of patients in speech perception tests. In fact, both F1 and F2 were reported important in vowel recognition for normal-hearing listeners [24]. Dowell et al. [24] found that the average scores on word recognition increased from 30% to 63% after switching from F0/F2 to F0/F1/F2 strategy.

Further improvements to the F0/F1/F2 strategy were made in the late 1980s, including the involvement of high-frequency information. MULTIPEAK (or MPEAK), a new coding strategy developed upon these changes, was used to extract both formants and high-frequency information from the speech signal (as shown in Fig. 7.7). The MPEAK strategy stimulates four electrodes at a rate of F0 pulses/sec (pps) for voiced sounds, and at an average rate of 250 pps for unvoiced sounds [57].

Although the MPEAK strategy has proved to be an efficient strategy for extracting important information from the speech signal, the performance is still limited. The MPEAK strategy and F0/F2 and F0/F1/F2 strategies tend to make errors in formant extraction, especially when the speech signal is embedded in noise. However, all the attempts made in the improvements of formant extraction methods motivated the development of the next generation coding strategies for CIs.
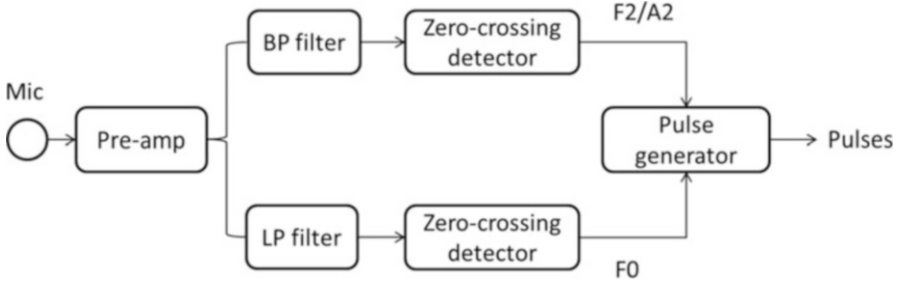
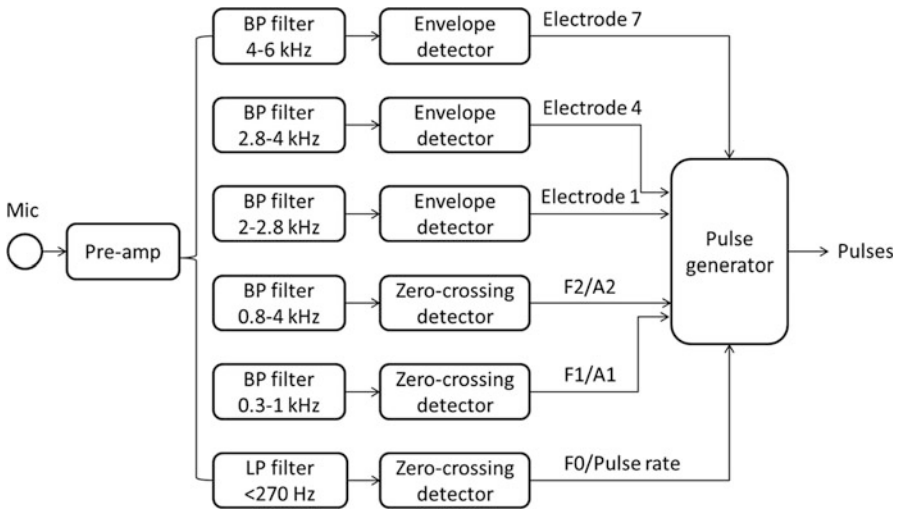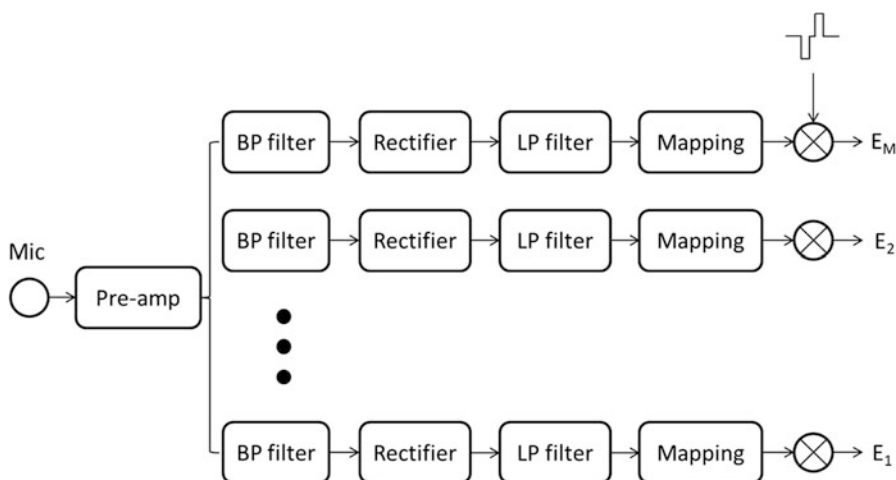**Fig. 7.6** Block diagram of F0/F2 strategy

Fig. 7.7 Block diagram of MPEAK strategy

7.3.3 Temporal Envelope-Based Strategies

Another thought of spectrum regeneration with electric stimulation was based on the implicit encoding of temporal envelope cues and could be traced back to earlier work in speech vocoder [25]. Most of algorithms implemented in current commercial devices origin from this idea.

7.3.3.1 Continuous Interleaved Sampling (CIS) Strategy

For modern multi-channel cochlear implants, which have M (e.g., 12–24) implanted electrodes, CIS is a strategy used in the speech processors of all major cochlear implant manufacturers [72]. CIS is a multi-band coding strategy, in which the temporal envelope of signal in each band is extracted at a cutoff frequency of

Fig. 7.8 Block diagram of CIS strategy

160–400 Hz. For each frame of sound, the signal is applied through M band-pass filters, and the envelopes of these frequency bands are extracted. The envelope also has to be compressed, usually logarithmically, to match the narrow dynamic range in electric stimulation. Then, all M frequency bands are stimulated in a non-overlapping sequence at a constant rate. In this pattern, the stimulation rate of each channel is relatively high and the interaction across electrodes can also be reduced. Meanwhile, the original spectrum of received sound is regenerated by M channels and one channel of the signal is produced by the stimulation of one electrode. The schematic diagram of CIS is shown in Fig. 7.8. According to Shannon et al. [56], four spectral bands in CIS processing can deliver acceptable speech intelligibility in quiet.

7.3.3.2 n-of-m Strategies

A group of coding strategies based on channel selection or "spectral peak picking" scheme is represented by "n-of-m strategy" (Fig. 7.9), which is designed in part to reduce the density of stimulation while still reserving the most important aspects of speech signals [38]. In each cycle, only N channels with largest amplitudes are selected from all M channels and stimulated. The deletion of stimulation from low-energy channels for each frame of sound may reduce the interference across electrodes and restrict the area of stimulated region in the cochlea. Taking the fact into consideration that low-level channels usually do not contain significant information, such "unmasking" may improve the perception of sounds by patients. In addition, selection of the channels containing higher energy in each frame may enhance the signal-to-noise ratio in signal domain situations.
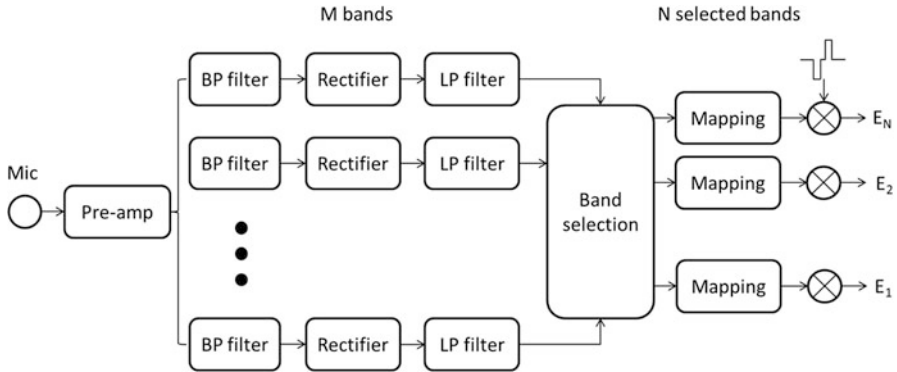
Fig. 7.9 Schematic diagram of n-of-m strategy

The ACE and SPEAK strategy (differ in stimulation rate), used in the Nucleus implant, consists of 22 fixed channels. The input signal is divided into 22 frequency bands for each frame just as CIS strategy. After the envelope information for each frequency band is extracted by rectifying and low-pass filtering, 6–10 frequency bands with the largest amplitudes are stimulated. The number of stimulated channels could be set by audiologists. Electrodes corresponding to the selected channels are then activated, and the original spectrum is reproduced by 6–10 fixed channels [49].

Advanced peak selection (APS) is a coding strategy employed by the Nurotron device [76]. The APS strategy can also be defined as an "n-of-m" strategy, with the number of frequency bands being 24. The number of channels being stimulated in each frame is typically set to 6–8, dependent on the number of available electrodes or the feedback from patients. In the APS strategy, stimulation rate can be adjusted to improve the representation of temporal fine structure. The typical stimulating rate of each selected electrode is normally set to 680 pps or 890 pps.

7.3.4 Coding Strategies with Advanced Cues

As described above, both n-of-m and CIS strategies only employ a certain number of channels to reproduce the original sound spectrum, which means only 12–24 electrodes can currently be implanted into a CI user's ear to generate 12–24 fixed channels. However, the population of auditory nerve fibers in a human cochlear is around 30,000. Due to the limitation of the electrode number and design, the spectral resolution of a CI user is normally worse than that of a normal-hearing listener, which severely weakens their pitch and tone perception. Therefore, a school of new coding strategies designed to improve pitch or tone perception of CI users has been proposed in recent years.

7.3.4.1 HiRes120 Strategy

Another alternative method is virtual channel strategy, in which the electrical stimulation pattern is shaped by current steering technique [22, 41]. To implement the virtual channel technique in a cochlear implant system, each electrode must have an independent power source to allow more than one electrode to be stimulated simultaneously. Theoretically, with simultaneous stimulation of neighboring electrodes, the locus of stimulation is controlled between fixed channels, creating virtual channels.

The HiRes120 strategy, used in the Advanced Bionics implant, is the first commercial virtual channel strategy [40]. Since the Advanced Bionics implant has 16 implanted electrodes, there are 15 electrode pairs that can be used to steer the electrical stimulation and 8 sub-channels within each electrode pair, generating 120 channels in total. Figure 7.10 is a diagrammatic representation of the HiRes120 strategy. Similar to CIS strategy, in each frame of sound, the signal is divided into 15 frequency bands and the envelope of each band is extracted. Next, 15 spectral peaks are also derived, which indicate the most important frequency component within each channel. These spectral peaks are then steered by corresponding electrode pairs based on the virtual channel technique. However, according to results from clinical tests, HiRes120 strategy did not achieve expectation of researchers.

7.3.4.2 C-Tone Strategy

CI signal processing significantly affects lexical tone recognition due to the restricted spectral resolution of CI users, which is to the disadvantage of overall speech understanding of tonal languages (e.g., [30]). One way to improve tone recognition rate is to deliver information other than temporal envelope. Since F0 has been found to carry most of the lexically meaningful information for tonal languages, Luo and Fu [47] evaluated a novel method to improve Chinese tone recognition in which amplitude contour was modified to better resemble the F0 contour. In this study, results showed significantly better tone recognition with the amplitude contour modification. An amplitude contour manipulation algorithm (C-tone) that originate from this idea was implemented in Nurotron implant system to challenge the difficulties in lexical tone recognition of CI users [51].

C-tone was implemented as a tone-enhanced version of APS strategy as shown in Fig. 7.11. A voice activity detector (VAD) is applied at the frontend of the algorithm process. In each frame, the first step of C-tone is to estimate the F0 with the average magnitude difference function (AMDF) algorithm [54]. Second, the input signal is passed through a similar process as APS strategy. Finally, the amplitude envelope of each selected stimulation channel is adjusted based on the relative change of F0 comparing to that estimated from the previous frame. An increment in F0 results in an enhancement in the amplitude envelope and vice versa. The preliminary data suggest that real-time enhancement of the amplitude envelope contour in C-tone may benefit Chinese CI users' tone recognition.
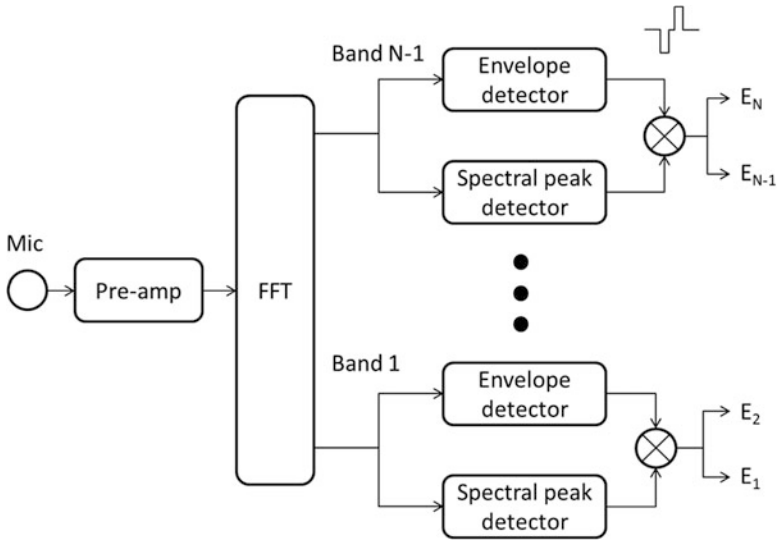
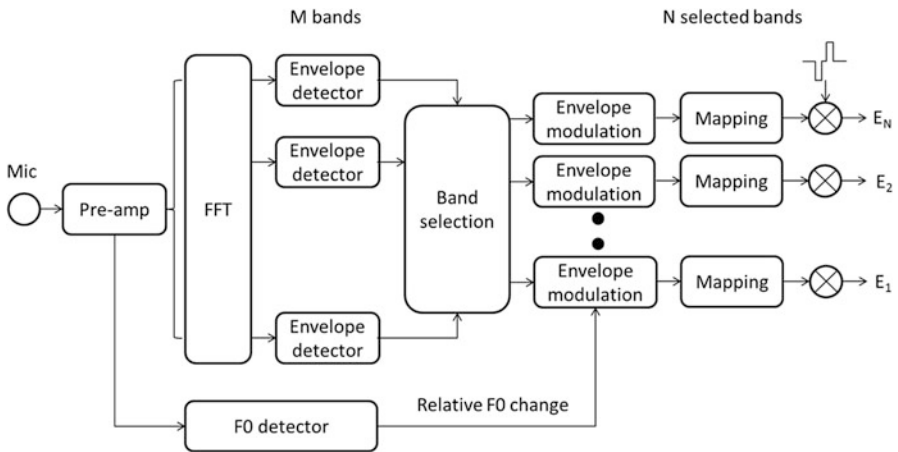**Fig. 7.10** Block diagram of HiRes120 strategy

Fig. 7.11 Block diagram of C-tone

7.3.4.3 Fine Structure Processing (FSP) Strategy

New processing options have also been introduced to increase the transmission of fine structure information compared with the CIS and other n-of-m strategies in current use. In one approach, the timing of positive zero crossings in the output of the four band-pass filters with the lowest center frequency dominates the presentation of a short group of pulses for the corresponding channels of stimulation as opposed to

the continuous presentation of pulses for standard CIS channels. This strategy is called the "fine structure processing" (FSP) strategy [55], applied in MED-EL's implant. In FSP, signals in low-frequency channels and in high-frequency channels are treated and processed differently. In low-frequency channels, the amplitude of output signal is determined by the total energy in this band. In high-frequency channels, however, signal is processed similar as that in CIS strategy.

The FSP and related approaches may provide an advantage compared with CIS and other envelope-based strategies with the delivery of fine structure information in the lower channels. With the help of additional fine structure information, FSP has been reported to enhance music or speech perception of CI users [2].

7.3.5   Pre-processing Techniques

Despite the good performance of CI in quiet, there are still significant gaps in performance between normal-hearing people and CI users. For example, the performance of CI users in speech perception is extremely poor with additive noise. At least a 15-dB loss in functional signal-to-noise ratio (SNR) could be produced in a steady-state noise background [75]. In a study by Firszt et al. [28], speech recognition was assessed using the hearing in noise test (HINT) sentences. Results revealed that CI recipients' performance on sentence recognition tasks was significantly poorer in noise compared with when listening at speech stimuli in quiet at a soft level. In Spahr and Dorman [61]'s study, it was reported that the average speech intelligibility performance of CI recipients is around 40% in tasks involving conversational speech presented at 10 dB SNR. The average recognition of conversational speech dropped to around 20% when the SNR level was lowered to 5 dB. Fetterman and Domico [27] had similar finding in their study, in which CI users were asked to identify speech in noise. Average sentence recognition scores of CI users decreased from 82% in quiet to 73% at 10 dB SNR and to 47% at 5 dB SNR.

The poor frequency selectivity of hearing-impaired listeners has been reported as a significant reason why they cannot distinguish speech signal from the noise as normal-hearing listeners [64]. Recent research efforts have been focusing on state-of-the-art noise reduction solutions much more to improve speech intelligibility in noisy environments. Since CIs deliver electrical pulses to stimulate auditory nerves to help restore hearing sensation, multiple signal processing algorithms have been applied to convert acoustic signals into electrical stimuli (e.g., [46, 74]). As we mentioned above, the majority of CI users can score high in open-set speech recognition tasks regardless of the device or speech coding strategy used (e.g., [58, 61]). However, few of them could overcome the problems of additive noise.

Many of current noise reduction algorithms can improve output SNR, but few of them can really enhance the speech intelligibility (e.g., [44]). The generated speech distortion has been considered as one of the reasons. A traditional method to reduce the effect of noise is to apply a gain calculated from estimated SNR level to suppress the noise. However, since the power of noise cannot be accurately estimated, the

speech signal can be either amplified or attenuated due to the underestimation or overestimation to the noise power, respectively. Considerable speech distortion is then introduced [39], resulting in no or even negative benefits in speech intelligibility [33].

In general, noise reduction algorithms designed for CIs could be divided into two classes: single-microphone and multi-microphone methods. Single-microphone approaches rely mostly on statistical models of speech and noise, and therefore can only remove noise with different temporal and spectral features as speech signals. In recent years, there has been a growing tendency toward the use of noise reduction methods with multiple microphones in CI devices (e.g., [42, 73]). Large improvements in SNR and therefore considerable benefits in speech intelligibility can be obtained, only if the target speech and the noise sources are located at different locations in space. In the following session, both single-channel and multi-channel noise reduction techniques are reviewed.

7.3.5.1 Single-Channel Noise Reduction Methods

One of the first proposed single-channel noise reduction algorithms is spectral subtraction, based on a maximum likelihood (ML) estimator, and has been implemented in numerous applications. Its efficiency and low computational complexity have resulted in its widespread use. The general idea of spectral subtraction is to estimate the spectrum of noise during gaps in the speech, and then to remove it from the noisy signal [66]. The performance of this class of algorithms depends critically on the accuracy of noise estimation. A conventional method to estimate the noise is to update the noise power cumulatively during speech gaps and hold it unchanged during speech frames. To determine when speech is present or absent, a voice activity detector (VAD) is required [4].

Despite its attractive simplicity, spectral subtraction has a number of shortcomings, which limit its use in applications such as hearing aids and CIs. One commonly audible artifact produced by the technique is termed "musical noise" and is generated primarily by inaccurate estimation of the noise spectrum. Since only the average power of the noise can be estimated over time, short-term, potentially important details, such as momentary spectral peaks and valleys, are ignored by the algorithm. As a result, after the estimated average noise is removed, those residual components can produce annoying tonal sounds, which can worsen, rather than improve, speech intelligibility and perceived quality.

Over the past three decades, much effort has gone into developing methods that remove or reduce musical noise [17, 52]. A common technique is to set up a noise floor, that when the signal level is under a certain threshold, it will be left unprocessed [4]. A factor could be used to control the strength of this technique, that how much the signal should be removed when its level is under the threshold. Moreover, it has been noticed that the influence of noise on speech signal may not be unified; it is rational to apply different control factors at different frequencies.

Wiener filtering is another well-studied technique in speech enhancement, based on optimal minimum mean square error (MMSE) estimator of each speech spectral component [13, 45]. Martin [48] developed an algorithm based on the combination of Wiener filtering and spectral subtraction to overcome the limitation of VAD, so that in a speech frame, noise information could still be updated by a Wiener filter. Extended Wiener filters have been proposed to further enhance the performance of noise reduction algorithms. Multi-channel Wiener filtering, for example, has been tested [68, 69]. In addition, the speech distortion weighted Wiener filter was developed to reduce speech distortion, in order to maintain speech intelligibility while cleaning speech [21, 62].

Most commercial CI devices employ single-channel noise reduction algorithm due to its simplicity and efficiency. A recent proposed technique named as eVoice applied in Nurotron speech processor, which can adapt to the external SNR conditions so as to generate stable auditory perception, was evaluated with speech perception test of CI users. Results are exhibited in Fig. 7.12. The percent of correct rates of subjects using APS strategy were compared with the performance of the
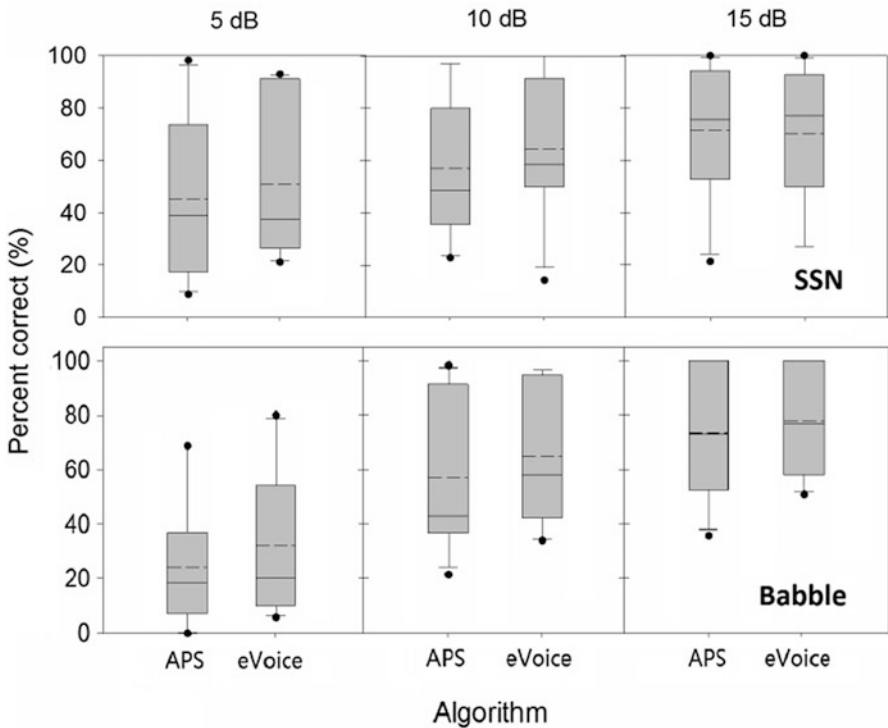
Fig. 7.12 Results of speech perception test in evaluating the effects of eVoice. *Notes*: APS represents using APS strategy along and eVoice indicates using eVoice as the pre-processing technique prior to the application of APS strategy. SSN and Babble represent speech-shaped noise and babble noise, respectively

same group of subjects when using APS and eVoice together. In summary, eVoice improves speech intelligibility of CI users in 5- and 10-dB SNR conditions in the presence of both speech-shaped noise and babble noise. Meanwhile, most subjects reported the preference of using eVoice in noisy environments.

### 7.3.5.2 Multi-Channel Noise Reduction Methods

Cocktail party problem [14] as one of the most challenging tasks for hearing-impaired listeners has been attempted to be solved via multi-channel algorithms. The crucial ability of completing this task is to separate the mixture of target speech and interfering noise or speech. One group of methods is blind source separation (BSS), which does not require the prior knowledge of microphone array and spatial information of target speech (e.g., [70, 71]). Information-based criteria are usually employed in such methods. A representative work was done by Douglas and Sun [23], using convolutive blind source separation with natural gradient algorithm to automatically resolve mixed recordings from the real environment. In this study, it was found that the modified BSS technique with linear prediction filters was able to complete the task of separating the mixture of two-channel speech signals.

Beamforming is another group of multi-microphone spatial enhancement technique via source separation and works by exploiting phase differences in the signals arriving at two spatially separated microphones from a particular direction. Beamformers can maximally attenuate noise at a null point whereas reserve the target speech in front (Fig. 7.13). This pattern of directionality can either be fixed to generate a static pattern of directionality or be adaptively updated to suppress moving noise sources. In order for beamforming to work, a number of assumptions typically have to be achieved: the target should always be located within a narrow range on angles in front of the listener and the noise source should be spatially separated from the target, meanwhile, the two microphones have to be well matched and calibrated.

Over the past two decades, a few beamforming techniques have been used to enhance speech perception of hearing-impaired listeners in noise. In a CI or hearing aids, the combination of two microphones can detect the differences in amplitude and phase of received signals and then generate the directionality of beam pattern to block noise coming from directions other than that of the target.

In 2005, BEAM strategy, a modified dual-microphone technique was implemented in the behind the ear (BTE) speech processor in Cochlear's Nucleus Freedom CI system. In BEAM, the first step is implemented through a spatially adaptive system that integrates the front directional microphone (which is changed to an omnidirectional microphone later in Nucleus 5 processor) and a rear omnidirectional microphone to separate speech from noise. The output from the rear omnidirectional microphone is firstly filtered through a fixed finite impulse response (FIR) filter and then subtracted from the delayed output from the front directional

Fig. 7.13 A typical beam pattern of beamforming technique. *Note*: 0° and 180° represent front and back, respectively
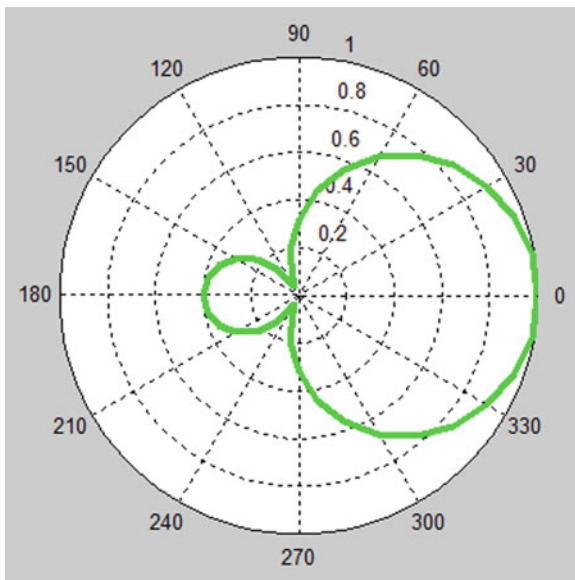
microphone to create the noise reference [73]. The filtered signal from the omnidirectional microphone is then added to the delayed signal from the directional microphone to create the speech reference. The reference signals are then delivered to an adaptive filter to remove additional noise, which can be updated with a least-mean-squares (LMS) or a normalized least-mean-squares (NLMS) method. This bilateral noise reduction system was tested and showed an average SRT improvement of 11 dB over a directional microphone.

7.4 Wireless Signal Transmission

In this section, we mainly focus on the analog circuit of cochlear implant system, and several critical analog blocks of wireless signal and power transmission are discussed in detail in the following parts.

As mentioned in the previous section, the internal unit of the cochlear implant system is powered by the inductive link for several considerations [76]. First, the skin thickness of the implanting location is about 3–10 mm, where the wireless transfer efficiency is still acceptable. Second, the expected implanting duration for the cochlear implant is more than 10 years, and it is difficult to use the implanted battery to sustain such a long period, because unlike pacemakers, the cochlear implant has to stimulate the nerve all the time so that its power consumption is relatively large. Third, both surgeon and patients request a small implanted device for easy operation in the surgery and gentle appearance from outside to see.
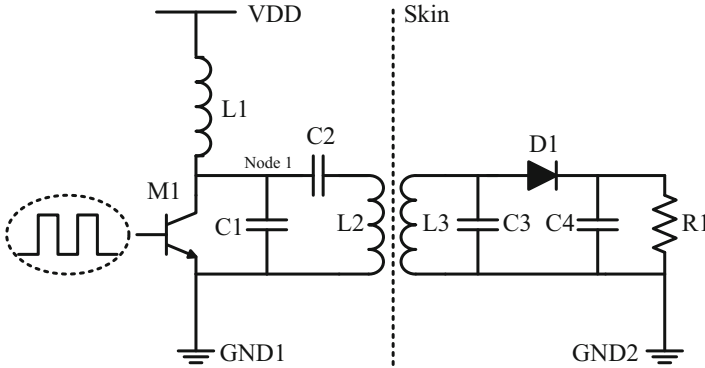
Fig. 7.14 A typical class E power amplifier with inductive link

Figure 7.14 shows the basic schematic of a power amplifier with an inductive link. The class E power amplifier drives the primary RF coil L2 that sends power inductively to the secondary RF coil L3. C2 and C3 are used to be resonant in series and in parallel with L2 and L3 at the working frequency, respectively. The RF signal on L3-C3 tank then is rectified to provide the power for the internal unit and stimulating electrodes. M1 is the main power transistor for the class E amplifier, which is usually controlled by the modulated signal. L1 is the choke inductor to provide supply current, and C1 is used to adjust the waveform of node 1 to make sure that M1 is on right at the moment when the voltage of node 1 is close to ground shown in Fig. 7.15a [60].

However, due to the variability of patient skin-flap-thickness and stimulating current, the equivalent load of the power amplifier varies. Therefore, in many cases as shown in Fig. 7.15b and c, the class E amplifier does not operate perfectly and the entire power transfer efficiency reduced. To solve this issue, many researches have been done. In Fig. 7.16a, the peak detector is used to find the zero crossing of current going through L2, and M1 is trigger by adding a delay t_{delay}, which can be expressed as:

$$t_{delay} = \frac{T}{2\pi}\left(\pi - \sin^{-1}\left(\frac{i_{dd}}{i_{L2,P}}\right)\right) \tag{7.1}$$

where T is the period of the input signal; i_{dd} is the supply current from L1; $i_{L2, P}$ is the peak current going through L2 [37]. Figure 7.16b shows another method that tries to achieve zero-voltage switching condition [3]. In this technique, when Vd is lower than the reference voltage, M1 is on and the switch losses are minimized. Both techniques show good results with different distances between the primary and secondary coils. However, these proposed circuits could consume additional power, especially because they are running at a high speed. In some cases, the saved power could be less than the power these circuits dissipate.
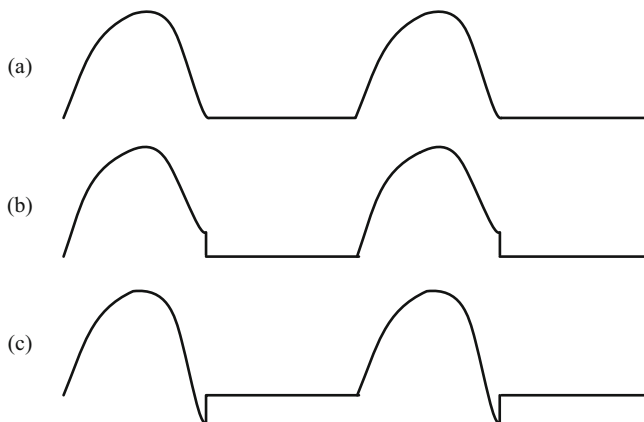
Fig. 7.15 Waveforms of node 1 when the coupling factor of the inductive link varies
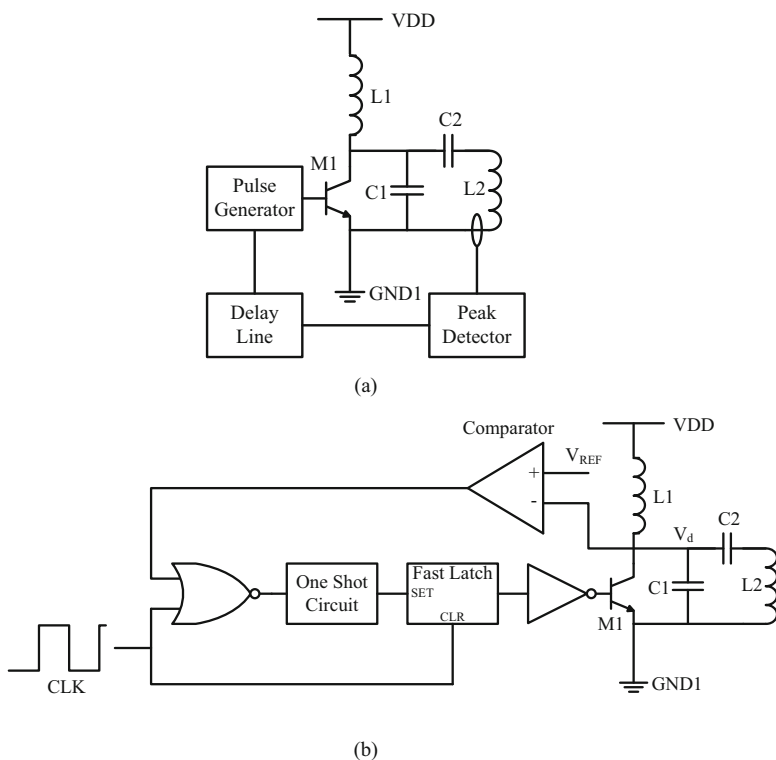
Fig. 7.16 (**a**) Using peak detector to find the zero crossing of current going through L2. (**b**) Using comparator to guarantee V_d is near ground when M1 is on

The efficiency of the inductive link is determined by the coupling coefficient k, the quality factor of L2 Q_2, the quality factor of L3 Q_3, and the effective quality factor of load network Q_L and can be simplified as:

$$\eta_{Link} = \left(\frac{k^2 Q_2 Q_3'}{1 + k^2 Q_2 Q_3'} \right) \left(\frac{Q_3}{Q_3 + Q_L} \right) \tag{7.2}$$

where $Q_3' = Q_3 Q_L / (Q_3 + Q_L)$. From (7.2), we can clearly see that with a higher coupling coefficient, the transfer efficiency of the inductive link increases. It means that the efficiency increases with thinner skin thickness. Also, Q_2 should be as large as possible to increase the efficiency. Normally k and Q_L varies in different circumstances so that it is difficult to find a determined Q_3 to maximize the efficiency. Moreover, the system usually uses on-off keying modulation, which means that the input signal of the amplifier is not a continuous signal. The complexity of the design needs to be more carefully considered.

7.5   ASIC Design

Stimulating auditory nerves and recording neural response are two main functions of the internal unit in a cochlear system. To reduce dimension and power consumption of implant, the internal circuit is implemented with application specific integrated circuit (ASIC). Usually, the function blocks inside the dashed border of Fig. 7.4 is achieved by ASIC.

7.5.1   Current Source

In Fig. 7.17, a current mode stimulating circuit is shown [77]. Twenty-four stimulating electrodes are connected to node E1, E2, ... E24, respectively. MP1 and MP2 are two reference electrodes. Two types of current sources, P-source and N-source, can be selected by controlling switch S5 and S6. The reason why current mode is chosen for stimulating circuit is because the charge injected into tissue could be precisely controlled. To clearly describe the mechanism of this circuit, choose electrode 1 as the stimulating electrode and MP1 as the reference electrode. Meanwhile, make S5 closed and S6 open to select P-type current source. In the cathodic phase, S2[1] and S3[1] are closed, and the current flows from MP1 to E1. In the anodic phase, S1[1] and S4[1] are closed and the current flows from E1 to MP1.

Stimulating charge balance is one of the most important factors to be considered in the circuit design. The tissue damage does not occur in chronic stimulation of cochlear implants if residual DC current is lower than 100 nA [34]. In this biphasic stimulation as explained above, the positive and negative charge going through the

Fig. 7.17 Current mode stimulating circuit
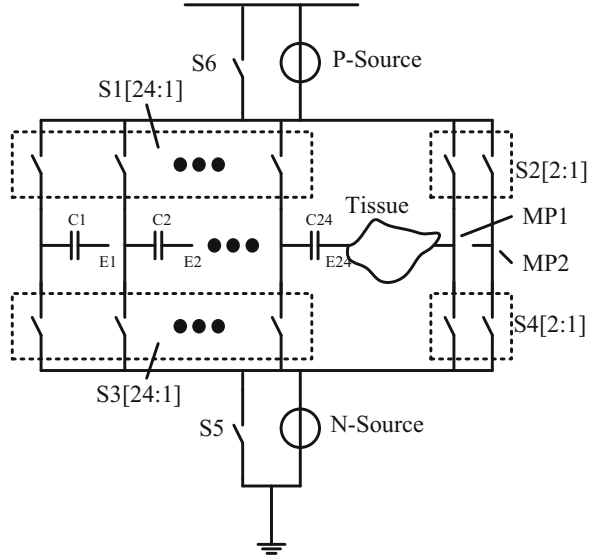
tissue should be balanced ideally, since both phases utilize the same current source. To further suppress imbalanced DC charge, a DC blocking capacitor, C_{block}, in series with each electrode is usually inserted as shown in Fig. 7.18. Moreover, when stimulation is completed, switches S7 and S8 are closed in Fig. 7.18 to guarantee that the stimulating and reference electrodes are on the same electrical potential [15].

7.5.2 Recording Circuit

A robust recording circuit is the key to successfully capture the electrically evoked compound action potential (ECAP) signal. As shown in Fig. 7.19, the recording circuit normally is composed of four blocks [12]. The targeted signal is received by the sensing electrode, and then transmitted to the band-pass filter to remove undesired noise. The variable gain amplifier (VGA), whose gain is set according to different circumstances, is used to amplify this signal, because the amplitude of this type of signals is only several millivolt or even smaller. At last, an analog-to-digital converter (ADC) is employed to measure this signal and send the data out.

Mismatch compensation is a critical technique for VGA design, since the amplitude of the input signal is comparable with the input offset of the operational amplifier. In Fig. 7.20, a typical VGA circuit with mismatch compensation is shown [53]. In this circuit, the first stage amplifier consists of Gm1, Gm2, and R, and A1 is the second stage amplifier. Switches S7, S8, S9, and S10 are used to change the gain of amplifier A1. The rest of switches are used for mismatch compensation of the first stage. In detail, S1, S2, S5, and S6 are turned on first. At

Fig. 7.18 Stimulating circuit with charge balancing techniques
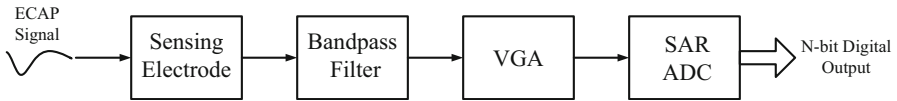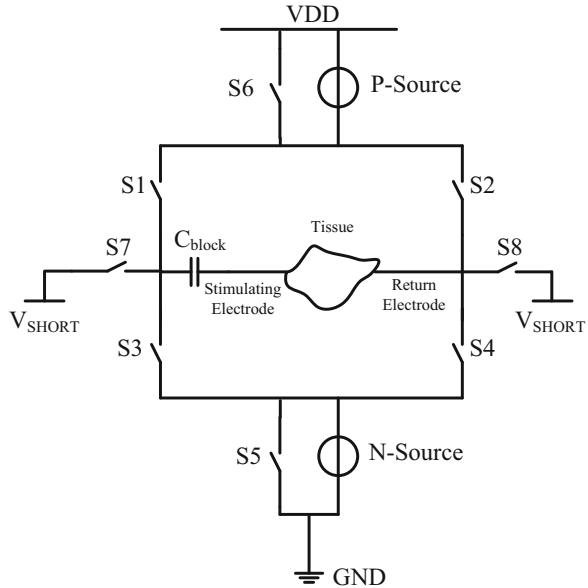
Fig. 7.19 A block diagram of neural response recording circuit

this moment, only the input offset V_{OS} is amplified by the first stage. Then S3 and S4 are also turned on, and the output of the first stage V_{OUT} becomes:

$$V_{OUT} = \frac{g_{m1}}{g_{m2}} V_{OS} \qquad (7.3)$$

where g_{m1} and g_{m2} are the trans-conductance of Gm1 and Gm2, respectively. The input offset information is stored in C3 and C4 by turning S1, S2, S3, S4, S5, and S6 off. Therefore, the offset of the first stage is cancelled by the output of Gm2.

   Low power, small area, and high acquisition precision are three major factors for ADC design in the cochlear implant, which should be considered carefully. Since the neural response is relatively slow (~KHz), the speed of this circuit is not needed to be very high. Based on the discussion above, the successive approximation (SAR) ADC is one of the most suitable candidates for ADC design in the internal unit [12]. Figure 7.21a shows a 12-bit fully differential SAR ADC circuit. The basic theory is using the output of a 12-bit DAC to compare with the input signal [19]. After comparing 12 times, the ADC finally gets all the digital output. Unlike flash ADC and pipeline ADC, SAR ADC only needs one comparator so that both
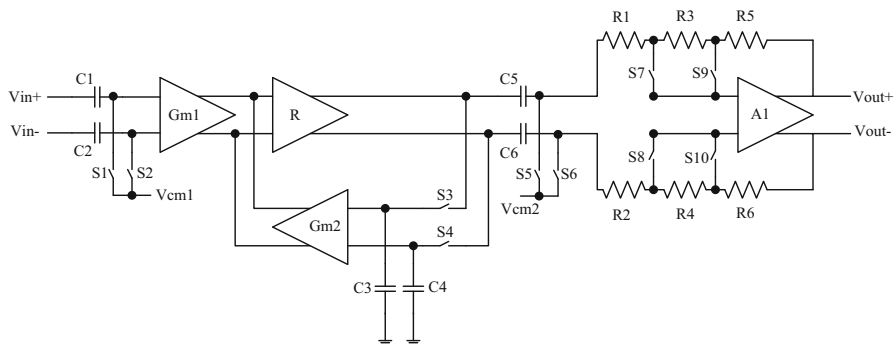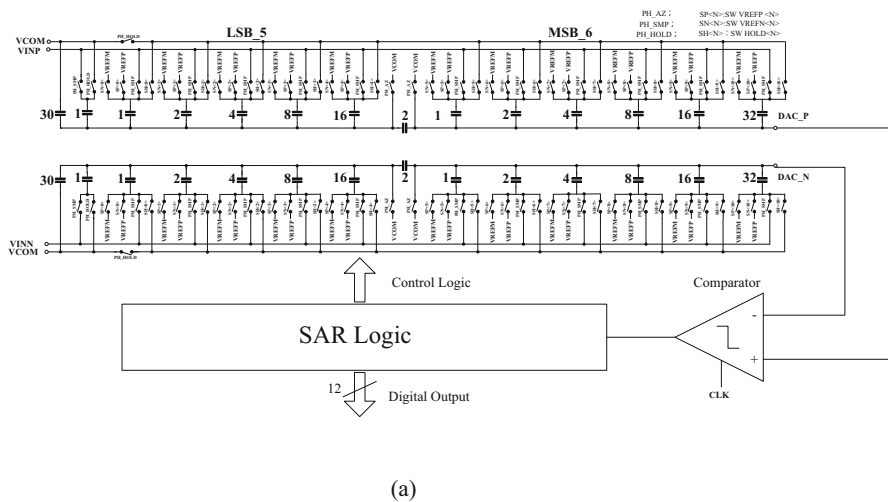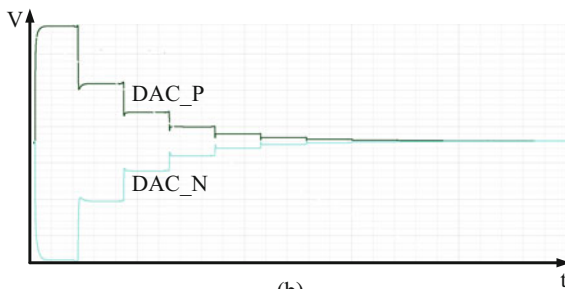
Fig. 7.20 Variable gain amplifier circuit with mismatch compensation

(a)

(b)

Fig. 7.21 (**a**) A 12-bit SAR ADC circuit. (**b**) Simulation waveforms of DAC_P and DAC_N

power and area are saved. Figure 7.21b shows the simulation results of DAC_P and DAC_N. We can clearly see that the comparator compares two input signals one stage by one stage in sequential way and the input of next stage is the subtraction of the output of this stage and the output of the DAC.

7.5.3 Reverse Telemetry Circuit

In a cochlear system, the implant in some cases needs to reversely transmit data to the speech processor, for example, neural impedance test data, neural response measurement data, or indication of operation status. Load-shift keying (LSK), which was referred as "reflectance modulation," is a commonly used technique for reverse telemetry [65]. The essence of LSK is the variation of the equivalent impedance in the primary coil, which could be influenced by changing the load of secondary coil. Therefore, this telemetry can be achieved using the same inductive link with forward transmission. Fig. 7.22a shows a modulation circuit that is based on a circuit configuration modulator [65]. When switch S1 is open, the circuit on the implant side is a full-wave rectifier. When S1 is closed, the circuit becomes a voltage clamp circuit. Using this method, the load of the secondary coil is successfully modulated by controlling S1. In Fig. 7.22b, LSK is realized by changing the resonant capacitor of the secondary coil [77]. This technique is especially effective for half-wave rectifier circuit.

The demodulator circuit is used to sense and digitize the variation of the signal amplitude on the external coil, which is modulated by the implant. Unlike other regular amplitude-shift keying (ASK) demodulator, this circuit is suffered from variable signal amplitudes, a shifting DC level, and an undetermined digitizing threshold due to the variation of patient's skin depth and the misalignment of the coils. Figure 7.23 shows that a demodulation architecture, which is based on a compact CMOS integrated circuit solution, is proposed to greatly enhance the transmission robustness, increase the maximum bit rate, reduce the bit error rate, and save the board area [35].

The entire architecture is composed of four blocks: sensor, rectifier, amplifier, and digitizer. An additional small coil (Fig. 7.24a) is introduced to pick up the modulated signal to separate the forward and reverse telemetry and reduce the interaction between each other. A half-wave rectification (Fig. 7.24 b) is implemented to filter high-frequency components and remove the negative part of the signal. In this block, the RC filter should be carefully designed to minimize the load of the additional coil to alleviate its effect on the main coil and save power consumption. The amplifier (Fig. 7.24c) is used to amplify the output of the rectifier. It has two modes: a normal mode and a sleep mode. The amplifier is in the sleep mode while the processor is transmitting regular data containing sound information to the implant. In this mode, a switch that is connected between the input of the amplifier and a constant DC voltage source is on and the DC level of the input is determined. Once the amplifier goes into the normal mode, the switch becomes off, and the common mode voltage of the input is still well defined. A high-pass feedback network is employed in the

Fig. 7.22 Reverse
telemetry circuit based on
(**a**) half-wave rectifier and
(**b**) full-wave rectifier

(a)

(b)
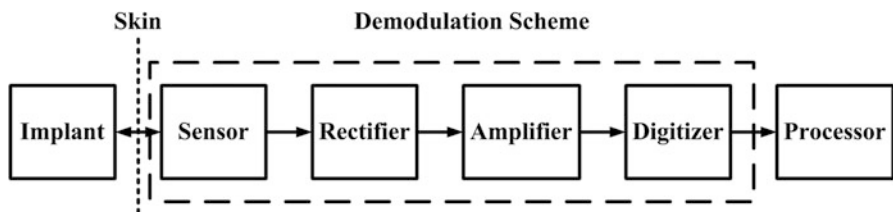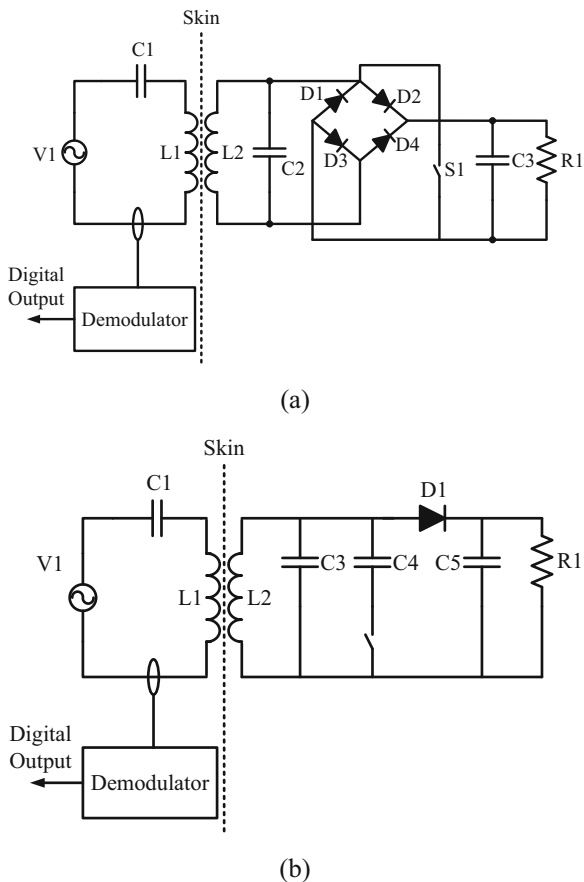
Fig. 7.23 A block diagram of the demodulator

amplifier so that the voltage on the capacitor in the network is the integral of the output signal. This voltage is used as a reference for the digitization block to differentiate digital "1" and "0". A Schmitt trigger (Fig. 7.24d) is implemented to convert the amplified analog signal to a clean digital signal. To further suppress random and deterministic noise, a hysteresis characteristic is utilized to avoid
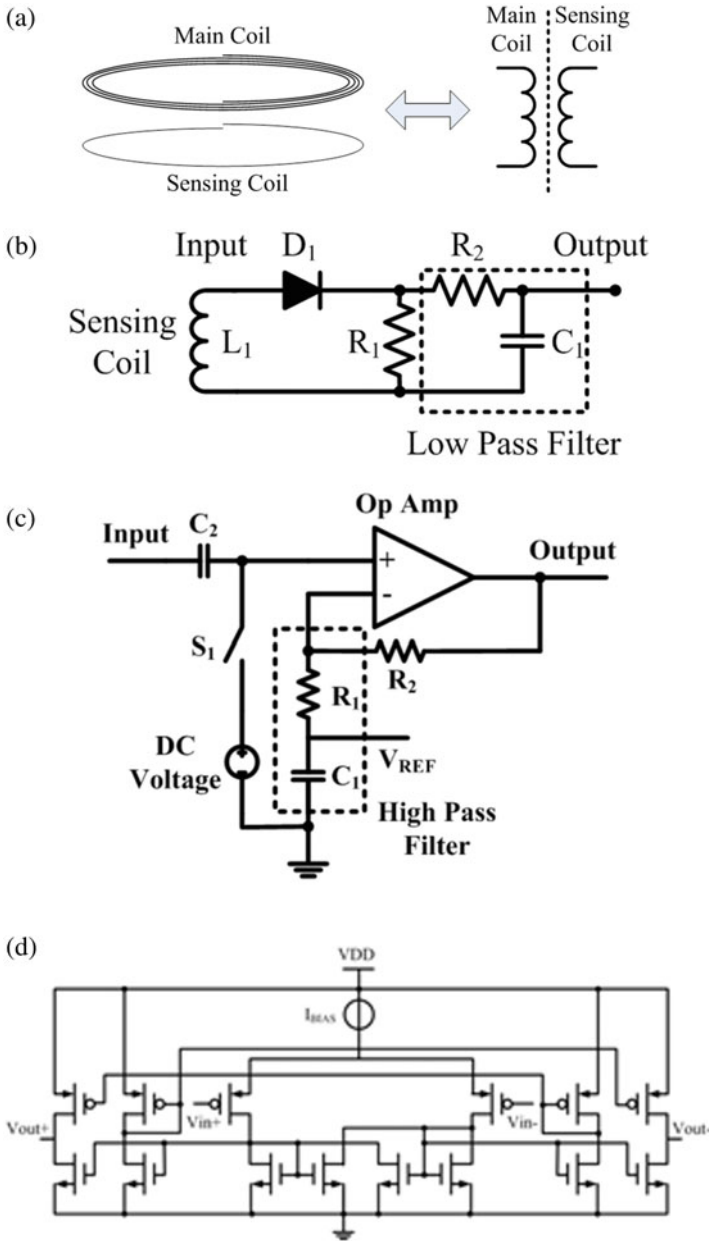
Fig. 7.24 (**a**) Sensor circuit. (**b**) Rectifier circuit. (**c**) Amplifier circuit. (**d**) Digitizer Circuit

undesirable data transition caused by a small disturbance near the threshold voltage. Figure 7.25 shows the outputs of the sensor, rectifier, amplifier, and digitizer. We can clearly see how the modulated signal is transformed to be digital data.

Fig. 7.25 Waveforms of the outputs of four main blocks: blue, purple, green, and yellow waveforms are the output of the sensor, the rectifier, the amplifier, and the digitizer, respectively

7.6 Neural Response Measurement

7.6.1 History

Neural response measurement (NRM) in cochlear implants is to detect and measure the electrically evoked compound action potential (ECAP) from the auditory nerve in cochlear implant (CI) recipients. With the development of the multi-electrode cochlear implant, there is a strong demand to request an easy and fast tool to give objective information directly from devices and patients themselves to surgeons and audiologists, because most of CI users are profoundly hearing-impaired people who have difficulty to communicate with other people. The ECAP has been demonstrated to be the best candidate, since the amplitude of the EAP could be proportional to the number of auditory nerve fibers activated.

In 1970s and 1980s, many researches have been done to test the ECAP in different animals [5, 11, 50, 63]. Compared with the acoustically evoked compound action potential (CAP), which has been studied much earlier than ECAP, ECAP is very difficult to be recorded, because the stimulating signal is always hundred or even thousand times larger than the response signal. In 1990, Brown et al. firstly used forward-masking subtraction method, which was originally proposed by Charlet de Sauvage et al., to measure the neural response in the human beings [6]. The results showed that the contamination of stimulus artifact on the recorded response was greatly reduced and ECAPs were successfully detected and measured.
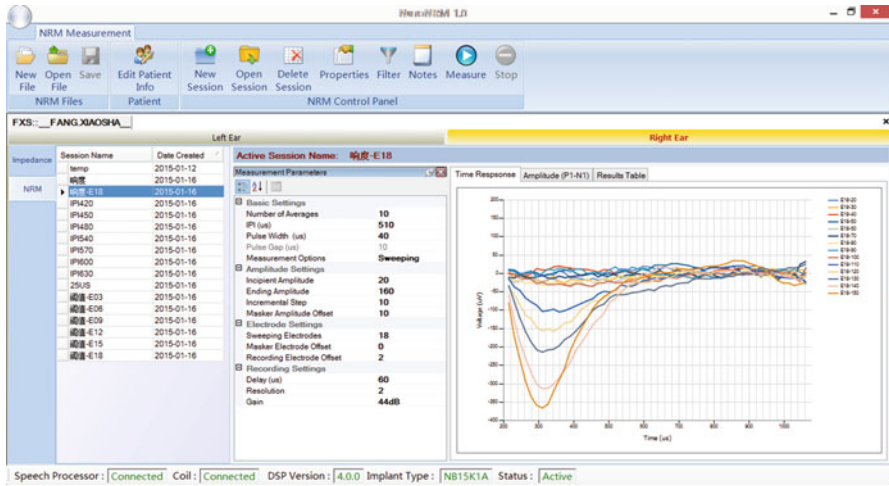
Fig. 7.26 Neural response measurement (NRM) tool

Based on this technique, the first commercial ECAP measurement tool, whose name was called "neural response telemetry" (NRT), was available in 1998. The initial results showed that based on a carefully designed protocol, the ECAP can be reliably recorded in most patients and most electrodes. After that, the similar tools with different names ("neural response imaging," "auditory nerve response telemetry," "neural response measurement") were issued by different brands of CI producers. Nowadays, ECAP measurement tools (Fig. 7.26) become one of the most useful tools to provide objective information of CI patients for clinical evaluation from surgeons and audiologists.

7.6.2 Electrically Evoked Compound Action Potential

Essentially, the ECAP is the Wave I of the auditory brainstem response (ABR). Once the auditory nerve is stimulated by an electrical signal, which is larger than a specific threshold, the ECAP is generated. Figure 7.27 shows two types of ECAPs, which were recorded with intra-cochlear electrodes in Nurotron Venus users. In most cases, the ECAP, as shown in Fig. 7.27a, is composed of a negative peak (N1) occurring at approximately 0.2–0.4 ms following stimulus onset and a much smaller positive peak (P2) at approximately 0.6–0.8 ms [1, 6, 7, 18]. But two-peak ECAPs as shown in Fig. 7.27b can also be occasionally recorded, whose incidence is around 10–20% [43, 67]. In this case, the N1 occurs at similar time as the one-peak case, but the P1 and the P2 typically occur at around 0.4–0.5 ms and 0.6–0.7 ms, respectively [43, 67].
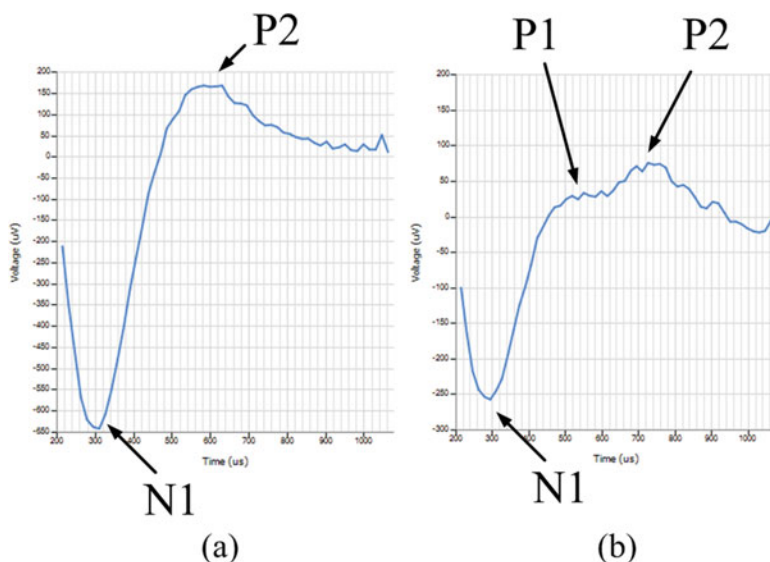
Fig. 7.27 The recorded ECAPs with (**a**) one positive peak and (**b**) two positive peaks

The amplitude of the ECAP varies from about 20 μV to 2 mV, and its maximum magnitude usually is larger than the electrically evoked ABR [8]. Because of its large amplitude, myogenic activity has little influence on the ECAP [32]. Moreover, maturation of the central auditory system also is not a main factor that will cause any changes in the ECAP. Therefore, the difference of ECAPs between adult and pediatric CI users is very small [6, 26, 31], and the recorded waveforms do not change with the increase of the duration of CI use. However, many factors also lead to the variation of the latency and amplitude of the ECAP recorded, for example, the stimulation level, the polarity of the stimulation, the surviving neural population, the intra-cochlear test electrode location, and so on. The amplitude of the ECAP is the voltage difference between N1 and P2 peaks. As shown in Fig. 7.28, ECAP amplitude increases as the stimulation level increases.

The ECAP threshold and slope of the ECAP amplitude growth, as shown in Fig. 7.29, are two major points in the neural response measurement, in which a number of researchers are interested. The ECAP threshold is the stimulation current level, at which the neural response measurement is able to capture the ECAP waveform. Many studies indicate that the ECAP threshold falls between the behavioral threshold (T-level) and comfort levels (C-level) of CI users [7, 9, 10, 18, 29, 59]. The slope of the ECAP amplitude growth is also widely used to objectively predict the fitting program of CI users [10, 29].
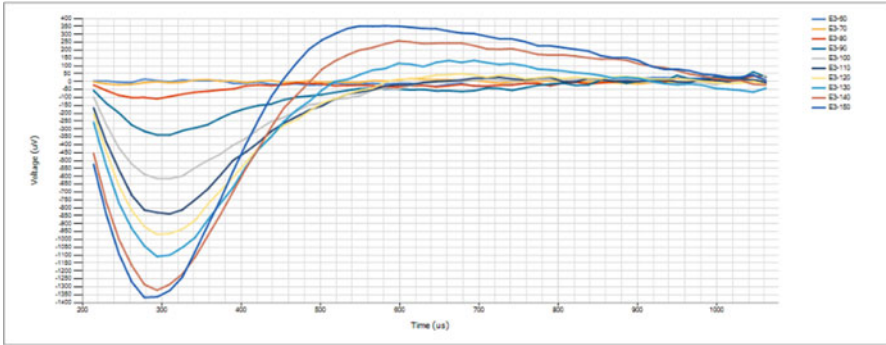
Fig. 7.28 Recorded ECAP waveform with different amplitudes of stimulation current
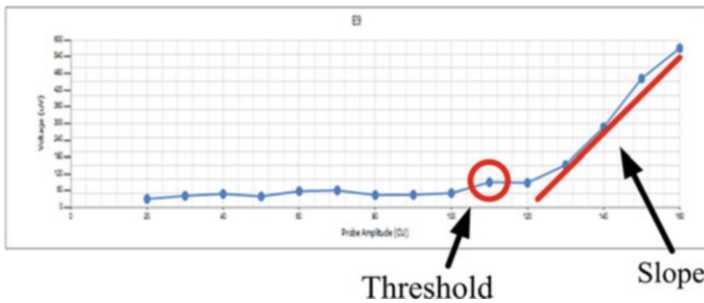

Fig. 7.29 The relationship between the stimulation current level and the amplitude of ECAP

7.6.3   Hardware Implementation

Hardware implementation is one of the key factors to successfully record the neural response. Figure 7.30 shows how the cochlear implant system realizes the NRM function. Generally, at the beginning the computer, where the NRM tool is installed and all the parameters are set, controls the speech processor to send a command to the implant with the information about the electrode and stimulation current level. The modulated signal, which is encoded by the speech processor according to this command, is transmitted through the inductive link between the external coil and the internal coil. The stimulator decodes the signal from the internal coil and sends a biphasic current pulse to the stimulating electrode (e.g., electrode 3 in Fig. 7.31). Once the electrode finishes the stimulation, the forward transmission is completed. After a determined delay, the recording electrode (e.g., electrode 5 in Fig. 7.31) starts to record the voltage signal it receives. This voltage signal firstly is amplified by an amplifier with a very large gain (usually more than 60 dB). Then the signal is digitized by a high-resolution ADC (usually more than 10 bits). Later, all the data are reversely transmitted to the speech processor by the
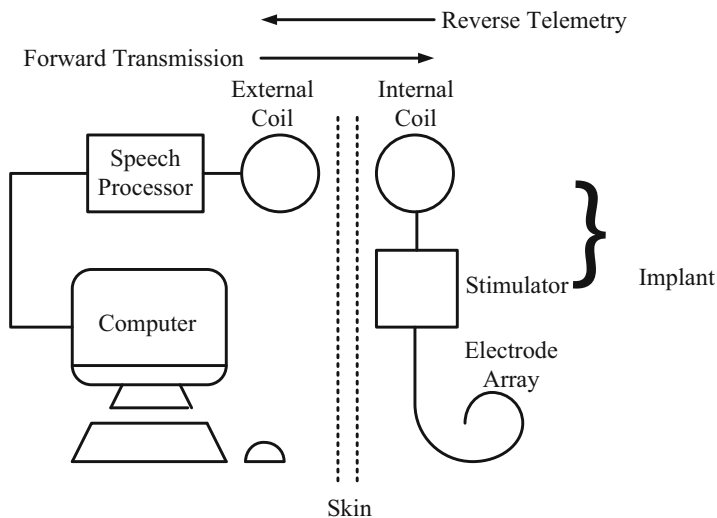
Fig. 7.30 The diagram of hardware implementation of neural response measurement
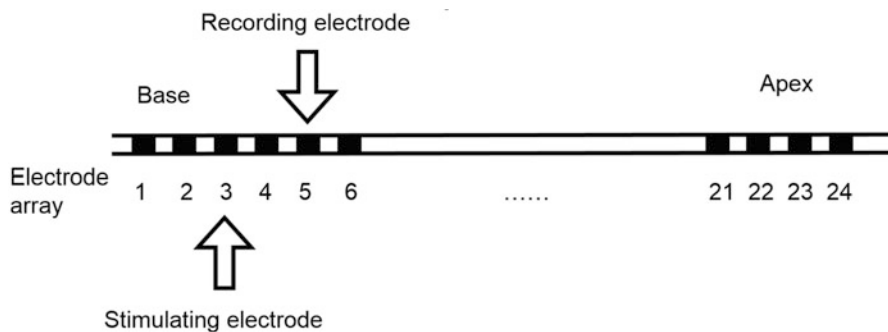
Fig. 7.31 Electrode array. *Note*: In this case, electrode 3 is the stimulating electrode, and electrode 5 is the recording electrode

reverse telemetry technique. In the end, the computer completes the analysis and provides the report based on the data which are sent from the speech processor.

The entire system is very flexible so that the tool could change a number of parameters. For example, the gain of the amplifier in the stimulator should be variable. In most cases, a large gain (e.g., 60 dB) is required to amplify very weak neural signal. By contrast, in some other cases, a relatively small gain (e.g., 40 dB) is necessary to avoid a severe saturation problem. In addition, one electrode should be able to consecutively generate two stimulating current pulses within a period, which varies from 50 μs to several milliseconds. Moreover, the turn-on time of the analog-to-digital converter (ADC) in the stimulator should also be well controlled, and the requirement of the ADC's turn-on duration time is at least 1 ms. Furthermore, the

roles between recording and stimulating electrodes can be easily changed or switched. In the real application, every electrode could be either a stimulating electrode or a recording electrode.

7.6.4 Measurement Techniques

The forward-masking subtraction method, which is briefly introduced above, now becomes the routine technique for most commercial neural response measurement tools [1, 6, 7, 9, 20]. The main purpose of this tool is to cancel the artifact caused by the probe stimulus, which is substantially larger than the neural response. The details of this method shown in Fig. 7.32 are described below.

Four types of stimulation are used each time in the measurement. For type A, the probe is stimulated alone at t_1. For type B, the masker is stimulated in the same electrode at t_0, and then the probe is stimulated at t_1. For type C, the masker alone is stimulated at t_0. For type D, zero stimuli for both masker and probe are presented. Each type of stimulation is measured separately. The main theory behind this technique is that the neurons in the auditory nerve will be in the refractory state for a short while after electrical stimulation. Therefore, the measurement results of type A, type B, type C, and type D, A, B, C, and D, are presented below, respectively:

$$A = SA + PA + PN \tag{7.4}$$

$$B = SA + MA + MN + PA \tag{7.5}$$

$$C = SA + MA + MN \tag{7.6}$$

$$D = SA \tag{7.7}$$

where SA is the system artifact; PA is the probe artifact; PN is the neural response caused by the probe; MA is the masker artifact; and MN is the neural response caused by the masker. In (7.5), the reason why PN is missed is because in this case, the auditory nerve is in the refractory state and has no response for the probe stimulus. Combining (7.4), (7.5), (7.6) and (7.7), the final measurement result of the ECAP (FMRE) is:

$$FMRE = A - B + C - D = PN. \tag{7.8}$$

Not surprisingly, the recorded signal is equal to the neural response caused by the probe. According to (7.8), it is known that the amplitude of the probe stimulus is variable and directly related to the amplitude of the ECAP. For the masker, the stimulating current should be at a high level to make sure enough neurons are stimulated by the masker and go into the refractory state [1].

Fig. 7.32 The forward-masking subtraction method. *Note*: For each case, the upper one is the electrical pulse generated by the stimulating electrode (SE), and the lower one is the measured signal recorded by the recording electrode (RE)
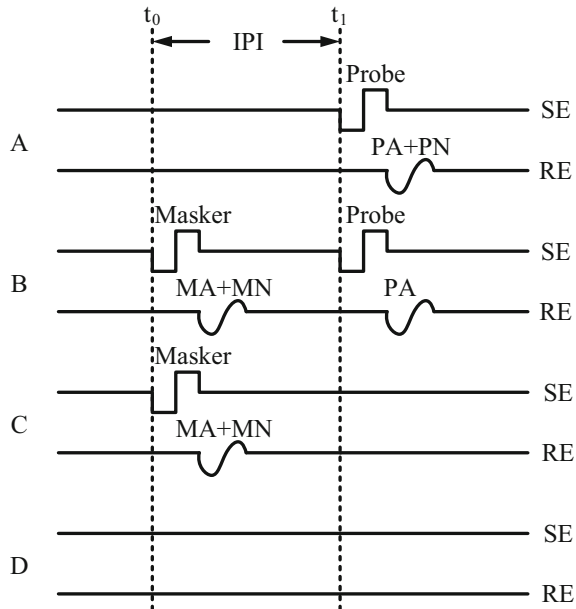
In practice, the results of this method are affected by several non-ideal factors. The saturation issue is one of the most serious factors, which could lead to the failure of neural response measurement. In Fig. 7.32, it shows that the signal the recording circuit received is comprised of the stimulus artifact and the neural response. However, the amplitude of the stimulus artifact is much larger than the neural response. Accordingly, if the amplitude of the stimulus artifact is too large so that the amplifier is saturated at its largest output, the ECAP could not be captured after measurement. In this case, reducing amplifier's gain and increasing the recording delay after stimulation could improve the final results of ECAP measurement.

In addition, changing the inter-pulse interval (IPI), which is the time difference between t_0 and t_1 in type B stimulation, could also change the amplitude of recorded ECAP. On one hand, the number of neurons in the refractory state after the masker stimulus in type B stimulation gradually decreases with increasing the IPI. Thus more and more neurons in the auditory nerve have responses to the probe stimulus in type B stimulation, which may reduce the amplitude of the ECAP based on (7.8). On the other hand, if the IPI is too short, the integration of probe and masker stimulation current may reduce the amplitude of the ECAP as well [1]. Figure 7.33 shows a group of ECAP signals, which were captured by NRM tool. It clearly shows that the amplitude of ECAP of this patient reaches the maximum value when the IPI is 510 μs.
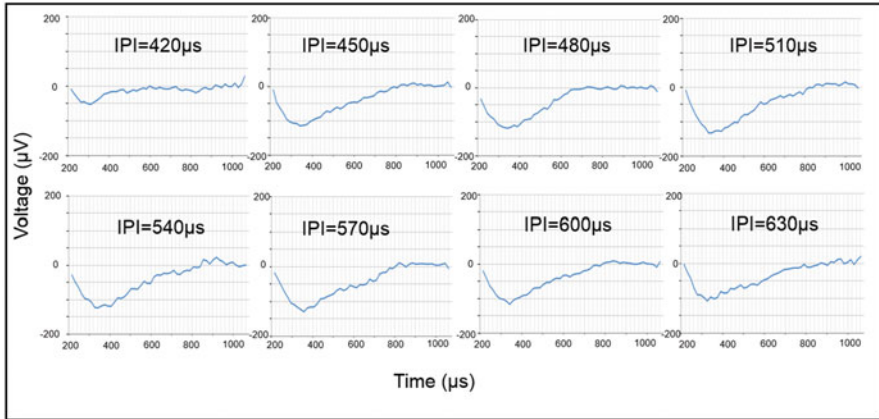
Fig. 7.33 The ECAP signal of patient P1 using NRM tool (stimulation of 130 CL was applied at electrode 12)

7.6.5 *Clinical Uses*

As mentioned in the previous section, the invention of the reliable ECAP measurement meets great demands from surgeons and audiologists for their clinical work. The neural response measurement now is clinically used in the following applications [36].

First, the ECAP measurement is used to evaluate and verify the neural response from the auditory nerve. In many cases, this objective information is very important for surgeons and audiologists. For example, surgeons can use it to monitor whether the electrode arrays are well placed in the cochlea in surgery. After surgery, the recovering condition of CI recipients varies significantly, and the audiologists can use this information to judge the effectiveness of the electrical stimulation in the auditory nerve fibers.

Second, the electrode and device can be functionally verified. Even though the impedance test also can offer useful information about the device in some degree, the capture of the ECAP signal is the direct proof that the device works properly inside the cochlea.

Third, the ECAP measurement creates a great convenience for programming the speech processor. As we all know, the first and very critical step to use CIs is to find a map with corresponding T and C levels, which is fitted with every user's own circumstance. Many studies prove that the NRM threshold fall between T- and C-levels [7, 9, 10, 18, 29, 59]. In Figs. 7.34, 21 adult subjects are tested using NRM tool, and the preliminary results also support this conclusion. Thus the ECAP threshold can guide audiologists how to start to test T and C levels individually. More importantly, for the people who poorly communicate with audiologists, for example, very young children, the results greatly assist audiologists to build relatively accurate maps for those people.
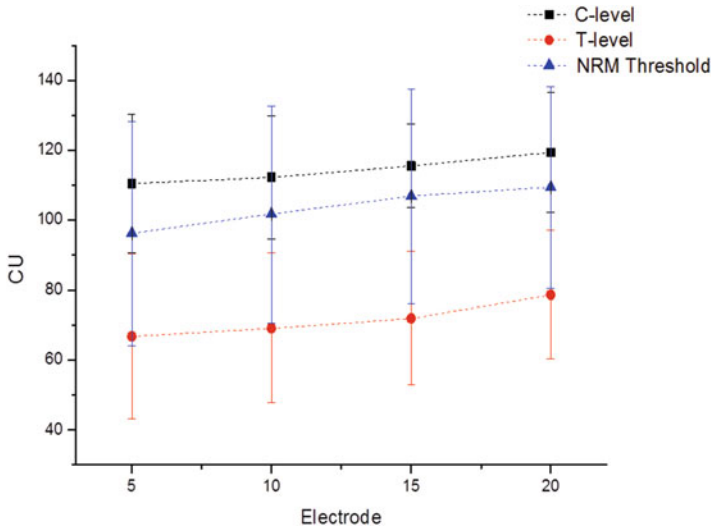
Fig. 7.34 Preliminary results of the relationship between NRM threshold and T- and C- levels using NRM tool

Compared with other measurement techniques, e.g., electrically auditory brainstem response (EABR), ECAP measurement is easy and convenient to operate, because it does not require special equipment, extra recording electrodes, and entirely different software. All the measurement is achieved based on the standard CI product itself and the tool is embedded into the programming software. Additionally, there is no strict requirement to limit patient's status so that it is easy to cooperate with patient to complete test, which is essentially useful for pediatric CI users. Moreover, the ECAP does not have an obvious difference between adults and children, a typical protocol with determined parameters can be used for most patients. Thus the operation of audiologists is much simplified. Because of the advantages discussed above, neural response measurement becomes a very promising technique for more clinical applications.

7.7 Emerging Technologies

Three pioneers of cochlear implant Graeme Clark, Ingeborg Hochmair, and Blake Wilson received the 2013 Lasker~DeBakey Clinical Medical Research Award for their outstanding contributions to the development of the modern cochlear implant. Meanwhile, active and diverse research is currently taking place in the area of cochlear implant. Compared with normal-hearing people, cochlear implant recipients find it hard to listen in noisy environment or to listen to music or tonal languages. Studies on conveying fine structure information, combined acoustic and electric hearing, and

bilateral implantation have been proposed to improve the performance of cochlear implant listeners in above mentioned difficult tasks. Recently, optogenetic stimulation of auditory nerve has been proposed to develop optical cochlear implant, which can significantly reduce the channel interference of electrical stimulation. Cochlear implant is on its way to confer more benefit to mankind.

References

1. Abbas PJ, Brown CJ, Shallop JK, Firszt JB, Hughes ML, Hong SH, Staller SJ (1999) Summary of results using the nucleus CI24M implant to record the electrically evoked compound action potential. Ear Hear 20:45–59
2. Arnoldner C, Riss D, Brunner M, Durisin M, Baumgartner WD, Hamzavi JS (2007) Speech and music perception with the new fine structure speech coding strategy: preliminary results. Acta Otolaryngol 127:1298–1303
3. Baker M, Sarpeshkar R (2007) Feedback analysis and design of RF power links for low-power bionic systems. IEEE Trans Biomed Circuits Syst 1:28–38
4. Boll SF (1979) Suppression of acoustic noise in speech using spectral subtraction. IEEE Trans Acoust Speech Signal Process 27:113–120
5. Brown CJ, Abbas PJ (1990) Electrically evoked whole-nerve action potentials: parametric data from the cat. J Acoust Soc Am 88:2205–2210
6. Brown CJ, Abbas PJ, Gantz B (1990) Electrically evoked whole-nerve action potentials: data from human cochlear implant user. J Acoust Soc Am 88(3):1385–1391
7. Brown CJ, Abbas PJ, Gantz B (1998) Preliminary experience with neural response telemetry in the nucleus CI24M cochlear implant. Am J Otol 19:320–327
8. Brown CJ, Hughes ML, Lopez SM, Abbas PJ (1999) Relationship between EABR thresholds and levels used to program the Clarion speech processor. Ann Otol Rhinol Laryngol 108(Suppl. 177):50–57
9. Brown CJ, Hughes ML, Luk B, Abbas PJ, Wolaver A, Gervais J (2000) The relationship between EAP and EABR thresholds and levels used to program the nucleus 24 speech processor: data from adults. Ear Hear 21:151–163
10. Cafarelli Dees D, Dillier N, Lai WK et al (2005) Normative findings of electrically evoked compound action potential measurements using the neural response telemetry of the nucleus CI24M cochlear implant system. Audiol Neurotol 10:105–116
11. Charlet de Sauvage R, Cazals Y, Erre JP, Aran JM (1983) Acoustically derived auditory nerve action potential evoked by electrical stimulation: an estimation of the waveform of single unit contribution. J Acoust Soc Am 73:616–627
12. Chaturvedi V, Anand T, Amrutur B (2013) An 8-to-1 bit 1-MS/s SAR ADC with VGA and integrated data compression for neural recording. IEEE Trans Very Large Scale Integr VLSI Syst 21(11):2034–2044
13. Chen JD, Benesty J, Huang Y, Doclo S (2006) New insights into the noise reduction Wiener filter. IEEE Trans Audio Speech Lang Process 14:1218–1234
14. Cherry C (1953) Some experiments on the recognition of speech with one and two ears. J Acoust Soc Am 25:975–981
15. Chun H, Yang Y, Lehmann T (2014) Safety ensuring retinal prosthesis with precise charge balance and low power consumption. IEEE Trans Biomed Circuits Syst 8(1):108–118
16. Clark GM, Tong YC, Dowell RC (1984) Comparison of two cochlear implant speech-processing strategies. Ann Otol Rhinol Laryngol 93:127–131
17. Crozier PM, Cheetham BMG, Holt C, Munday E (1993) Speech enhancement employing spectral subtraction and linear predictive analysis. Electron Lett 29:1094–1095
18. Cullington H (2000) Preliminary neural response telemetry results. Br J Audiol 34:131–140

19. Culurcielllo E, Andreou A (2003) An 8-bit, 1mW successive approximation ADC in SOI CMOS. In: Proceedings of IEEE international symposium on circuit and system, IEEE, Bangkok, Thailand pp 301–304

20. Dillier N, Lai WK, Almqvist B, Frohne C, Müller-Deile J, Stecker M, von Wallenberg E (2002) Measurement of the electrically evoked compound action potential via a neural response telemetry system. Ann Otol Rhinol Laryngol 111(5):407–414

21. Doclo S, Spriet A, Wouters J, Moonen M (2007) Frequency-domain criterion for the speech distortion weighted multichannel Wiener filter for robust noise reduction. Speech Comm 49:636–656

22. Donaldson GS, Kreft HA, Litvak L (2005) Place-pitch discrimination of single- versus dual-electrode stimuli by cochlear implant users (L). J Acoust Soc Am 118(2):623–626

23. Douglas SC, Sun XA (2003) Convolutive blind separation of speech mixtures using the natural gradient. Speech Comm 39:65–78

24. Dowell R, Seligman P, Blamey P, Clark G (1987) Evaluation of a two-formant-estimating speech processor for a multiple-channel cochlear prosthesis. Ann Otol Rhinol Laryngol 96 (Suppl. 128):132–134

25. Dudley H (1939) The vocoder. Bell labs record, 18(4), pp 122–126

26. Eisen MD, Franck KH (2004) Electrically evoked compound action potential amplitude growth functions and HiResolution programming levels in pediatric CII implant users. Ear Hear 25:528–538

27. Fetterman BL, Domico EH (2002) Speech recognition in background noise of cochlear implant patients. Otolaryngol Head Neck Surg 126:257–263

28. Firszt JB, Holden LK, Skinner MW, Tobey EA, Peterson A, Gaggl W, Runge-Samuelson CL, Wackym PA (2004) Recognition of speech presented at soft to loud levels by adult cochlear implant recipients of three cochlear implant systems. Ear Hear 25:375–387

29. Franck KH, Norton SJ (2001) Estimation of psychophyical levels using the electrically evoked compound action potential measured with the neural response telemetry capabilities of Cochlear Corporation's CI24M device. Ear Hear 22:289–299

30. Fu QJ, Zeng FG, Shannon RV, Soli SD (1998) Importance of tonal envelope cues in Chinese speech recognition. J Acoust Soc Am 104:505–510

31. Gordon KA, Papsin BC, Harrison RV (2004) Toward a battery of behavioral and objective measures to achieve optimal cochlear implant stimulation levels in children. Ear Hear 25:447–463

32. He S, Teagle HFB, Buchman CA (2017) The electrically evoked compound action potential: from laboratory to clinic. Front Neurosci 11(Article 339):1–20

33. Hu Y, Loizou PC (2007) A comparative intelligibility study of single-microphone noise reduction algorithms. J Acoust Soc Am 122:1777

34. Huang C, Shepherd R, Center P, Seligman P, Tabor B (1999) Electrical stimulation of the auditory nerve: direct current measurement in vivo. IEEE Trans Biomed Eng 46(4):461–469

35. Huang Y, Xia B, Wang S, Sun X (2015) A novel demodulation technique in reverse telemetry for cochlear device. In: Conference on implantable auditory prostheses, p 119

36. Hughes ML (2010) Fundamentals of clinical ECAP measures in cochlear implants, Part 1: use of the ECAP in speech processor programming, 2nd edn, Audiology Online, November 8, 2010, Article 2347

37. Kendir GA, Liu W, Bashirullah R, Wang G, Humayun MS, Weiland J (2005) An optimal design methodology for inductive power link with class-E amplifier. IEEE Trans Circuits Syst Regul Pap 52(5):857–866

38. Kiefer J, Hohl S, Stürzebecher E, Pfennigdorff T, Gstöett-ner W (2001) Comparison of speech recognition with different speech coding strategies (SPEAK, CIS, and ACE) and their relation-ship to telemetric measures of compound action potentials in the nucleus CI 24M cochlear implant system. Audiology 40(1):32–42

39. Kim G, Loizou PC (2011) Gain-induced speech distortions and the absence of intelligibility benefit with existing noise-reduction algorithms. J Acoust Soc Am 130:1581–1596

40. Koch DB, Osberger MJ, Segal P, Kessler D (2004) HiResolution and conventional sound processing in the HiResolution bionic ear: using appropriate outcome measures to assess speech recognition ability. Audiol Neurootol 9(4):214–223
41. Koch DB, Downing M, Osberger MJ, Litvak L (2007) Using current steering to increase spectral resolution in CII and HiRes 90K users. Ear Hear 28(2 Suppl):39S–41S
42. Kokkinakis K, Loizou PC (2008) Using blind source separation techniques to improve speech recognition in bilateral cochlear implant patients. J Acoust Soc Am 123:2379–2390
43. Lai WK, Dillier N (2000) A simple two-component model of the electrically evoked compound action potential in the human cochlea. Audiol Neurootol 5:333–345
44. Li N, Loizou PC (2008) Factors influencing intelligibility of ideal binary-masked speech: implications for noise reduction. J Acoust Soc Am 123:1673–1682
45. Lim JS, Oppenheim AV (1979) Enhancement and bandwidth compression of Noisy speech. Proc IEEE 67:1586–1604
46. Loizou PC, Poroy O, Dorman M (2000) The effect of parametric variations of cochlear implant processors on speech understanding. J Acoust Soc Am 108:790–802
47. Luo X, Fu QJ (2004) Enhancing Chinese tone recognition by manipulating amplitude envelope: implications for cochlear implants. J Acoust Soc Am 116:3659–3667
48. Martin R (1994) Spectral subtraction based on minimum statistics. In: Proceedings European signal process, Edingburgh, Scotland, U.K. pp 1182–1185
49. McDermott HJ, McKay CM, Vandali AE (1992) A new portable sound processor for the University of Melbourne/Nucleus Limited multielectrode cochlear implant. J Acoust Soc Am 91(3367–3371):1992
50. Nagal D (1974) Compound action potential of the cochlear nerve evoked electrically. Arch Otorhinolaryngol 206:293–298
51. Ping L, Wang N, Tang G, Lu T, Yin L, Tu W, Fu QJ (2017) Implementation and preliminary evaluation of 'C-tone': a novel algorithm to improve lexical tone recognition in Mandarin-speaking cochlear implant users. Cochlear Implants Int 18(5):240–249
52. Plapous C, Marro C, Scalart P (2006) Improved signal-to-noise ratio estimation for speech enhancement. IEEE Trans Audio Speech Lang Process 14:2098–2108
53. Razavi B (2001) Design of analog CMOS integrated circuits. McGraw-Hill, New York, pp 471–479
54. Ross M, Shaffer H, Cohen A, Freudberg R, Manley H (1974) Average magnitude difference function pitch extractor. IEEE Trans Acoust Speech Signal Process 22:10
55. Schatzer R, Krenmayr A, Au DK, Zierhofer C (2010) Temporal fine structure in Cochlear implants: preliminary speech perception results in Cantonese speaking implant users. Acta Otolaryngol 130:1031–1039
56. Shannon RV, Zeng FG, Kamath V (1995) Speech recognition with primarily temporal cues. Science 270:303–304
57. Skinner MW, Holden LK, Holden TA (1991) Performance of postlinguistically deaf adults with the wearable speech processor (WSP III) and mini speech processor (MSP) of the nucleus multi-electrode Cochlear implant. Ear Hear 12:3–22
58. Skinner MW, Holden LK, Whitford LA, Plant KL, Psarros C, Holden TA (2002) Speech recognition with the nucleus 24 SPEAK, ACE, and CIS speech coding strategies in newly implanted adults. Ear Hear 23:207–223
59. Smoorenburg GF, Willeboer C, van Dijk JE (2002) Speech perception in nucleus CI24M cochlear implant users with processor settings based on electrically evoked compound action potential thresholds. Audiol Neurootol 7:335–347
60. Sokal NO, Sokal AD (1975) Class-E- a new class of high-efficiency tuned single-ended switching power amplifiers. IEEE J Solid State Circuits 10(3):168–176
61. Spahr AJ, Dorman MF (2004) Performance of subjects fit with the advanced bionics CII and nucleus 3G cochlear implant devices. Arch Otolaryngol Head Neck Surg 130:624–628
62. Spriet A, Moonen M, Wouters J (2004) Spatially pre-processed speech distortion weighted multi-channel Wiener filtering for noise reduction. Signal Process 84:2367–2387

63. Stypulkowski PH, van den Honert C (1984) Physiological properties of the electrically stimulated auditory nerve. I. Compound action potential recordings. Hear Res 14:205–223
64. Summers IR, Al-Dabbagh AD (1982) Simulated loss of frequency selectivity and its effects on speech perception. Acoust Lett 5:129–132
65. Tang Z, Smith B, Schild JH, Peckham PH (1995) Data transmission from an implantable biotelemeter by load-shift keying using circuit configuration modulator. IEEE Trans Biomed Eng 42(5):524–528
66. Vary P (1985) Noise suppression by spectral magnitude estimation – mechanism and theoretical limits. Signal Process 8:387–400
67. van de Heyning P, Arauz SL, Atlas M, Baumgartner WD, Caversaccio M, Chester-Browne R et al (2016) Electrically evoked compound action potentials are different depending on the site of cochlear stimulation. Cochlear Implants Int 17:251–262
68. Van den Bogaert T, Doclo S, Wouters J, Moonen M (2009) Speech enhancement with multichannel wiener filter techniques in multimicrophone binaural hearing aids. J Acoust Soc Am 125:360–371
69. Van Dun B, Wouters J, Moonen M (2007) Multi-channel wiener filtering based auditory steady-state response detection. In: IEEE international conference on acoustics, speech and signal processing, Honolulu, Hawaii, USA pp 929–932
70. Van Gerven S, Van Compernolle D (1995) Signal separation by symmetric adaptive decorrelation: stability, convergence, and uniqueness. IEEE Trans Signal Process 43:1602–1612
71. Weinstein E, Feder M, Oppenheim AV (1993) Multi-channel signal separation by decorrelation. IEEE Trans Signal Process 1:405–413
72. Wilson BS, Finley CC, Lawson DT, Wolford RD, Eddington DK, Rabinowitz WM (1991) Better speech recognition with cochlear implants. Nature 352:236–238
73. Wouters J, Vanden Berghe J (2001) Speech recognition in noise for cochlear implantees with a two-microphone monaural adaptive noise reduction system. Ear Hear 22:420–430
74. Zeng FG (2004) Trends in cochlear implants. Trends Amplif 8:1–34
75. Zeng FG, Nie K, Stickney GS, Kong YY, Vongphoe M, Bhargave A, Wei C, Cao K (2005) Speech recognition with amplitude and frequency modulations. Proc Natl Acad Sci U S A 102:2293–2298
76. Zeng FG, Rebscher SJ, Fu QJ, Chen H, Sun X, Yin L, Ping L, Feng H, Yang S, Gong S, Yang B, Kang HY, Gao N, Chi F (2015) Development and evaluation of the Nurotron 26-electrode cochlear implant system. Hear Res 322:188–199
77. Zeng F, Rebscher S, Harrison W, Sun X, Feng H (2008) Cochlear implants: system design, integration, and evaluation. IEEE Rev Biomed Eng 1:115–142

Chapter 8
Neuromodulation for Pain Management

Jing Wang and Zhe Chen

Abstract Pain is a salient and complex sensory experience with important affective and cognitive dimensions. The current definition of pain relies on subjective reports in both humans and experimental animals. Such definition lacks basic mechanistic insights and can lead to a high degree of variability. Research on biomarkers for pain has previously focused on genetic analysis. However, recent advances in human neuroimaging and research in animal models have begun to show the promise of a circuit-based neural signature for pain. At the treatment level, pharmacological therapy for pain remains limited. Neuromodulation has emerged as a specific form of treatment without the systemic side effects of pharmacotherapies. In this review, we will discuss some of the current neuromodulatory modalities for pain, research on newer targets, as well as emerging possibility for an integrated brain-computer interface approach for pain management.

8.1 Introduction

Pain is a complex human experience which contains sensory, affective, and cognitive dimensions. The sensory component of pain provides information about the exact location, timing, and character of a noxious stimulus – the stimulus that provokes pain. The affective component includes feelings of annoyance, anger,

---

J. Wang (✉)
Department of Anesthesiology, Perioperative Care and Pain Medicine, Department of Neuroscience and Physiology, New York University School of Medicine, New York, NY, USA
e-mail: Jing.Wang2@nyumc.org

Z. Chen
Department of Psychiatry, Department of Neuroscience and Physiology, New York University School of Medicine, New York, NY, USA

sadness, anxiety, and depression in response to that noxious stimulus. Finally, the cognitive component of pain dictates behavioral responses to this stimulus. During a painful episode, these three components are integrated and contribute to the full experience of pain.

The Webster dictionary definition of pain is "physical suffering or discomfort caused by illness or injury." However, this definition does not provide any anatomical or mechanistic dimensions. Nor does it necessarily delineate the contribution of the three components of pain. Compatible with this vague definition, the clinical diagnosis of pain is established purely by verbal report and thus remains highly subjective. Therefore, an objective diagnosis of pain can greatly improve both our scientific understanding of pain and its clinical management.

At the treatment level, pharmacological options are limited. Opioids remain the most efficacious analgesics, and these drugs have been utilized for pain management for over 1000 years. Opioids, however, carry significant side effects, including constipation, sedation, respiratory depression, immunosuppression, neuro-hormonal dysregulation, dependence, and addiction. There is currently a great debate regarding the use of opioids in the management of chronic non-malignant pain. Despite enormous research over the last century, most of which focuses on spinal and peripheral nervous systems, there have been relatively few new discoveries of pharmacological therapy for pain. Neuromodulation, on the other hand, has emerged as a potentially more specific form of treatment without the systemic side effects of pharmacotherapies. In this review, we will discuss some of the current neuromodulatory treatment modalities for pain, as well as ongoing research to identify newer targets. We will also discuss the possibility for an integrated brain-computer interface approach for pain management that involves both decoding pain signals and neuromodulation of pain.

8.2 Spinal Neuromodulation for Pain

8.2.1 Theory for Spinal Cord Modulation

One of the key concepts in the scientific understanding of pain comes from a classic paper by Melzack and Wall [1]. In this paper, Melzack and Wall argued that there are possible gates of control for nociceptive and non-nociceptive signals at the spinal cord level. More specifically, pyramidal or excitatory neurons in the spinal dorsal horn (SDH) receive sensory inputs – both nociceptive and non-nociceptive – from the peripheral primary sensory neurons, and then in turn transmit this sensory information by projection to the thalamus and brain stem. The SDH, however, also contains interneurons, which are GABAergic and inhibitory. These interneurons also receive peripheral sensory information, but instead of projecting to the brain, they project to other pyramidal neurons in the SDH to inhibit these neurons from providing ascending signals. Thus, non-nociceptive sensory inputs to the SDH can activate interneurons to inhibit the pain signal – in a sense shutting the gate for pain.

Based on this theory for gate control, spinal cord stimulation (SCS) was developed as a way to treat pain. It was thought that external electric stimulator can simulate the firing of interneurons to inhibit ascending pyramidal neurons in the SDH. As a result, SCS can inhibit the transmission of the pain signal from the periphery to the brain. Surgically, SCS includes a trial phase and a permanent implantation phase. During the trial phase, a trial stimulator is implanted into the epidural space under fluoroscopy guidance. The stimulator is then turned on, and the frequency of the stimulation and the location of the stimulator are adjusted over a period of hours to ensure patient comfort and analgesic effects. As the goal of the SCS therapy is to replace the actual pain sensation with paresthesia, the SCS leads need to cover the body area where the patient's pain is generated [2]. If the trial is successful and the patient is able to tolerate the side effects, a permanent implant is then done in the operating room. The permanent implantation is procedurally similar to the trial lead placement, but the leads and battery are implanted in a pocket inside the patient. The battery can be remotely charged. In some cases, permanent lead implantation is done by laminectomy and the leads are sutured to the dura to ensure stable placement [2].

8.2.2 Current Clinical Practice

The frequency of spinal cord stimulation is typically 40–60 Hz [2]. Newer advances, however, include the use of very high-frequency stimulation (10,000 Hz) and burst stimulation. Through mechanisms that are not entirely understood, such higher frequency stimulations have been shown in a limited number of preliminary studies to confer superior pain relief compared with traditional stimulation protocols [3–7].

Numerous studies have confirmed the analgesic efficacy for SCS. In two recent meta-analyses of SCS treatment, it was found that >50% of the patients experienced pain relief with an average follow-up of 24 months [8, 9]. The pain syndromes most responsive to therapy include lumbosacral radiculitis that is refractory to pharmacological and interventional treatments, failed back surgery syndrome, diabetic peripheral neuropathy, and other distal peripheral neuropathic syndromes [2]. In Europe, SCS has also been utilized for ischemic chest pain [2].

8.2.3 Limitations of Spinal Modulation for Pain

Despite its efficacy in pain treatment, there are several distinct disadvantages for SCS. First, the SCS is implanted in the epidural space, and with a constant movement of the spine, there is a high risk for lead displacement, with rates reported to be as high as 30% in some studies [10]. Another key disadvantage of SCS is that it requires constant stimulation. This is because while SCS was developed as a neuromodulation technique, it was not developed as a demand-based neuromodulation technique. As a

result, many patients develop tolerance to SCS, and in a significant subset of patients, SCS loses its analgesic efficacy over time. In addition, continuous stimulation makes side effects more problematic. The main side effect of SCS is paresthesia. Over time, many patients elect to turn off the SCS due to the continuous bothersome paresthesia.

Theoretically, a demand-based approach to neuromodulation can alleviate many of the side effects associated with SCS. SCS would be turned on only when pain is sensed. This way, the patient will not experience a long period of paresthesia when there is no pain signal. The design for a demand-based neuromodulation approach, however, requires real-time decoding of pain signals, which has not been achieved at the level of SDH and DRG neurons.

8.3 Brain Neuromodulation for Pain

After it first emerged 70 years ago, brain neuromodulation has been studied to be a treatment modality for refractory pain conditions. Some of the earlier studies are in rodents. A number of brain targets have been sought, with the overall goal of reducing the activities in these pain-producing or processing regions with high-frequency stimulations in a protocol that is similar to deep brain stimulation (DBS) utilized for Parkinson's disease [11]. In some cases, direct stimulation with lower frequency has been attempted to activate the region of interest. These targets include the anterior cingulate cortex (ACC), motor cortex, sensory thalamus, intralaminar parafascicular complex (CMP), periacqueductal gray (PAG), and nucleus accumbens (NAc). A number of studies targeting these areas have shown a varying degree of success in pain relief.

8.3.1 Current Practice of Brain Modulation for Pain

Cortical Stimulations
The ACC is well known to be a critical hub for the processing for the affective component of pain [12–22]. Not surprisingly, it was one of the first regions to be targeted for pain relief. The first case series of electrical stimulation of the ACC as a treatment for chronic pain was published in 1960 [23]. A large number of these cases involved pain from spinal cord injuries [24, 25]. In these studies, bilateral stimulation using a DBS protocol achieved temporary pain relief as measured by the patient's pain reporting and medication dosages. In particular, patients who received ACC stimulation reported a decrease in the affective component of pain. It was reported that these patients still felt pain, but "it didn't bother" them as much. However, pain relief was not found to be enduring. In a more recent study of 15 patients with chronic pain, chronic DBS of the ACC using implanted electrodes produced an analgesic effect in five patients [26]. The side effects have in general been mild in most studies.

Although not a region known for pain processing, the motor cortex has also been targeted for pain relief. Motor cortex stimulation (MCS) has been evaluated particularly in central pain syndromes such as post-stroke pain or refractory trigeminal neuralgia. The rationale for MCS comes from the observation that motor cortex stimulation achieved sensory responses, and treatment as early as in 1971 has shown partial analgesic effects [27]. Modern approach to MCS began with a study in 1991, where eight of 12 patients were able to experience some degree of pain relief after 1 year of MCS with implanted electrodes [28]. A number of studies since then have demonstrated efficacy for MCS, particularly for post-stroke pain syndrome, where up to 70% of patients responded positively, and facial pain, with up to 80% efficacy [29–34]. In these studies, a chronic implant with stimulation of 5–130 Hz has been investigated to be efficacious.

Subcortical Stimulations

The role of the sensory thalamus in pain regulation is well established, as studies have shown that thalamic injury such as in the case of stroke can lead to persistent central pain or post-stroke pain. The thalamus is a highly heterogeneous structure, and the regions involved in pain processing include the ventroposterior lateral (VPL) and ventroposterior medial (VPM) nuclei. Whereas the lateral thalamus is thought to project to the somatosensory cortex (S1) and provide accurate sensory information related to pain, the VPM has been shown to project to a variety of cortical and subcortical structures and is thought to be involved in the affective processing of pain. Hyperactivity of the thalamus has been observed in neuropathic pain conditions [35–37]. In an early and well-cited study, four of five facial pain patients who received chronic VPM stimulation demonstrated pain relief [38]. Subsequently, stimulation of both VPM and VPL regions have been carried in a number of studies. Studies have shown that contralateral VPM stimulation can result in persistent analgesia as well as paresthesia, whereas study with neuropathic pain patients showed that thalamic stimulation can result in improvement in pain scores [39–41]. The technical difficulty associated with thalamic stimulation, however, is considerable, due to its position in the brain and its numerous subdivisions with highly divergent functions. Perhaps as a result of these anatomic and structural concerns, more recent studies have shown more conflicting results [42, 43].

The PAG projects to the rostroventral medial medulla (RVM), which in turn projects to the spinal dorsal horn neurons, and depending on the exact neuronal subgroups and circuit dynamics, this projection can provide either descending inhibition or facilitation of ascending pain signals [44]. Given its well-established involvement in descending pain regulation, the PAG has been pursued as a promising target in a number of studies [45–47]. Recent data, however, did not demonstrate consistent and enduring pain relief [24, 43, 48–51]. Some of these studies showed that PAG stimulation results in pain relief, whereas other studies did not demonstrate persistent analgesic effect. These divergent results may be due to the fact that the PAG can project to the RVM, but it projects to two distinct populations of RVM cells. Whereas the off cells in the RVM produce pain relief, the on cells actually give rise to pain intensification. As a result, a constant stimulation approach

without differentiating on- or off-cells in the PAG may not be highly effective. Furthermore, PAG stimulation appears to cause significant side effects including nausea, nystagmus, vertigo, and nausea [45].

Additional targets in the brain include the NAc, CMP, hypothalamus (HT), and the internal capsule (IC). The NAc forms the ventral striatum and is known for its role in reward-based behaviors [52]. However, the NAc has also been shown in recent studies to play a crucial role in pain and analgesia [53–55]. Specifically, studies have shown that the projection from the medial prefrontal cortex (PFC) to the NAc can produce relief of both sensory and affective components of pain in acute as well as chronic pain conditions [56]. There are in fact case studies of post-stroke (central) pain where stimulation of the NAc when combined with PAG stimulation can achieve significant pain relief [57]. Meanwhile, the CMP has high levels of expression of opioid receptors and is anatomically connected to the thalamus, ACC, and NAc, and thus it has also been postulated to function as a target for pain treatment [58]. Surgical stimulation of the CMP, however, has achieved variable results. Some studies have shown CMP stimulation to have modest analgesic effects in central or neuropathic pain syndromes, whereas other studies have failed to reproduce such results with any significant time frame [59–61]. Finally, a recent number of studies have shown that DBS of the posterior HT demonstrated relief for cluster headache as well as for cephalgias [62–64]. The rationale for this approach is that cluster headache has a circadian component, which in turn is regulated in large part by the posterior HT [65]. These studies, however, are relatively small in sample size. Meanwhile, the earliest study on IC stimulation in 1974 showed analgesic efficacy [66, 67]. Subsequent studies in this area have also shown that DBS in this area may have a role in reducing neuropathic pain [68–70]. The mechanisms for the analgesic effects of IC stimulation, however, are not well understood.

8.3.2   Technical Considerations for Brain Modulation for Pain

Electrical leads for MCS or DBS are typically two side by side four-contact electrodes. MCS is achieved with an amplitude of 0.5–10 volts, with frequency ranging from 5 to 130 Hz, with 40–100 Hz being the most common, and pulse widths spanning from 60 to 450 ms. Meanwhile, standard DBS electrodes can be implanted for pain similar to implants for Parkinson's patients. Unfortunately, due to the small number of studies, the difficulty in enrollment, and the nature of the implantation surgery, MCS and DBS protocols have not been well investigated in studies using large sample sizes. Important factors for consideration for cortical and subcortical stimulation include the duration of stimulation, frequency of stimulation, and the possibility of low-frequency stimulation to activate neurons vs high-frequency stimulation to inhibit neuronal activities. The desired outcome would be for the device to perform stimulation or inhibition of the neuronal networks during

the occurrence of pain episodes. The ultimate goal, meanwhile, is to achieve demand-based automated stimulation. The accomplishment of this goal, however, requires accurate decoding of the pain signals in the brain.

8.4 Decoding Pain in the Brain

8.4.1 Electrophysiological Recordings in Rodents and Non-human Primates

From a neural coding perspective, the goal of pain encoding is to understand how neurons represent and transmit the information of pain. Current decoding of pain relies on neuroimaging techniques such as fMRI or PET. These neuroimaging studies have a few critical limitations. First, at the anatomical level, fMRI imaging experiments cannot provide desirable single-cell resolution. Second, fMRI measurements reflect the blood-flow changes, and such changes indirectly indicate brain activity. Therefore, it only measures the correlation between blood flow and neural activity instead of direct neurophysiological measurements. Nociceptive information is distributed so widely that blood-flow changes sometimes cannot accurately depict primary and secondary neural responses. Third, imaging studies cannot identify the causal relationship between circuit change and pain behaviors. This lack of causality limits the mechanistic insight that neuronal codes can provide. Fourth, the limited temporal resolution of imaging studies precludes the analysis of ultrafast circuit and synaptic events. It is the last constraint that makes various imaging techniques less ideal tools for real-time decoding in the brain. Due to these limitations, circuit mechanisms of pain, particularly the affective and cognitive dimensions of pain, remain poorly defined. On the other hand, in vivo electrophysiological recordings in animal studies have provided insight on pain mechanism at cellular and circuit levels and at a millisecond timescale. Below we will review a few important electrophysiological studies in rodents and non-human primates. We focus on the primary neural circuits that modulate the pain stimuli, including thermal, mechanical, inflammatory, and neuropathic pain.

Recent animal research on pain has focused on spinal and peripheral systems. Spinal cord and peripheral systems mostly inform nociception. Pain, however, is a multi-dimensional experience and includes sensory, affective, and cognitive dimensions. Therefore, attempts to decode pain should ideally include circuitry in the brain. Meanwhile, there is no "pain cortex," as pain is perceived and processed in a distributed network [71]. Among the many brain areas, the S1 and ACC are two of the most studied areas for pain-related responses. The S1 has long been thought to encode the sensory component of pain, whereas the ACC has been known as a key anatomic region for understanding the aversive and other affective manifestations of pain [72, 73]. Other brain regions that are engaged in pain processing include the medial prefrontal cortex (mPFC) [74], insular cortex [75],

NAc [76], thalamus including the thalamic reticular nucleus (TRN), medial dorsal (MD) nucleus, and other thalamic nuclei [77, 78].

In rodent experiments, neurophysiological recordings in pain studies were reported in both anesthetized and freely behaving animals. For instance, it was found that neurons in the TRN and ventroposterior lateral nucleus responded to CO_2 laser in anesthetized rats [79]. These neurons have shown specificity in their responses and hence have been thought to be nociceptive thalamic neurons. However, in another independent report, it was found that none of the mechanical nociceptive neurons showed a clear relationship between discharge and thermal pain temperature [80]. The differences in these studies may be attributed to the fact that animals were under anesthesia, which can make the magnitude and duration of the sensory information transfer variable.

Physiological recordings in conscious, behaving rats have been collected in S1 and ACC [81–83], as well as in VPL and MD [83]. Specifically, S1 and VPL are within the lateral sensory pain pathway, whereas ACC and MD are within the medial pathway more involved in the affective and cognitive processing of pain. Kuo and Yen [81] compared noxious responses in S1 and ACC and observed that ACC neurons were less frequently activated and had a longer latency of onset in response to thermal pain induced by a CO_2 laser [81]. Additional experiments showed that neuronal responses in both the S1 and ACC increased with the intensity of the laser heat; and the stimulus-response curve of S1 ensemble activity had a steeper slope than that of the ACC. Furthermore, S1 neurons were better at coding laser-heat intensity than ACC neurons, whereas more ACC neurons were involved in conditioned fear associated with an electric shock than S1 neurons. These results suggest differential contributions of the S1 and ACC to sensory and affective dimensions of pain. With the simultaneous recording of multiple brain areas in lateral and medial pain pathways, Zhang et al. [83] reported significant correlations between laser intensity and the number of responsive neurons, the firing rates, as well as the mass spike counts. In addition, their results also showed a comparable coding capacity of medial and lateral pain pathway neurons [83]. Furthermore, Zhang et al. used a linear discriminant analysis for pain intensities based on the mass spike counts of neuronal recordings from multiple brain areas. Although several electrophysiological investigations in rats similar to the above studies have established that activities in the S1 and ACC are altered by pain stimuli, very little effort has been devoted specifically to decoding analysis, especially for the onset detection of pain signals.

In non-human primate experiments, Chudler et al. [84] have found that nociceptive neurons in the S1 of anesthetized monkeys were responsive to noxious thermal stimulation applied to the face [84]. One type of nociceptive S1 neurons showed increased firing rate with increasing stimulus intensity, whereas another type of nociceptive S1 neurons showed saturated response once reaching a plateau above a specific temperature. At the behavioral level, the intensity of pain sensation or pain rating in some ways parallels the neuronal responses of nociceptive S1 neurons. In another study, Iwata et al. [85] recorded ACC neurons from awake behaving monkeys [85]. Positively and negatively modulated ACC neurons were reported in

response to a heat stimulus on the face. Their results further suggested that ACC neurons are involved in the attention to pain and escape from pain but not in the sensory-discriminative aspect of pain.

8.5 Potential for a Demand-Based Neuromodulation Approach

From a treatment perspective, a neuromodulation is a potential option for refractory pain. As discussed above, both spinal and brain stimulation has the potential for modulating the pain experience [86]. In addition to therapeutic benefits, the use of brain stimulation also allows mechanistic understanding of brain circuits that underlie the pain experience. However, current techniques such as deep brain stimulation or transcranial magnetic stimulation (TMS) lack optimal targets in the brain and require constant stimulation resulting in unacceptable side effects.

Demand-based neuromodulation, or closed-loop control for pain, provides an appealing alternative strategy. This strategy can be combined with either spinal or brain modulation. The realization of a demand-based neuromodulatory approach depends critically on two factors: first, accurate and timely identification of the pain signal, and second, low-latency neuromodulatory control. In other words, timing matters in closed-loop neuromodulation therapy [87].

8.5.1 Challenges for Demanded-Based Pain Modulation

In neuroscience and clinical experiments, a closed-loop brain-machine interface (BMI) offers a powerful platform to investigate the causal link between brain circuits and behavior [88]. A basic closed-loop BMI system for pain modulation (Fig. 8.1) would consist of a detection arm (which is aimed for detecting the onset of pain signals) and a treatment arm (which is aimed for delivering neuromodulation).

For the detection arm, the central challenge in change-point detection is the speed and accuracy of detection. In real-time processing, the objective of *quickest detection* is to detect changes as quickly as possible in an online fashion, and the requirement of time-delay for closed-loop feedback usually lies within tens or hundreds of milliseconds.

For the treatment arm, the first step is to identify effective neural circuits for modulating pain. Some candidate targets have been discussed above, including the nucleus accumbens [89], ACC [90], and thalamus [79, 91]. The second step is to apply neuromodulation methods. There are also a few strategies based on invasive or noninvasive stimulations. In animal studies, the emergence of optogenetics [56, 92–96] and chemogenetics [96] offer intriguing options. While not yet applicable in humans due to the nature of viral transfer, these techniques allow quick and
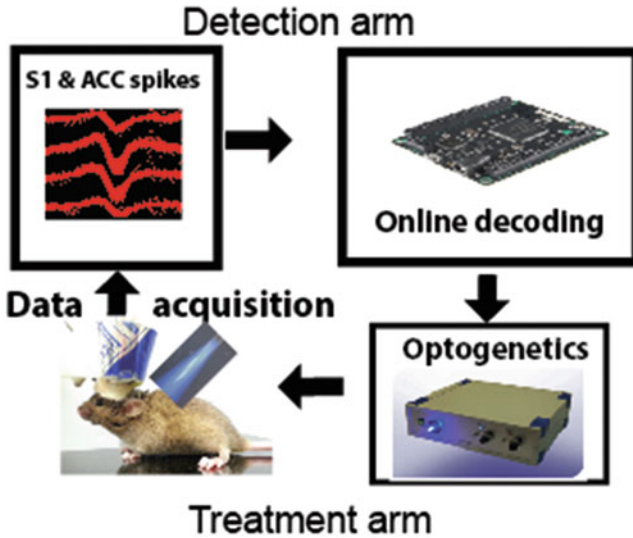
Fig. 8.1 A schematic of the rodent closed-loop BMI system. A closed-loop system consists of the detection arm (detection of the onset of pain signals via online neural decoding) and treatment arm (neuromodulation via electrical or optogenetic stimulation)

targeted methods to alter brain circuits. Such techniques can be used to perform feasibility studies for therapeutics as well as to probe circuits in basic mechanistic investigations.

8.5.2 Pilot Rodent Studies

In our investigations, we have used a rat model to study mechanisms of acute pain, including acute thermal pain and acute mechanical pain. In thermal pain experiments, we used a blue diode-pumped solid-state laser applied 1 mm from the plantar surface of the hind paw contralateral to the brain recording site to generate pain in freely moving rats. The laser was turned on by a transistor-to-transistor pulse generator until paw withdrawal was observed. The fiber output power was calibrated by compact power and energy at the beginning of every recording day [90, 97]. We used custom-designed microdrives (32 channels) to simultaneously record neuronal ensemble spike activity from the rat S1 and ACC areas. Both spike (>300 Hz) and local field potential (<300 Hz) data were obtained.

For detection of the onset of pain signals, we have designed model-based and model-free algorithms based on the input of (off-line or on-line) sorted neuronal ensemble spike activity [97–99].

A Model-Based Approach

Notations: Given C neuronal recordings, let $\mathbf{y}_k = [y_{1,\,k}, \ldots, y_{C,\,k}]$ denote a C-dimensional population vector, with each element consisting of the neuronal spike count at the kth time bin (bin size Δ); let $\exp.(\boldsymbol{\eta}_k)$ denote the Poisson firing rate vector for C neurons. We assumed that the data follows a latent-state Poisson linear dynamical system (PLDS), where the latent univariate variable z_k denotes an unobserved common input that drives neuronal ensemble spiking activity $\mathbf{y}_k$ as follows [97, 98]:

$$z_k = az_{k-1} + \epsilon_k \tag{8.1}$$

$$\boldsymbol{\eta}_k = \mathbf{c}z_k + \mathbf{d,} \tag{8.2}$$

$$\mathbf{y}_k \sim Poisson(\exp(\boldsymbol{\eta}_k)\Delta), \tag{8.3}$$

where the state Eq. (8.1) is a first-order autoregressive (AR) model ($0 < |a| < 1$) driven by a Gaussian noise process with zero mean and variance $N(0, \sigma^2)$. We used an iterative expectation-maximization (EM) algorithm to estimate the latent state (E-step) and the unknown parameters $\{a, \mathbf{c}, \mathbf{d}, \sigma^2\}$ (M-step). Alternatively, we transformed the Poisson population vector (nonnegative) into a Gaussian random vector and obtained a transformed linear dynamical system (TLDS). In this case, the inference procedure was simpler due to the approximation methods. In on-line applications, once the model parameters are identified, we used a recursive (forward) filter to estimate the latent state variable [97, 99].

From the estimated latent state $\hat{z}_k$, we further computed the Z-score related to the baseline: $Z = \frac{z - \text{mean}(z_{\text{baseline}})}{\text{SD}(z_{\text{baseline}})}$. Under the assumption that the Z-score is standard normally distributed, we converted it to the one-tailed P-value. The criterion of Z-score change was determined by a critical threshold for reaching statistical significance.

A Model-Free Approach

We designed a greedy CUSUM (cumulative sum) algorithm. The CUSUM method is aimed to detect a change point based on the instantaneous log-likelihood ratio (LLR):

$$\text{LLR}_{f_1 \| f_0} = y\log\frac{\lambda_1}{\lambda_0} - (\lambda_1 - \lambda_0) \tag{8.4}$$

where λ_0 and λ_1 are the rate parameters of two Poisson distributions f_0 and f_1. We assume that the baseline rate λ_0 is known or can be estimated directly from data. We define an empirical criterion for a significant change in λ_1 such that $\lambda_1^{sig} = \lambda_0 \pm 2\sqrt{\lambda_0}$ in either a positive or negative direction. The CUSUM algorithm computes the instantaneous LLR $s_{c,\,k}$ for the cth neuron and update the cumulative sum as follows:

$$S_k = \max_c\{S_{c,k}\} = \max_c\{\max\{0, S_{c,k-1} + s_{c,k}\}\} \tag{8.5}$$
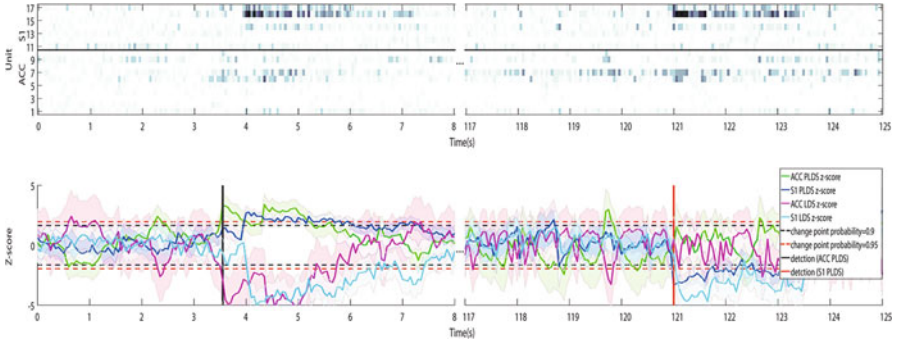
Fig. 8.2 Online detection of the onset of thermal acute pain. *Top*: Spike counts of simulta-
neously recorded, online-sorted 17 units (seven S1 units and ten ACC units) from a freely behaving
rat. *Bottom*: Continuous tracking and detection of pain signals derived from the rat S1 and ACC
activity. Shaded area denotes the CI of Z-score. Vertical lines denote the moments of change-point
detection. In this example, the detection results of the PLDS were better than those derived from the
TLDS and model-free method (not shown) [100]

where $S_0 = 0$. The technical details are referred to [99]. Once the cumulative sum S_k
is above a predetermined threshold θ_0 and the trend continuous more than two
consecutive steps, then a decision is made and S_k is reset. The threshold θ_0 in the
CUSUM algorithm controls the false alarm rate. An empirical choice is to use the
test statistic (twofold log-likelihood) being a chi-square distribution with 1 degree of
freedom: $\chi^2_{1,(1-\alpha)}$. If we set $\alpha = 0.01$, we have $\theta_0 = 0.5 \times 6.64 = 3.38$.

To illustrate these two methods, we apply these two methods to simultaneous
recordings of rat S1 and ACC neuronal populations. Two representative examples of
online detection of pain signals are shown in Fig. 8.2.

Therefore, as these pilot studies demonstrate, the S1 and ACC neuronal ensemble
activity encode important information about pain signals. Even more importantly,
these experiments demonstrate that integrating neural signals from multiple brain
areas will further improve the decoding accuracy for the onset of pain. Developing
online statistical methods for detecting the onset of pain signals in closed-loop neural
interfaces can open new research opportunities for both acute and chronic pain. Such
methods, when combined with spinal or brain modulation, can have the potential to
achieve pain control with limited side effects.

8.6 Summary

Pain is a complex experience. In a subset of patients who suffer from chronic pain, it
is a debilitating experience. The current state-of-the-art neuromodulation therapy is
spinal cord stimulation. While this treatment modality is well validated, it continues
to have side effects. Neuromodulation in the brain, meanwhile, has also been

explored, but optimal targets remain lacking. Recent advances in neuro-engineering and computational neuroscience, however, when combined with an improved understanding of neurocircuitry of pain, allow for the possibility of demand-based neuromodulation of pain. The possibility of a brain-computer interface approach can allow better mechanistic understanding of basic pain mechanisms, and at the same time, it can provide much-needed treatment for refractory pain syndromes.

References

1. Melzack R, Wall PD (1965) Pain mechanisms: a new theory. Science 150(3699):971–979
2. Deer TR et al (2014) The appropriate use of neurostimulation of the spinal cord and peripheral nervous system for the treatment of chronic pain and ischemic diseases: the Neuromodulation Appropriateness Consensus Committee. Neuromodulation 17(6):515–550. discussion 550
3. Liem L et al (2015) One-year outcomes of spinal cord stimulation of the dorsal root ganglion in the treatment of chronic neuropathic pain. Neuromodulation 18(1):41–48. discussion 48-9
4. De Ridder D et al (2013) Burst spinal cord stimulation for limb and back pain. World Neurosurg 80(5):642–649 e1
5. De Ridder D et al (2010) Burst spinal cord stimulation: toward paresthesia-free pain suppression. Neurosurgery 66(5):986–990
6. Van Buyten JP et al (2013) High-frequency spinal cord stimulation for the treatment of chronic back pain patients: results of a prospective multicenter European clinical study. Neuromodulation 16(1):59–65. discussion 65-6
7. Tiede J et al (2013) Novel spinal cord stimulation parameters in patients with predominant back pain. Neuromodulation 16(4):370–375
8. Taylor RS et al (2014) Predictors of pain relief following spinal cord stimulation in chronic back and leg pain and failed back surgery syndrome: a systematic review and meta-regression analysis. Pain Pract 14(6):489–505
9. Grider JS et al (2016) Effectiveness of spinal cord stimulation in chronic spinal pain: a systematic review. Pain Physician 19(1):E33–E54
10. Deer TR et al (2014) The appropriate use of neurostimulation: avoidance and treatment of complications of neurostimulation therapies for the treatment of chronic pain. Neuromodulation 17(6):571–598
11. Levy RM, Lamb S, Adams JE (1987) Treatment of chronic pain by deep brain stimulation: long term follow-up and review of the literature. Neurosurgery 21(6):885–893
12. Turnbull IM (1972) Bilateral cingulumotomy combined with thalamotomy or mesencephalic tractotomy for pain. Surg Gynecol Obstet 134(6):958–962
13. Craig AD et al (1996) Functional imaging of an illusion of pain. Nature 384(6606):258–260
14. Rainville P et al (1997) Pain affect encoded in human anterior cingulate but not somatosensory cortex. Science 277(5328):968–971
15. Foltz EL, White LE (1968) The role of rostral cingulumotomy in "pain" relief. Int J Neurol 6(3–4):353–373
16. Talbot JD et al (1995) Evaluation of pain perception after anterior capsulotomy: a case report. Somatosens Mot Res 12(2):115–126
17. Koyama T, Kato K, Mikami A (2000) During pain-avoidance neurons activated in the macaque anterior cingulate and caudate. Neurosci Lett 283(1):17–20
18. Koyama T et al (2001) Anterior cingulate activity during pain-avoidance and reward tasks in monkeys. Neurosci Res 39(4):421–430
19. Qu C et al (2011) Lesion of the rostral anterior cingulate cortex eliminates the aversiveness of spontaneous neuropathic pain following partial or complete axotomy. Pain 152(7):1641–1648

20. Johansen JP, Fields HL, Manning BH (2001) The affective component of pain in rodents: direct evidence for a contribution of the anterior cingulate cortex. Proc Natl Acad Sci U S A 98(14):8077–8082
21. LaGraize SC et al (2006) Selective regulation of pain affect following activation of the opioid anterior cingulate cortex system. Exp Neurol 197(1):22–30
22. Lubar JF (1964) Effect of medial cortical lesions on the avoidance behavior of the cat. J Comp Physiol Psychol 58:38–46
23. Lewin W, Whitty CW (1960) Effects of anterior cingulate stimulation in conscious human subjects. J Neurophysiol 23:445–447
24. Boccard SG et al (2013) Long-term outcomes of deep brain stimulation for neuropathic pain. Neurosurgery 72(2):221–230. discussion 231
25. Spooner J et al (2007) Neuromodulation of the cingulum for neuropathic pain after spinal cord injury. Case report. J Neurosurg 107(1):169–172
26. Boccard SG et al (2014) Deep brain stimulation of the anterior cingulate cortex: targeting the affective component of chronic pain. Neuroreport 25(2):83–88
27. Lende RA, Kirsch WM, Druckman R (1971) Relief of facial pain after combined removal of precentral and postcentral cortex. J Neurosurg 34(4):537–543
28. Tsubokawa T et al (1991) Chronic motor cortex stimulation for the treatment of central pain. Acta Neurochir Suppl (Wien) 52:137–139
29. Katayama Y, Tsubokawa T, Yamamoto T (1994) Chronic motor cortex stimulation for central deafferentation pain: experience with bulbar pain secondary to Wallenberg syndrome. Stereotact Funct Neurosurg 62(1–4):295–299
30. Katayama Y, Fukaya C, Yamamoto T (1998) Poststroke pain control by chronic motor cortex stimulation: neurological characteristics predicting a favorable response. J Neurosurg 89(4):585–591
31. Herregodts P et al (1995) Cortical stimulation for central neuropathic pain: 3-D surface MRI for easy determination of the motor cortex. Acta Neurochir Suppl 64:132–135
32. Ebel H et al (1996) Chronic precentral stimulation in trigeminal neuropathic pain. Acta Neurochir 138(11):1300–1306
33. Nguyen JP et al (2000) Treatment of central and neuropathic facial pain by chronic stimulation of the motor cortex: value of neuronavigation guidance systems for the localization of the motor cortex. Neurochirurgie 46(5):483–491
34. Garcia-Larrea L et al (1999) Electrical stimulation of motor cortex for pain control: a combined PET-scan and electrophysiological study. Pain 83(2):259–273
35. Lenz FA et al (1989) Characteristics of the bursting pattern of action potentials that occurs in the thalamus of patients with central pain. Brain Res 496(1–2):357–360
36. Tasker RR et al (1987) Thalamic microelectrode recording and microstimulation in central and deafferentation pain. Appl Neurophysiol 50(1–6):414–417
37. Lenz FA et al (1987) Abnormal single-unit activity recorded in the somatosensory thalamus of a quadriplegic patient with central pain. Pain 31(2):225–236
38. Hosobuchi Y, Adams JE, Rutkin B (1973) Chronic thalamic stimulation for the control of facial anesthesia dolorosa. Arch Neurol 29(3):158–161
39. Mazars G, Merienne L, Cioloca C (1974) Treatment of certain types of pain with implantable thalamic stimulators. Neurochirurgie 20(2):117–124
40. Mazars G, Merienne L, Ciolocca C (1973) Intermittent analgesic thalamic stimulation. Preliminary note. Rev Neurol (Paris) 128(4):273–279
41. Turnbull IM, Shulman R, Woodhurst WB (1980) Thalamic stimulation for neuropathic pain. J Neurosurg 52(4):486–493
42. Marchand S et al (2003) Analgesic and placebo effects of thalamic stimulation. Pain 105(3):481–488
43. Coffey RJ (2001) Deep brain stimulation for chronic pain: results of two multicenter trials and a structured review. Pain Med 2(3):183–192

44. Heinricher MM, Cheng ZF, Fields HL (1987) Evidence for two classes of nociceptive modulating neurons in the periaqueductal gray. J Neurosci 7(1):271–278
45. Richardson DE, Akil H (1977) Pain reduction by electrical brain stimulation in man. Part 1: acute administration in periaqueductal and periventricular sites. J Neurosurg 47(2):178–183
46. Richardson DE, Akil H (1977) Pain reduction by electrical brain stimulation in man. Part 2: chronic self-administration in the periventricular gray matter. J Neurosurg 47(2):184–194
47. Hosobuchi Y, Adams JE, Linchitz R (1977) Pain relief by electrical stimulation of the central gray matter in humans and its reversal by naloxone. Science 197(4299):183–186
48. Nandi D et al (2003) Thalamic field potentials in chronic central pain treated by periventricular gray stimulation -- a series of eight cases. Pain 101(1–2):97–107
49. Owen SL et al (2007) Deep brain stimulation for neuropathic pain. Acta Neurochir Suppl 97(Pt 2):111–116
50. Green AL et al (2004) N-of-1 trials for assessing the efficacy of deep brain stimulation in neuropathic pain. Neuromodulation 7(2):76–81
51. Bittar RG et al (2005) Deep brain stimulation for pain relief: a meta-analysis. J Clin Neurosci 12(5):515–519
52. Nestler EJ, Carlezon WA Jr (2006) The mesolimbic dopamine reward circuit in depression. Biol Psychiatry 59(12):1151–1159
53. Goffer Y et al (2013) Calcium-permeable AMPA receptors in the nucleus accumbens regulate depression-like behaviors in the chronic neuropathic pain state. J Neurosci 33(48):19034–19044
54. Su C et al (2015) Persistent pain alters AMPA receptor subunit levels in the nucleus accumbens. Mol Brain 8(1):46
55. Baliki MN et al (2010) Predicting value of pain and analgesia: nucleus accumbens response to noxious stimuli changes in the presence of chronic pain. Neuron 66(1):149–160
56. Lee M et al (2015) Activation of corticostriatal circuitry relieves chronic neuropathic pain. J Neurosci 35(13):5247–5259
57. Mallory GW, Abulseoud O, Hwang SC, Gorman DA, Stead SM, Klassen BT, Sandroni P, Watson JC, Lee KH (2012) The nucleus accumbens as a potential target for central poststroke pain. Mayo Clin Proc 87(10):1025–1031
58. Weigel R, Krauss JK (2004) Center median-parafascicular complex and pain control. Review from a neurosurgical perspective. Stereotact Funct Neurosurg 82(2–3):115–126
59. Andy OJ (1980) Parafascicular-center median nuclei stimulation for intractable pain and dyskinesia (painful-dyskinesia). Appl Neurophysiol 43(3–5):133–144
60. Krauss JK et al (2002) Deep brain stimulation of the centre median-parafascicular complex in patients with movement disorders. J Neurol Neurosurg Psychiatry 72(4):546–548
61. Ray CD, Burton CV (1980) Deep brain stimulation for severe, chronic pain. Acta Neurochir Suppl (Wien) 30:289–293
62. Franzini A et al (2003) Stimulation of the posterior hypothalamus for treatment of chronic intractable cluster headaches: first reported series. Neurosurgery 52(5):1095–1099. discussion 1099-101
63. Schoenen J et al (2005) Hypothalamic stimulation in chronic cluster headache: a pilot study of efficacy and mode of action. Brain 128.(Pt 4:940–947
64. Green AL et al (2006) Deep brain stimulation for neuropathic cephalalgia. Cephalalgia 26(5):561–567
65. Magis D, Schoenen J (2012) Advances and challenges in neurostimulation for headaches. Lancet Neurol 11(8):708–719
66. Fields HL, Adams JE (1974) Pain after cortical injury relieved by electrical stimulation of the internal capsule. Brain 97(1):169–178
67. Adams JE, Hosobuchi Y, Fields HL (1974) Stimulation of internal capsule for relief of chronic pain. J Neurosurg 41(6):740–744
68. Hosobuchi Y, Adams JE, Rutkin B (1975) Chronic thalamic and internal capsule stimulation for the control of central pain. Surg Neurol 4(1):91–92

69. Namba S et al (1984) Electrical stimulation of the posterior limb of the internal capsule for treatment of thalamic pain. Appl Neurophysiol 47(3):137–148
70. Namba S et al (1985) Sensory and motor responses to deep brain stimulation. Correlation with anatomical structures. J Neurosurg 63(2):224–234
71. Mano H, Seymour B (2015) Pain: a distributed brain information network? PLoS Biol 13(1): e1002037
72. Sewards TV, Sewards MA (2002) The medial pain system: neural representations of the motivational aspect of pain. Brain Res Bull 59(3):163–180
73. Bushnell MC, Ceko M, Low LA (2013) Cognitive and emotional control of pain and its disruption in chronic pain. Nat Rev Neurosci 14(7):502–511
74. Apkarian AV et al (2004) Chronic back pain is associated with decreased prefrontal and thalamic gray matter density. J Neurosci 24(46):10410–10415
75. Segerdahl AR et al (2015) The dorsal posterior insula subserves a fundamental role in human pain. Nat Neurosci 18(4):499–500
76. Baliki MN et al (2012) Corticostriatal functional connectivity predicts transition to chronic back pain. Nat Neurosci 15(8):1117–1119
77. Lenz FA et al (2004) The role of the thalamus in pain. Suppl Clin Neurophysiol 57:50–61
78. Dostrovsky JO (2000) Role of thalamus in pain. Prog Brain Res 129:245–257
79. Yen CT, Shaw FZ (2003) Reticular thalamic responses to nociceptive inputs in anesthetized rats. Brain Res 968(2):179–191
80. Peschanski M, Guilbaud G, Gautron M (1981) Posterior intralaminar region in rat: neuronal responses to noxious and nonnoxious cutaneous stimuli. Exp Neurol 72(1):226–238
81. Kuo CC, Yen CT (2005) Comparison of anterior cingulate and primary somatosensory neuronal responses to noxious laser-heat stimuli in conscious, behaving rats. J Neurophysiol 94(3):1825–1836
82. Kuo CC et al (2009) Differential involvement of the anterior cingulate and primary sensori-motor cortices in sensory and affective functions of pain. J Neurophysiol 101(3):1201–1210
83. Zhang Y et al (2011) Ensemble encoding of nociceptive stimulus intensity in the rat medial and lateral pain systems. Mol Pain 7:64
84. Chudler EH et al (1990) Responses of nociceptive SI neurons in monkeys and pain sensation in humans elicited by noxious thermal stimulation: effect of interstimulus interval. J Neurophysiol 63(3):559–569
85. Iwata K et al (2005) Anterior cingulate cortical neuronal activity during perception of noxious thermal stimuli in monkeys. J Neurophysiol 94(3):1980–1991
86. Riva-Posse P et al (2013) Practical considerations in the development and refinement of subcallosal cingulate white matter deep brain stimulation for treatment-resistant depression. World Neurosurg 80(3–4):S27.e25–S27.e34
87. Sun FT, Morrell MJ (2014) Closed-loop neurostimulation: the clinical experience. Neurotherapeutics 11(3):553–563
88. Thakor NV (2013) Translating the brain-machine interface. Sci Transl Med 5(210):210ps17
89. Rauschecker JP et al (2015) Frontostriatal gating of tinnitus and chronic pain. Trends Cogn Sci 19(10):567–578
90. Zhang Q et al (2017) Chronic pain induces generalized enhancement of aversion. elife 6: e25302
91. Wilson HD, Uhelski ML, Fuchs PN (2008) Examining the role of the medial thalamus in modulating the affective dimension of pain. Brain Res 1229:90–99
92. Daou I et al (2013) Remote optogenetic activation and sensitization of pain pathways in freely moving mice. J Neurosci 33(47):18631–18640
93. Iyer SM et al (2014) Virally mediated optogenetic excitation and inhibition of pain in freely moving nontransgenic mice. Nat Biotechnol 32(3):274–278
94. Gu L et al (2015) Pain inhibition by optogenetic activation of specific anterior cingulate cortical neurons. PLoS One 10(2):e0117746

95. Zhang Z et al (2015) Role of Prelimbic GABAergic circuits in sensory and emotional aspects of neuropathic pain. Cell Rep 12(5):752–759
96. Iyer SM et al (2016) Optogenetic and chemogenetic strategies for sustained inhibition of pain. Sci Rep 6:30570
97. Chen Z et al (2017) Deciphering neuronal population codes for acute thermal pain. J Neural Eng 14(3):036023
98. Chen Z, Wang J (2016) Statistical analysis of neuronal population codes for encoding acute pain. In: Proceedings of IEEE ICASSP. IEEE Press, New York, pp 829–833
99. Chen Z, Hu S, Zhang Q, Wang J (2017) Quickest detection for abrupt changes in neuronal ensemble spiking activity using model-based and model-free approaches. In: Proceedings of the IEEE conference neural engineering. IEEE Press, New York, pp 481–484
100. Hu S, Zhang Q, Wang J, Chen Z (2017) Real-time particle filtering and smoothing algorithms for detecting abrupt changes in neural ensemble spike activity. J Neurophys 119(4):1394–1410

Chapter 9
Future of Neural Interfaces

Farah Laiwalla and Arto Nurmikko

Abstract The technological ability to capture electrophysiological activity of populations of cortical neurons through chronic implantable devices has led to significant advancements in the field of brain-computer interfaces. Recent progress in the field has been driven by developments in integrated microelectronics, wireless communications, materials science, and computational neuroscience. Here, we review major device development landmarks in the arena of neural interfaces from FDA-approved clinical systems to prototype head-mounted and fully implantable wireless systems for multi-channel neural recording. Additionally, we provide an outlook toward next-generation, highly miniaturized technologies for minimally invasive, vastly parallel neural interfaces for naturalistic, closed-loop neuroprostheses.

Keywords Brain-computer interfaces · Wireless neural interfaces · Spatially distributed neural sensors · Neuroprostheses

9.1 Overview: Where We Are Now

This volume contains many illustrative examples of the early development and specific applications, across a spectrum of contemporary techniques, whereby direct electronic access to brain circuits, primarily from/to the neocortex, offers opportunities for basic brain science, emergence of medical devices for assisting and/or correcting neurological deficits, as well as discovering potential device-based therapies as an alternative to pharmaceuticals. The emergence of electronic neural interfaces, in particular, reflects outcomes of worldwide multidisciplinary work over the past two decades whereby device engineering, neuroscience, and clinical needs have met at the intersection of fundamental and applied brain science. Here,

F. Laiwalla · A. Nurmikko (✉)
School of Engineering, Brown University, Providence, RI, USA
e-mail: arto_nurmikko@brown.edu

we consider progress—and challenges ahead—for the development of brain-computer interfaces for neural prostheses. We narrow the focus to cortical brain-computer interfaces (BCI) in offering a subjective view of future assistive technologies, particularly those applicable to severe neurological injury to the motor system such as in case of paralysis from neuromotor diseases, stroke, or spinal cord injury. To gain a broader perspective, the reader is referred elsewhere for reviews of neural interfaces including those which engage deeper brain structures such as deep brain stimulation (DBS) which has reached medical device maturity in widespread treatment of, e.g., Parkinsonian disorder [33]. The DBS technology is one example of neuromodulation application of electrical stimulation; many other approved electrical stimulation-based medical devices are also in widespread clinical use, such as spinal cord treatment for chronic pain.

When compared to maturity of the DBS-like neuromodulation technologies, and leaving questions about their therapeutic efficacy to clinicians, cortical BCIs are still at relative infancy, limited at this writing to perhaps up to a dozen human pilot trials worldwide. The fundamental challenges are, in our opinion, considerably more difficult than devices which deploy electrical stimulation from a handful of electrodes near/at the anatomical central or peripheral nervous system target. In particular, for BCIs, one must be able to record cortical circuit activity at sufficient level of detail and then decode typically many parallel channels of electrophysiological activity (action potentials, field potentials, etc.). The decoding, in turn, for essentially reconstructing cortical network activity in a predictive context requires sophisticated computational models and tools to decipher, e.g., a subject's intention to move a limb.

One set of illustrative examples of progress is from research where intracortical microelectrode arrays (MEA) are used to record population dynamics from (<1 cm^2 area) cortical patches at single neuron-level and subsequent application of stochastic state-space dynamical models to decode, e.g., movement planning intention of a subject. The genesis and progress have been well documented in a number of review articles and book chapters. Suffice it to say here that from early discoveries in non-human primates [9, 21, 30, 51], the adaptation of these methods has enabled tetraplegic subjects to control communication devices and electromechanical devices such as robotic arms and hands [3, 13, 22, 23, 46, 52]. The cortical locations where such recordings are made have typically involved primary and/or premotor and parietal areas where, e.g., direction and velocity tuning is distinctly encoded in subsets of neurons. While specific tuning properties of neurons can be helpful across a population which is part of an interconnected network with manifolds of internal state representation (e.g., motor and visual cortices), new decoding techniques are emerging using, e.g., deep learning methods, where presence of such tuning properties is not necessary for successful decoding.

While it follows from biophysical fundamentals that intracortical probes with their inherently single-neuron space-time resolution offer the most direct means to communicate with neuronal populations and their associate networks, they are by no means the only, and not always necessary, requirement for building electronic neural interfaces for prosthetic and other assistive use. As shown elsewhere in this volume,

whether scalp-based (EEG) electrode arrays [36], epidural or subdural electrocorticography (ECoG) [34, 50], peripheral nerves, or elsewhere, there are multiple means to acquire meaningful control signals for assistive use. Broadly, for any assistive medical technology, the overall cost-to-benefit calculations must weigh in many factors: engineering and technological complexity, required medical procedures (such as surgery), safety and reliability—and above all, the level of required performance of the neural interface from the user's point of view.

This chapter examines electrophysiological BCIs only. While the brain is an electrical (electrochemical) biological machine with remarkable level of performance (e.g., per Watt of metabolic power) and lends itself readily to electrophysiology, active research is being pursued to search for neural interfaces relying on recording/stimulation modalities which range from optical to acoustic (ultrasound), to magnetic to chemical modalities, and combinations thereof. Time will tell if these alternative biophysical agents/modalities can compete or augment the direct electrical/electronic approaches.

We summarize in Sect. 2 some recent progress where innovation of *wireless* neural interfaces can now be envisioned to enable mobile BCIs, for untethered movement of subjects. In Sect. 3, we peek into the early ambitious efforts to develop very large-scale neural recording and microstimulation systems where scaling the electrophysiological access to, say, thousands of cortical points requires entirely new ways of approaching the problem, from developing new types of neural probes to re-examining systems level neuroengineering concepts.

9.2 Examples of State-of-the-Art Electronic Brain Interfaces

From a systems level perspective, a brain-computer interface may be broadly partitioned into (i) the physical neural probe (electrodes), (ii) an electronic custom integrated circuit (IC) core for signal acquistion, (iii) the (generally noisy) signal conditioning and telemetry, and (iv) the computing modules with dedicated back-end hardware embedding computational algorithms specific to the neural decoding task. The last decade has seen significant advances in each of these areas, even if a challenging road still lies ahead to meet the overarching goal of developing versatile BCI systems that can adaptively engage with the underlying non-stationary neural circuits in a closed-loop fashion, while compatible with long-term chronic implantation of neural probes in a (future) mobile subject without eliciting significant immune response.

The fundamental challenges of chronic intracortical or deep-brain neural probe design are manifold. First, it is arguably desirable that the spatial scale and density of microscale probes reach close to single neuron resolution (say, ~20–100 μm electrode proximity for a layer V pyramidal neural cell body). Second, the probe material in direct electrical contact with tissue must enable high signal to noise ratio (SNR)

recordings and high-charge-density biphasic microstimulation (the latter being critical for eventual fully closed-loop BCIs) while maintaining designed form factor (rigidity, etc.) and microscale surface characteristics that hopefully limit unavoidable immunologic response. There have been multiple recent reports of successful refinement of electrode microfabrication methodologies to yield, for example, high-density surface ECoG electrodes [26, 49], as well as penetrating 3-D probes [40] approaching an electrode pitch of tens of microns for high-density neural sampling. In contrast to traditional epi and intracortical approaches, Oxley et al. [37] have described a minimally invasive intravascular approach for the placement of a "stentrode" in cortical veins to access neural information at high spatial resolution (where the latter approach is currently being commercialized by Synchron med). Meanwhile, material science research has provided several promising candidates for the integration of next-generation BCI probes in addition to established work horses of Pt and IrOx, from silicon-carbide [15, 16], carbon nanotubes [12], nanoelectronic threads [32] to hybrids of conductive polymers like poly(3,4-ethylenedioxythiophene) (PEDOT) [10, 11, 27]. Success of optical techniques such as optogenetics has led to the development of hybrid probes integrating, for example, optical stimulation and electronic recording onto the same intracortical platform [22, 28, 45], where the latter target closed-loop hybrid optoelectronic BCIs in rodents and non-human primates. Successful transitioning of these novel experimental probe technologies for a chronic implantable BCI is the next major challenge and goal.

The electronic core of a BCI system invariably includes signal amplifiers, conditioning (filters) and dedicated analog-to-digital neural signal conversion. A number of groups worldwide have been developing custom IC solutions for low-power and low-noise neural signal acquisition, particularly focusing on channel scalability (from a handful to >100) and ease of physical integration with the typically monolithic multi-element neural probe. While it is not possible to review these developments exhaustively here, we highlight one recent work, namely, the "Neuropixel" probe system where up to 1356 recording channels were microfabricated within one silicon shank with integrated CMOS signal preconditioning [25, 39]. Systems such as these which allow high-resolution, sub-acute (up to a few months) of robust, wired access to the brain are instrumental in driving neuroscientific knowledge forward, yet are limited for translational chronic use by the complex percutaneous connectors in terms of full subcutaneous implantation. In general, adding a wireless telecommunication capability to neural probes defines one crucial need to extend the utility of these methods to freely moving animals and clinical applications.

9.2.1 BCI Going Wireless: General Considerations

In designing wireless neural interfaces, it is important to consider the requirements and constraints in the full ecosystem context. Relevant questions to ask up front might include, e.g., how a given intracortical MEA or subdural ECoG array may be interfaced with the electronic payload, the latter now located within the hermetically

sealed envelope of the wireless device system. A key question is where within or on the body will the electronics package locate. We start with the design where the system electronics are configured as a head-mounted compact package whereby percutaneous/transcranial connectorization from, e.g., an MEA, is required. One rationale for this configuration as a starting choice on the wireless path is that silicon-based commercial intracortical MEAs are now widely available with a variety of channel counts compatible with small-animal (rodent) as well as non-human and human primate models, including reasonable chronic robustness demonstrated in clinical trials.

Given that contemporary intracortical (or subdual ECoG) sensor arrays typically sample on the order of 100 nodes (single neurons for MEAs, summated field potentials for ECoGs), it is remarkable how such pronounced under-sampling of neuronal population can be successful in enabling subjects to control, e.g., a robotic hand/arm with multiple degrees of freedom of motion. The good news is that this limited amount of neural data sets not unreasonable requirements for wireless telemetry. As also noted elsewhere in this volume, much credit to BCI development must be assigned to (scalable) sophisticated statistical models of neuronal dynamics which have produced powerful algorithms for effective decoding of, e.g., patient's movement intention, from this under-sampled pool of "noisy" brain signals, for real-time assistive device use. Since the "noise" typically hides valuable neural information, it is important that the signal fidelity of a wireless link be maintained (use of data compression techniques must thus be approached judiciously). The wireless neural population data provides direct inputs to the neuro-computational decoding models. There are numerous approaches to neural decoding; one representative example is state-space dynamical modeling, which distils multidimensional neural data (spikes and field potentials) to lower dimensional cortical state representation, suitable for interpretation both by visualization (graphics algorithms), as well as for prosthetic use through forwarding the outputs to assistive electronic devices (e.g., direct cortically operated laptops). The role of machine learning applied to neural decoding and encoding is a rapidly evolving new area of computational neuroscience, with very promising preliminary results suggestive of significant performance and efficiency benefits for real-time BCIs. We bypass the field of neural decoding/encoding in this article and refer the reader to the rich literature, which by now exists for this topic.

From a generic system level view, a fully wired BCI instrumentation collects the raw neural (multi-channel) data via multi-wire cables into electronic neural signal processors (composed of combinations of analog and digital electronics). The digitized data is fed to computers where even today's desktop machines have enough on-board processing power to carry out much of neural decoding to run a simple set of assistive devices. Figure 9.1 shows a block diagram of the basic electronic ecosystem which is more or less common to most (non-human and human) primate researchers in the field.

The next level of significance in advancing this type of electronic brain interface neurotechnology (even if still in early days) is to "untether the patient" by engineering direct wireless access to neural probes such as depicted in Fig. 9.2. While for external body wearable biosensors (whether EEG, EKG, etc.), the transition to a

Fig. 9.1 A block diagram view of a multi-channel neural recording system for brain-computer interface applications. Multi-channel implantable microelectrode arrays are connectorized using wire bundles, and external cabled electronics and computers are used for signal acquisition and processing
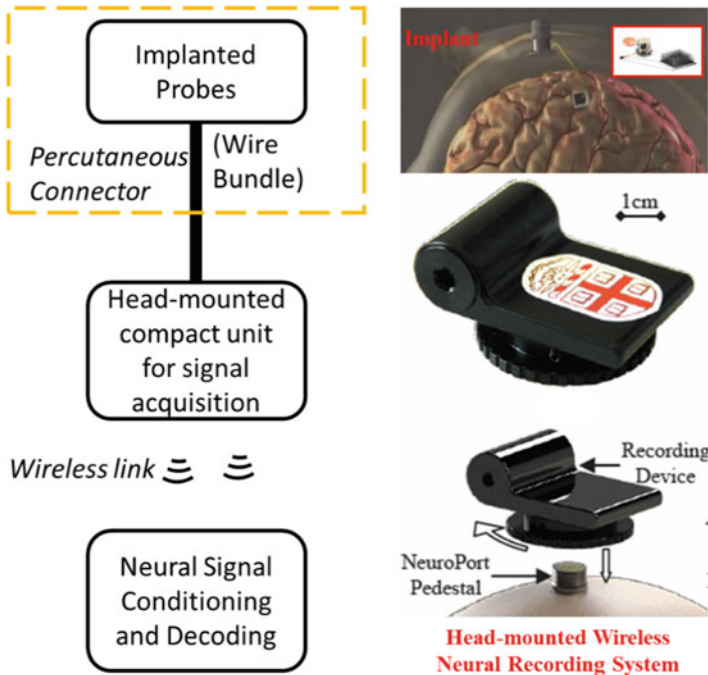
Fig. 9.2 Block diagram and representative device view of a head-mounted wireless neural recording system [55]. Integrated microelectronics are placed within a compact package powered by a replaceable Li-ion battery

wireless system for enhancing subject's mobility is already possible by adapting any number of wireless electronics developed in the past decade for consumer and industrial use, the situation for implanted wireless BCIs poses a number of challenges. These include the following which must be designed and ultimately integrated seamlessly into one viable medical grade implant device system:

- Very low-power and high-fidelity analog and digital (custom) application specific integrated circuits (ASICs) for broadband (spikes, field potentials) neural signal acquisition and electrical microstimulation.
- Very low-power radio frequency transmitter capable of high data rate transmission (~100 MBits/s and beyond), custom designed as an integrated circuit ("RF ASIC").
- Connectorization of the multi-element neural probe front-end (such as one or more MEAs) to and integration with the on-board ASICs.
- Packaging the electronics within a compact housing which is hermetically viable for long-term chronic use.
- Designing external RF receivers which capture the wirelessly emitted, digitally-encoded signals for inputs to computational devices for decoding.
- Strategy for powering the implant electronics (internal battery or RF inductive coupling by external coils).

These engineering challenges are further bound by the first priority in any medical device candidate—safety—which overrides even the main functional claim of the device, here the neurotechnological performance. In the wireless device system which we use here as an example (from our laboratories), safety has multiple components such as (and revisited further below):

- Electrical safety: the electrical energy required by the active ASICs in the implant must have zero accidental probability of discharging into the body/brain tissue.
- Mechanical safety: if the implant unit locates, for example, in the subject's head, the packaging of the electronics must be correspondingly impact-proof.
- Chemical safety: the hermetic sealing of the electronics package must ensure that there is no leakage of toxic or other chemically harmful materials into tissue.
- Thermal safety: ensure that maximum temperature, e.g., in the subcutaneous vicinity of the implant during operation (or recharging batteries), does not exceed $\Delta T < 2.0\ ^{\circ}\text{C}$ and that corresponding temperature rise in the cortical space are kept at $\Delta T < 0.1\ ^{\circ}\text{C}$.
- Electromagnetic (EM) safety: RF (or similar wireless) signal and power transmission of the device are secure, and are not susceptible to external EM interference by ambient RF traffic and vice versa.

Most of these requirements follow the footsteps of established protocols, such as those for pacemakers or cochlear implants for human use, thereby mirroring established regulatory guidelines determined by FDA in the USA. We note, however, that at the frontiers of neurotechnology such as discussed in this volume, the device systems involve considerably complex electronics and require orders of magnitude larger wireless data rates so that early discussions by the technology developers with regulatory agencies is very important.

A number of neurotechnology research groups have developed compact, externally head-mounted wireless neural recording systems as the first step, whereby this approach has allowed leveraging commercially available microelectronics for the development of proof-of-concept wireless BCI systems. Among some of the earliest innovation in this arena, a set of contributions came from the Shenoy group at Stanford. This team has built a series of incrementally sophisticated "Hermes" series of wireless neural recording platforms [12, 19, 30, 38] beginning from a two-channel Hermes-B [41] to a 96-channel battery-operated Hermes-E [17]. In the laboratories of the authors of this chapter, we have similarly developed an external battery-operated, 96-channel broadband neural recording system, featuring custom ICs for neural signal capture and conditioning as well as a dedicated RF IC for 3.5 GHz short-range (~4 m), very-low power wireless transmission with a net power consumption of 61.2 mW [55]. The latter is now a licensed technology which is commercially available, allowing animal researchers to conduct studies on freely moving animals, for example in the context of foraging and naturalistic locomotion.

In addition to the systems level achievements highlighted above, new research is particularly focused at pushing the limits of microelectronic technology to attain improved performance for wireless neural recording with ever-shrinking power budgets. This research extends from subsystems utilizing commercial technologies such as UWB radios, WiFi, and Zigbee to highly optimized low-power integrated approaches. For example, a 4096 channel multiplexed ECoG recording chip with 64-channel amplifiers and 5.12 Mbps data rata, transmitted at 7.8 GHz using UWB radio has been described by Ando et al. [2] with a net power consumption of 1400 mW. Schwarz et al. [42] similarly describe a 128-channel head-mounted system working with microwire array implants, but now integrating the capability for on-board neural signal processing and bidirectional communications with a power consumption of 264 mW, or ~2 mW per channel. Several other groups have described multi-channel ASICs with sub-milliwatt power consumptions per channel while representing various trade-offs between signal compression and power budgets [5, 8]. Finally, multi-modal sensing and stimulation, for example, integrating dopamine sensing and electrical stimulation alongside electrical neural recording [7, 22], and approaches incorporating optogenetic approaches, are increasingly building a niche in the BCI component level landscape which is anticipated to grow significantly in future.

9.2.2 Fully Implanted Wireless Devices—A Case Example

The development of head-mounted and other outside-body wireless neural recording systems has provided a new BCI tool for neuroscience research by enabling more complex and naturalistic animal experiments. However, the need for a percutaneous connection still poses a limitation for BCI use of these systems, in particular, limiting their translation into the human/clinical BCI domain. In considering the bridge from a head-mounted to a fully implanted wireless neural

interface device system, we reiterate key challenges which have to be addressed, typically through extensive animal testing and performance validation:

- Implantation of the system's electronic components within the body in a hermetically encapsulated unit, and choice for the anatomical location of this payload relative to the actual neural probes, where the electronic package has a form factor compatible with subcutaneous placement, for example, in the epicranial space.
- ASIC design and optimization for ultra-low power, consistent with thermal safety guidelines defined by FDA for active brain implants (maximum of 0.5 °C increment in tissue temperature). Extensive thermal simulations and metrology of implants in animal models are typically required.
- Implant power management (rechargeable batteries or continuous inductive coupling) and transcutaneous wireless communication, mitigating the impact of tissue RF absorption, and keeping within the specific absorption rate (SAR) limits prescribed by *IEEE Std C95.1–2005*.

The basic microelectronic building blocks of a fully implantable neural interface system are nearly identical to those described in previous sections; the caveat is that now the spatial scale and performance metrics and requirements (such as those listed above) for a fully implantable device are far more stringent. As the case example for this chapter, the authors' labs have developed a 100-channel hermetically-sealed, fully implantable broadband wireless neural recording system utilizing a 100-channel neural amplifier ASIC, 12-bit SAR ADCs, and a custom RF transmitter IC. The components mirror those developed for the head-mounted system described previously, but now focus on a system architecture with a titanium (Ti)-based hermetic enclosure. The Ti-enclosure has been equipped with a sapphire window to provide full electromagnetic transparency for wireless charging and telecommunications. Further, a custom planar interconnect interface has been built to feed the 100 microwires from the intracortical MEA to the active electronics via multi-channel custom high-density hermetic feedthroughs as shown in Fig. 9.3 [6]. In keeping with the need for further
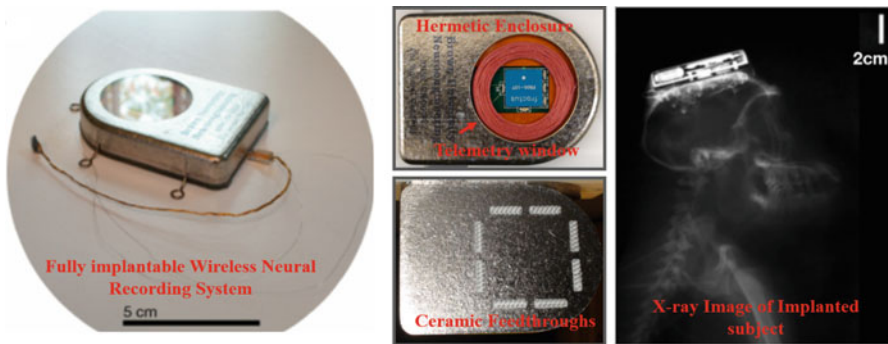

Fig. 9.3 A fully implantable wireless device for neural recording using titanium hermetic enclosure, ceramic feedthroughs, and a sapphire window for broadband wireless communication. Device is powered using a rechargeable Li-ion battery, with multi-hour operation between recharges

electronic integration, there have been several recent efforts to develop system on chip electronics (SoC), where a single chip solution provides neural recording in conjunction with wireless charging, compressive sensing or spike detection, electrical stimulation and bidirectional telecommunications [4, 31, 36]. These advancements are important elements for the further development of fully-implantable systems, but the most critical current bottle-neck for these devices is the availability of scalable hermetic packaging solutions. Hermetic sealing approaches being further studied include ceramic, metallic, or thin-film materials, among others. In addition to the materials choice, a major engineering challenge is to microfabricate the large number of electrical "feedthroughs" without compromising the hermeticity of the implant.

9.3 New Horizons: Large-Scale Neural Interfaces to 10,000 Nodes and Beyond

There has been significant progress in enhancing and maintaining neural access through dense-electrode arrays and biocompatible surface modifications as described in previous sections, yet the scalability of practical neural interfaces to orders of magnitude higher numbers of recording and/or stimulating nodes (thousands and tens of thousands) remains a persistent challenge. As we move from the realm of highly controlled, experimental BCIs to more naturalistic, deployable systems, neural task complexity (NTC) is expected to grow. To gauge the expected number of microelectrode sites with increasing NTC, Gao et al. [18] have postulated that neural decoding would be critically dependent on access to significantly higher numbers of neurons at high densities, ideally from an anatomically diverse neural population. Figure 9.4 represents the outcome from a high-dimensionality neural state-space dynamical theoretical model. Current monolithic multi-electrode constructs are, in our view, inherently incompatible with large-scale implementations of BCIs due to a variety of anatomical and fabrication constraints. For example,
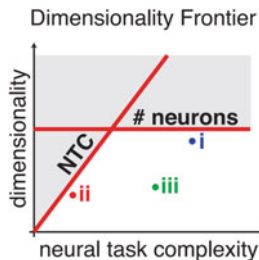
Fig. 9.4 A dimensionality frontier in motor cortical data. Allowed possibilities of dimensionality D and neural task complexity, NTC, exhibit three distinct regimes: (i) the number of recorded neurons M but not NTC restricts dimensionality, (ii) NTC but not M restricts D, and (iii) D is far less than both M and NT C, reflecting an unexplained circuit constraint beyond smoothness and task simplicity. (Courtesy of [18])

traditional hermetic sealing approaches require bulky Ti or ceramic cases, which add significant volume overhead to device size. The intricacy of interconnect design, particularly in the case of a multi-areal implant, is an added complication. While the short tethers between intracortical arrays and the wireless electronics described in the previous section represent a significant improvement over percutaneous tethers, they are still relying on the traditional monolithic intra- or epicortical electrode arrays. Looking forward, one needs to consider paradigm shifts in approaching future BCI-compatible neural interface designs to mitigate these issues in the design of vastly scalable systems. One such approach is to split individual recording and/or neurostimulation electrodes into separate autonomous microscale active electronic chiplets, each with its own internal electronics and (wireless) means to communicate with a central information processing hub. The idea takes advantage of the remarkable progress made by silicon microelectronics in the past 20 years which has pushed component and transistor sizes deep into the sub-100 nm regime. For neural and BCI applications, having access to such CMOS technologies is very attractive provided that commensurate expertise is available for custom design of "mixed-signal" CMOS chips (analog-digital-RF).

Among contemporary work is the concept of free-floating individual "neural dust" sensors in conjunction with a sub-cranial interrogator which was proposed by a number of neuroengineering researchers, most notably Seo et al. [43] (we show concrete examples from our own work below to illustrate a related approach for wireless microsensors and stimulators). The proposed system by Seo et al. [43] involves ultrasonic power and telemetry to circumvent the challenges of efficient electromagnetic energy coupling at millimeter-scale and has been demonstrated at the level of a single 1 mm^3 recording node in the peripheral nervous system [44]. While the concept is presented as an ultra-miniaturizable sensor system, the authors identify several fabrication and materials challenges requiring further advances in CMOS die post-processing completion of microscale implantable microdevices. Elsewhere, a purely electromagnetic-based distributed neural sensor has been demonstrated by Yeon et al. [53], where a three-coil resonant near field inductively coupled system is used to improve the efficiency of wireless power transfer to a millimeter-sized free-floating wireless implantable neural recording system (FF-WINeR). The approach to assembling the FF-WINeR sensor node by manual techniques is also described by Yeon et al. [54] including integration of microwire electrodes, ASICs with through-silicon vias (TSVs), discrete microcoils, and surface mount components. Finally, hermetic sealing with polymeric film deposition (parylene in this case) was applied to form a single "push-pin" recording node measuring $1.05 \times 1.05 \times 0.3$ mm^3. Here too, the authors outline a number of challenges ahead in scaling to many devices given the number of heterogeneous materials and the complexity plus fabrication requirements comprising each sensor node.
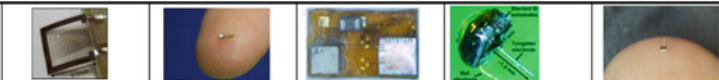
With these snapshots of recent early work, we support the view that spatially distributed sensor systems, once developed as full-fledged medical devices can contribute to future breakthroughs in the field of BCIs while providing new tools for brain science. There are, however, several caveats for the development of a truly

scalable distributed sensor system. First, it is imperative that it be possible to pursue the fabrication of sensors in a uniform, high throughput batch process. Second, sophisticated and ultra-miniaturized sensor node electronics are needed to support semi-autonomous operation including critical functions such as memory and networking. Third, the full neural interface system needs to be defined in the context of a highly-efficient multi-node telecom network. This includes the design and implementation of a compact wearable telecommunications hub that would drive and tune the performance specifications of individual sensor nodes in an adaptive fashion, depending on the specific neural interface application. Fourth, the next frontier in BCI development beyond neural recording for decoding must include neural encoding implemented as patterned cortical microstimulation by a spatially distributed ensemble. This capability needs to be integrated into the individual nodes to form an independent, bidirectional neural interfacing element. Fifth, for chronic implants, it is critical to develop the means for (thin film) hermetic seals which provide a chemically impermeable envelope for the microdevices over decades in the body environment. Finally, the implementation of any neural interface system for use in a human subject requires a real-time neural encoding/decoding using a wearable neurocomputational processor with wireless telemetry to supporting computational platforms, including cloud computing. The concept image of Fig. 9.5 shows schematically the general approach (with some specifics to the approach adopted in the authors' laboratories).

Designing a system to meet the above-mentioned caveats is a challenging proposition on multiple levels. Recent work in our laboratories has focused on developing a spatially distributed implantable wireless "cortical communication" system toward these aspirations, which is built around $500 \times 500\ \mu m$ individually addressable custom microelectronic "neurograins" chiplets (see Fig. 9.6, which also
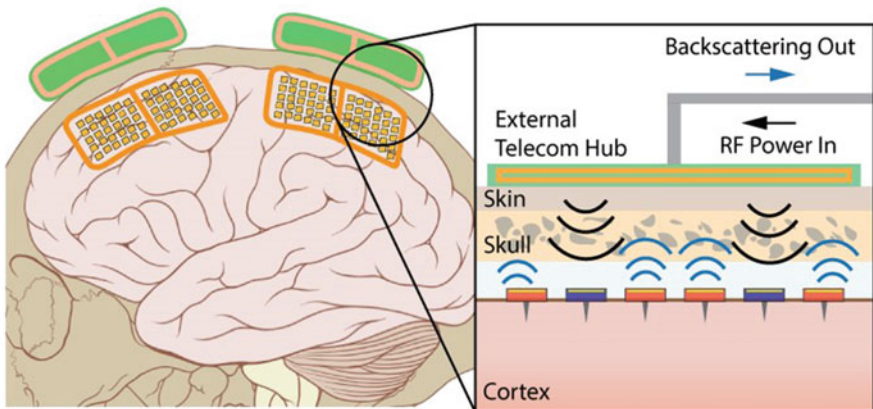
Fig. 9.5 Overview diagram of the spatially distributed implanted wireless neurograin read-out-write-in network—in full deployable system context. Here, two cortical areas are targeted. The external telecom hub in this representation is synonymous with neural computation engine

Reference	[Muller R et al 2018]	[Seo D et al, 2016]	[Johnson B et al 2018]	[Yeon P et al [2018]	Brown/UCSD work
Applications	Recording (CNS)	Recording (PNS)	Stimulation (PNS)	Recording (CNS)	Record./Stim. (CNS)
Number of Ch	64	1	1	1	Up to 800
IC Area [mm²]/Ch	0.09 (Note A)	0.032 (Note B)	1	1.1	0.25
Total Volume [mm³]	-	2.4	2.2	<1	<0.0075 (note C)
Power Consumption [uW]/Ch	3.4	120	9.7	<300	<30
Input Ref.Noise [uVrms]	1.3	180	-	3.78	1.6
Wireless Powering	300MHz RF	1.85MHz Ultrasonic	1.85MHz Ultrasonic	131 MHz RF	915 MHz RF
Telemetry	LSK	Backscattering	Backscattering	IR-UWB	BPSK (TDMA)
Data rate (Mbps)	1	0.5	-	0.8	10
Power supply (V)	0.5	-	3 V	1.8	0.7
ADC	VCO	-	-	VCO	SAR
ADC Resolution	15	8	-	10	8
Technology	65 nm CMOS	Discrete	65 nm CMOS	0.35 um CMOS	65 nm CMOS
Hermetic Sealing	?	?	?	?	ALD > 10 years

Note A: A multichannel system that shares many of the components across the channels
Note B: The ASIC an incomplete system – many of area savings come from using external components such as piezoelectric transducers
Note C: Volume savings include thin substrate but includes hermetic seals.

Fig. 9.6 Comparison of some mm-scale neural microdevices using electrical and/or ultrasound

compares several other recent microdevices). Each chiplet integrates RF-energy harvesting, broadband neural recording or cortical microstimulation. Ensembles of neurograins operate as a synchronized, networked bidirectional RF telecommunication network, scalable in principle across populations of nodes up to tens of thousands. We have chosen to utilize near-field electromagnetic coupling at ~1 GHz to mitigate RF tissue absorption for SAR compliance and designed a single RF-channel simultaneous power-data link for network level simplicity. An external RF telecommunications hub, implemented as a wearable module, wirelessly manages implant performance, and is envisioned also to integrate real-time data processing for neural decoding [19, 20]. Further, we have addressed the microscale packaging challenge by utilizing a batch-process stacked multi-layer thin-film deposition process which is able to yield packaged individual devices that are <0.01 mm^3 in physical volume. This thin film hermetic sealing technique using atomic layer epitaxy, has been demonstrated to provide implant impermeability in accelerated lifetime tests exceeding 10 years [24]. These features have been validated in the context of ex vivo rodent brain slices as well as acute in vivo experiments [29], and now mature for transition to a specific application context.

The above-described system from our labs is one example of an approach for a completely untethered neural interface system that is minimally invasive from the perspective of implant volume burden. Alternative approaches involve flexible, floating epicortical probes with very high channel counts [48] versus integration of genetic approaches to modify neural responsiveness (optogenetics, etc.) toward the realization of next-generation highly efficient, integrated neural interface systems.

9.4 Summary: Outlook for High-Performance BCIs

In this chapter, we have described approaches to high data rate neural interfaces via examples of technical solutions to intracortical/intracranial recording systems. While early clinical trials are under way, and mainly use well-established, but bulky cabled systems, there is a need and opportunity to invest resources to pursue innovative approaches across the entire ecosystem from micro- and optoelectronic probe arrays to chipscale integration of tailored on-chip signal processing and storage functions, to name two areas.

The microminiaturization approaches reviewed here offer a particular opportunity to enhance the functionality of the wireless interfaces by adding neuromodulation/stimulation capabilities. Among such functions is the implementation of patterned electrical (e.g., [14, 47]) or/and optical microstimulation for enabling truly bidirectional communication opportunities with the brain. Efforts to develop such multinode targeted microstimulation tools are being pursued in several academic and commercial laboratories and are likely to reach primates in the near term. These efforts must link closely with neural decoding/encoding models using combination of theoretical neuroscience and machine learning tools.

We re-emphasize the importance of close synergy between closed-loop sense/stimulate-based algorithms which have recently made progress in deep brain stimulation [1]; however, the challenges encountered herein, for bidirectional interfaces comprising hundreds of channels (nodes) and beyond require that large amounts of real-time data, recorded from the nervous system, must be processed and decoded (e.g., [38, 52]). Among the many challenges to this aspiration are the inherent variability and statistical entropy-driven fluctuations in neural circuits, the latter requiring approaches which can adapt to such "non-stationarities."

References

1. Afshar P, Khambhati A, Stanslaski S, Carlson D, Jensen R, Dani S, . . ., Denison T (2013) A translational platform for prototyping closed-loop neuromodulation systems. Front Neural Circuits 6:117

2. Ando H, Takizawa K, Yoshida T, Matsushita K, Hirata M, Suzuki T (2016) Wireless multichannel neural recording with a 128-mbps UWB transmitter for an implantable brain-machine interfaces. IEEE Trans Biomed Circuits Syst 10(6):1068–1078

3. Aflalo T, Kellis S, Klaes C, Lee B, Shi Y, Pejsa K, . . ., Liu C (2015) Decoding motor imagery from the posterior parietal cortex of a tetraplegic human. Science 348(6237):906–910

4. Biederman W, Yeager DJ, Narevsky N, Leverett J, Neely R, Carmena JM, . . ., Rabaey JM (2015) A 4.78 mm 2 fully-integrated neuromodulation SoC combining 64 acquisition channels with digital compression and simultaneous dual stimulation. IEEE J Solid State Circuits 50(4):1038–1047

5. Bonfanti A, Ceravolo M, Zambra G, Gusmeroli R, Borghi T, Spinelli AS, Lacaita AL (2010) A multi-channel low-power IC for neural spike recording with data compression and narrowband 400-MHz MC-FSK wireless transmission. In: 2010 Proceedings of ESSCIRC, September. IEEE, pp 330–333

6. Borton DA, Yin M, Aceros J, Nurmikko A (2013) An implantable wireless neural interface for recording cortical circuit dynamics in moving primates. J Neural Eng 10(2):026010

7. Bozorgzadeh B, Schuweiler DR, Bobak MJ, Garris PA, Mohseni P (2016) Neurochemostat: a neural interface SoC with integrated chemometrics for closed-loop regulation of brain dopamine. IEEE Trans Biomed Circuits Syst 10(3):654–667

8. Brenna S, Padovan F, Neviani A, Bevilacqua A, Bonfanti A, Lacaita AL (2016) A 64-channel 965-μW neural recording SoC with UWB wireless transmission in 130-nm CMOS. IEEE Trans Circuits Syst Express Briefs 63(6):528–532

9. Carmena JM, Lebedev MA, Crist RE, O'Doherty JE, Santucci DM, Dimitrov DF, . . ., Nicolelis MA (2003) Learning to control a brain–machine interface for reaching and grasping by primates. PLoS Biol 1(2):e42

10. Castagnola E, Maiolo L, Maggiolini E, Minotti A, Marrani M, Maita F, . . ., Fadiga L (2015a) PEDOT-CNT-coated low-impedance, ultra-flexible, and brain-conformable micro-ECoG arrays. IEEE Trans Neural Syst Rehabil Eng 23(3):342–350

11. Castagnola V, Descamps E, Lecestre A, Dahan L, Remaud J, Nowak LG, Bergaud C (2015b) Parylene-based flexible neural probes with PEDOT coated surface for brain stimulation and recording. Biosens Bioelectron 67:450–457

12. Chen G, Dodson B, Hedges DM, Steffensen SC, Harb JN, Puleo C, . . ., Davis RC (2018) Fabrication of high aspect ratio millimeter-tall free-standing carbon nanotube-based microelectrode arrays. ACS Biomater Sci Eng 4(5):1900–1907

13. Collinger JL, Wodlinger B, Downey JE, Wang W, Tyler-Kabara EC, Weber DJ, . . ., Schwartz AB (2013) High-performance neuroprosthetic control by an individual with tetraplegia. Lancet 381(9866):557–564

14. Dadarlat MC, O'doherty JE, Sabes PN (2015) A learning-based approach to artificial sensory feedback leads to optimal integration. Nat Neurosci 18(1):138

15. Deku F, Cohen Y, Joshi-Imre A, Kanneganti A, Gardner TJ, Cogan SF (2018) Amorphous silicon carbide ultramicroelectrode arrays for neural stimulation and recording. J Neural Eng 15(1):016007

16. Diaz-Botia CA, Luna LE, Neely RM, Chamanzar M, Carraro C, Carmena JM, . . ., Maharbiz MM (2017) A silicon carbide array for electrocorticography and peripheral nerve recording. J Neural Eng 14(5):056006

17. Gao H, Walker RM, Nuyujukian P, Makinwa KA, Shenoy KV, Murmann B, Meng TH (2012) HermesE: a 96-channel full data rate direct neural Interface in 0.13μm CMOS. IEEE J Solid State Circuits 47(4):1043–1055

18. Gao P, Trautmann E, Byron MY, Santhanam G, Ryu S, Shenoy K, Ganguli S (2017) A theory of multineuronal dimensionality, dynamics and measurement. bioRxiv 1:214262

19. Heelan C, Komar J, Vargas-Irwin CE, Simeral JD, Nurmikko AV (2015) A mobile embedded platform for high performance neural signal computation and communication. In: 2015 IEEE biomedical circuits and systems conference (BioCAS), October. IEEE, pp 1–4

20. Heelan C, Nurmikko AV, Truccolo W (2018) FPGA implementation of deep-learning recurrent neural networks with sub-millisecond real-time latency for BCI-decoding of large-scale neural sensors (104 nodes). In: 2018 40th annual international conference of the ieee engineering in medicine and biology society (EMBC), July. IEEE, pp 1070–1073
21. Hochberg LR, Serruya MD, Friehs GM, Mukand JA, Saleh M, Caplan AH, ..., Donoghue JP (2006) Neuronal ensemble control of prosthetic devices by a human with tetraplegia. Nature 442(7099):164
22. Hochberg LR, Bacher D, Jarosiewicz B, Masse NY, Simeral JD, Vogel J, ..., Donoghue JP (2012) Reach and grasp by people with tetraplegia using a neurally controlled robotic arm. Nature 485(7398):372
23. Jarosiewicz B, Sarma AA, Bacher D, Masse NY, Simeral JD, Sorice B, ..., Cash SS (2015) Virtual typing by people with tetraplegia using a self-calibrating intracortical brain-computer interface. Sci Trans Med 7(313):313ra179
24. Jeong J, Laiwalla F, Lee J, Ritasalo R, Pudas M, Larson L, ..., Nurmikko A (2019) Conformal hermetic sealing of wireless microelectronic implantable Chiplets by multilayered atomic layer deposition (ALD). Adv Funct Mater 29(5):1806440
25. Jun JJ, Steinmetz NA, Siegle JH, Denman DJ, Bauza M, Barbarits B et al (2017) Fully integrated silicon probes for high-density recording of neural activity. Nature 551(7679):232
26. Khodagholy D, Gelinas JN, Thesen T, Doyle W, Devinsky O, Malliaras GG, Buzsáki G (2015) NeuroGrid: recording action potentials from the surface of the brain. Nat Neurosci 18(2):310
27. Kozai TD, Catt K, Du Z, Na K, Srivannavit O, Razi-ul MH, ..., Cui XT (2016) Chronic in vivo evaluation of PEDOT/CNT for stable neural recordings. IEEE Trans Biomed Eng 63(1):111–119
28. Kwon KY, Lee HM, Ghovanloo M, Weber A, Li W (2015) Design, fabrication, and packaging of an integrated, wirelessly-powered optrode array for optogenetics application. Front Syst Neurosci 9:69
29. Lee J, Mok E, Huang J, Cui L, Lee AH, Leung VW, Mercier P, Shellhammer S, Larson L, Asbeck A, Song YK, Nurmikko A, Laiwalla F (2019) An implantable wireless network of distributed microscale sensors for neural applications. IEEE EMBS conference on neural engineering 2019
30. Leuthardt EC, Schalk G, Wolpaw JR, Ojemann JG, Moran DW (2004) A brain–computer interface using electrocorticographic signals in humans. J Neural Eng 1(2):63
31. Liu X, Zhang M, Xiong T, Richardson AG, Lucas TH, Chin PS, ..., Van der Spiegel J (2016) A fully integrated wireless compressed sensing neural signal acquisition system for chronic recording and brain machine interface. IEEE Trans Biomed Circuits Syst 10(4):874–883
32. Luan L, Wei X, Zhao Z, Siegel JJ, Potnis O, Tuppen CA, ..., Dunn AK (2017) Ultraflexible nanoelectronic probes form reliable, glial scar–free neural integration. Sci Adv 3(2):e1601966
33. McDermott H (2016) Neurobionics: treatments for disorders of the central nervous system. In: Neurobionics: the biomedical engineering of neural prostheses. Wiley, Hoboken, pp 213–230
34. Mestais CS, Charvet G, Sauter-Starace F, Foerster M, Ratel D, Benabid AL (2015) WIMAGINE: wireless 64-channel ECoG recording implant for long term clinical applications. IEEE Trans Neural Syst Rehabil Eng 23(1):10–21
35. Mirbozorgi SA, Bahrami H, Sawan M, Rusch LA, Gosselin B (2016) A single-chip full-duplex high speed transceiver for multi-site stimulating and recording neural implants. IEEE Trans Biomed Circuits Syst 10(3):643–653
36. Müller-Putz GR, Schwarz A, Pereira J, Ofner P (2016) From classic motor imagery to complex movement intention decoding: the noninvasive Graz-BCI approach. In: Progress in brain research, vol 228. Elsevier, pp 39–70
37. Oxley TJ, Opie NL, John SE, Rind GS, Ronayne SM, Wheeler TL, ..., Steward C (2016) Minimally invasive endovascular stent-electrode array for high-fidelity, chronic recordings of cortical neural activity. Nat Biotechnol 34(3):320

38. Park YS, Hochberg LR, Eskandar EN, Cash SS, Truccolo W (2013) Early detection of human epileptic seizures based on intracortical local field potentials. In: 2013 6th international IEEE/EMBS conference on neural engineering (NER), November. IEEE, pp 323–326

39. Raducanu BC, Yazicioglu RF, Lopez CM, Ballini M, Putzeys J, Wang S et al (2016) Time multiplexed active neural probe with 678 parallel recording sites. In: 2016 46th European solid-state device research conference (ESSDERC). IEEE, pp 385–388

40. Rios G, Lubenov EV, Chi D, Roukes ML, Siapas AG (2016) Nanofabricated neural probes for dense 3-D recordings of brain activity. Nano Lett 16(11):6857–6862

41. Santhanam G, Linderman MD, Gilja V, Afshar A, Ryu SI, Meng TH, Shenoy KV (2007) HermesB: a continuous neural recording system for freely behaving primates. IEEE Trans Biomed Eng 54(11):2037–2050

42. Schwarz DA, Lebedev MA, Hanson TL, Dimitrov DF, Lehew G, Meloy J, . . ., Ramakrishnan A (2014) Chronic, wireless recordings of large-scale brain activity in freely moving rhesus monkeys. Nat Methods 11(6):670

43. Seo D, Carmena JM, Rabaey JM, Alon E, Maharbiz MM (2013) Neural dust: an ultrasonic, low power solution for chronic brain-machine interfaces. arXiv preprint arXiv:1307.2196

44. Seo D, Neely RM, Shen K, Singhal U, Alon E, Rabaey JM, . . ., Maharbiz MM (2016) Wireless recording in the peripheral nervous system with ultrasonic neural dust. Neuron 91(3):529–539

45. Seymour EÇ, Freedman DS, Gökkavas M, Özbay E, Sahin M, Ünlü MS (2014) Improved selectivity from a wavelength addressable device for wireless stimulation of neural tissue. Front Neuroeng 7:5

46. Simeral JD, Kim SP, Black MJ, Donoghue JP, Hochberg LR (2011) Neural control of cursor trajectory and click by a human with tetraplegia 1000 days after implant of an intracortical microelectrode array. J Neural Eng 8(2):025027

47. Tabot GA, Dammann JF, Berg JA, Tenore FV, Boback JL, Vogelstein RJ, Bensmaia SJ (2013) Restoring the sense of touch with a prosthetic hand through a brain interface. Proc Natl Acad Sci 110(45):18279–18284

48. Tsai D, Sawyer D, Bradd A, Yuste R, Shepard KL (2017) A very large-scale microelectrode array for cellular-resolution electrophysiology. Nat Commun 8(1):1802

49. Viventi J, Kim DH, Vigeland L, Frechette ES, Blanco JA, Kim YS, . . ., Wulsin DF (2011) Flexible, foldable, actively multiplexed, high-density electrode array for mapping brain activity in vivo. Nat Neurosci 14(12):1599

50. Wang W, Collinger JL, Degenhart AD, Tyler-Kabara EC, Schwartz AB, Moran DW, . . ., Kelly JW (2013) An electrocorticographic brain interface in an individual with tetraplegia. PLoS One 8(2):e55344

51. Wessberg J, Stambaugh CR, Kralik JD, Beck PD, Laubach M, Chapin JK, . . ., Nicolelis MA (2000) Real-time prediction of hand trajectory by ensembles of cortical neurons in primates. Nature 408(6810):361

52. Wodlinger B, Downey JE, Tyler-Kabara EC, Schwartz AB, Boninger ML, Collinger JL (2014) Ten-dimensional anthropomorphic arm control in a human brain– machine interface: difficulties, solutions, and limitations. J Neural Eng 12(1):016011

53. Yeon P, Mirbozorgi S, Ash B, Eckhardt H, Ghovanloo M (2016) Fabrication and microassembly of a mm-sized floating probe for a distributed wireless neural interface. Micromachines 7(9):154

54. Yeon P, Gonzalez JL, Zia M, Rajan SK, May GS, Bakir MS, Ghovanloo M (2017) Microfabrication, assembly, and hermetic packaging of mm-sized free-floating neural probes. In 2017 IEEE biomedical circuits and systems conference (BioCAS), October. IEEE, pp 1–4

55. Yin M, Borton DA, Komar J, Agha N, Lu Y, Li H, . . ., Larson L (2014) Wireless neurosensor for full-spectrum electrophysiology recordings during free behavior. Neuron 84(6):1170–1182